



**Republic of Iraq**

**Ministry of Higher Education & Scientific Research**

**University of Kerbala**

**College of Engineering**

**Civil Engineering Department**

**Experimental and Numerical Study of Concrete-Filled  
Double Skin Steel Tubular Columns Under Lateral Cyclic  
Loading**

A thesis Submitted to the Council of the Faculty of the College of Engineering/University of Kerbala in Partial Fulfillment of the Requirements for the Master Degree in Civil Engineering

**By:**

**Zainab Fadhil Kadhim**

**Supervisors**

**Assist prof. Dr. Bahaa Hussain Al- Abbas**

**Assist prof. Dr. Ali Ghanim Abbas Al- Khafaji**

April 2024

Ramadan 1445

**بِسْمِ اللَّهِ الرَّحْمَنِ الرَّحِيمِ**

**((وَقُلْ أَعْمَلُوا فِيسِرَى اللَّهِ**

**عَمَلِكُمْ وَرِسُولَهُ وَالْمُؤْمِنُونَ))**

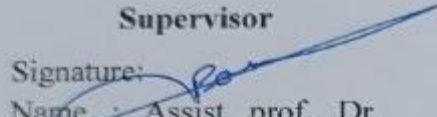
**صَدَقَ اللَّهُ الْعَلِيَّ الْعَظِيمَ**

**(التوبة: من آية 105)**

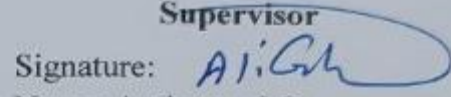
### Examination committee certification

We certify that we have read the thesis entitled " **Experimental and Numerical Study of Concrete-Filled Double Skin Steel Tubular Columns Under Lateral Cyclic Loading** " and as an examining committee, we examined the student " **Zainab Fadhil Kadhim** " in its content and in what is connected with it and that, in our opinion, it is adequate as a thesis for the degree of Master of Science in Civil Engineering.

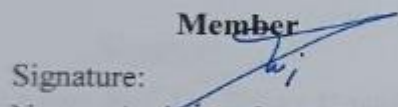
#### Supervisor

Signature:   
Name : Assist prof. Dr.  
Bahaa Hussain Al- Abbas  
Date: / / 2024

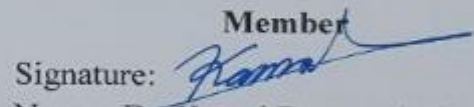
#### Supervisor

Signature:   
Name: Assist prof. Dr.  
Ali Ghanim Abbas Al- Khafaji  
Date: / / 2024

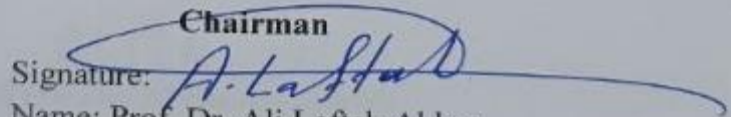
#### Member

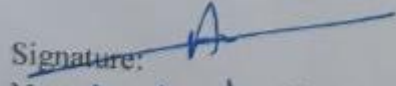
Signature:   
Name : Assist prof. Dr. Zainab  
Muhammad Ridha Abdul Rasoul  
Date: / / 2024


#### Member

Signature:   
Name : Dr. Kamal Darweesh Ibrahim  
Date: / / 2024

#### Chairman

Signature:   
Name: Prof. Dr. Ali Laftah Abbas  
Date: / / 2024

Signature:   
Name Dr. Awad Ali sagheer  
Head of the Department of Civil Engineering  
Date: / / 2024

Signature:   
Name : Assit. Prof. Dr. Haider Nadhom Azziz  
Dean of the Engineering College  
Date: 5/5/2024

### Supervisor certificate

We certify that the thesis entitled " **Experimental and Numerical Study of Concrete-Filled Double Skin Steel Tubular Columns Under Lateral Cyclic Loading** " was prepared by **Zainab Fadhil Kadhim** under our supervision at the Department of Civil Engineering, Faculty of Engineering, University of Kerbala as a partial fulfillment of the requirements for the Degree of Master of Science in Civil Engineering.

Signature: 

Assist prof. Dr. Bahaa Hussain Al- Abbas

Date: / / 2024

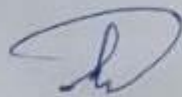
Signature: 

Assist Prof. Dr. Ali Ghanim Abbas Al- Khafaji

Date: / / 2024

### **Linguistic certificate**

I certify that the thesis entitled " **Experimental and Numerical Study of Concrete-Filled Double Skin Steel Tubular Columns Under Lateral Cyclic Loading** " which has been submitted by **Zainab Fadhil Kadhim**, has been proofread, and its language has been amended to meet the English style.



Signature:

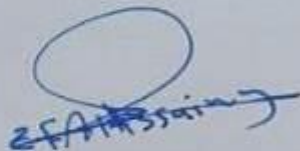
Hawra Mohamed Ali:

Date: 29/4 / 2024

### Undertaking

I certify that the research work titled " **Experimental and Numerical Study of Concrete-Filled Double Skin Steel Tubular Columns Under Lateral Cyclic Loading** " is my own work. The work has not been presented elsewhere for assessment. Where material has been used from other sources, it has been properly acknowledged and referred.

Signature:

A handwritten signature in blue ink, appearing to read 'Zainab Fadhil Kadhim', with a large circular flourish above it.

Zainab Fadhil Kadhim

Date 28/ 4/ 2024

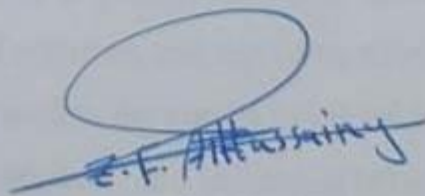
## **Dedication**

*To the Prophet of God Mohammed, his daughter Fatima Al-Zahara,  
and Twelve Infallible Imams, especially Al Imam -Almahdi Al Montather,  
( My God's prayers upon them all).*

## Acknowledgments

By The Name of **Allah**, the most thanks and praise first of all, we would like to be grateful to almighty **Allah**, for giving us a chance to complete this thesis. We do pray to his greatness to enable us to finish this study. Without his permission, we cannot make it possible. I am deeply grateful to my advisors, **Assist Prof. Dr. Bahaa Hussain Al-Abbas, and Prof. Dr. Ali Ghanim Abbas Al- Khafaji** for their support and invaluable guidance throughout my master's research. Their experiences and suggestions have been invaluable to me and have played a crucial role in the success of this thesis. Thanks also to the **civil engineering department, the construction material laboratory, at the University of Kerbala, and Al Sebtayn company for specialized structural and chemical surveys and soil investigation**, for providing me with the opportunity to complete my research and for all of the resources and support they provided. I would like to extend a special thanks to my friends, who went above and beyond to help me with my work. Very special thanks to **my family** for their love and support during this process. Without them, I would not passed this stage.

Finally, I would like to thank all of the participants in my study for their time and willingness to share their experiences. This work would not have been possible without their contribution.



Zainab Fadhil Kadhim



## **Abstract**

The lateral cyclic behavior of composite concrete and double-skin steel tube columns is one of the construction methods used at the current time. The current study consists of two tubes outer and inner welded together perfectly and filled with two types of concrete: normal and high strength. Twelve composite columns represented the testing samples, six of them had square sections, and the other were circular. They were divided into six groups all subjected to cyclic lateral load: The first group consisted of two samples; circular and square. These samples were filled with normal concrete and subjected to cyclic lateral load only. The second group was the same construction as the previous group and was subjected to a scaled axial dead load of only about (40) kN. The third group also had the same construction and description as the 1st and 2nd groups and was subjected to an axial load (dead and live) scaled load of about (70) kN. The fourth group consists of two samples; circular and square. These samples were filled with high-strength concrete, and subjected to cyclic lateral load only. The fifth group was the same construction as the previous group and subjected to an axial dead load of only about (40) kN. The sixth group had the same construction and description as the 4th and 5th groups and was subjected to axial (dead plus live) loads of about (70) kN. The variables of experimental work and the numerical study included tube shape, type of concrete, and the value of axial load. The cyclic responses, including failure modes, the curves of lateral load —displacement, the protocol of cyclic load with time, and validation between numerical study used (ABACUS program) and experimental work. The experimental and numerical study compared the effect of the type of concrete

that filled the composite columns and found that specimens filled with high-strength concrete(HSC) resisted the effects of lateral cyclic loading more than the same with normal concrete strength (NSC), for the circular section as a percentage of (6.68 %,9.20%,21.10%) respectively as the value of axial loads. For the square section, the resistance of lateral cyclic loading was increased as a percentage of (3.07%, 6.26%, and 9.53%) respectively according to the value of axial loads, compared with columns filled with normal concrete strength (NSC), which means the influence of high-strength concrete enhanced the performance of the resistance of composite columns to lateral cyclic loading. The shape's effect, also considered in this study, the results show that circular sections have a resistance of lateral cyclic loads greater than the square section at the same conditions both for normal and high-strength concrete.

## Table of Contents

Examination committee certification.....	
Supervisor certificate.....	
Linguistic certificate.....	
Undertaking.....	
Acknowledgments.....	
Abstract.....	ii
Table of Contents.....	iii
List of Tables.....	viii
List of Figures.....	x
List of Abbreviations.....	v
List of Symbols.....	v
Chapter1:Introduction.....	1
1.1 Composite Columns.....	1
1.1.1 General.....	1
1.1.2 Composite Column's Type.....	1
1.1.2.1 Concrete-filled Sections.....	2
1.1.2.2 Totally or partially encased Sections.....	2
1.1.3 Advantages of Composite Columns.....	4
1.2 Cyclic Load.....	5
1.3 Types of Concrete.....	7
1.4 Differences between Normal and high-strength concrete properties.....	8
1.5 Objectives of the Present Study.....	9
1.6 Thesis Layout.....	9
Chapter2: Literature Review.....	11

2.1 Introduction.....	11
2.2 Composite Columns.....	11
2.3 High-strength concrete filled (CFST).....	30
2.4 Influence of (CFST) cross-sectional shape:.....	34
2.5 Summary:.....	37
Chapter3: Experimental Work.....	39
3.1 General.....	39
3.2 Details of Specimens.....	40
3.3 Materials .....	48
3.3.1 Cement.....	48
3.3.2 Fine aggregate (sand).....	51
3.3.3 Coarse Aggregate (Gravel) .....	52
3.3.4 Water.....	54
3.3.5 Silica Fume... ..	54
3.3.6 Superplasticizer.....	56
3.3.7 Steel Tube.....	57
3.4 Concrete Mixing .....	60
3.4.1 Normal Concrete (NSC) .....	60
3.4.2 High Strength Concrete (HSC):.....	61
3.5 Fresh Concrete Test .....	62
3.5.1 Slump Test .....	62
3.6 Hardened Concrete's Mechanical Characteristics.....	63
3.6.1 Compressive Strength.....	63
3.6.2 Splitting Tensile Strength .....	64

3.6.3 Flexure tensile Strength .....	65
3.7 Processing of Specimens.....	66
3.8 Support industry .....	68
3.9 Application of Axial Loads.....	74
3.10 Application of Cyclic Loading .....	75
Chapter4: Results and Discussion.....	76
4.1 General.....	76
4.2 Mechanical Properties of NSC and HSC.....	77
4.2.1 Compressive Strength Results .....	77
4.2.2 Splitting Tensile Strength Results.....	78
4.2.3 Flexure tensile Strength (Modulus of Rupture (fr )).....	80
4.2.4 Modulus of Elasticity .....	81
4.3 Nominal Axial Load: .....	82
4.4 Failure Modes .....	83
4.5 Load-Displacement Behavior .....	91
4.6 Skeletons Curve. ....	99
4.7 Parameters Influence.....	100
4.7.1 Influence of type of concrete: .....	100
4.7.1.1 Square Section .....	100
4.7.1.2 Circular Section .....	101
4.7.2 Influence of Shape of Steel Tube Cross Section: .....	103
4.7.2.1 High-Strength Concrete Specimens.....	103
4.7.2.2 Normal Strength Concrete Specimens.....	104
4.7.3 Influence of Value of Axial Loads: .....	106

4.7.3.1 High-Strength Circular Specimens: .....	106
4.7.3.2 High-Strength Square Specimens: .....	107
4.7.3.3 Normal Strength Circular Specimens: .....	108
4.7.3.4 Normal Strength Square Specimens: .....	110
Chapter5: Finite Element Simulation.....	112
5.1 General.....	112
5.2 Parts of Model.....	112
5.3 Materials Properties .....	114
5.3.1 Concrete Material Representing. ....	115
5.3.2 Steel Material Representing.....	116
5.3.3 Sections.....	117
5.4 Assembly.....	117
5.5 Interaction .....	118
5.6 Meshing.....	119
5.7 Loading and boundary conditions.....	120
5.8 Results and Analysis .....	122
5.8.1 Validation of Numerical Study.....	123
5.9 Parametric Study.....	134
5.9.1 Reinforcement specimens simulation .....	135
5.9.2 Reinforcement Details .....	135
5.9.3 Parametric Study Results and Analysis .....	136
5.9.3.1 Validation of parametric study .....	136
Chapter6 : Conclusions.....	143
6.1 Introduction.....	143

6.2 Conclusions.....	143
6.3 Recommendations.....	145
References.....	147
Appendixes.....	1
Appendix A .....	1
Silica Fume Properties.....	1
Superplasticizer (Glenium 54).....	3
Appendix B .....	5
Design of Axial and Lateral Load for( CFST ) Columns.....	5

## List of Tables

Table 2-1 The Results of Composite Columns with Various Steel Layer Thickness .....	15
Table 3-1 Details of Area and Moment of Inertia of Composite Columns...	42
Table 3-2 Details of concrete-filled circular double-skin columns.....	47
Table 3-3 Details of concrete-filled square double skin column (CFSDS)...	48
Table 3-4 Physical characteristics of The Cement .....	49
Table 3-5 Chemical Construction of Cement.....	50
Table 3-6 Gradation of Sand .....	51
Table 3-7 The Chemical Composition of Sand .....	52
Table 3-8 Coarse Aggregate Grading Results .....	53
Table 3-9 Chemical Characteristics of Coarse Aggregate (Gravel).....	53
Table 3-10 Properties of Silica Fume .....	55
Table 3-11 properties of the steel coupon .....	58
Table 3-12 Amounts of the Materials measured by (kg)/ One Cubic Meter of Normal Concrete (NC) Mix.....	61
Table 3-13 Amounts of the Materials by (kg) for One Cubic Meter of High Strength Concrete (HSC) Mix: .....	62
Table 4-1 Compressive Strength of Concrete Mixes .....	77
Table 4-2 Results of three cylinders of each type of concrete .....	79
Table 4-3 Results of three prisms for each type of concrete and average.....	80
Table 4-4 Average Modulus of Elasticity. ....	81
Table 4-6 The failure modes of the CFDST column.....	98
Table 5-1 Concrete Damage Plasticity Value[50].....	115
Table 5-2:Effect of Mesh Size on Ultimate Load and Deflection.....	120



Table 5-3 Validation of Lateral Load Value of Experimental and Numerical Results.....	124
Table 5-4 Validation between Lateral Load for The Model in F.E and Model Strengthen with Reinforcement Steel .....	137

## List of Figures

Figure 1-1 Concrete Filled Section[1] .....	3
Figure 1-2 Totally Concrete Filled Section[1] .....	3
Figure 1-3 Partially Encased Concrete Filled Section[1] .....	4
Figure 1-4 Different Types of Cyclic Load and Material Response .....	6
Figure 2-1 Three types of load application. Load applied to (a) the Concrete section, (b) the steel section, and (c) the entire section, (d) The section of the columns.....	12
Figure 2-2 Concrete -Filled Double -Skin Steel Tube (CFDST) Details.....	13
Figure 2-3 Boundary Condition Diagram and Finite Element Model. (a) Boundary Condition Diagram; (b) Cross-Section Details; (c) Finite Element Model; (d) Core Concrete Model (e) Steel Tube Mode .....	16
Figure 2-4 Details of Different Types of CFDST .....	17
Figure 2-5 Numerical and Experimental Curves of Lateral Force-Displacement .....	18
Figure 2-6 P-M Interaction Curve of SRC Column As Per Eurocode 4.....	19
Figure 2-7 (a) Test Set-up Schematic (b) Test Specimens (c) LVDT Position .....	19
Figure 2-8 Composite Columns Boundary Conditions .....	20
Figure 2-9 Protocol of Cycles with Displacement .....	20
Figure 2-10 Failure Mode for Specimens.....	21
Figure 2-11 Cyclic Lateral Load -Displacement Curve .....	23
Figure 2-12 The Details of Lateral Displacement Curve and Failure Mode.	24
Figure 2-13 Failure Modes for Experimental and Numerical Specimens....	27
Figure 2-14 Testing Setup .....	28
Figure 2-15 Test Setup and Failure Mode of Specimens .....	29

Figure 2-16 Cross-Section of CFDST .....	30
Figure 2-17 Details of Specimens .....	31
Figure 2-18 Dimension details of test specimens.....	32
Figure 2-19 Failure Mods for Specimens .....	33
Figure 2-20 Specimens Details.....	35
Figure 2-21 Different Cross SectionsCFT.....	36
Figure 3-1 Flow Chart for Experimental Work.Error! Bookmark not defined.	
Figure 3-2 Cross Section in CFDST.....	40
Figure 3-3 Sieve Analysis Chart for Sand.....	52
Figure 3-4 Sieve analysis chart for Coarse Aggregate .....	54
Figure 3-5 descriptions of dimension coupon as per ASTM-A370 .....	58
Figure 3-6 stress-strain curve .....	59
Figure 3-7 Brsim Dimensions Details .....	66
Figure 3-8 Details of Lower Support and Stiffeners. ....	71
Figure 3-9 Testing Machine .....	73
Figure 3-10 Displacement history of all specimens .....	75
Figure 4-1 Flow Chart of Specimens Test.....	76
Figure 4-2Critical column load combination[49].....	83
Figure 4-3 Load Displacement Diagram for CNS-C1 Specimen.....	92
Figure 4-4 Load Displacement Diagram for CNS-C2 Specimen.....	92
Figure 4-5 Load Displacement Diagram for CNS-C3 Specimen.....	93
Figure 4-6 Load Displacement Diagram for CNS-S1 Specimen .....	93
Figure 4-7 Load Displacement Diagram for CNS-S2 Specimen .....	94
Figure 4-8 Load Displacement Diagram for CNS-S3 Specimen .....	94
Figure 4-9 Load Displacement Diagram for CHS-C1 Specimen.....	95
Figure 4-10 Load Displacement Diagram for CHS-C2 Specimen.....	95

Figure 4-12 Load Displacement Diagram for CHS-S1 Specimen .....	96
Figure 4-13 Load Displacement Diagram for CHS-S2 Specimen .....	97
Figure 4-14 Load Displacement Diagram for CHS-S3 Specimen .....	97
Figure 4-15 Skeleton Curve for All Specimens .....	99
Figure 4-16 Skeleton Curve of CHS-S1 and CNS-S1 .....	100
Figure 4-17 Skeleton Curve of CHS-S2 and CNS-S2 .....	100
Figure 4-18 Skeleton Curve of CHS-S3 and CNS-S3 .....	101
Figure 4-19 Skeleton Curve of CHS-C1 and CNS-C1 .....	101
Figure 4-20 Skeleton Curve of CHS-C2 and CNS-C2 .....	102
Figure 4-21 Skeleton Curve of CHS-C3 and CNS-C3 .....	102
Figure 4-22 Skeleton Curve of CHS-C1 and CHS-S1 .....	103
Figure 4-23 Skeleton Curve of CHS-C2 and CHS-S2 .....	103
Figure 4-24 Skeleton Curve of CHS-C3 and CHS-S3 .....	104
Figure 4-25 Skeleton Curve of CNS-C1 and CNS-S1 .....	104
Figure 4-26 Skeleton Curve of CNS-C2 and CNS-S2 .....	105
Figure 4-27 Skeleton Curve of CNS-C3 and CNS-S3 .....	105
Figure 4-28 Skeleton Curve of CHS-C3 and CHS-C2 .....	106
Figure 4-29 Skeleton Curve of CHS-C3 and CHS-C1 .....	106
Figure 4-30 Skeleton Curve of CHS-C2 and CHS-C1 .....	107
Figure 4-31 Skeleton Curve of CHS-S3 and CHS-S2 .....	107
Figure 4-32 Skeleton Curve of CHS-S3 and CHS-S1 .....	108
Figure 4-33 Skeleton Curve of CHS-S2 and CHS-S1 .....	108
Figure 4-34 Skeleton Curve of CNS-C3 and CNS-C2 .....	109
Figure 4-35 Skeleton Curve of CNS-C3 and CNS-C1 .....	109
Figure 4-36 Skeleton Curve of CNS-C2 and CNS-C1 .....	110
Figure 4-37 Skeleton Curve of CNS-S3 and CNS-S2 .....	110
Figure 4-38 Skeleton Curve of CNS-S3 and CNS-S1 .....	111

Figure 4-39 Skeleton Curve of CNS-S2 and CNS-S1 .....	111
Figure 5-1 Part Modeling for Square Columns .....	113
Figure 5-2 Part Modeling for Circular Columns .....	114
Figure 5-3 Compressive Stress-Strain Behavior .....	116
Figure 5-4 Tensile Stress-Strain Behavior .....	116
Figure 5-5 Assembly for Square and Circular Models.....	117
Figure 5-6 Models Interaction Simulations.....	118
Figure 5-7 Typical Applied Meshing for Square and Circular Model.....	119
Figure 5-8 Displacement and Rotation Degree of Freedom.....	121
Figure 5-9 Boundary Conditions and Lateral Displacement on Model .....	121
Figure 5-10 Boundary Conditions, Lateral Displacement, and Axial Force on Model.....	122
Figure 5-11 Failure Mode Validation between Experimental and F.E Work .....	123
Figure 5-12 Stresses in Model Group One CNS-C (a) Stresses in Concrete(b) Stresses in Steel Tube .....	126
Figure 5-13 Stresses in Model Group Two CHS-C (a) Stresses in Concrete(b) Stresses in Steel Tube.....	127
Figure 5-14 Stresses in Model Group Three CNS-S (a) Stresses in Concrete(b) Stresses in Steel Tube.....	128
Figure 5-15 Stresses in Model Group Four CHS-S (a) Stresses in Concrete(b) Stresses in Steel Tube.....	129
Figure 5-16 Load Displacement Diagram for CNS-C1 Specimen.....	129
Figure 5-17 Load Displacement Diagram for CNS-C2 Specimen.....	130
Figure 5-18 Load Displacement Diagram for CNS-C3 Specimen.....	130
Figure 5-19 Load Displacement Diagram for CNS-S1 Specimen .....	130

Figure 5-20 Load Displacement Diagram for CNS-S2 Specimen .....	131
Figure 5-21 Load Displacement Diagram for CNS-S3 Specimen .....	131
Figure 5-22 Load Displacement Diagram for CHS-C1 Specimen.....	131
Figure 5-23 Load Displacement Diagram for CHS-C2 Specimen.....	132
Figure 5-24 Load Displacement Diagram for CHS-C3 Specimen.....	132
Figure 5-25 Load Displacement Diagram for CHS-S1 Specimen .....	132
Figure 5-26 Load Displacement Diagram for CHS-S2Specimen .....	133
Figure 5-27 Load Displacement Diagram for CHS-S3Specimen .....	133
Figure 5-28 The Deformed Shape of Composite Column Model.....	134
Figure 5-29 Reinforcement Details for Specimens (a) Square Section Specimens (b) Circular Section Specimens.....	136
Figure 5-30 Stresses in Strengthen Circular Columns CHS-CR (a) Stresses in Concrete(b) Stresses in Steel Tube(c) Stresses in reinforcement steel ...	138
Figure 5-31 Stresses in Strengthen Square Columns CHS-SR (a) Stresses in Concrete(b) Stresses in Steel Tube(c) Stresses in reinforcement steel .....	140
Figure 5-32 Comparison of Load Displacement Diagram between CHS-C3 and CHS-CR Mode.....	140
Figure 5-33 Comparison of Load Displacement Diagram between CHS-S3 and CHS-SR Model.....	141

## List of Abbreviations

Symbols	Description
ASTM	American society for testing materials
ACI	American concrete institute
CFST	Concrete-filled steel tube
CCFST	Circular concrete-filled steel tube
SCFST	Square concrete-filled steel tube
RCFST	Rectangular concrete-filled steel tube
CFDST	Concrete-filled double steel tube
(AISC)	American institute of steel construction
FEA	Finite Element Applications
RC	Reinforced concrete
LVDT	Linear variation displacement transducer
CES	Concrete encased steel
HSC	High-strength concrete
NSC	Normal-strength concrete
MBCC GROUP	Master building construction chemical group
USA	United States of America
GPGPUs	General-purpose graphics processing units
HPC	High-performance computing
CPUs	Central processing units
FIB	The International Federation for Structural Concrete

## List of Symbols

$(D_i/D_o)$	the ratio of inner to outer diameter
$(D/t)$	diameter-thickness ratio
$D$	Diameter of circular tube
$D_o, D_i$	Outer and inner diameter of circular tube
$B$	Width of square tube
$B_o, B_i$	Outer and inner width of square tube
$I_x$	Moment of inertia about x-axis
$A_c$	Area of concrete
$A_s$	Area of steel
$f_y$	Specified yield strength for steel
$f_c'$	Specified cylinder compressive strength of concrete
$E_s$	Modules of elasticity of steel
$E_c$	Modules of elasticity of concrete
$f_u$	The ultimate strength of steel
$MPa$	Mega Pascal N/mm <sup>2</sup>
$f_s$	The tensile stress of splitting
$f_r$	Flexural tensile strength( modulus of rupture )
$P_o$	Nominal strength load
$D.L$	Dead load
$L.L$	Live load
$LCF$	Low cycle fatigue
$PPC$	Portland Pozzolana Cement
$SCC$	Self-Compacting Concrete
$STRC$	Steel Tube-Reinforced Concrete



***CHAPTER***

***ONE***

## **Chapter1 :Introduction**

### **1.1 Composite Columns**

#### **1.1.1 General**

These days, among the many buildings we see, both large and small, present and ancient, the modern structures are the ones that catch our attention the most since they represent remarkable achievements in science and engineering. , now the goal has switched to designing safe structures while considering the project's economic implications in terms of towers and blocks. Another name for them might be "vertical cities" which consists of having more ground space available and the capacity to fit more people in a smaller area. As a result, it offers us advantages like a nice skyline, significant sites, and sustainable land use. The main purpose for these is to attain the stability, strength, and stiffness of the construction; to do so, innovation was introduced. "Composite Construction" The industry for non-residential high-story structures is governed by composite construction. For more than twenty years, this has been the state. One way to sum up why composite construction is often so good is this: steel is good in tension, and concrete is good in compression. This allows for an increase in strength and stiffness with low material consumption. These two materials' structural complementarities can be combined to create a highly effective and lightweight design. Another advantage of composite systems is their ability to save building time. Reduced floor depths made possible by composite construction can also have a significant positive impact on service costs[1].

#### **1.1.2 Composite Column's Type**

Concrete infill steel columns use the advantages of both steel and concrete. Usually, plain or reinforced concrete is filled with a steel hollow

section that is circular or rectangular. When a strong and effective structural system is required, it is usually used as beams in low-rise industrial structures and as columns in high-rise and multi-story buildings. Such structural solutions have a lot of benefits in terms of construction sequence as well as structural performance. The innate buckling issue in thin-walled steel tubes is either avoided or limited because of the concrete core. Furthermore, the steel shell's application of a confinement effect enhances the ability of the concrete in-fill. Another benefit, such as the cross-sectional material distribution, aids in the system's overall structural performance efficiency. Columns' behavior in tension and buckling is more effective because of the steel cover on the outside. Also provides the maximum stiffness since the material is located farthest from the centroid. The combination with the high modulus of elasticity of the steel investigated the high impact on the moment of inertia. On the other hand, the core of concrete has a high resistance of axial compression strength[1].

**1.1.2.1 Concrete-filled sections**

- Circular concrete-filled steel tube.
- Rectangular concrete-filled steel tube.
- Square concrete-filled steel tube.

**1.1.2.2 Totally or partially encased sections**

- Totally encased concrete fill sections
- Partially encased concrete fill sections

The different cross-sectional forms of the composite members are shown in Figures 1-1, 1-2, and 1-3 The first type of composite columns represented by a partial encasement method, in which concrete is poured between the edges of the steel section, can be employed to reduce the need for temporary

formwork while maintaining the usage of the universal components of the composite elements see Figure 1-1, due to the concrete's adequate shielding, this steel web has very strong fire resistance. The steel section encased in concrete Figure 1-2, and 1-3 was the second and third form of a composite column, because of its low grade and requirement for resisting fire, this column is contained by concrete. Previous research has indicated that using high-strength concrete is better as it improves column durability and can also have fewer cross-sections. Currently, concrete-filled pipes are used more commonly than concrete-covered steel components because of their inappropriate appearance and the requirement for molds to pour concrete Figure 1-1. Also, using steel tubes as prefabricated molds speeds up a building, enhances appearance, and filling concrete provides high fire resistance. [1].

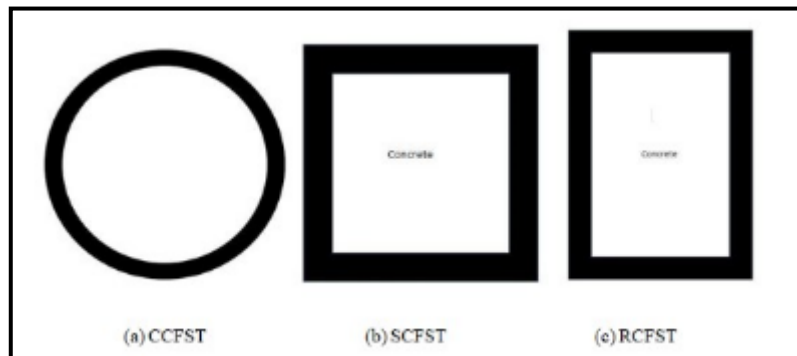


Figure 1-1 Concrete Filled Section[1]

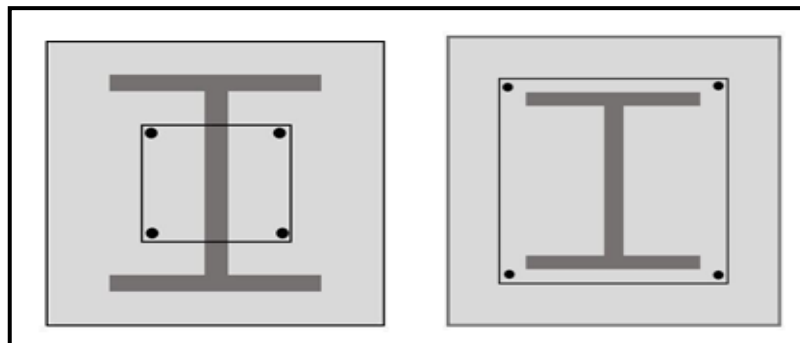


Figure 1-2 Totally Concrete Filled Section[1]

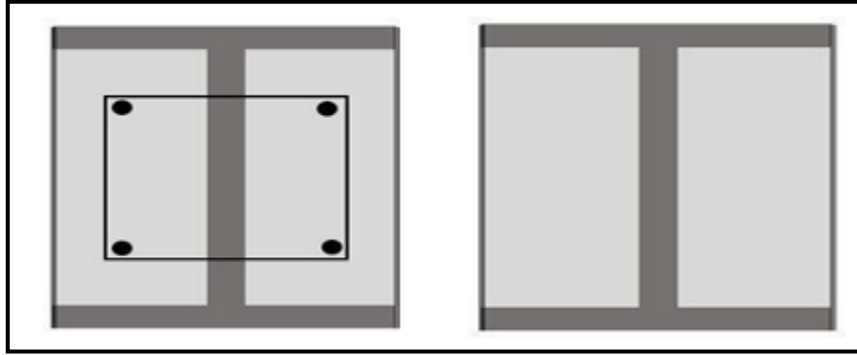


Figure 1-3 Partially Encased Concrete Filled Section[1]

### 1.1.3 Advantages of Composite Columns

There are many advantages to using composite columns as follows:

- To expand the availability of usable floor space for a given strength.
- The concrete-encased columns, offer excellent resistance to corrosion and fire.
- Its application offers financial benefits over the more traditional use of reinforced concrete or structural steel.
- The columns' outside measurements remain constant throughout multiple stories, making architectural detailing and construction easier see Plate 1-1.
- If the tubular sections are filled with concrete, there is no need to add more reinforcing steel.
- Drying shrinkage and creep are significantly reduced in composite members than the other reinforced concrete [1].



Plate 1-1 Application of Composite Columns Building

## 1.2 Cyclic Load

"**Cyclic loading**" means the continuous and repeated application of a load (variable stresses, strains, forces, etc.) on a structural element or a material that eventually results in fatigue and material degradation[2]. Materials that are subjected to cyclic loading tend to fatigue more quickly and at lower loads than they would normally.

**Fatigue** is the gradual and localized damage of a material's molecular structure caused when the structure or material is exposed to cyclic loading, which ultimately leads the material to lose its strength. One of the reasons the load required for fatigue failure is far less than the material's ultimate tensile strength is the repeated stress, strain, tension, and tensile load acting in this kind of situation. The continuous and repeated application of a load in a horizontal direction, on an object or structural component, is known as lateral loading. As a result, lateral force may be a shear or bend in the direction of the force of the material, which could ultimately lead to material failure. Materials deteriorate due to shearing under lateral load.

**Yield stress:** is defined as a minimum stress in which a material begins to deform without a noticeable increase in load. In another way, the yield stress, which is a measurement of the material structure's strength, is the lowest stress necessary to cause a material to flow. The rate of deformation (strain rate) and, more significantly, the temperature at which the deformation occurs affect the stress yield occurs. Engineering materials can exhibit many types of cyclic plastic deformation, such as mean stress relaxation, ratcheting, and low cycle fatigue (LCF), as illustrated in Figure 1-4. Mean stress relaxation happens during asymmetric strain cycling, ratcheting results from asymmetric stress cycling, and LCF typically occurs during symmetric strain cycling[3].

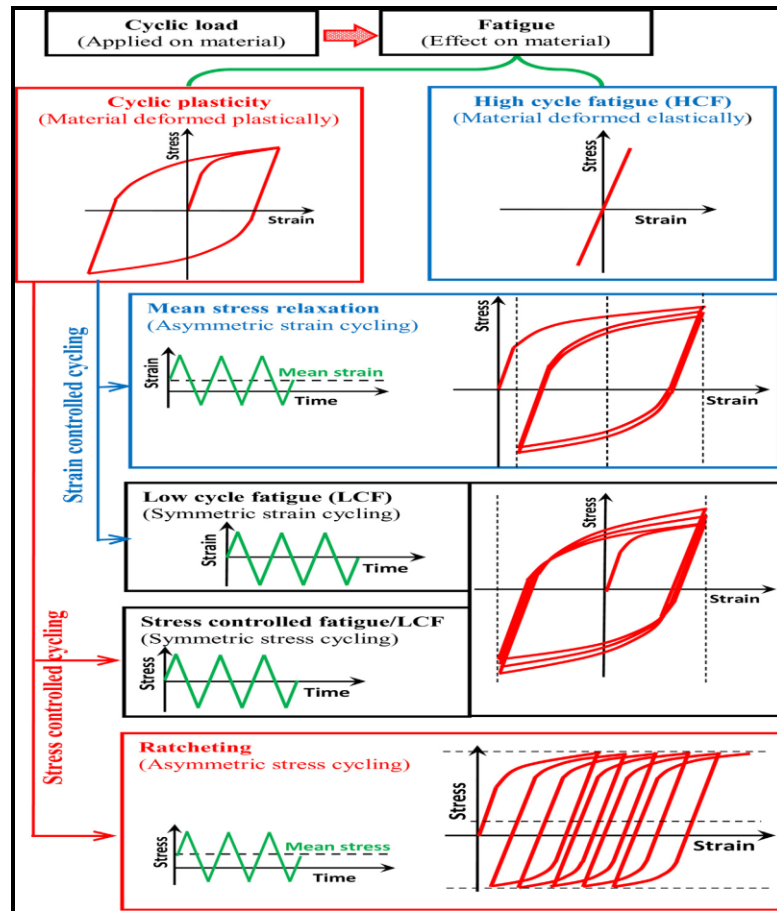


Figure 1-4 Different Types of Cyclic Load and Material Response

### 1.3 Types of Concrete

Concrete is a building material that is composed of cement, sand, and coarse aggregates- mixed with water that hardens in time. Concrete works employ a variety of cement types, each with different characteristics and uses. Portland Pozzolana Cement (PPC), rapid hardening cement, sulfate-resistant cement, and other types. The ratio of water to cement is a significant factor that affects different features, including workability, strength, and durability. The water-cement ratio must be required to produce concrete workability. The hydration reaction begins when cement combined with water reacts with it. Concrete is used to build a variety of structural components, including footings, lintels, beams, slabs, and columns, according to ACI 301 Specifications for Structural Concrete and ACI 318 Building code requirements for structural concrete. Nowadays, several kinds of concrete are produced to be used in the construction of buildings and other structures. These have specific characteristics and properties that raise the standard of construction to meet specifications. Based on its compressive strength, concrete is divided into two types for use in construction: normal concrete and high-strength concrete. Normal concrete has a compressive strength that lies between 15 to 45 MPa .[4]. The strength of the high-strength concrete will be greater than 55 MPa [5].The characteristics that once distinguished normal concrete from high-strength concrete have also improved. Compared to high-strength concrete, normal-strength concrete is more commonly employed in applications. Using high-strength concrete serves its main purpose of reducing weight, preventing creep or permeability, enhancing the structure's durability, and taking into account special architectural requirements that call for components to support larger loads.



#### **1.4 Differences between Normal and high-strength concrete properties[4]:**

- **The workability factors of concrete with normal and high strengths**

It is well-known that the workability factor indicates how easy it is to concrete placed, compact, and finish while it is still fresh. Normal-strength concrete has acceptable workability. High-strength concrete mix is frequently sticky and challenging to handle.

- **Bleeding Elements Concrete with Normal and High Strength**

Bleeding is the term for the formation of a layer of water on top of the fresh concrete condition, which is caused by the settlement of cement and aggregate particles in the fresh concrete mix settling. The high-strength concrete does not bleed in contrast to the normal-strength concrete. This is a result of the increased cementitious material content and lower water content of the high-strength concrete.

- **Concrete's Permeability in Normal and High Strengths**

The permeability of the concrete directly affects all durability issues, including resistance to corrosion, chemical assaults, and creep. Damage only happens when a foreign particle enters the concrete. Concrete's permeability is determined by the permeability characteristics of the paste and aggregates that are mixed into the concrete.

Reduction in permeability contributes to:

- Increasing resistance to chemical and sulfate attacks
- Resistance to the entry of chlorides;
- Resistance to corrosion

## **1.5 Objectives of the Present Study**

The main goal of the research project is to study the behavior of different shapes of double-skin tubular columns filled with two types of concrete subjected to lateral cyclic loading. The most important points investigated were as follows:

- 1 . Experimental work to study the behavior of different shapes of double skin steel tubes filled with two types of concrete, normal and high-strength concrete.
2. Study the effect of different values of axial loads on the columns concurrently with the effect of lateral cyclic loading.
4. Using the Finite Element program (ABAQUS), to analyze and discuss the results, and submit a parametric study case.

## **1.6 Thesis Layout**

Six chapters in this research of this thesis were represented, as follows:

**Chapter One:** Introduce the basic information and commonality introduction considered composite columns, and cyclic loads.

**Chapter Two:** A review of the literature is provided, which includes an overview of the applications, studies, and papers related to concrete-filled steel tubes. It also includes experimental and research investigations concerning normal and high strengths under cyclic loads.

**Chapter Three:** This chapter included a summary of the materials and test findings used in the current study, the concrete mixing and casting techniques used in the concrete for the column, steel tube installation procedure, instrumentation, and testing setup.

**Chapter Four:** presents the experimental results and the influence of the study's chosen parameters on the failure mode, ultimate load, and deflection.

The European Code (EN 2014), the American Institute of Steel Construction (AISC), and the American Concrete Institute (ACI) design strengths were compared with the testing results of the maximum strength. After that, there is a discussion of how these parameters effect.

**Chapter Five:** Include the numerical study of the load-displacement and find the results, compare it with experimental results, and submit a parametric study, by using ABAQUS program.

**Chapter Six:** Includes the principal conclusions and overall research program findings. There are also suggestions made for future research.

***CHAPTER***  
***TWO***

## **Chapter2 : Literature Review**

### **2.1 Introduction**

The composite columns have low cost because of their low cross-section and ability to withstand high seismic and wind loads. Composite columns are widely used at current time because it has many advantages, such as the high tensile strength of steel and economic benefits, and the ability to resist high compression strength for concrete makes the two materials work together well.

### **2.2 Composite Columns.**

[Johansson and Gylltoft, \(2002\)](#) [6] in this study 13 circular steel concrete composite columns specimens were tested experimentaly and analytically. This study explores the mechanical behavior of concrete-filled steel tube (CFST) columns, focusing on the bond strength between steel tubes and concrete cores and the enhanced compressive strength due to confinement. The research aims to improve the use of high-strength concrete and enhance its mechanical properties. Figure 2-1 ,and Plate 2-1 shows different modes of failure according to the type of specimens. For the concrete filled columns, buckling mode type at failure varied according to how the load was applied to the column section.In stub columns with the load applied to the entire section or the concrete section, the concrete core exhibited greater compressive stresses than predicted. The efficiency of the steel tube in confining the concrete core was greater when the load was applied only to the concrete section.

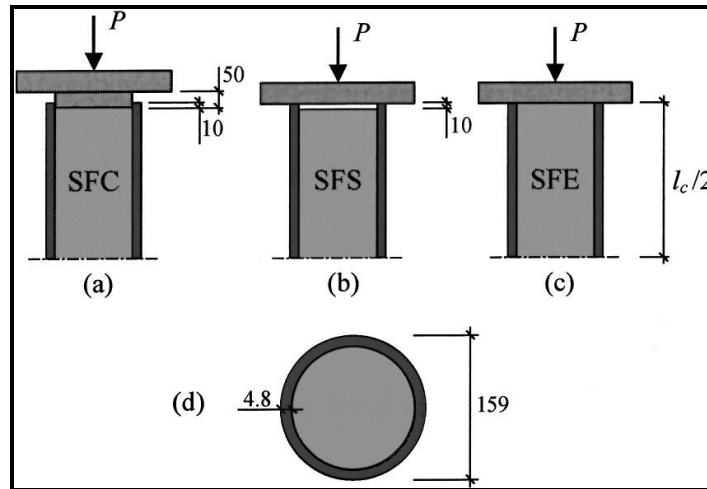


Figure 2-1 Three types of load application. Load applied to (a) the Concrete section, (b) the steel section, and (c) the entire section, (d) The section of the columns

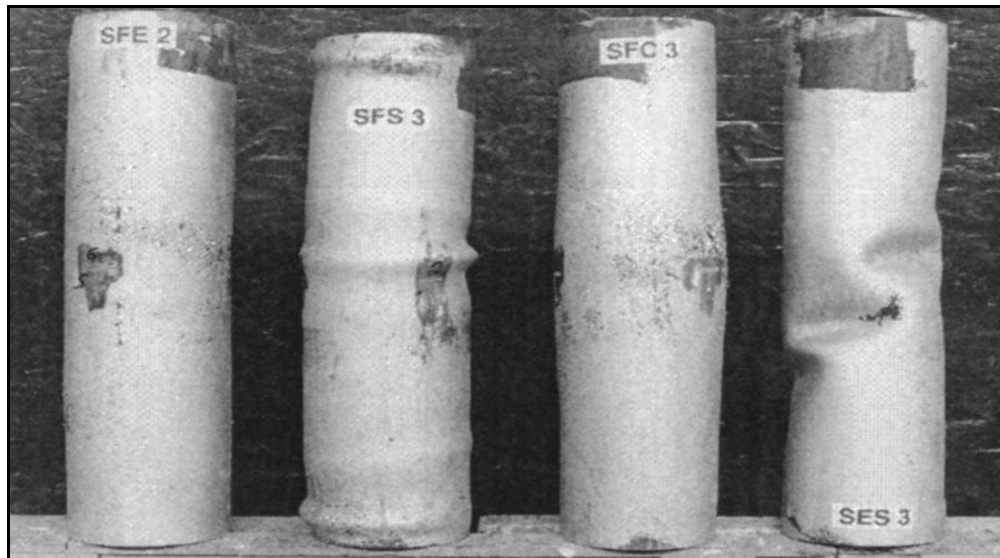


Plate 2-1 Failure Mode of Specimens (SFE) Entire Section, (SFS) Section with Steel, (SFC) Section with Concrete, (SES) Empty Steel Tube.

J. Pan, and Chen,(2017) [7] nine scaled columns were presented ,The damages that happen in reinforced concrete (RC) frame structures as a result of earthquakes appear in columns more than other structures even some RC frames are damaged because of column failure. The columns must have adequate inelastic deformation and energy dissipation capabilities to avoid

collapsing. Due to the low ductility of concrete, concrete covers on columns can also split apart during earthquakes, further reducing the column's stiffness. The results indicate that Engineered cementitious composite ECC and Reinforced Engineered cementitious composite ECC/RC have better ductility, better energy dissipation capacity, and slower stiffness degradation than RC columns, also indicate that the number of stirrups can be properly reduced in ECC and ECC/RC composite columns because of the high-shear strength of ECC. Vernardos and Gantes, (2019) [8] examined the compressive behavior of stub "Concrete-filled double-skin Steel Tubular" CFDST components using extensive analysis of several experimental projects conducted over 20 years. The CFDST concept's efficiency is measured by contrasting the final strength and energy absorption of CFDST members with those of their components functioning in isolation. (CFDST) members, also known as "steel-concrete-steel sandwich tubular" ones, are composed of two concentric steel tubes with varying diameters and an intermediate concrete core, the details of (CFDST) appear in Figure 2-2.

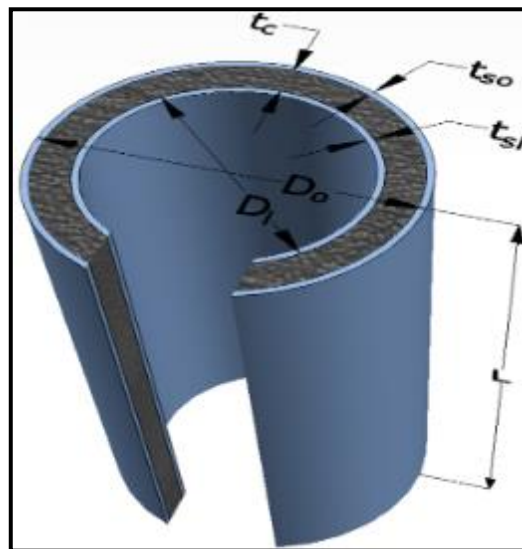


Figure 2-2 Concrete -Filled Double -Skin Steel Tube (CFDST) Details

Concrete-filled double-skin Steel Tubular (CFDST) members have significantly covered the necessary improvement space. Since a significant portion of the concrete in CFST members is replaced by a relatively thin steel tube, CFDST members typically have lower weights and noticeably higher strength-to-weight ratios. The steel tubes can be used as forms for pouring concrete, just like the outer tube of a CFST member, and, on the other hand, because the inner tube may act as longitudinal reinforcement. The legs of deep-water platforms, pressure pipes, and high-rise bridges are just a few structural applications that have already made use of these benefits.

[Behnamnia and Barati, \(2019\)](#) [9] saw that one of the main benefits of using the concrete-filled steel tube (CFST) was the decrease in steel usage consequently the cost of the project was reduced. Using steel with concrete led to the enhancement of seismic performance by increasing the strength of columns while reducing the dimensions of structural members. In this research, cyclic seismic loads were applied to eight steel specimens with identical concrete-filled circular sections and concrete grades of 30 Mpa, both with and without reinforcing. The results were compared. The displacement, stress, damage parameter, and plastic strain values of the composite column for each specimens modeled in the current investigation are summarized in Table 2-1 below. The results indicate that the composite column reduced displacement and damage when the thickness was increased. Furthermore, throughout the whole area, with the increased thickness, the plastic strain has considerably decreased. Consequently, it follows that using composite columns with a suitable steel layer thickness may greatly improve the concrete column's strength under the lateral cyclic load.



Table 2-1 The Results of Composite Columns with Various Steel Layer Thickness

Sample	Damage Parameter	Strain of composite section	Stress of composite section	Stress of steel jacket (MPa)	Displacement (mm)
1	3.45	0.0594	370	370	68
2	2.89	0.0435	360	320	59
3	1.318	0.02752	349	283	55
4	1.02	0.0185	328	223	47

The study found that increasing the steel layer thickness to 20 mm increased the steel's effectiveness in controlling column behavior, reducing displacement, and enhancing lateral loading resistance.

[Fa-xing Ding, Yi-fan Chen \(2020\)](#) [10] rectangular concrete-filled steel tubes, or RCFSTs, are extensively used in many engineering domains, including the construction of bridges and buildings. In this study, the researchers enhanced 3-dimensional finite element simulations to comprehensively investigate the composite action of RCFST columns under lateral shear forces. as shown in Figure 2-3. The models included the enhanced material constitutive models and provided full information on the interactions between the concrete core and the encased steel tube. Investigations were shown into the composite effect and interactions between the concrete core and encased steel tube under various configurational dimensions and loading states.

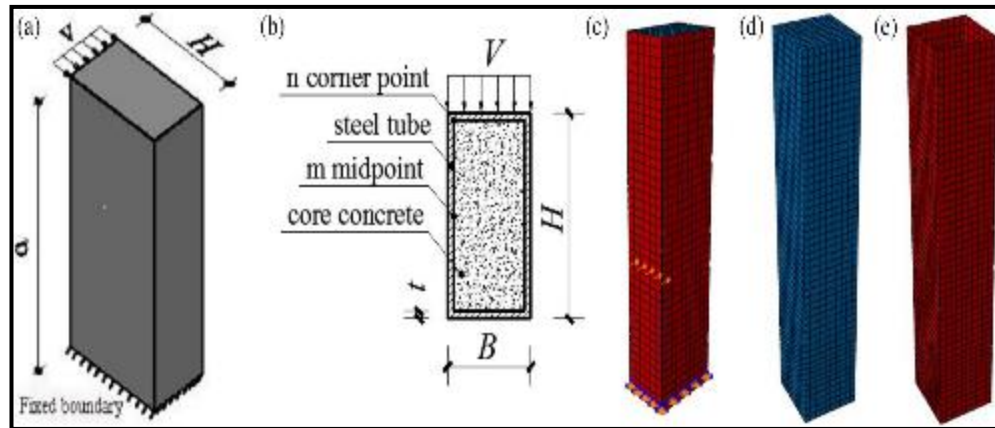


Figure 2-3 Boundary Condition Diagram and Finite Element Model. (a) Boundary Condition Diagram; (b) Cross-Section Details; (c) Finite Element Model; (d) Core Concrete Model (e) Steel Tube Model

When the suggested estimates were compared to the design regulations that were in place in various nations, the results were found to be more accurate than the others. İpek and Mete ( 2020) [11] were modeled 72 specimens using Finite Element method to simulate the behavior of the concrete-filled double skin steel tubular (CFDST). Considering different outer and inner steel tube diameters, different outer and inner steel tube thicknesses, and two different concrete strengths. Figure 2-4 show some CFDST member types.  $D$ ,  $D_o$ ,  $D_i$ ,  $B$ ,  $B_o$ , and,  $B_i$  in the figures means, the outside and inner dimensions of a square and a circular steel tube, where  $t_o$  and  $t_i$  represent the inner and outer steel thickness of tubes, consequently in that order. The hollow circular had been studied in the CFDST members' performance. The confirmed FEM model showed that the concrete compressive strength and the diameters and thicknesses of the inner and outer steel tubes had an impact on the ultimate axial strengths of the CFDST columns. The FEM model indicated that the ultimate axial strength increased when the outer steel tube's diameter and thickness increased. Additionally, the results of the FEM model

demonstrated that the CFDST columns' ability to carry more weight was enhanced when the concrete's compressive strength was raised..

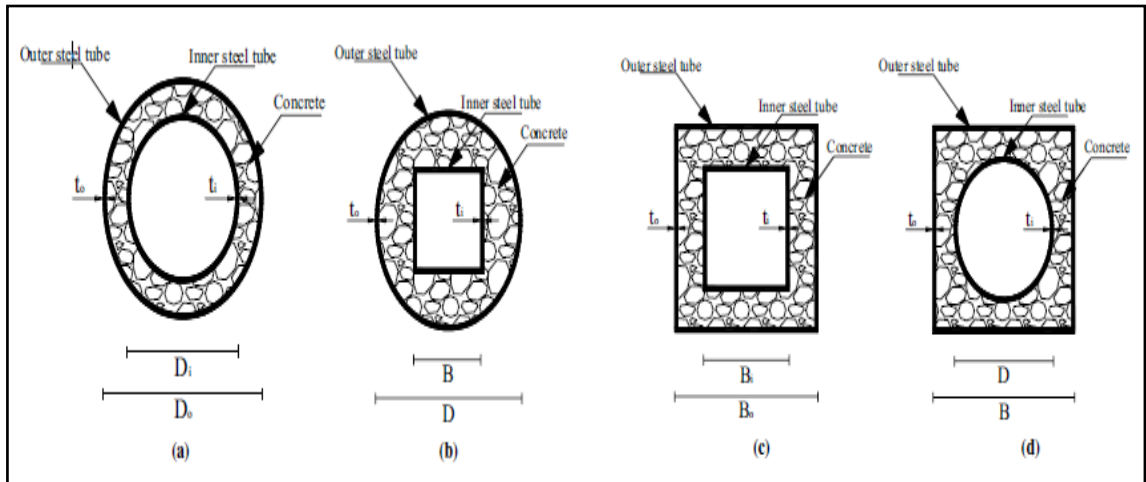


Figure 2-4 Details of Different Types of CFDST

Alsamawi and Boumechra (2021) [12] the responses of composite columns to different axial loads and horizontal cyclic loads are presented in this research. The main aim of this research was to analyze and compare the reactions (load displacement) of various composite column types under cyclic loads. To do this, a finite element model was created for each column, and the ANSYS code is used to perform the finite element analysis of composite columns. The non-linearity of contact friction and the elastoplasticity of materials are taken into account in the numerical model. The goal of this research was to examine enclosed composite columns subjected to cyclic loads with a focus on various steel section types. The impact of axial load levels, ductility, energy dissipation, the peak lateral load, and the skeleton curve were the parameters that are being examined. The lateral force-displacement curve that was implemented in this study is shown in Figure 2-5 below.

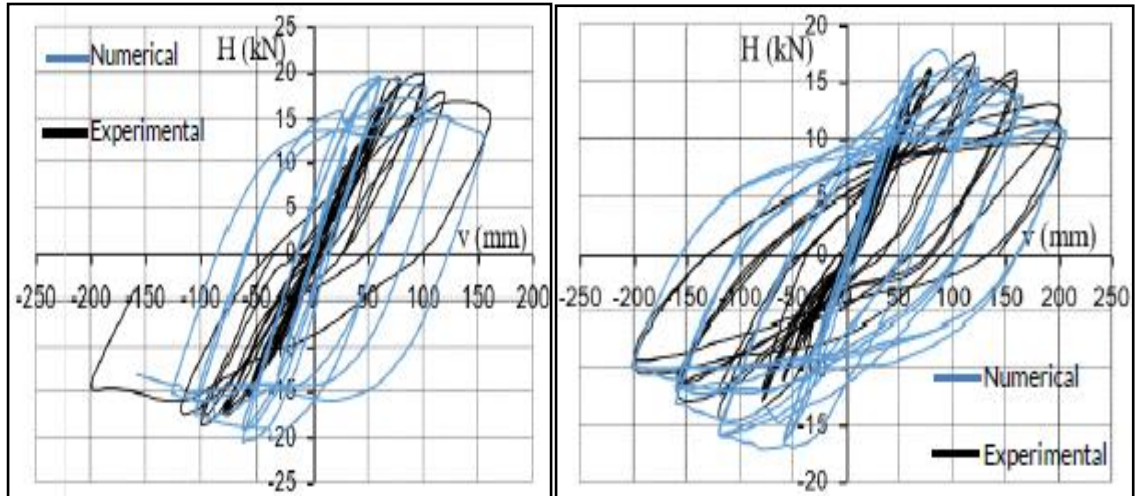


Figure 2-5 Numerical and Experimental Curves of Lateral Force-Displacement

For the two studied specimens of fully encased composite columns, the better ductility and energy dissipation the axial load level should not exceed an upper-limit value of 0,6. Beyond this limit, the composite columns are not so efficient. [Sahoo \(2021\)](#)[13] the experimental and numerical study on structural steel-reinforced concrete (SRC) columns under combined axial and lateral cyclic loadings was presented in this research. Peak lateral strength, mode of failure, hysteretic response, stiffness degradation, and energy dissipation potential of SRC columns were the main parameters that were studied. The flexural capacity of the SRC columns under various axial load levels has been predicted parametrically using the finite element software ABAQUS. Additionally. The majority of the experimental and numerical data points in the tension damage regions fall inside or on top of the unfactored P-M envelopes of these two standards. In the compression damage zone, the data points were discovered to lie outside of the P-M envelopes as shown in Figure 2-6. The Eurocode 4 (2004) requirements show a more reliable forecast of the failure loads under the uniaxial bending situation for the SRC columns planned to fail in the compression damage. saw Figure 2-7.

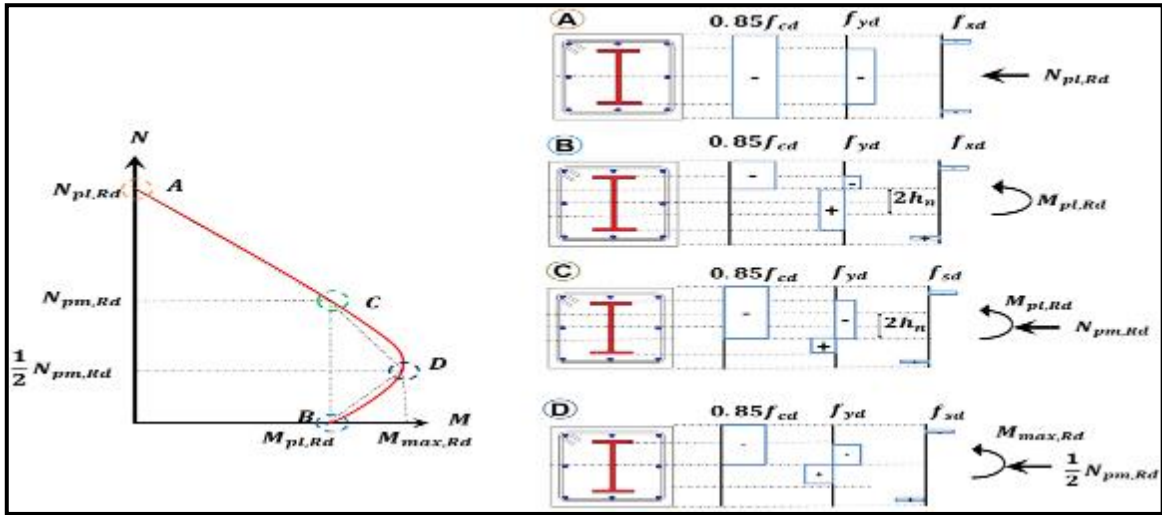


Figure 2-6 P-M Interaction Curve of SRC Column As Per Eurocode 4

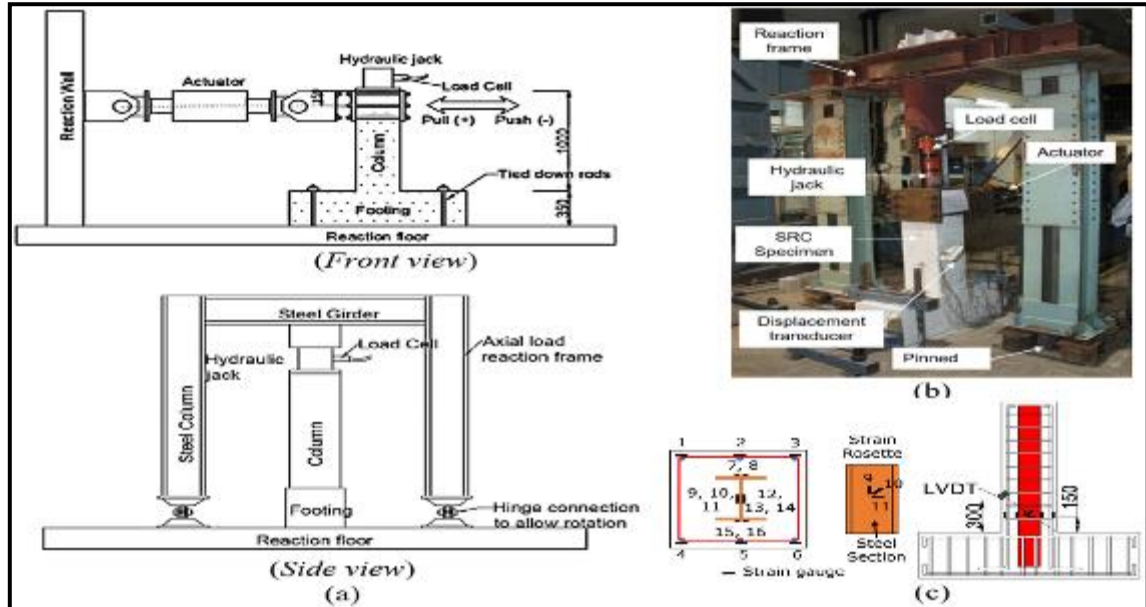


Figure 2-7 (a) Test Set-up Schematic (b) Test Specimens (c) LVDT Position

The study found that lateral drifts and flexure-dominated failures were more common in SRC specimens with larger stirrup ratios and encased steel cross-sections. [Alsamawi \(2022\)](#) [14] used a finite element program (ANSYS) to study the effect of increasing the strength and performance of the composite column, research should be done on the influence of the steel-concrete coefficient of friction and the cover concrete on the behavior (strength, ductility, stiffness, and energy dissipation) of composite columns subjected

to combined axial load and cyclically increasing lateral load. Eleven columns were built to investigate the coefficient of friction effect in the dynamic behavior of the cyclic load, while eight columns were constructed to investigate the cover concrete effect. The dimensions of specimens and boundary conditions are shown in Figure 2-8. The researcher used in this study had a constant axial load of  $P=1333.8\text{kN}$ , which represented 20% of the composite cross-section's plastic resistance to compressive axial force at the top surface of the column.



Figure 2-8 Composite Columns Boundary Conditions

The history of horizontal displacement can be observed in Figure 2-9 as a sequence of displacement cycles that have been completely reversed.

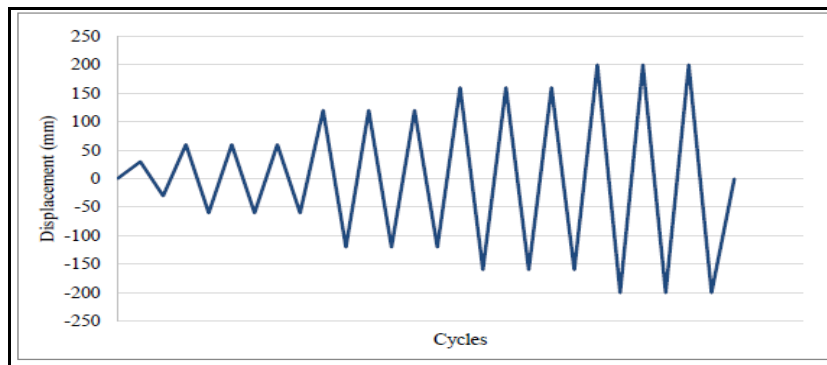


Figure 2-9 Protocol of Cycles with Displacement

Figure 2-10 shows numerically the failure mode, and the equivalent stress (Von-Mises) distribution specimens. It is clear that the columns reach the bottom to the plastic mode while the top is still in the elasticity

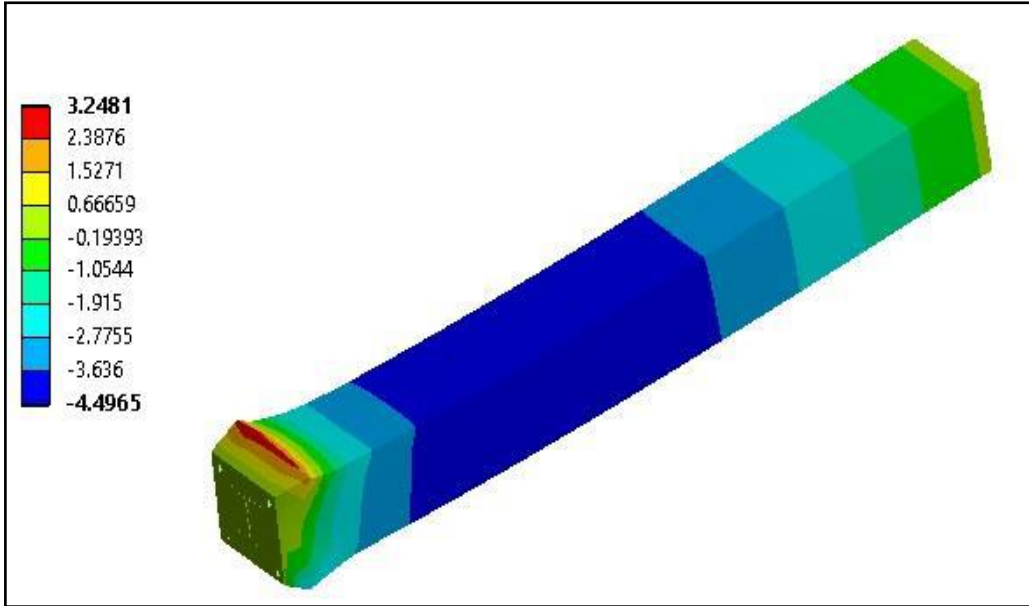


Figure 2-10 Failure Mode for Specimens

The findings illustrate that the cover concrete slightly affects, the composite columns in contrast to the effects of the coefficient of friction because of the composite work between the steel section and the concrete, For the composite column to have better friction and a higher dynamic dissipative capacity, it is necessary to use the sandblasting method in the steel.

Prasanta (2023) [15] investigated the hysteretic behavior, ultimate lateral strength, energy dissipation capacity, and ductility of partially confined concrete-filled steel tubular (PCCFST) square columns under combined axial and cyclic lateral loadings. The findings showed that the height and diameter of the inner CHS impact the column's cyclic performance, with maximum lateral force and vitality increasing up to 1.5D the details of the lateral test are shown in Plate 2-2 below.

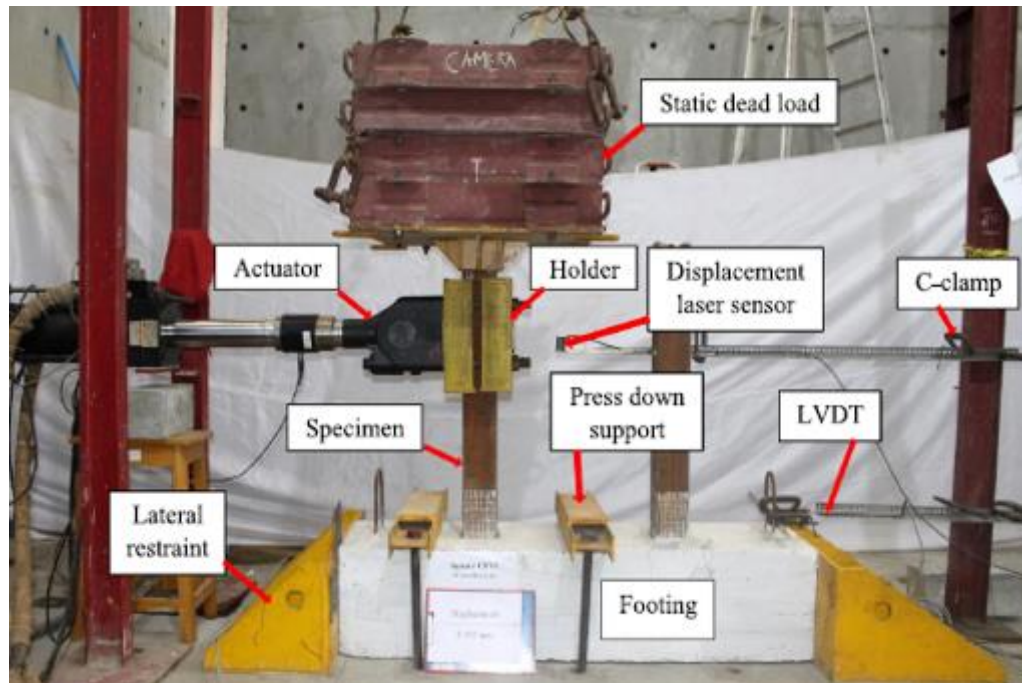


Plate 2-2 Lateral Cyclic Load Test

Chang-Geun (2012)[16] attempted a new technique for seismically strengthened reinforced concrete composite columns by applying High-Performance fiber-reinforced cementitious composites (HPFRCs) instead of concrete locally in the column's plastic hinge region. The goal was to increase the seismic strength and performance of reinforced concrete columns. With sustaining the tensile stress after cracking and exhibiting various micro-cracking behaviors, HPFRC exhibits high ductile tensile stresses of approximately 2-3%. Several column tests with a constant axial load and a cyclic lateral load were conducted. One typical reinforced concrete column and three specimens of reinforced concrete composite cantilever columns were planned and produced. The HPFRC was applied locally in the column plastic hinge zone in place of concrete. It was determined from the studies that the developed HPFRC-applied reinforced concrete columns reduced bending and shear fractures in the flexural critical



zone of the reinforced concrete columns in addition to improve cyclic lateral load and deformation capacities. Figure 2-11 shows the lateral load–top displacement hysteretic behavior of each column.

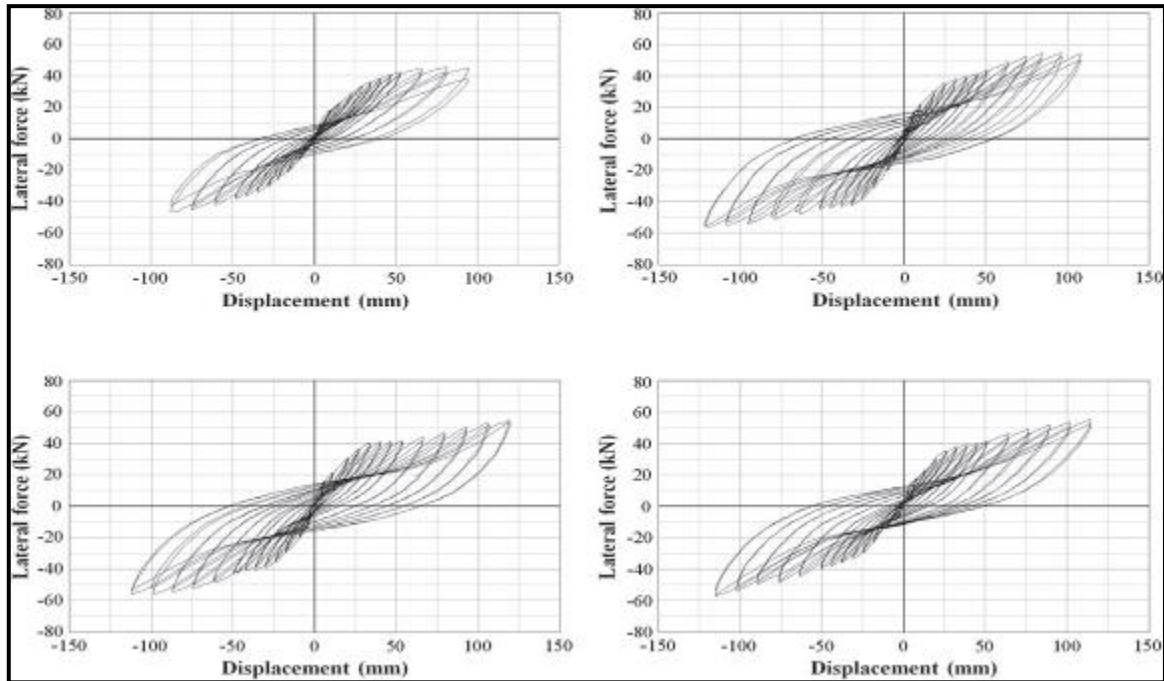


Figure 2-11 Cyclic Lateral Load -Displacement Curve

Duarte (2015) [17] studied the cyclic behavior of short steel tubes filled with Rubberized Concrete (RuC), a composite material that combines concrete and rubber particles. The three cross-sectional shapes of the tested specimens—square, rectangular, and circular—were described. , three steel grades (S235, S275, S355), three concrete mixtures (0%, 5%, 15% of rubber particle content), with two levels of axial load (10%, and 20% from the plastic axial load). The loading protocol, test rig, and experimental process were then thoroughly explained. The experimental results are thoroughly reviewed, with particular attention paid to the energy-based ductility factors, failure modes, hysteretic and envelope curves, and column cyclic strength. as shown in Figure 2-12.

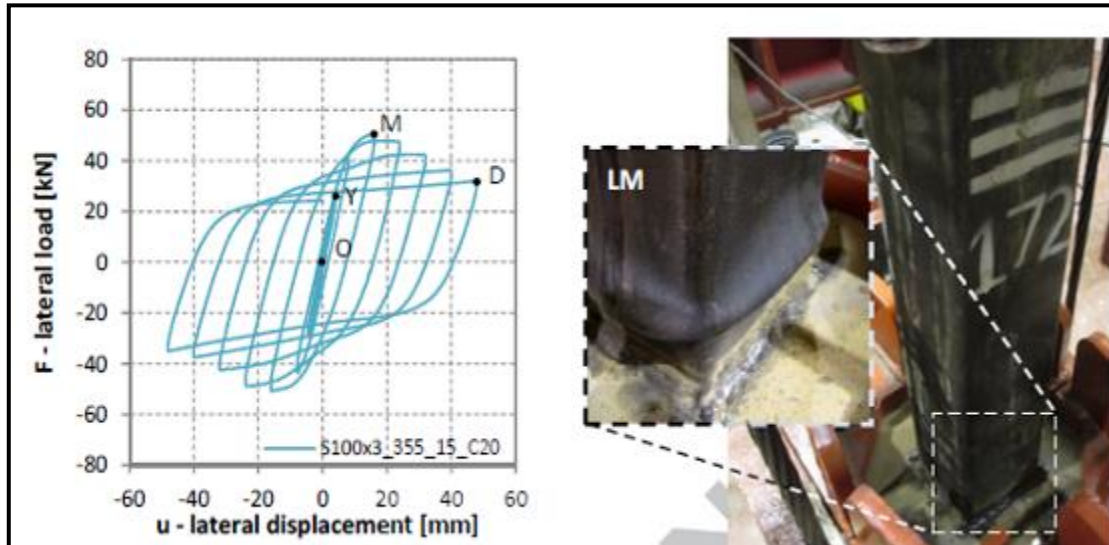


Figure 2-12 The Details of Lateral Displacement Curve and Failure Mode

The main achievement is that a concrete mix containing only 5% rubber particles simultaneously results in the lowest cyclic strength decrease (5%) and the highest ductility increase (52%). This makes this mix the best choice for use in seismic areas where energy dissipation and ductility requirements are essential. [Teng, \(2016\)](#) [18] five large-scale columns were prepared and tested; two of the columns were tested under a combination of axial compression and monotonic lateral loading, and the remaining three under a combination of axial compression and cyclic lateral loading. Each of the five columns had a circular section with a diameter of 318 mm, a height of 1625 mm, and 3 mm thickness of the steel tubes. For the three specimens, an FRP jacket was applied to provide additional confinement to the potential plastic hinge region which was assumed to be 500mm from the column footing. They found that the FRP jacket can effectively delay or even prevent the foot local buckling failure at the end of a cantilevered CFT column subjected to both cyclic lateral loading and constant axial compression. The buckling deformations in columns with a thick FRP jacket may be forced and appear

above the FRP jacketed zone. [Pedro Faustino \(2016\)](#) [19] presented a six reinforced concrete (RC) columns were subjected to cyclic lateral and axial loading under a variety of strengthening methods and situations. Carbon-fiber-reinforced polymer (CFRP) sheets were used for confinement strengthening; CFRP laminates and CFRP confining jackets for longitudinal strengthening; stainless steel bars and CFRP jackets for longitudinal strengthening; tested columns until reinforcing steel failure; CFRP confining jacket repair; and longitudinal strengthening with stainless steel bars. After analyzing the test results regarding energy dissipation and the load-displacement relationship, it was determined that using CFRP confinement in conjunction with external longitudinal strengthening is a practical and effective method for performance retrofitting and upgrading, with good ductile behavior, the load capacity increase resulting from strengthening reached 36–46%. [Chahmi Oucif1 \(2017\)](#)[20] conducted numerical analyses on square-reinforced concrete columns. A comparison of experimental tests and numerical modeling of reinforced concrete columns reinforced with fiber-reinforced polymer (GFRP) and steel bars was presented in the first section. The study found that numerical models for reinforced concrete columns reinforced with GFRP and steel bars replicated experimental behavior, providing confidence for researchers and engineers in assessing cyclic behavior. Comparative analysis showed that adding more GFRP layers reduced residual displacement and limited crack breadth, demonstrating the effectiveness of using more layers to strengthen square RC columns. [Fang Yuan \(2019\)](#) [21]. suggested a novel method for enhancing the plastic hinge zone's seismic behavior of such components by using high-ductility engineered cementitious composites (ECCs), see Plate 2-3. Under reversed cyclic loads, several hybrid FRP–steel-reinforced ECC–

-concrete columns were investigated. A thorough investigation was conducted into how the columns' failure mode, crack pattern, load-carrying capacity, residual deformation, ductility, and energy-dissipation capacity were affected by the types of reinforcement, axial force ratios, and reinforcement ratios. The local buckling of the FRP bars was effectively eliminated and the seismic performance was much enhanced by the replacement of concrete with ECC in the plastic hinge zone. The hybrid-reinforced composite column showed significantly lower residual deformation and higher post-yielding stiffness when compared to the steel-reinforced ECC–concrete composite column, the ultimate strength increased and the deformation capacity decreased as the axial force ratio increased.

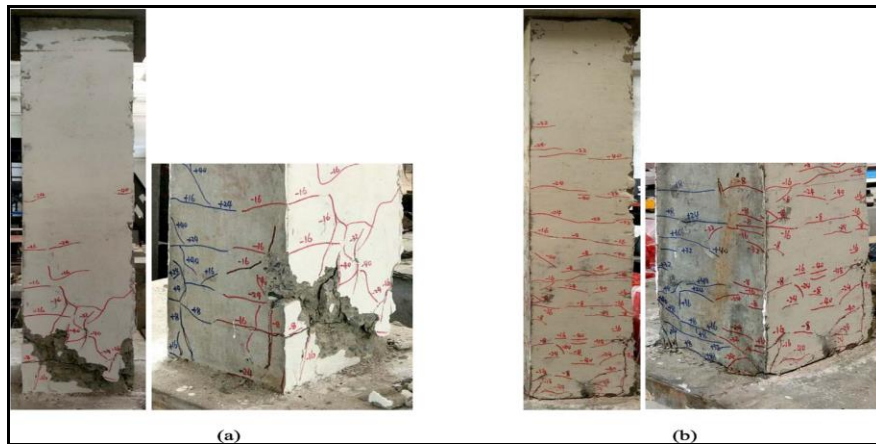


Plate 2-3 The Failure Modes and Crack Patterns of (a) Hybrid-Reinforced Concrete Column, (b) Hybrid-Reinforced ECC–Concrete Composite Column

Zhichao Huang (2019)[22] used sixteen hollow and composite columns casted with high-strength steel plates under axial compression, the ultimate capacity, and the local buckling behavior were examined. An explicit numerical model was generated and cross-checked with the results of the experiment. In the current model, residual stresses and initial defects were also taken into account. Numerous parametric studies were conducted on steel and composite columns with different ratios of width to thickness ( $b/t$ ).

Figure 2-13 showed different failure modes of numerical, and experimental cases of specimens

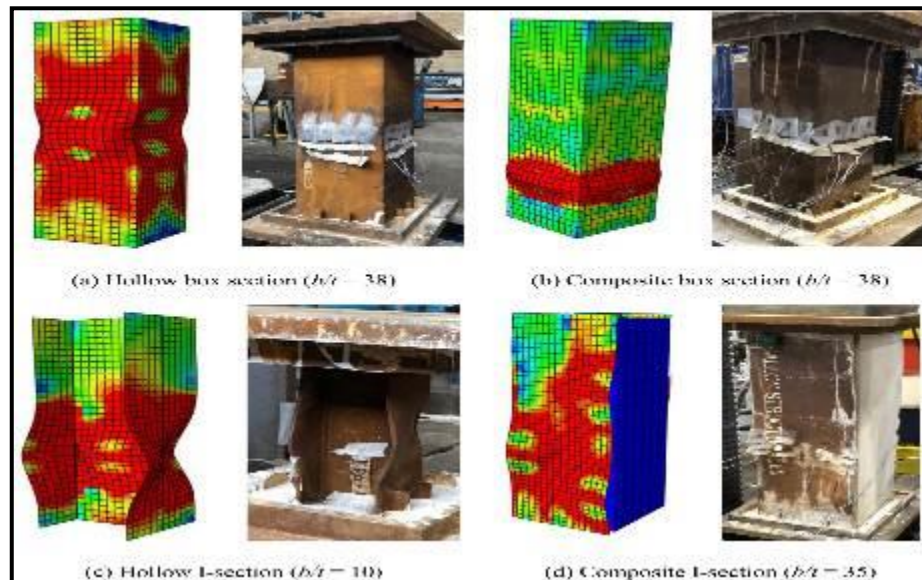


Figure 2-13 Failure Modes for Experimental and Numerical Specimens

A numerical model was created to predict the local buckling and post-local buckling response of box and I-section columns. The model takes into account the effects of residual stresses and initial geometric flaws. The test results were used to validate this model. Numerical results were used to calculate yield slenderness limitations, which were then compared to current codes of practice for hollow steel and composite sections that included high-strength steel plates. [Yuhong Yan, \(2019\) \[23\]](#), examined one square RC column and 14 square RC columns reinforced with circular steel tubes filled with Self-Compacting Concrete SCC under constant axial stress and lateral cyclic loading. Figure 2-14 shows the instrumentation architecture and loading system. A 2000 kN hydraulic jack provided the vertical constant axial load, which was observed using a force transducer. Between the distribution beam and the tested column, a slip device was inserted. An anchoring 600 kN horizontal jack was used to apply the low reversed cyclic

lateral loading against the reacting-force wall. To measure the lateral displacement, a linear variable differential transformer was mounted at the lateral load point. The column footing was secured in both vertical and horizontal directions at the bottom.

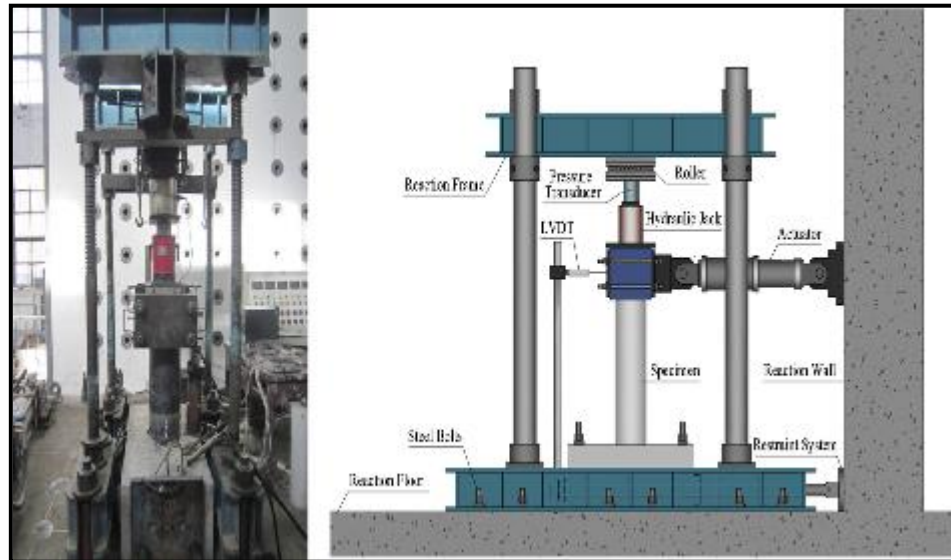


Figure 2-14 Testing Setup

The strengthened columns significantly improved seismic performance, as evidenced by an increase in the ultimate lateral load and energy dissipation capacity. Because of its improved plastic deformation capacity, the thickness of the steel tubes had a positive impact on envelope curves, ductility, stiffness, and energy dissipation capacity, as well as hysteresis behavior. It was also found that the axial load ratio affected seismic performance; a higher ratio led to an increase in ultimate lateral load and a lower energy dissipation capacity. [Hasan Elci \(2020\)](#) [24] examined six-column specimens and performed a total of 18 column tests throughout three test stages. The test columns were subjected to a cyclic lateral load pattern and the maximum axial load ( $N_d = 0.40A_c f_c$ ) in all tests. NSC was used to repair the severely damaged columns after the first and second test stages. Before the final test phase, though, more reinforcement using CFRP

confinement was put into place. The lateral strengths, drift ductility, energy dissipation capacities, and lateral stiffness obtained from each test were compared, and the evolution of damage for the test columns was reported. Figure 2-15 shows the details of test setup and failure mods of specimens.

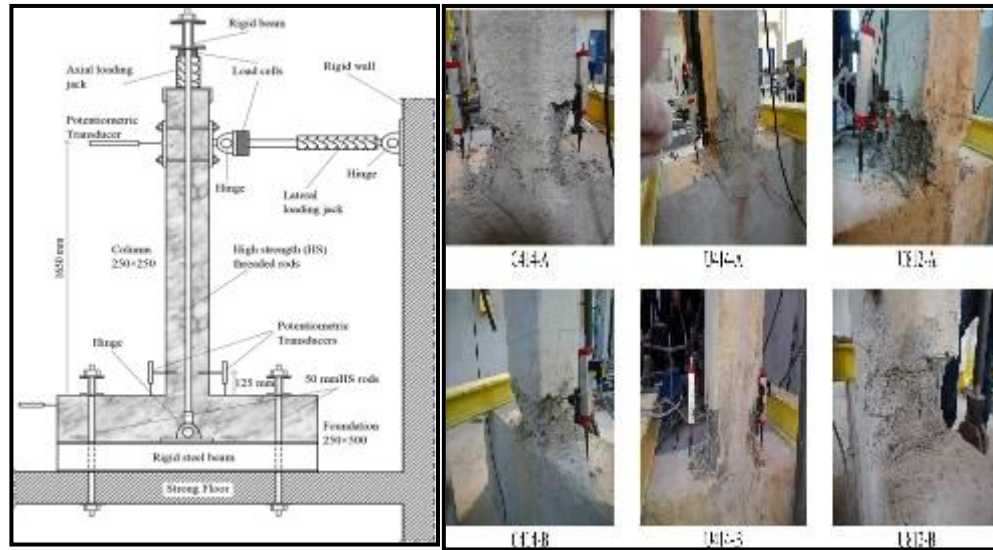


Figure 2-15 Test Setup and Failure Mode of Specimens

This suggests that strengthening using CFRP confinement could enhance their seismic performance.

F. C. Wang and H. Y. Zhao, (2020) [25] presented that concrete made with slag aggregate from blast furnaces, it showed that the usage of slag aggregate instead of normal aggregate was possible to increase the concrete's split tensile strength, flexural strength, and compressive strength. The findings suggested that adding furnace slag to concrete as a coarse aggregate could enhance the material's mechanical properties. The results showed that it was possible to alternate out coarse aggregate with waste glass or steel slag Figure 2-16 shows the details cross-section in CFDST.

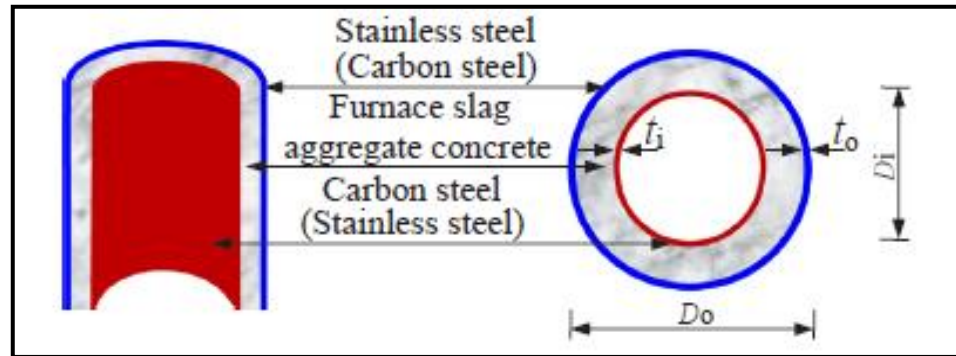


Figure 2-16 Cross-Section of CFDST

### 2.3 High-strength concrete filled (CFST).

Ishvarbhai, (2014) [26] introduced a numerical model for nonlinear inelastic analysis of high-strength thin-walled rectangular CFST slender beam-columns under constant axial and cyclically varying lateral loading. The model accounts for progressive cyclic local buckling of steel tube walls under stress gradients, providing a more accurate simulation of actual cyclic local and post-local buckling behavior than the modified stress-strain curve method. The model can be used to validate other numerical techniques and develop new composite design codes for high-strength CFST columns. Due to their superior structural performance, including high strength, high stiffness, high ductility, and energy absorption capacity, CFST slender beam columns have been employed more and more in composite structures and bridges in seismic regions. In seismic areas, thin-walled CFST slender beam columns may be subjected to both cyclically variable lateral loading from the earthquake and a constant axial load from upper levels. The strength and ductility of thin-walled CFST slender beam columns decreased by cyclic local buckling. To improve the cyclic performance of thin-walled CFST slender beam-columns under nonlinear analytical methodologies, cyclic local buckling effects must be taken into consideration . Jianwei Zhang



(2019) [27] used six full-sized, high-strength concrete columns with high-strength steel bars that were tested experimentally. Five steel tube-reinforced concrete STRC composite columns and one conventional RC column were subjected to cyclic horizontal loading. The effects of adding steel tubes, the inner steel tube's cross-sectional shape, and the strength corresponding to the outer and core concrete, as well as the steel fiber content of the outer concrete, were examined and compared. The details of the specimens are in Figure 2-17 below.

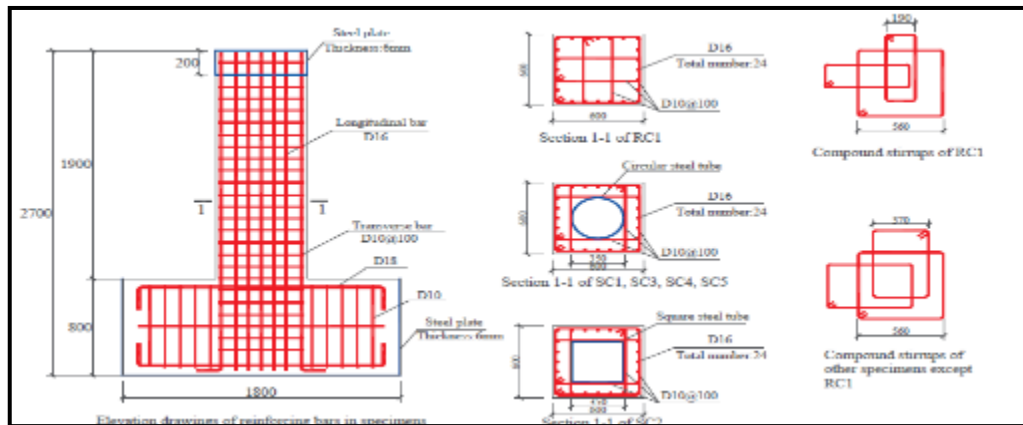


Figure 2-17 Details of Specimens

Inner steel tubes, longitudinal steel bars, outer concrete, and core concrete, are the components of high-strength STRC composite columns. For strength design, circular steel tubes are advised because of their lower steel ratio and low cost-effectiveness. Using C90 and C70 grade core and exterior concrete can lead to improved cyclic behavior when there is reasonable strength matching. The addition of steel fibers to exterior concrete decreases damage degree, residual deformation, and crack width, and increases ductility and energy consumption. Binglin Lai (2019) [28] evaluated the axial compressive behavior of short columns composed of high-strength Concrete, and Encased Steel (CES). Under monotonic pure compression, six

specimens of high-strength concrete were evaluated. The study investigates the primary factors that impact the ultimate strength of these composite columns, such as the concrete's strength, the transverse reinforcement bars' spacing, and the addition of steel fibers in high-strength concrete, as showed in Plate 2-4, and Figure 2-18 respresented the dimension of test specimens.

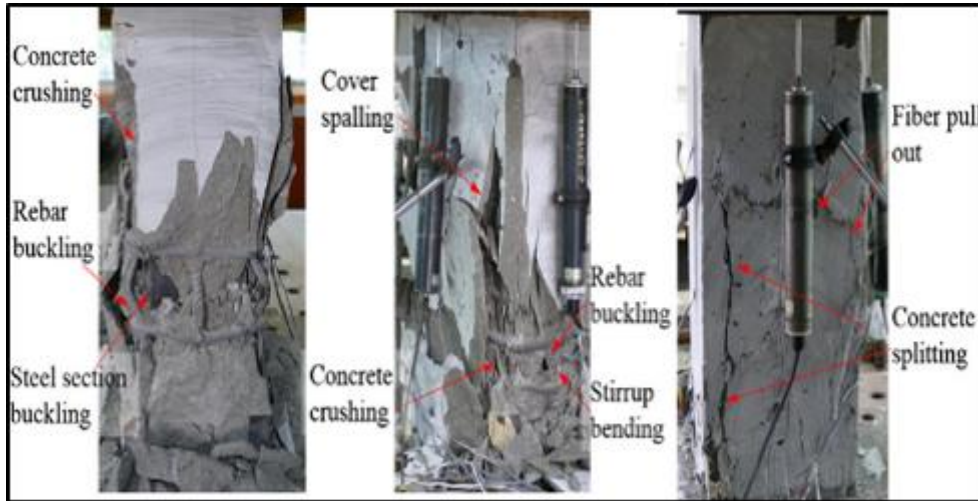


Plate 2-4 Failure Mode View

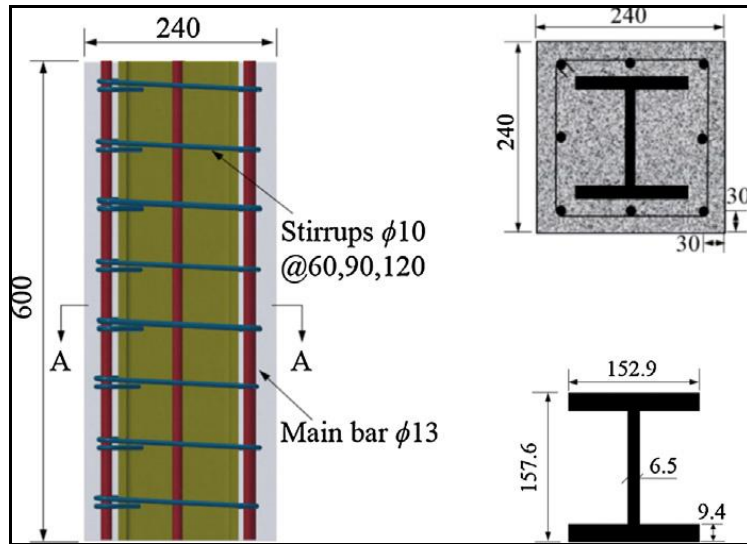


Figure 2-18 Dimension details of test specimens.

The results of the experimental work indicated that the concrete cover spalling failure mode of CES columns with high concrete strength C120 causes a sudden drop in compression capacity once peak resistance is

reached; the test results also showed that the provision of 0.5% volume of steel fiber can prevent the concrete cover spalling, and hence the load carrying capacity. The maximum resistance of CES columns with concrete strengths greater than C90 MPa is overestimated by the code methods, however, they provide an excellent prediction of CES columns with normal strength steel and concrete grade up to C90. [Jian-Tao Wang \(2021\)](#) [29] investigated the bearing capacity and damage behavior of circular high-strength concrete-filled thin-walled steel tubular (HCFTST) columns. The relation between moment and axial force was first examined using the finite element method. To create a workable design approach, the effects of important factors such as the peak strain of the concrete, material strengths, and diameter-to-thickness (D/t) ratios have been studied. Figure 2-19 shows the failure modes of specimens.

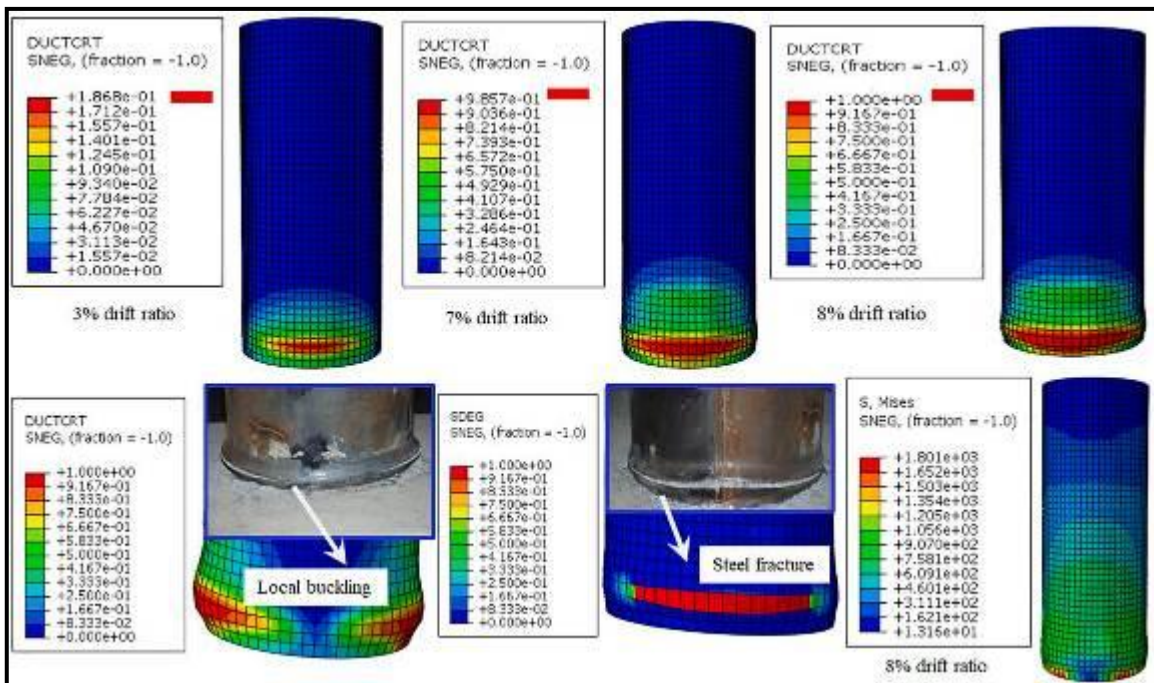


Figure 2-19 Failure Mods for Specimens

According to the study, moment axial force curves can be pushed inward by reducing concrete strength, raising steel yield strength, and changing the D/t ratio. The tested bearing capacity and the suggested parabolic moment-axial force curve had been aligned. The restoring force model offers helpful guidelines for the design and analysis of HCFTST columns.

#### **2.4 Influence of (CFST) cross-sectional shape:**

[Xiao and Zhang, \(2007\)](#) [30], six circular columns, four square columns, and four diamond columns, are designed and investigated experimentally under low frequency cyclic lateral load with very high constant axial load level. Structural engineers frequently focus more on the seismic performance of RC columns during the seismic design of RC frame structures than on other components like beams. The numerical study showed that, in addition to the axial load level and shear span-to-depth ratio, shear deformation may have an important effect on the lateral load-displacement curves, particularly for diamond sections and short columns. For the same axial compressive stress ratio, shear span to depth ratio, and volumetric ratio of stirrups, the seismic performance of circular columns was the best, square and diamond columns come next. Shear load capacity increased as the axial compressive stress ratio increased, while deformation ability decreased at decreased conditions of column section shape, shear span to depth ratio, and stirrup volumetric ratio. [Weiqing Zhu \(2016\)](#) [31] presented an experimental study on the seismic behavior of steel-reinforced high-strength concrete (SRHC) columns. The axial load level, stirrup arrangement, structural steel details, and studs were the main experimental parameters for a total of 21 SRHC columns tested under simulated earthquake loading conditions. The details

of specimens at the end testing frame, are shown in Figure 2-20 and Plate 2-5 respectively.

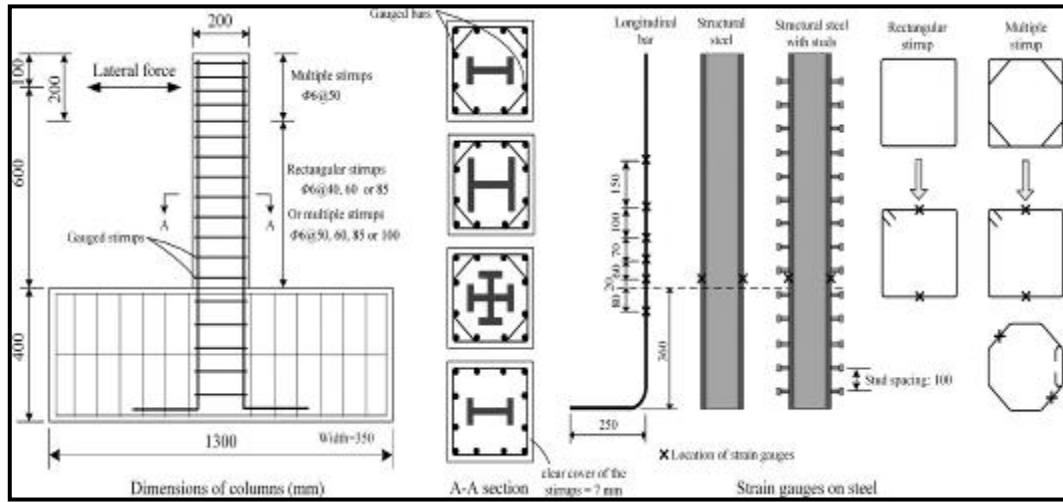


Figure 2-20 Specimens Details



Plate 2-5 Testing Frame

According to the study, high-rise structures in seismically active areas can benefit from using SRHC columns with multiple stirrups and structural steel ratios because of their excellent seismic performance. Stirrups had little effect on initial stiffness and lateral force, but they had a favorable impact on energy dissipation and deformation capacity. Farajpourbonab (2018) [32]

compared between standard CFT and steel-reinforced concrete fiber (CFT) columns, as shown in Figure 2-21, the study examined the mechanical and hysteretic behavior. Under cyclic displacement history, cross-steel reinforcement for CFT columns results increased energy absorption. degradation happens at greater lateral drift ratios and the shear strength of SRCFT columns increased compared to CFT columns. The study also found that the performance of SRCFT columns under axial loading is highly influenced by the type of reinforcing steel section. Because of the confinement effect of the concrete and the higher moment inertia of the C-Cross specimen, it performs better than the CB 200 and C 2 IPE.

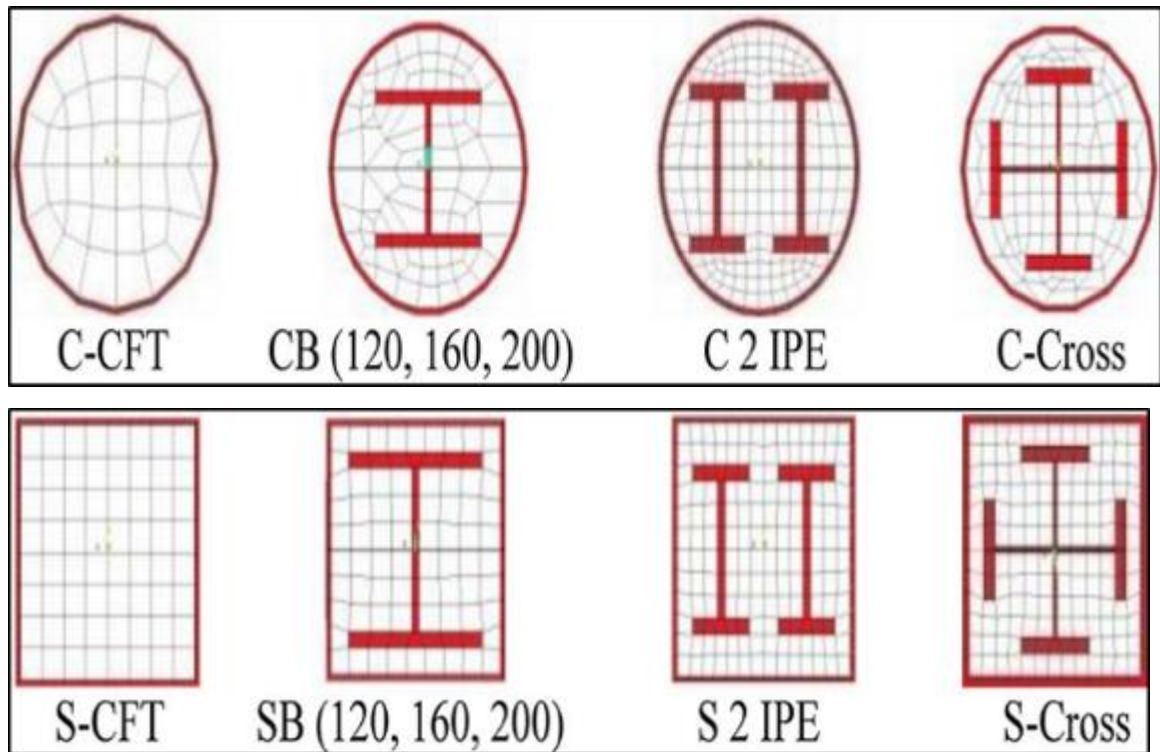


Figure 2-21 Different Cross Sections CFT

Junchang (2021) [33] introduced a series of axial compression tests performed on a circular concrete-filled double steel tubular column (CFDST) with a square hollow section (SHS). Additionally, three-

dimensional models used as a modified restricted concrete constitutive model for the core concrete are produced for such columns using the finite element (FE) program ABAQUS. By contrasted the FE model with the experimental data, the model's accuracy is confirmed as shown in Plate 2-6. Used the verified FE model, the impacts of different parameters on the load-axial strain response of CFDST short columns are investigated. The proposed formulas for determining the bearing capacity of CFDST short columns are based on the confined concrete model.

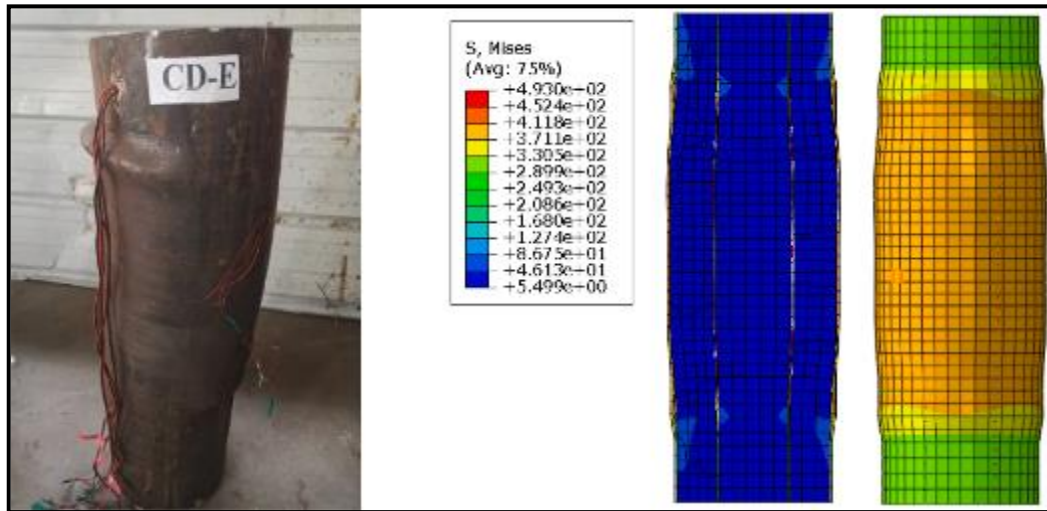


Plate 2-6 Experimental and Numerical Failure Mode of Composite Column

## 2.5 Summary:

1-The advantage of using Concrete-filled double-skin Steel Tubular(CFDST) instead of (CFST) members, since a significant portion of the concrete in CFST members is replaced by a relatively thin steel tube, CFDST members typically have lower weights and noticeably higher strength-to-weight-ratios. In terms of construction costs, they can be very effective. The steel tubes can be used as forms for pouring concrete, just like the outer tube of a CFST member, and, on the other hand, because the inner tube may act as longitudinal reinforcement

2- The efficiency of using the steel tube in confining the concrete core was greater when the load was applied only to the concrete section, composite columns have better ductility, better energy dissipation capacity, and slower stiffness degradation than RC columns.

3-Adding some materials, like Rubberized Concrete (RuC), and fiber-reinforced polymer (FRP), may enhance the performance of the composite columns.

4- Increasing the thickness of the steel tubes had a positive impact on envelope curves, ductility, stiffness, and energy dissipation capacity, as well as hysteresis behavior, also the use of high-strength longitudinal and transverse reinforcements in confined concrete columns can improve bearing capacity and deformability.

The studies that were covered in this chapter concluded that few earlier studies had been done to predict the behavior of cyclic loading on CFDST columns concerning the effect of the value of axial load with various types of concrete filled and different shapes of steel tubes. An experimental work and a numerical study investigation were conducted using multiple parameters, including the type of concrete filled and the shape of the steel tube section used for the cyclic loading instance.

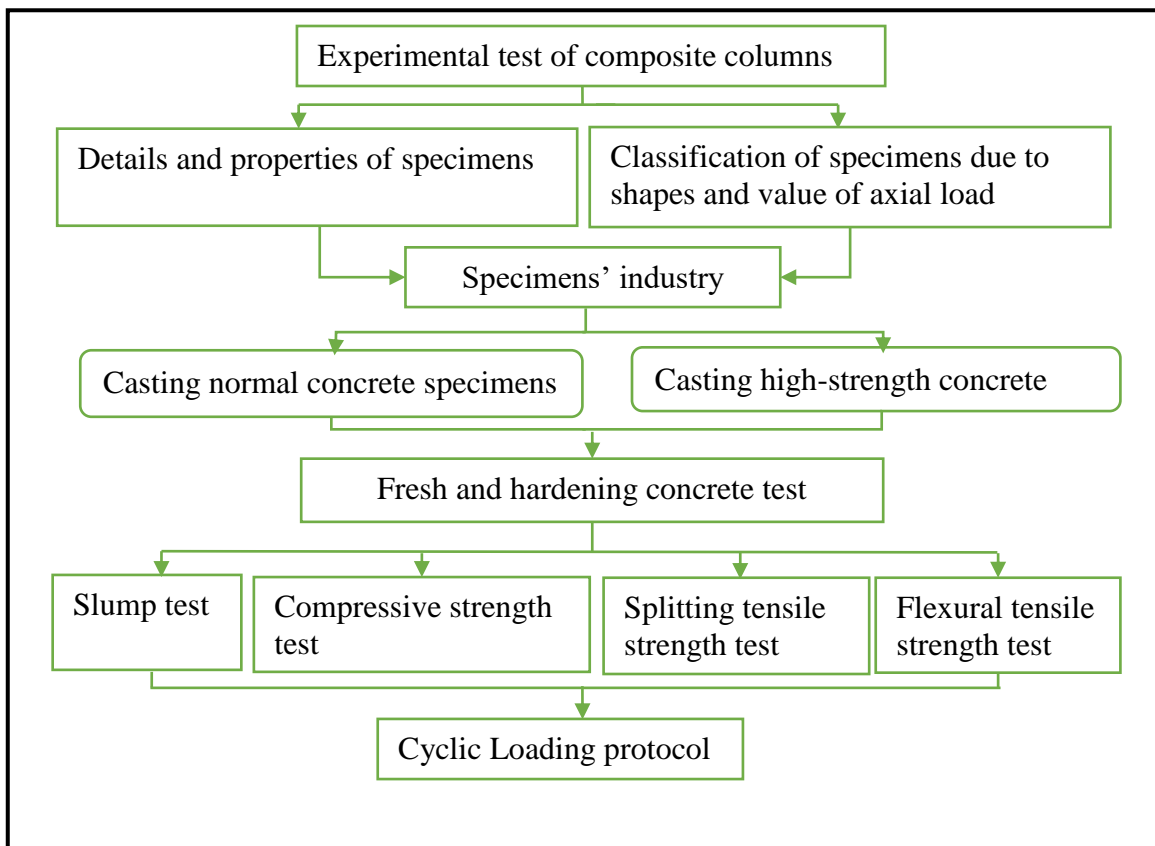


***CHAPTER***  
***THREE***

## Chapter3 : Experimental Work

### 3.1 General

The main focus of this research working is to study the behavior of composite columns (concrete-filled steel tubes) subjected to lateral cyclic load. Many main parameters have been studied and discussed in this research, such as the shape of the steel tube, the value of axial load, and the type of concrete filled. This chapter explains the concrete-filled double-skin portion, the properties of the materials used, different types of concrete mixtures, the material characteristics of concrete samples, and the concrete-filled double-skin specimen testing procedure. All the tests and work had been implemented in the College of Engineering of the University of Karbala laboratories. Figure 3-1 shows the main details of the experimental work.



### 3.2 Details of Specimens

The present experimental program consisted of all the units tested in this study, such as samples of cylinders, and twelve concrete-filled double-skin tubular columns (CFDST) specimens, which have been examined to represent all variables of the research plan. (CFDST) was made up of inner and outer tubes, as well as filled with concrete between them. Six of these specimens were cast with normal concrete while in other specimens six columns were filled with high-strength concrete. The selection of dimensions of the column depending on the scale factor with the value of (1:4) from the actual short columns with dimensions (400\*400\*3250) mm for square cross-section, and investigate the equivalent area of steel and concrete between circular and square cross-section as possible. The total length of specimens is (800 mm), The side length of the outer and inner square tubes is equal to (100) mm, and (50) mm respectively. For circular tube ,the external and internal diameters of the cross-section are (115) mm and (61) mm respectively as shown in Figure 3-2.

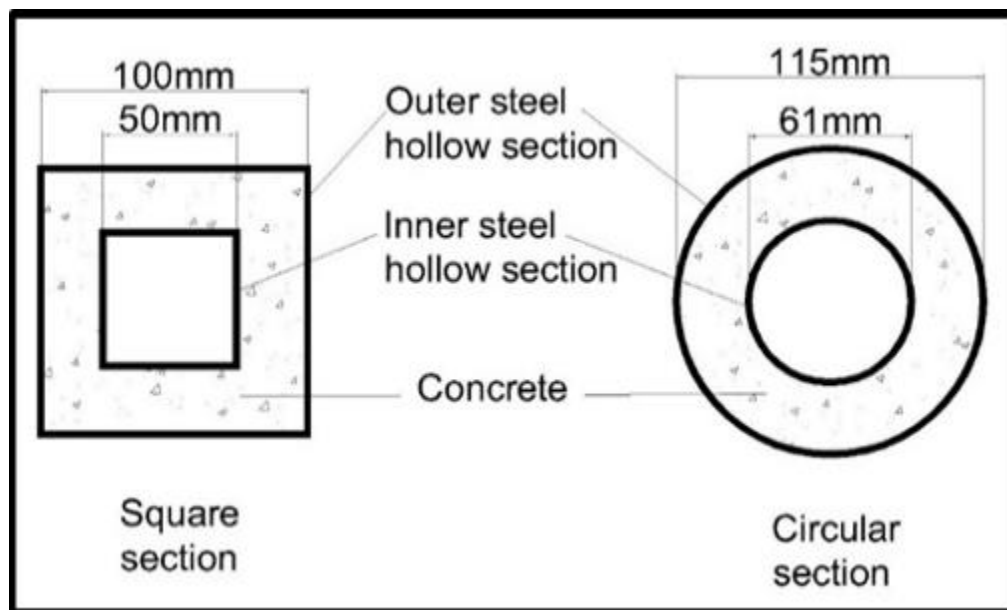


Figure 3-1 Cross Section in CFDST

With consideration- as possible- the equivalent area of concrete ( $A_c$ ) and steel ( $A_s$ ) and moment of inertia ( $I_x$ ) between two shapes of composite columns (square and circular) with a constant thickness of steel tube for square and circular sections is (2.75) mm. The thickness of the steel tube had been satisfied The ACI-code 318M-14 (10.3.1.6)[34] the determinant of the thickness of the steel tube that encased a concrete core for composite columns shall be at least (a) or (b) as shown in Appendix B:

(a)  $b\sqrt{\frac{fy}{3Es}}$  for each face of width (square)

(b)  $h\sqrt{\frac{fy}{8Es}}$  for circular sections of diameter  $h$

Plate 3-1 shows the inner and outer steel tube detailing, and Table 3-1 shows the equivalent between square and circular sections about the area of concrete and steel and the moment of inertia, the calculations and details were cleared up in Appendix B.

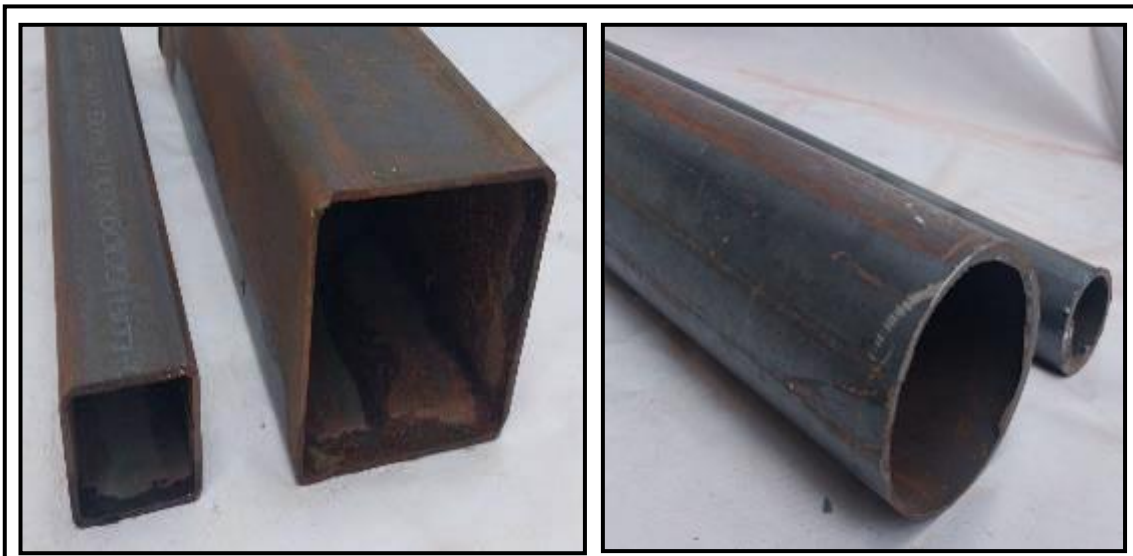


Plate 3-1 Inner and Outer Steel Section

Table 3-1 Details of Area and Moment of Inertia of Composite Columns

Square Composite Columns	Circular Composite Columns
$A_c = 6430 \text{ mm}^2$	$A_c = 6494 \text{ mm}^2$
$A_s = 1650 \text{ mm}^2$	$A_s = 1520 \text{ mm}^2$
$I_x = 7.8 \cdot 10^6 \text{ mm}^4$	$I_x = 7.9 \cdot 10^6 \text{ mm}^4$

All the specimens were divided depending on the type of concrete and the value of axial load with a constant length and thickness of tube for all specimens into six groups the details of the specimens as below:

- **First group:** this group consists of two specimens; the first one is composed of two tubes of steel with a circular outer and inner section, while the other specimen consists of a square outer and inner tube. These specimens were filled with normal concrete and colored orange, with a total length of 800 mm for both specimens. This group was subjected to cyclic lateral load only without exposure to an axial load. This parameter studied the effect of the lateral cyclic load only without the effect of axial load as shown in Plate 3-2.

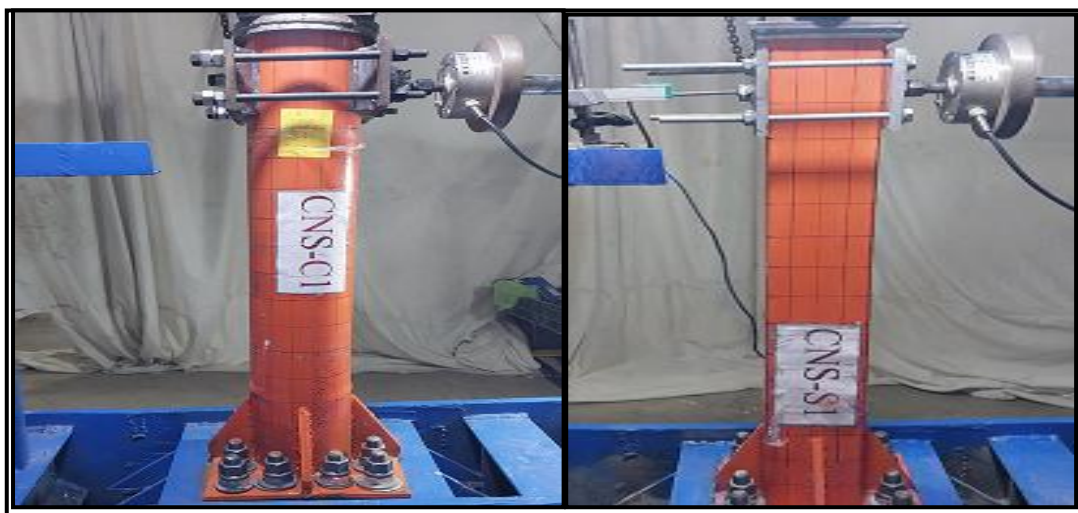


Plate 3-2 CNS-C1 and CNS-S1 Details

- **Second group:** this group consists of two specimens, the first one was composed of two tubes of steel with circular outer and inner sections, and the other specimen had a square outer and inner tube. These specimens were cast with normal concrete and colored orange, had a length of 800 mm for both specimens subjected to cyclic lateral and an axial dead load only represented the effect of dead load only about (40) kN this value had been calculated as from actual construction section multiplied by a scale factor (1:4) the details of specimens in appendix B. See Plate 3-3.



Plate 3-3 CNS-C2 and CNS-S2 Details

- **Third group:** this group consists of two specimens, the first one was composed of two tubes of steel with circular outer and inner sections, and the other specimen had a square outer and inner tube. These specimens

were cast with normal concrete colored orange and a length of 800 mm for both specimens. This group subjected to cyclic lateral and axial (dead plus live) load is (70) kN approximately. This value had been calculated from the actual construction section multiplied by a scale factor (1:4). The details of dimensions and load cleared in Appendix B, show Plate 3-4.



Plate 3-4 CNS-C3 and CNS-S3 Details

- **Fourth group:** this group consists of two specimens; the first one is composed of two tubes of steel with a circular outer and inner section, while the other specimen consists of a square outer and inner tube. These specimens were filled with high-strength concrete and colored yellow has a length of 800 mm for both specimens and were subjected to cyclic

lateral load only this parameter studied the effect of the lateral cyclic load only without the effect of axial load, as shown in Plate 3-5.

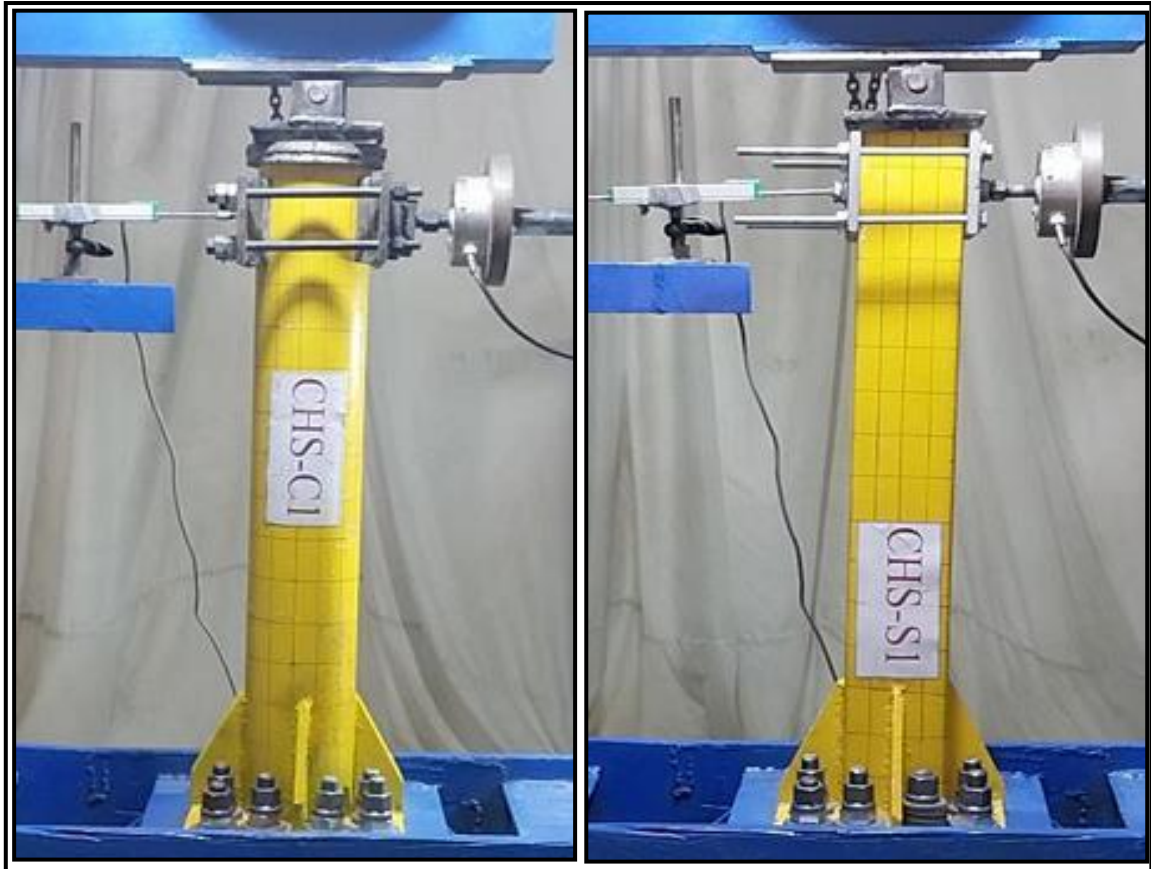


Plate 3-5 CHS-C1 and CHS-S1 Details

- **Fifth group:** this group consists of two specimens, the first one was composed of two tubes of steel with a circular outer and inner section, and the other specimen was with a square outer and inner tube. These specimens were filled with high-strength concrete colored yellow and a length of 800 mm for both specimens. This group subjected to cyclic lateral and axial dead load only is about (40) kN, this value had been calculated from the actual construction section multiplied by a scale factor (1:4) the details of dimensions and load cleared in Appendix B, see Plate 3-6.





Plate 3-6 CHS-C2 and CHS-S2 Details

- **Sixth group:** this group consists of two specimens, the first one was composed of two tubes of steel with a circular outer and inner section, and the other specimen was with a square outer and inner tube. These specimens were filled with high-strength concrete colored yellow and a length of 800 mm for both specimens. Subjected to cyclic lateral and axial (dead plus live) load, is (70) kN approximately, this value had been calculated from the actual construction section multiplied by a scale factor (1:4) the details of dimensions and load cleared in Appendix B, as shown in Plate 3-7.

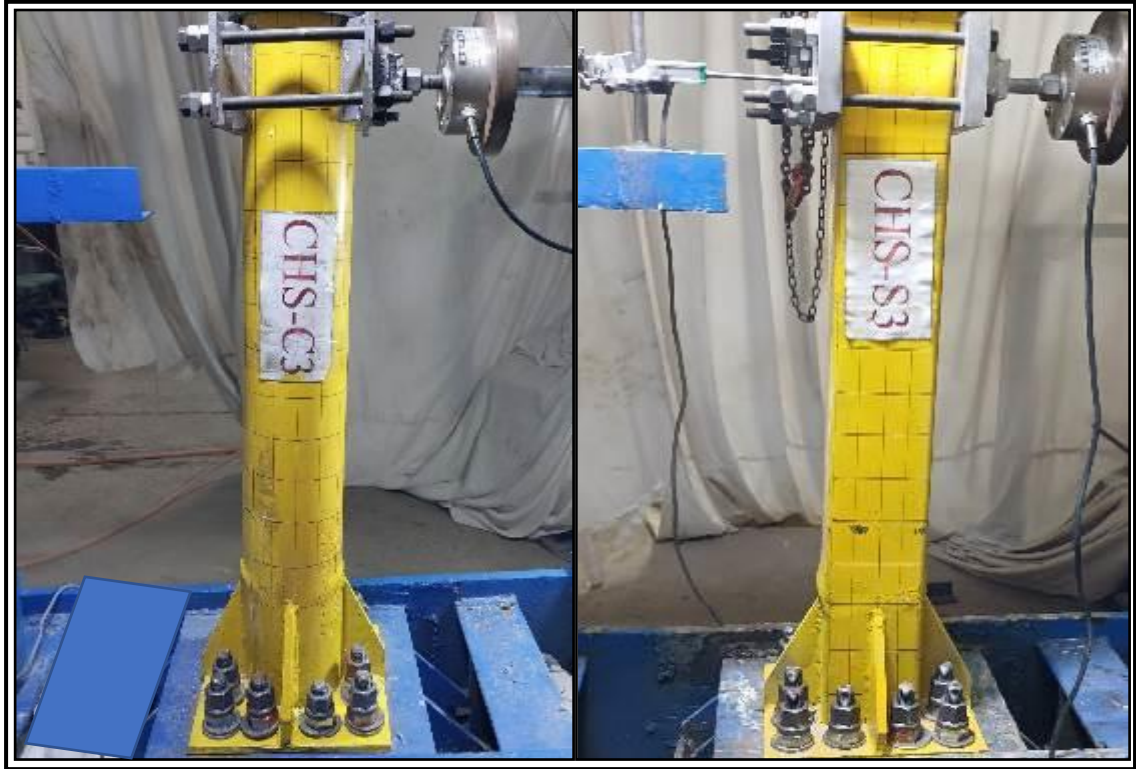


Plate 3-7 CHS-C3 and CHS-S3 Details

All specimens with details of the type of concrete, names, and axial load parameters shown in Tables 3-2 and 3-3 respectively.

Table 3-2 Details of concrete-filled circular double-skin columns.

Type of concrete used in specimen	Specimen designation	Parameter of specimen
Normal concrete	CNS-C1	Lateral cyclic load only
	CNS-C2	Lateral cyclic load +Axial Dead load
	CNS-C3	Lateral cyclic load +Axial Dead and Live load
High strength Concrete	CHS-C1	Lateral cyclic load only
	CHS-C2	Lateral cyclic load +Axial Dead load
	CHS-C3	Lateral cyclic load +Axial Dead and Live load

Table 3-3 Details of concrete-filled square double skin column (CFSDS).

Type of concrete used in specimen	Name of specimen	Parameter of specimen
Normal concrete	CNS -S1	Lateral cyclic load only
	CNS -S2	Lateral cyclic load +Axial Dead load
	CNS -S3	Lateral cyclic load +Axial Dead and Live load
High Strength Concrete	CHS -S1	Lateral cyclic load only
	CHS -S2	Lateral cyclic load +Axial Dead load
	CHS -S3	Lateral cyclic load +Axial Dead and Live load

### 3.3 Materials

Some structural materials used in this study to complete its requisites as itemized lower:

#### 3.3.1 Cement

In the local market, there are several commercial cement products. KARASTA as Portland-limestone cement was the type of cement used for this research it is traditional cement form CEM II/A-L, which is industrial by LAFARGE HOLCIM, Karbala Cement Manufacturing Limited, KCML, this type of cement is shown in Plate 3-8. Both HSC and NSC mixtures in the experimental work, this type of cement been used in it. To prevent moisture exposure cement was kept in a dry place. The physical characteristics and chemical construct of this type of cement are shown in Tables 3-4 and 3-5 respectively. The results of this test show that the cement satisfied Iraqi Specification No.5/1984[35].



Plate 3-8 Cement Used in this study

Table 3-4 Physical characteristics of The Cement

Physical Properties	Test Result	Iraqi specification
Initial setting (min)	150	More than 45 min
Final setting (hr.)	240	Less than 600 min.
Compressive strength for cement at 2 days of age at 28 days of age	15 MPa 35 MPa	Not less than 10 MPa Not less than 32.5 MPa

Table 3-5 Chemical Construction of Cement

Compound Composition	Chemical Composition	Weight (%)	Iraqi specification %
<b>Lime</b>	CaO	63.00	-
<b>Silica</b>	SiO <sub>2</sub>	21.46	-
<b>Alumina</b>	Al <sub>2</sub> O <sub>3</sub>	4.28	-
<b>Iron oxide</b>	Fe <sub>2</sub> O <sub>3</sub>	5.20	-
<b>Magnesia</b>	MgO	2.28	5 % max
<b>Sulfate</b>	SO <sub>3</sub>	2.12	2.5 % max
<b>Loss on ignition</b>	L.O. I	1.34	4% max
<b>Insoluble residue</b>	IR	0.9	1.5% max
<b>Lime saturation Factor</b>	L.S. F	0.90	0.66-1.02
<b>Tri Calcium Aluminates</b>	C <sub>3</sub> A	2.54	-
<b>Tri Calcium Silicate</b>	C <sub>3</sub> S	46.13	-
<b>Dia Calcium Silicate</b>	C <sub>2</sub> S	26.73	-
<b>Tetra calcium alumina ferrite</b>	C <sub>4</sub> AF	15.82	-

Physical ,and Chemical tests were implemented in the College of Engineering / Karbala University's Materials Laboratory as shown in Plate 3-9.



Plate 3-9 Chemical and Physical Test for Cement

### 3.3.2 Fine aggregate (sand)

Al-Akhaidher normal sand with the optimum particle size (4.75 mm) was used in this study for a traditional concrete mixture see Plate 3-10. The grade and chemical characteristics of this type of sand are shown in Tables 3-6 and 3-7 consequently. This type of sand was fitting under Iraqi Specification No.45/1984[36]. These tests were implemented in the Laboratory of Materials in the Engineering College / University of Karbala.



Plate 3-10 Sieve Analyses for Fine Aggregate

Table 3-6 Gradation of Sand

Sieve size (mm)	Passing accumulative %	Specification limits %Iraqi specification Zone No.
10	100	100
4.75	94.5	100-90
2.36	79.8	100-75
1.18	65.9	90-55
0.6	44.6	59-35
0.3	11.4	30-8
0.15	0.2	10-0

Table 3-7 The Chemical Composition of Sand

Property	Test result	Specification limits % Iraqi specification
Material Passing 75 $\mu\text{m}$ Sieve	3.6 %	< 5 %
Sulfate content (SO <sub>3</sub> )	0.4 %	$\leq$ 0.5 %

Figure 3-3 shows that the grade of the sand used in this study is within the acceptable range compared with the upper and lower limits of grading.

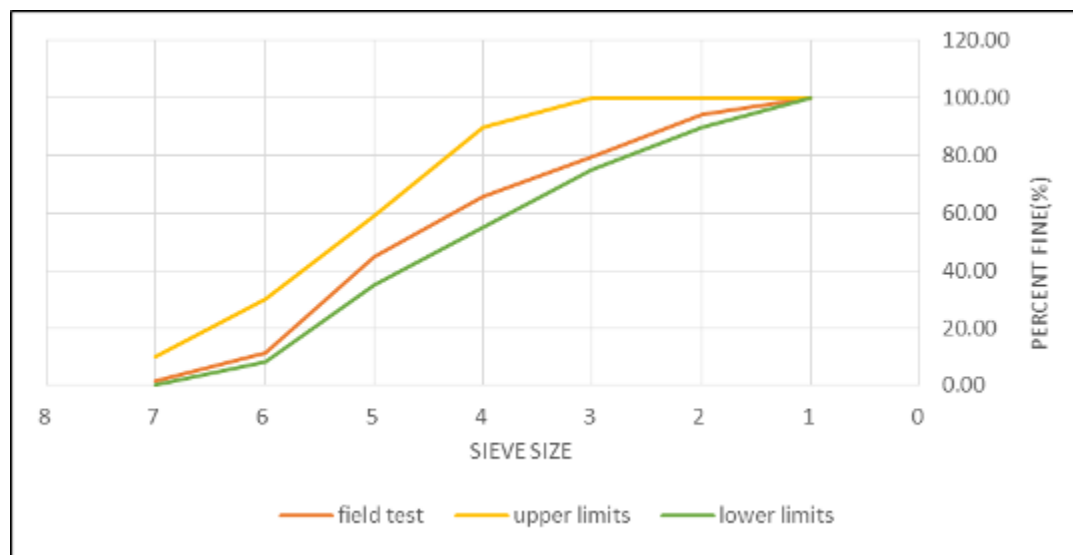


Figure 3-2 Sieve Analysis Chart for Sand

### 3.3.3 Coarse Aggregate (Gravel)

One of the materials that was entered in the concrete mixture is a coarse aggregate made from crushed river gravel gained from Al-Akhaidher with a maximum size particle of (9.5) mm. It had been washed with a water weller to clean it from flauts, and dry it by leaving it in the air before using it as clear in Plate 3-11.



Plate 3-11 Coarse Aggregate

The test consequences of coarse aggregate implemented to the Iraqi specification limits are shown in Table 3-8 and 3-9 respectively. Test results of the coarse aggregate presented that this kind has been adequate according to the Iraqi specification No.45/1984 [36].

Table 3-8 Coarse Aggregate Grading Results

Sieve size (mm)	Passing %	Specification limits % Iraqi specification
14	100	100
10	100	85-100
4.75	2.8	0-25
2.36	0.6	0-5

Table 3-9 Chemical Characteristics of Coarse Aggregate (Gravel)

Properties	Results of Test	Specification limits % Iraqi specification
Passing Material from 75 $\mu$ m Sieve	1.5%	$\leq 3\%$
Content of (SO <sub>3</sub> ) Sulfa	0.054 %	$\leq 0.1\%$



Figure 3-4 shows that the grade of the coarse aggregate used in this research is within the acceptable range compared with the upper and lower limits of grading.

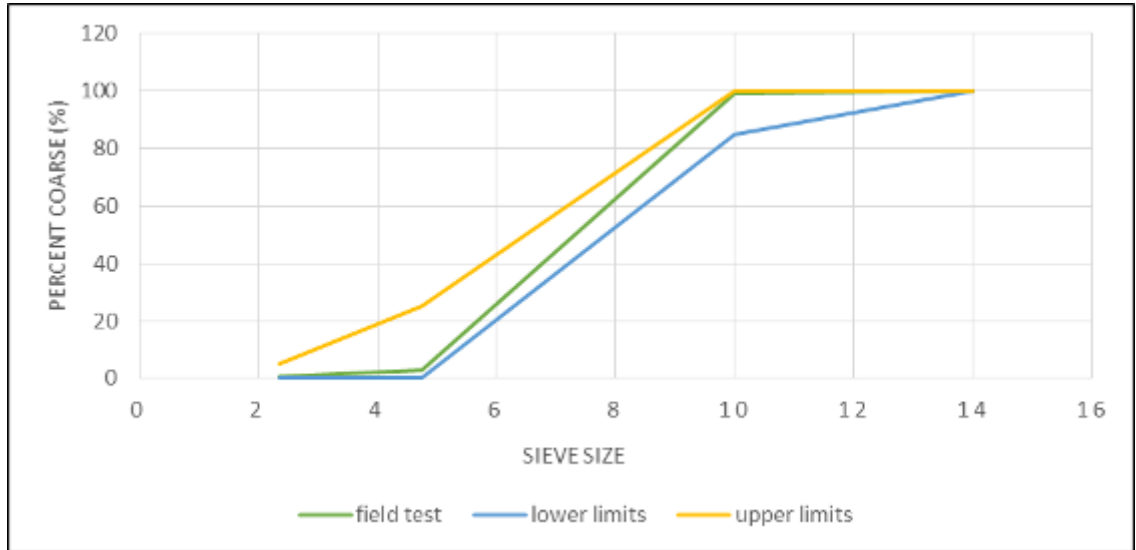


Figure 3-3 Sieve analysis chart for Coarse Aggregate

### 3.3.4 Water

All type of concrete mixtures used in this study was mixed and cured with water.

### 3.3.5 Silica Fume

(MasterRoc MS610) the type of silica fume that was used in the HSC mixtures of the experimental program as clarified in Appendix (A). This type was a high-quality silica fume powder for high-performance concretes, it changes the structures of concrete mixtures from porous and makes it more resistant to external effects. It helped to increase the strength considerably enhanced resistance to chemical and mechanical occurrence, disallowed bleeding and segregation in fresh concrete, reduced accelerator consumption, and its very thick layers of possible. Table 3-10 shows the physical and chemical characteristics of this type of silica fume. The results

show that it was agreeable with the standard specification of (ASTM C1240 – 03a)[37]. In this study, the content of silica used in HSC mixtures was 12.7 % of the weight of cement, as recommended in the datasheet[38]. Plate 3-12 appear a silica fume.



Plate 3-12 Silica Fume powder  
Table 3-10 Properties of Silica Fume

Property	Result from Data Sheet	Limit of specification requirements ASTM C1240 – 03a
Color	Grey powder	---
Density(kg/m <sup>3</sup> )	600	(500-700)
Chloride content	<0.1%	

### 3.3.6 Superplasticizer

A high-performance concrete superplasticizer based on modified polycarboxylic was used in this experimental work for the HSC and NSC mixture as explained in Appendix (A)[39]. It was supplied by MBCC GROUP under the name of (Master Glenium 54), this type is suitable for making many types of concrete and is suitable to containing all Portland cement types and cementitious materials like Microsilica, Fly ash (PFA), and Ground granulated blast furnace slag GGBS. The main advantage of it is to reduce the content of water in the mixture and it has also several benefits, increasing the compressive strength earlier, increasing the strength of flexural, the resistance of carbonation became better, decreasing permeability, reducing the creep and shrinkage, and increased the durability. Plate 3-13 shows the type of glinume that used in this study. The features of this type of superplasticizer are found in the datasheet in Appendix A, where it conforms to the requirements of superplasticizer according to ASTM-C 494/C 494M – 04 [40].



**Plate 3-13** Master Glenium 54

### 3.3.7 Steel Tube

The test was done on a steel tube to show the properties of the material, a tensile stress of coupon, elongation, and modulus of elasticity. The tensile coupon curve of samples taken out from manufactured tubes was the same by a similar procedure. The coupon and tensile test is implemented as seen in Plate 3-14. Three pieces of tensile coupon were tested to measure the average tensile strength and to measure stress in yield point ( $f_y$ ), the strength in ultimate ( $f_u$ ), and modulus of elasticity ( $E_s$ ) of steel were showed in Table 3-11. The sample formatting, geometric features, and dimensions of the steel coupon were superposed with ASTM-A370 requisites. Figure 3-5 shows the details of the coupon as per ASTM-A 370 – 03a [41]. All samples were tested at Al Sebtayn company for specialized structural and chemical surveys and soil investigation.



Plate 3-14 specimens of coupon



Figure 3-4 descriptions of dimension coupon as per ASTM-A370

Table 3-11 properties of the steel coupon

No .of coupon	Yielding stress (Fy) Mpa	Ultimate stress(Fu) Mpa	Elongation at fracture %	Modulus of elasticity(Es) (Mpa)	Thickness (t)
1	320	397	22.41	206985	2.75
2	315	399	23.25	204884	2.75
3	311	394	25.07	191820	2.75
<b>Average</b>	315.33	386.66	23.57	201229	2.75

Plate3-15 shows the coupon inside the tensile testing machine in the laboratory where steel tubes tested



Plate 3-15 Tensile Testing Machine

Plate 3-16 appear the coupons after tensile failure and the curve of stress failure in the computer.

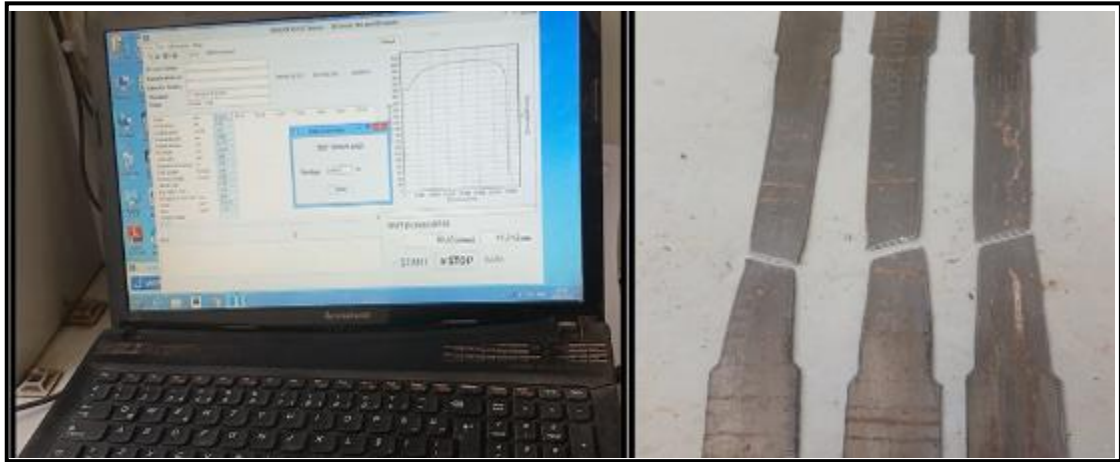


Plate 3-16 Coupons After Tensile Failure

From computer data recorded in the test of steel, the relationship between stress and strain is seen in Figure 3-6.

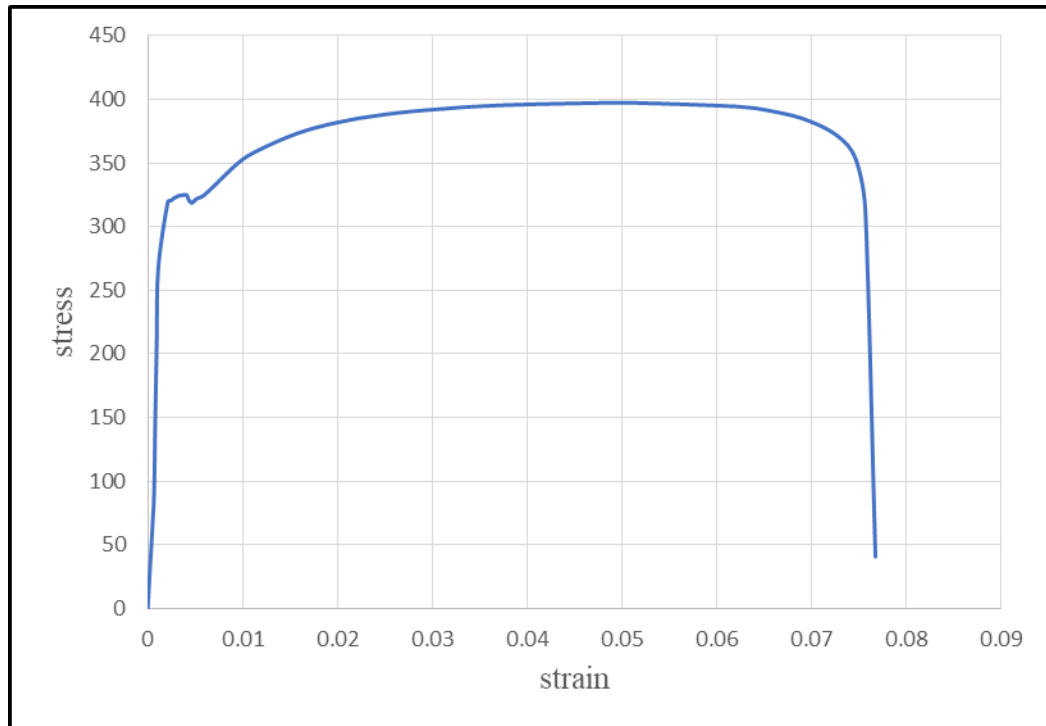


Figure 3-5 stress-strain curve

### 3.4 Concrete Mixing

#### 3.4.1 Normal Concrete (NSC)

This type of concrete mixture essentially contains cement, sand, coarse aggregate, water, and a small amount of superplasticizer. In this form of mixture, the compressive strength ranged between (25-35 ) MPa. To attain the optimal mixing design, mixes were done in the laboratory to acquire final amounts ((1) cement: (1.8) fine sand:(2.6) coarse aggregate) and the water-to-cement ratio was 0.4. Table 3-12 shows produce quantities by weight of materials per cubic meter. mixing was done using a mechanical mixer as shown in Plate 3-17. The mixture procedure was done by admixture of dry materials like cement, fine sand, and coarse aggregate after mixing for two minutes. Then, water and superplasticizer were applied and mixed to get an alliterative mix for two minutes.



ate 3-17 Mechanical Machine Supply Normal Concrete (NC)

Table 3-12 Amounts of the Materials measured by (kg)/ One Cubic Meter of Normal Concrete (NC) Mix.

Elements	Amounts (kg/m <sup>3</sup> )
Cement	400
Coarse aggregate	1062
Fine sand	720
Superplasticizer	6 (in litter units)
Water	160

### 3.4.2 High Strength Concrete (HSC):

This type of concrete mix essentially contains cement, fine sand, coarse aggregate, water, silica fume, and superplasticizer. In this type of mix, the compressive strength value ranges between (55-65) MPa. To reach the best-mixture design, many trials of mixes were implemented in the laboratory to gain typical quantities being ((1) cement: (1.3) fine sand:(1.9) coarse aggregate) and the ratio of water to cement is( 0.27). Table 3-13 shows product amounts by weight of materials per cubic meter accept superplasticizer that measured by litter units. mixing was done using a mechanical mixer, the materials of the mixture and specimens of the concrete test are shown in Plate 3-18. The mixing process was done by combining dry materials like cement, fine sand, coarse aggregate, and silica fume then mixing for two minutes consequently. After that, water and superplasticizer were added and mixed to obtain a typical mixture for two minutes, this type of concrete was cured in water





Plate 3-18 High Strength Concrete Mixture

Table 3-13 Amounts of the Materials by (kg) for One Cubic Meter of High Strength Concrete (HSC) Mix:

Elements	Amounts (kg/m <sup>3</sup> )
Cement	550
Coarse aggregate	1060
Fine sand	720
Silica fume	70
Superplasticizer	16 (in litter units)
Water	155

### 3.5 Fresh Concrete Test

#### 3.5.1 Slump Test

One of the significant tests for the consistency and achievement of concrete mixes is the test of slump. This test was implemented typically to (ASTMC143)[42]. The test contains a truncated cone its dimensions is the height 300mm. The top diameter was 100 mm and the bottom diameter is 200 mm. Three layers were achieved for the fresh concrete, every layer was compacted by a steel rod by stroking the fresh concrete layer 25 strokes uniformly and consistence method by the steel rod. After the three layers of

fresh concrete filled the cone, it was raised gradually, then the variance was measured between the top cone and the surface of the concrete from the upper as clear in plate 3-19 (a) The American code states that the amount of precipitation that is allowed in a column ranges between 25 and 100 mm according to (ACI 211.1-91). Plate 3-19 (b) shows the procedure of the slump test in the laboratory. The result of a normal concrete slump was 50 mm, and the result of a high concrete slump is 123mm because the mixture contains a greater amount of superplasticizer that makes it like the self-compact texture.

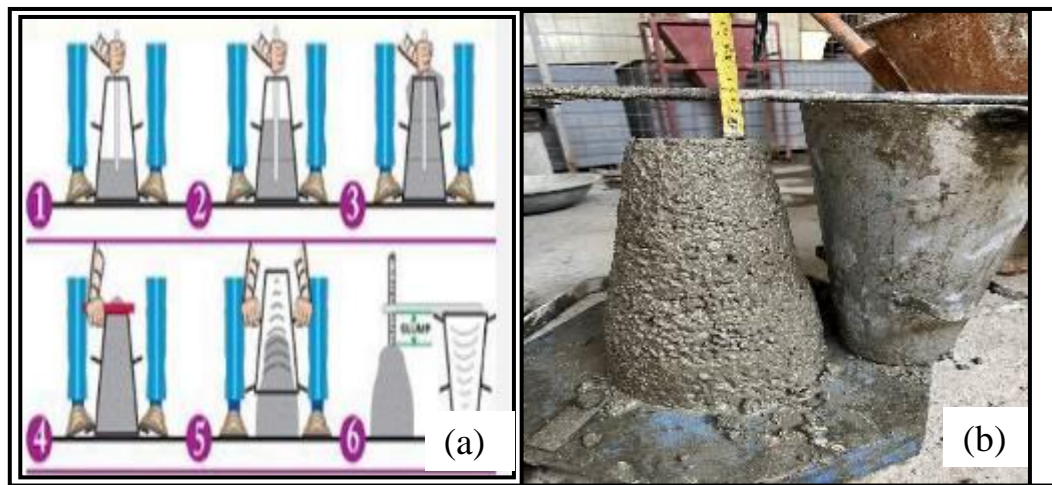


Plate 3-19 Slump Test

### 3.6 Hardened Concrete's Mechanical Characteristics

Some of the concrete mix's characteristics have been considered in evaluating performance, and they are as follows:

#### 3.6.1 Compressive Strength

The compressive strength test was conducted on a (100 \* 200) mm cylinder according to ASTM C 39/C 39M – 03 [43] using a digital machine its a compressive capacity of 2000 kN as clear in Plate 3-20. The cylinders were tested after 28 days of submerging them in a basin of water to

investigate the curing procedure for each NSC and HSC. The average value of three samples was occupied to signify the compressive strength.



Plate 3-20 Compressive Strength Machine

### 3.6.2 Splitting Tensile Strength

The splitting tensile strength was established using cylinders of (100\*200) mm lie crosswise according to the ASTM C 496 M-04[44]. A digital machine with a capacity of 2000 kN was used to perform this test as shown in Plate 3-21. The test was done to the cylinders after age 28 days of curing in water. The mean of three specimens was used to display the tensile strength for both NSC and HSC. The splitting tensile strength can be calculated from the equation 3-1 as below:

$f_s = \frac{2p}{\pi DL} \dots\dots\dots$	<b>3-1</b>
---	------------

**Where**

- fs: Tensile stress of splitting (MPa)
- P: Ultimate implemented load (N)
- L: Length of cylinder (mm),
- D: Diameter of cylinder (mm)



Plate 3-21 Splitting Tensile Test

### 3.6.3 Flexure tensile Strength

The test of flexure tensile strength which is shown in Plate 3-22, was carried out according to ASTM C78 and ASTM C1609-12 [45] specification for NSC and HSC respectively. Simply supported prismatic samples measuring 100 x 100 x 500 mm were used to determine the flexure tensile strength under three-point loading as shown in Figure 3-7. The modulus of rupture (flexure tensile strength) was considered by the following equation numbering 3-2.

---


$$f_r = \frac{3PL}{2bd^2} \quad \dots\dots\dots 3-2$$


---

where:

$f_r$  = Flexural tensile strength( modulus of rupture )(MPa),

$P$  =ultimate value for the implemented load (N),

$L$ = length of the prisms (mm).

$b$  = width of the prisms (mm),

$d$  = depth of prisms (mm).

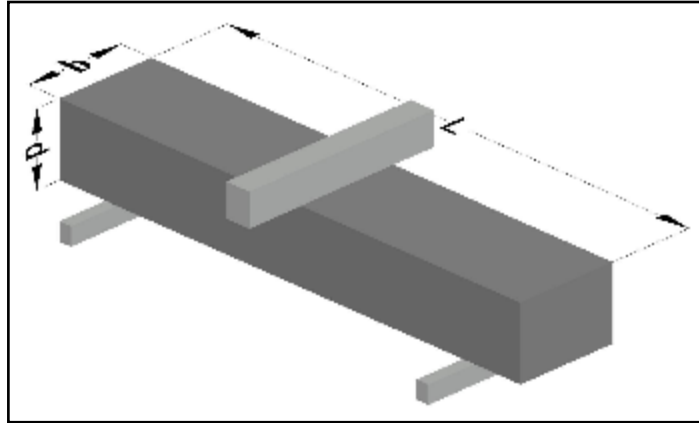


Figure 3-6 Brisim Dimensions Details



Plate 3-22 Flexure Tensile Test

### 3.7 Constructing of Specimens

The structure of the steel tube was made by the Turkish Toscelik Company, and the typical length of the steel tube was 6000 mm. After that, the tubes which length of 6000 mm were divided to obtain the needed length of the specimens. To investigate the alignment between the inner and outer tubes' centers, the inner tubes were accurately located at the center of the outer tubes in the test specimen setting process. To let the concrete be cast, the top hollow of the steel tube was left unlocked, and a plate with a

thickness of (10) mm had been welded to the tube's base. To achieve a uniformly distributed load transference about the cross-section throughout the test process, an angle grinder handled tool to ensure it is smooth and on the level on its upper face as shown in Plate 3-23.



Plate 3-23 Top Surface Preparation

In CFDS 1, during the process of casting the upper hollow of the inner tube had been covered carefully to avoid fresh concrete inflowing inside it, which is not required for the study. After the casting process is complete it can remove the cover and prepare the sample for test. After that, the specimens were protected from corrosion when the curing process was begun by cleaning them carefully and painting them with two layers of anti-corrosion paint as shown in Plate 3-24.



Plate 3-24 Preparing and Casting Specimens

The curing process started in the basin provided with heaters to keep the degree of concrete temperature constant according to ASTM- C 511 – 03 Standard [46], specimens were submerged in water for 28 days.

### 3.8 Support industry

To make the fixed support, the upper support consists of a square plate welded with a square ring like a cap has a thickness of (10) mm and welded with it six steel bullburn inside it a steel rod that the bullburn help the column to slide right and left easily. For the circular columns, the upper support consists of a circular plate welded with a circular ring that has a thickness of (10) mm and has the same details as the square columns, as shown in plate 3-25.

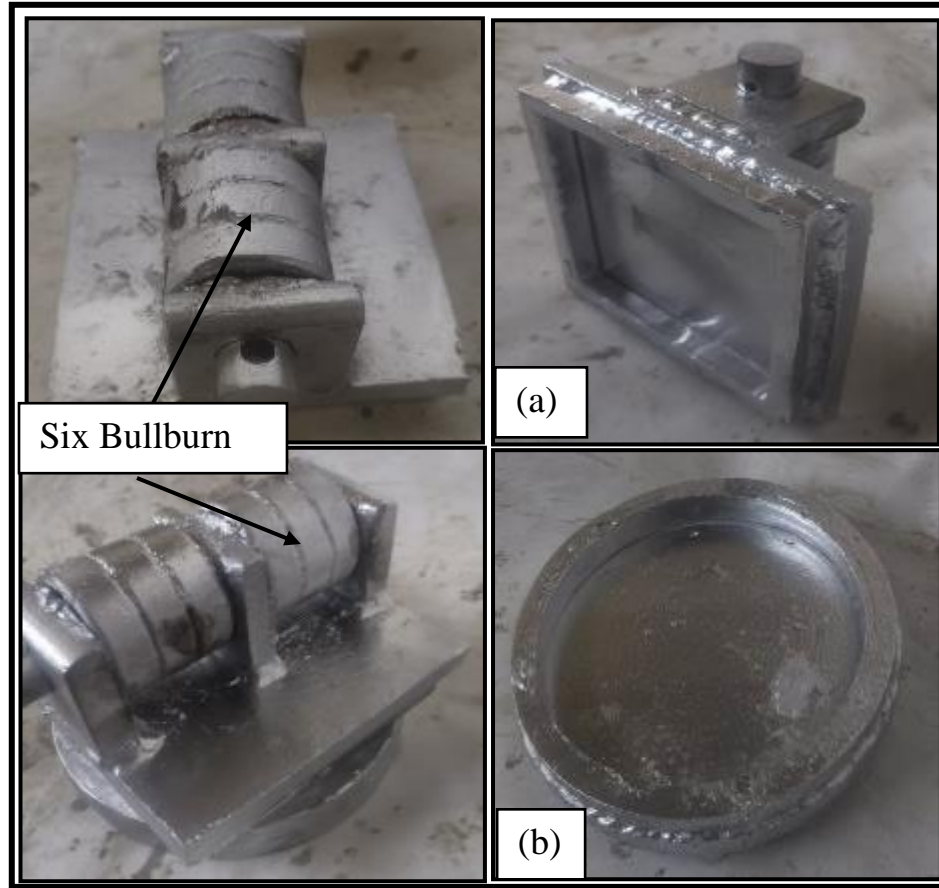


Plate 3-25 Upper Steel Caps (a) Square Cap (b) Circular Cap

To achieve a uniform distribution of axial load an arm of steel had been fixed in the side of the steel girder that was placed between the upper support and the vertical hydraulic jack as shown in plate 3-26.

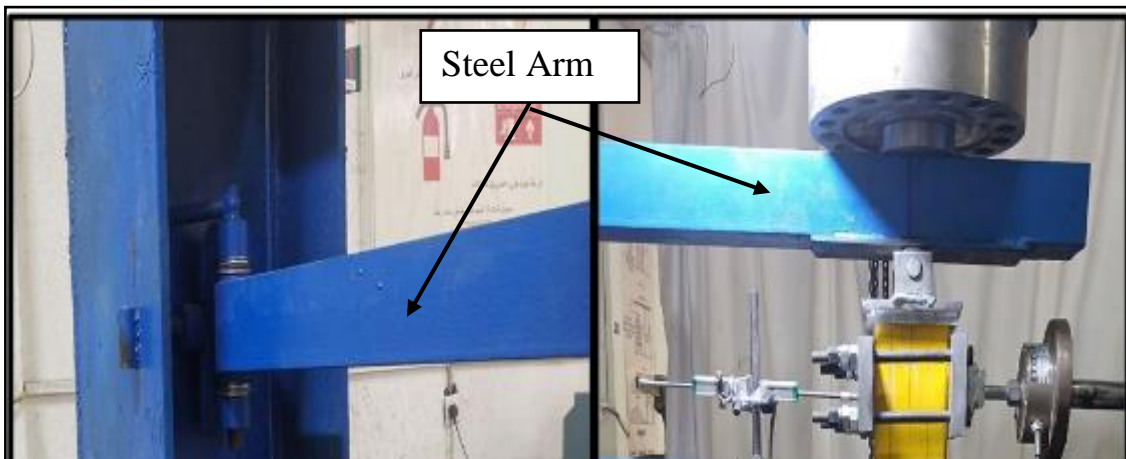


Plate 3-26 Steel Arm



To make the specimen able to move with the Lateral hydraulic jack right and left two plates with a thickness (of 10 mm) were made and linked together with four bolts that joined with the lateral load cell with steel bolts to ensure the complete touch between the two steel plates and the specimens, for square specimens, the plate was square planer plate, and for circular specimens, a curve in the plate was made to prevent any lateral movement in the opposite side of the motion, so when the lateral jack pushed to the right the specimen moves to the right by this pincers and move to left when the hydraulic jack moves left the details of this plates and bolts can be shown in Plate 3-27.

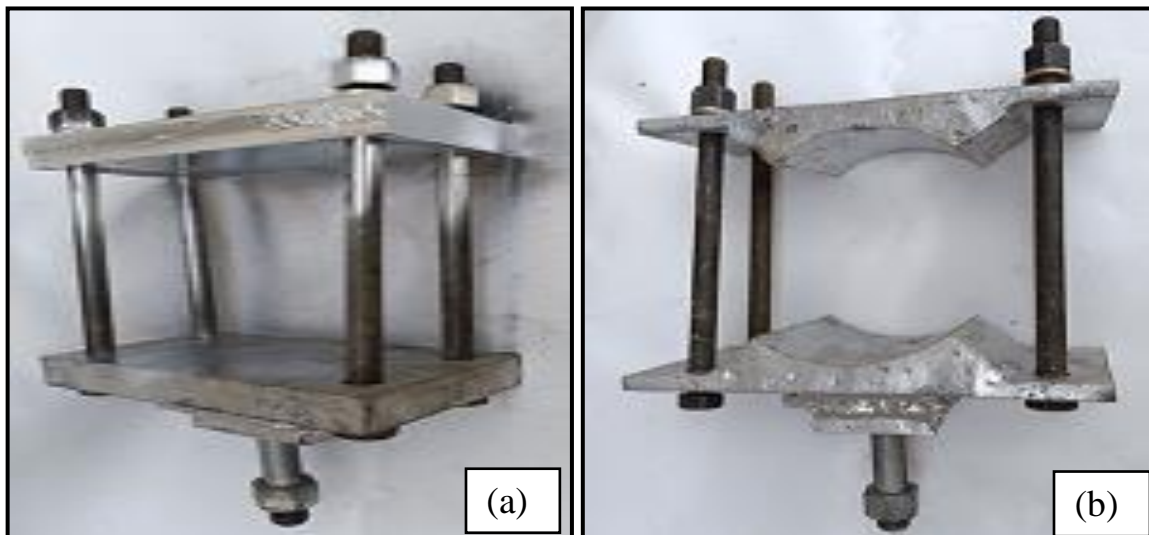


Plate 3-27 Steel Pencers (a) For Square Specimens (b) For Circular Specimens

To achieve the fixation case in the lower support a square steel plate were provided with a thickness (of 10) mm and dimensions (of 220\*220) mm, it has (12) holes and is linked with a base plate- that was fixed in the rigid girder -by heavy steel bolts and twelve nuts fixed with steel washers to prevent the movement as possible and to support the column from bottom four steel stiffeners with triangle shape welded with the outer tube, Plate 3-

28 showed the bottom plate and bolts distribution, and Figure 3-8, show details of stiffeners.

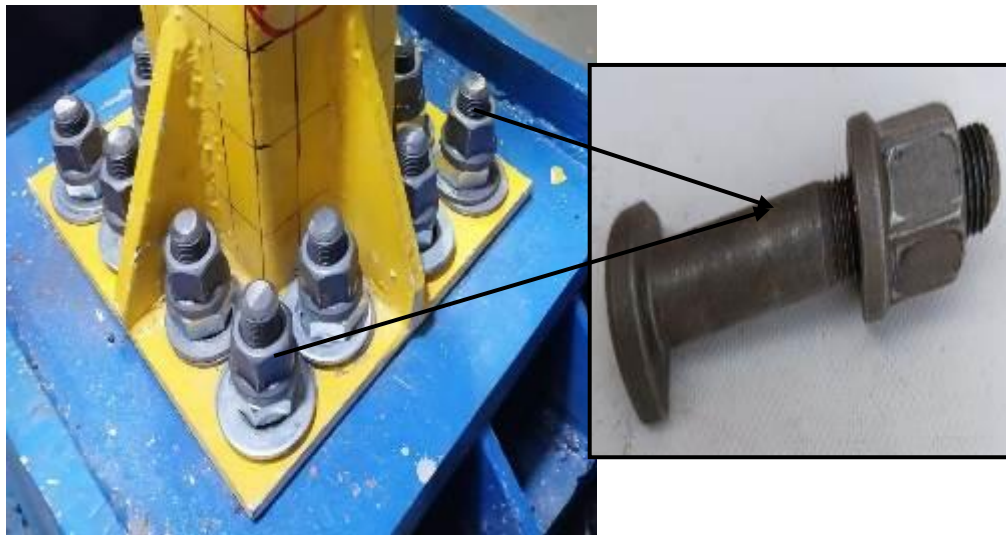


Plate 3-28 Lower Support Details

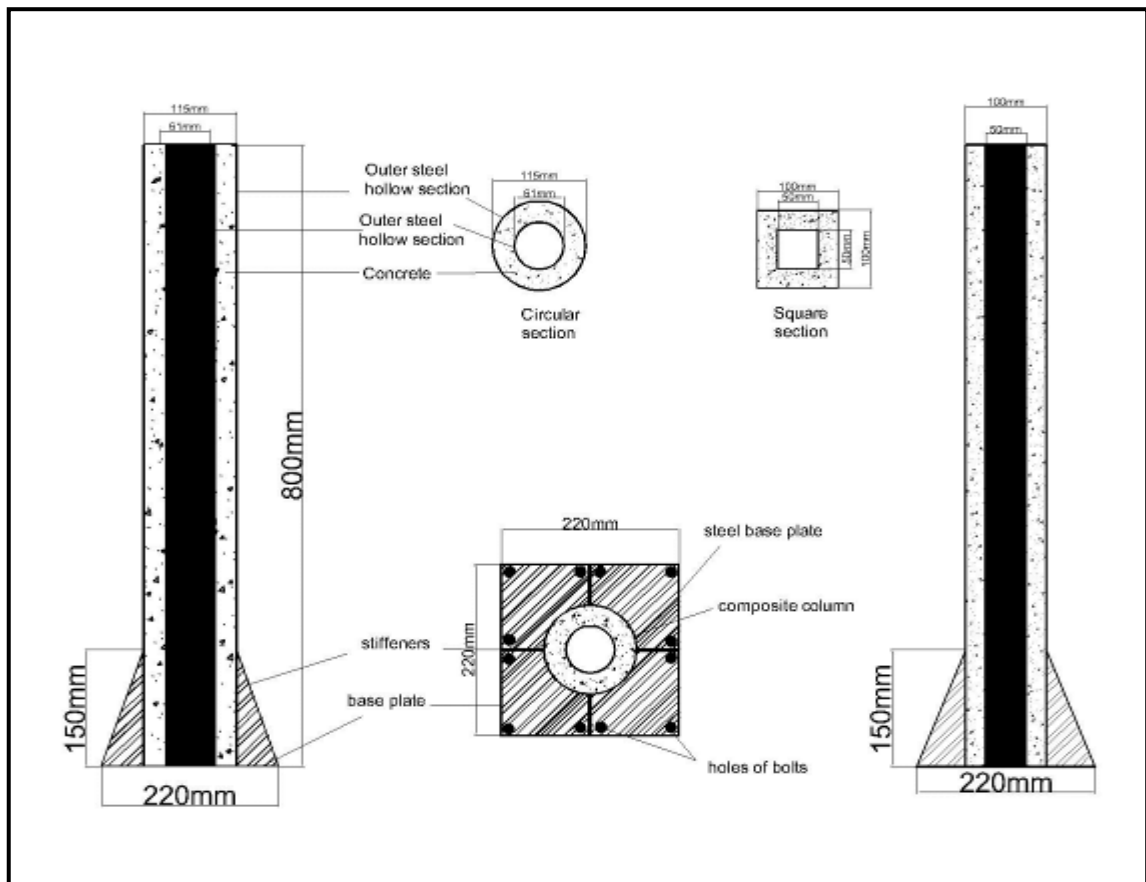


Figure 3-7 Details of Lower Support and Stiffeners.

The overall view of the test system and view used in the experimental work. After 28 days of the casting process of the HSC and NSC composite columns, the curing of specimens with water was finished, and the column specimens were removed from water basins. Then it is prepared by cleaning and painting to clarify the variables and show forms of failure. During the test process, steel caps were set on the upper of the column to distribute the axial load and fixed the column from the upper, while the column's lower support was fixed. To find out the change in lateral displacement of the column during the testing process, a linear Variation Displacement transducer (LVDT) was provided. The horizontal deflection was measured in the upper of the column. The machine hydraulic jack was provided and has a capacity of approximately 100kN. The test was performed on the columns up to failure. The load was recorded by two load cells (vertical and horizontal) linked to the computer as shown in Figure 3-9 and Plate 3-29. Excel program data representing the displacement history works automatically with positive and negative values of displacement was carried out in this test setup, all these details are shown in Plate 3-30.

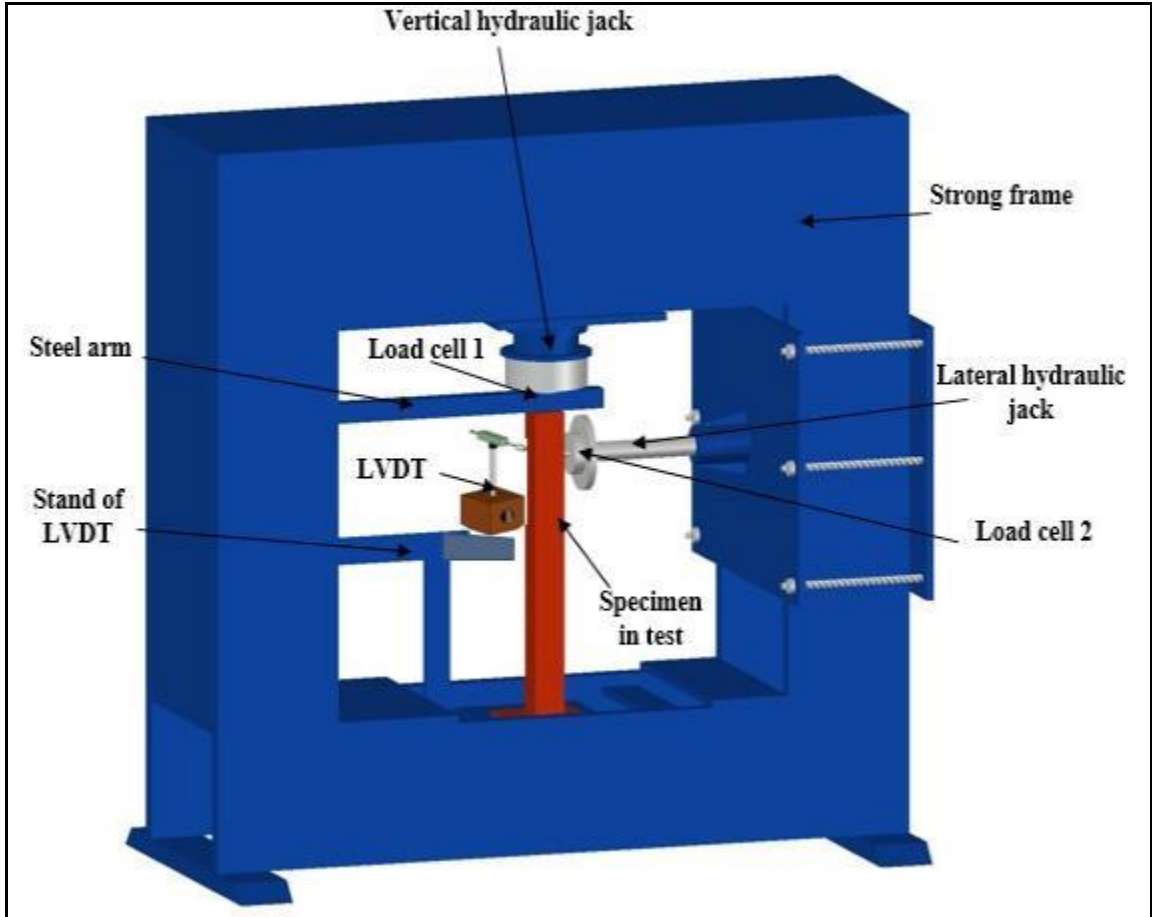


Figure 3-8 Testing Machine

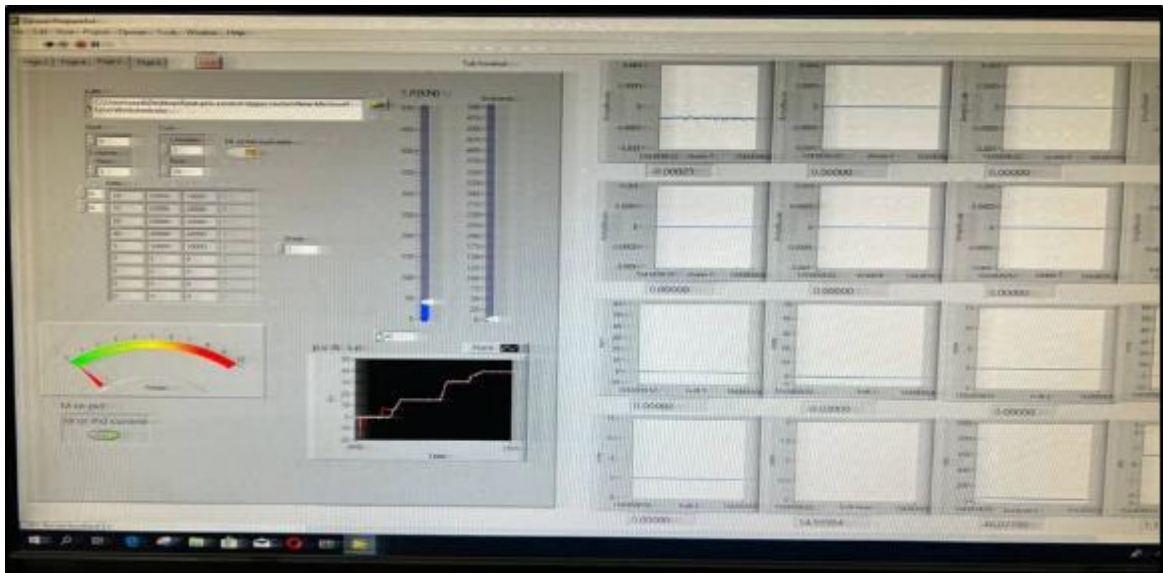


Plate 3-29 Computer Program Test

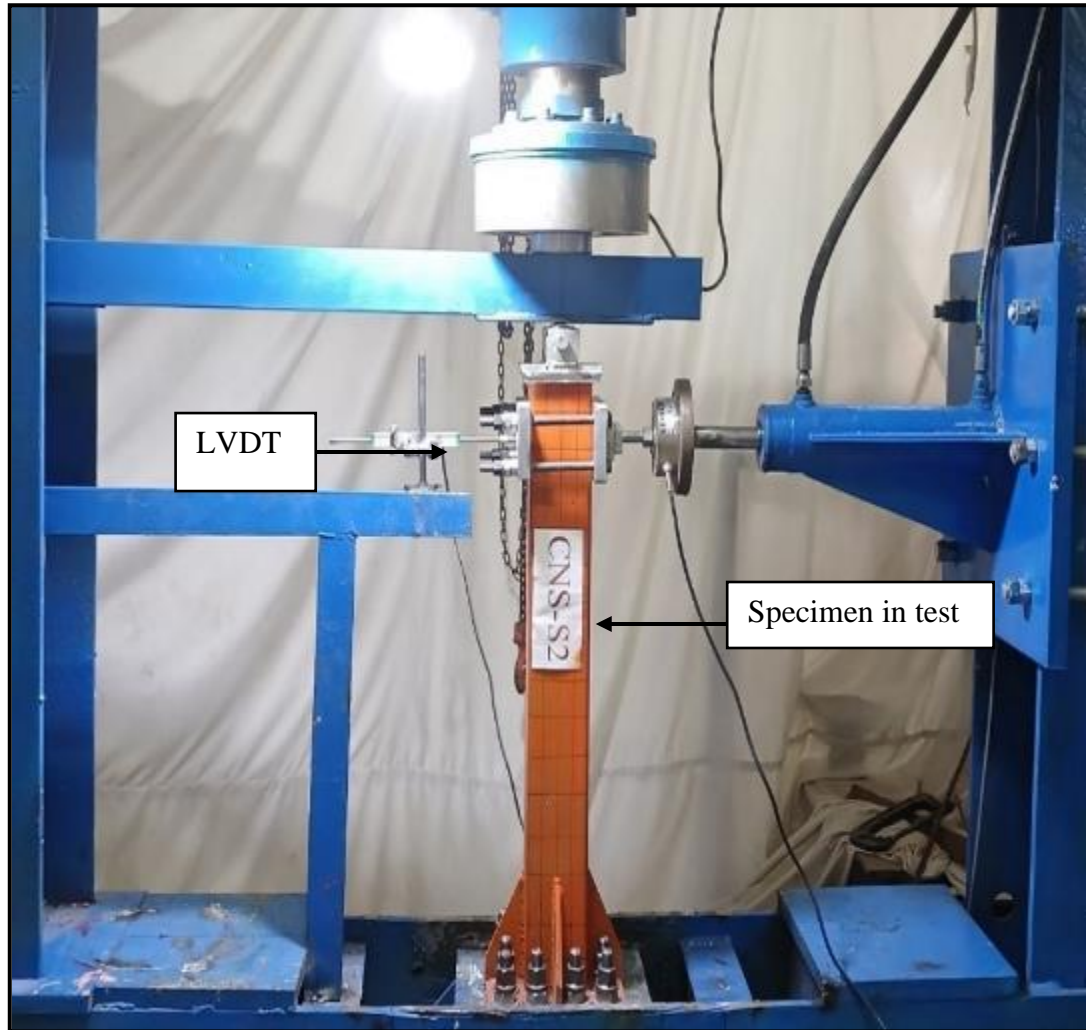


Plate 3-30 Vertical and Horizontal Jack details

### 3.9 Application of Axial Loads.

axial load value in this study was represented in three cases:

- The first case represented the effect of lateral load only without considering the effect of axial load (assume axial load zero) this case had been represented to study the effect of lateral load only in the construction stage.
- The second case represented the effect of dead load only as a value of self-weight of a typical slab assumed to have a dimension (5000\*5000)  $mm^2$  with (220)  $mm$  thickness and the finishing tiles over it (50)  $mm$  that

carried by a short column with dimensions of (400\*400\*3250) *mm* multiplied by a scale factor (1:4). The result of this calculations is about (40) kN as details in Appendix B.

- The third case represented the effect of dead load plus live load as a value self-weight of a typical slab assumed to have a dimension (5000\*5000) *mm*<sup>2</sup> with (220) *mm* thickness and the finishing tiles over it (50) *mm*, and live load about (1-1.25) kN/m<sup>2</sup> that carried by a short column with dimensions of (400\*400\*3250) *mm* multiplied by a scale factor (1:4). The result of this calculations is about (70) kN as details in Appendix B.

### 3.10 Application of Cyclic Loading

The testing process was: The cyclic lateral loading test began from (2,-2)mm displacement to( 42,-42) mm with two-cycle for each magnitude of displacement applied as an excel program worked automatically in the computer Figure 3-10, shows the cyclic protocol dependent on displacements. The Axial loading is divided into three types: The first group has four specimens with zero axial loads, the second group with an axial dead load of about (40kN) only, and the last group with axial dead and live load of approximately (70 kN).

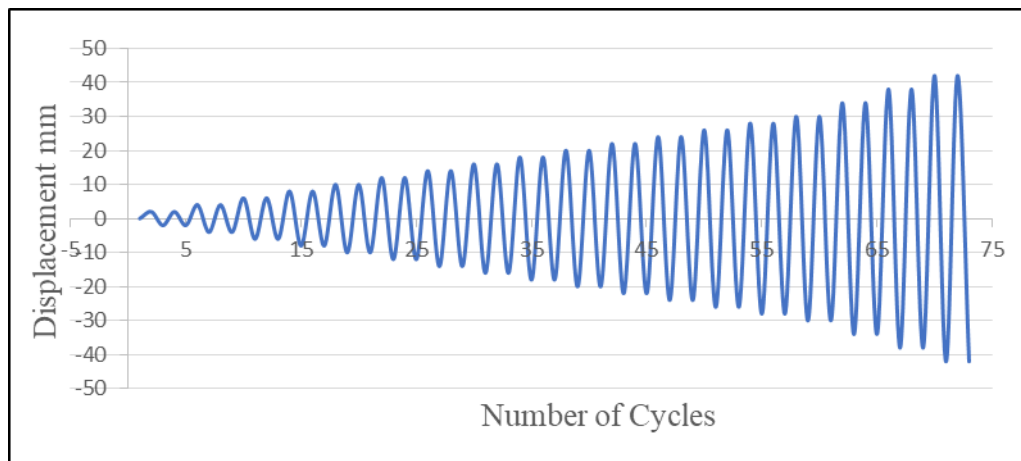


Figure 3-9 Displacement history of all specimens

***CHAPTER***  
***FOUR***

## Chapter4 : Results and Discussion

### 4.1 General

The main focus of this research is to study the behavior of concrete-filled double-skin columns subjected to cyclic lateral load under different cases of axial load experimentally. The mechanical properties of normal concrete (NSC) and high-strength concrete (HSC) have been introduced first in this chapter. The result of an experimental test of the behavior of twelve concrete-filled double-skin columns is presented in this chapter. The tested composite columns were divided according to the type of mixture into two groups: columns filled with high-strength concrete and others with normal concrete. The experimental variables included the shape of the composite column by two types square and circular columns. The effect of these variables was studied and discussed, load-deflection behavior, and the modes of failure of the specimens. Figure 4-1 shows the flow chart of experimental columns test and analysis results and its discussion.

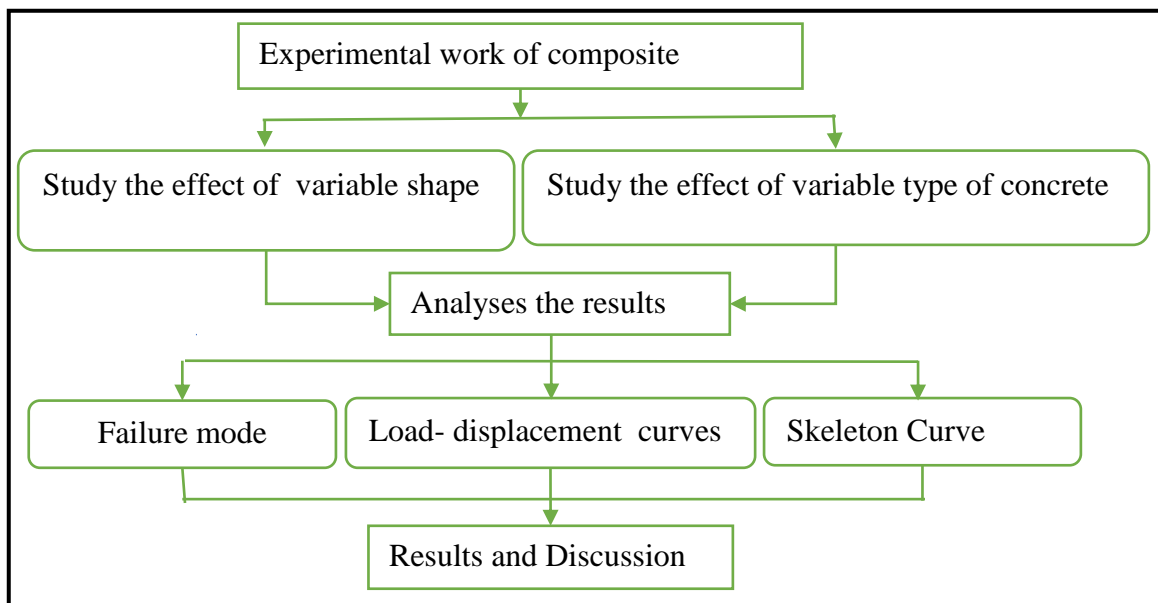


Figure 4-1 Flow Chart of Specimens Test



## 4.2 Mechanical Properties of NSC and HSC

The mechanical properties of the samples of concrete that have been tested in this study contained compressive strength, tensile strength, and modulus of elasticity. The average values of three samples were recorded to represent each test of the mechanical properties.

### 4.2.1 Compressive Strength Results

One of the most essential characteristics of the hardened concrete is compressive strength. To determine how this feature affects the behavior of composite columns, two types of concrete --NSC and HSC-- have been used in this study. The compressive test results of the two mixtures are shown in Table 4-1. The average value of three-cylinder samples had been taken to represent the compressive strength.

Table 4-1 Compressive Strength of Concrete Mixes

No. of specimen	Normal concrete NSC	High-strength concrete HSC
	100*200 Cylinder (MPa)	100*200 Cylinder (MPa)
1	28.4	66.5
2	30.9	66.9
3	35.7	71.1
<b>average</b>	<b>31.66</b>	<b>68.16</b>

The results showed that the compressive strength of high-strength concrete samples larger than the compressive strength of the normal concrete samples with a magnitude of 36.5 MPa. Plate 4-1 shows the failure modes of cylinders for each mixture .



Plate 4-1 Failure Mode of Samples (a) NSC samples (b) HSC samples.

#### 4.2.2 Splitting Tensile Strength Results

An indirect method to assess the tensile of the concrete, in this test standard cylinder (100\*200) mm, is used by laying horizontally and applying the force radially which causes a crack along the cylinder vertically as shown in Plate 4-2.



Plate 4-2 Failure Mode of Different Types of Concrete in Splitting Test (a) HSC  
(b) NSC

Three cylinders were used in this test for each type of concrete, and the results of this test are shown in Table 4-2 and take the average.

Table 4-2 Results of three cylinders of each type of concrete

No. of specimen	Normal concrete (MPa)	High strength concrete (MPa)
1	3.4	5.3
2	3.7	5.5
3	3.9	6.1
Average	3.67	5.63

The results of the splitting test indicate that the tensile strength of high-strength concrete is more than normal concrete by approximately 2.0 MPa.

**4.2.3 Flexure tensile Strength (Modulus of Rupture ( $f_r$ ))**

To obtain the modulus of rupture for NSC and HSC, three prism specimens with dimensions (100×100×500) mm were tested under one concentrated load as shown in Plate 4-3, and Table 4-3 clear the results of flexural tensile strength and their average of both type of concrete.



Plate 4-3 Failure Mode of Flexural Strength of Different Types of Concrete  
(a) NSC sampels (b) HSC sampels .

Table 4-3 Results of three prisms for each type of concrete and average.

No. of specimen	Normal concrete (MPa)	High strength concrete (MPa)
1	3.74	4.96
2	3.87	5.36
3	4.58	5.98
<b>Average</b>	4.06	5.43

The experimental values for the modulus of rupture indicated that HSC flexural strength has a magnitude greater than the flexural strength of NSC by 1.37 MPa.

#### 4.2.4 Modulus of Elasticity

The modulus of elasticity was calculated for each mix of NSC and HSC using equation 4-1, which represented the formula of modulus of elasticity for normal concrete according to the ACI-318 formula [34].

$$E_c = 4700 \sqrt{f_c} \dots\dots\dots 4-1$$

Equation 4-2 represented the formula of modulus of elasticity for high strength of concrete according to the ACI 363R-23 [5].

$$E_c = 3320 \sqrt{f_c} + 6900 \dots\dots\dots 4-2$$

The value of the modulus of elasticity for each mixture is calculated by the previous equations represented in Table 4-4.

Table 4-4 Average Modulus of Elasticity.

No. of specimen	Modulus of elasticity (Ec) for High strength concrete (Mpa)	Modulus of elasticity (Ec) for Normal Concrete (Mpa)
1	33973	25047
2	34000	26126
3	34894	28082
<b>Average</b>	34289	26418

Through the calculations of the modulus of elasticity for High strength concrete, it was found an increase in the modulus of elasticity where the

average value of elasticity modulus in the mixture of high strength was 34289 MPa and the average value of modules for normal concrete was 26418 MPa .

### 4.3 Nominal Axial Load:

The columns are generally known as compression members, and usually carry bending moment in one or two directions. The most common types of RC columns are:

- 1- Columns have a longitudinal bar with lateral ties
- 2- Columns have a longitudinal bar with continuous spirals.
- 3- Composite members with steel pipe or tubing.

The nominal strength axial load can be evaluated by the equation 4-3 which is represented according to the ACI -318 code, recognizing the nonlinear response of steel and concrete materials.

---

---

$$P_o = 0.85 * f_c * A_c + f_y * A_s \dots\dots\dots 4-3$$

---

---

Where:

$P_o$ :Nominal strength load

$f_c$ : Specified compressive strength of concrete

$A_c$ :Area of the concrete section

$f_y$ :Specified yield strength for steel

$A_s$ :Area of steel

Figure 4-2 considered the factored maximum load combination linked with maximum axial force and maximum bending moment according to ACI code 440.11-22(R10.4.2)[47].

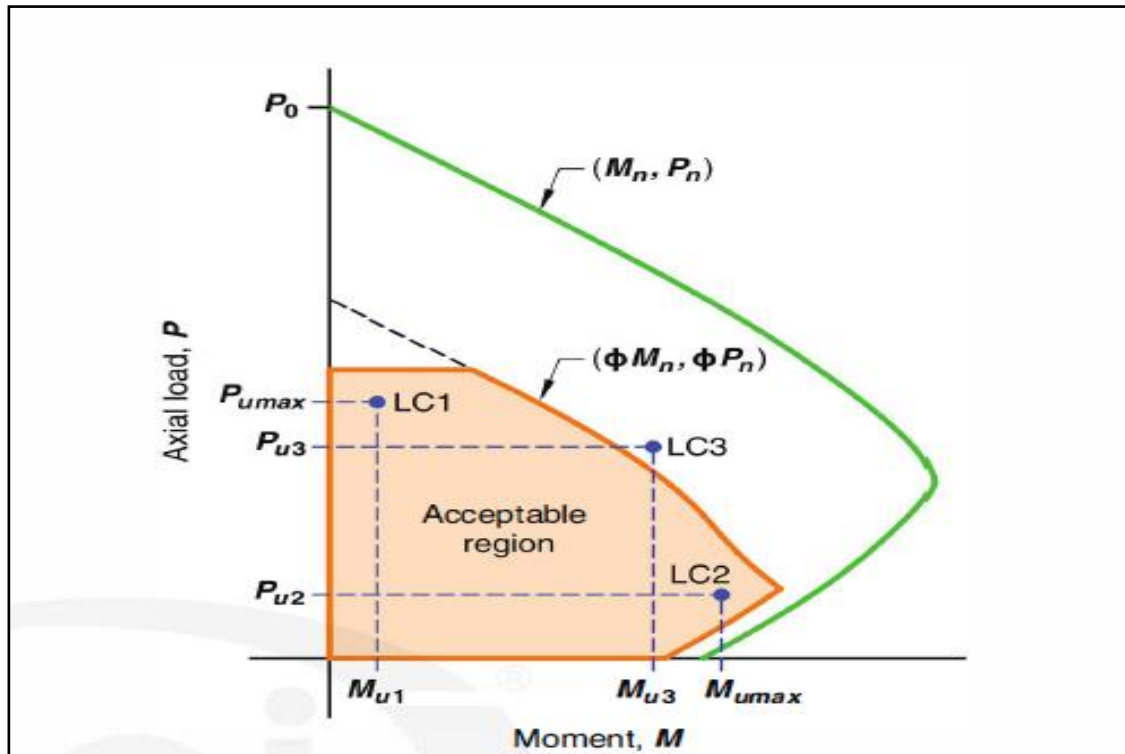


Figure 4-2 Critical column load combination[47]

#### 4.4 Failure Modes

Generally, the shape of the steel tube and the type of concrete are important factors that affect and give an important indicator of the shape of the column's failure. The modes of failure of the CFDST circular and square columns are shown in Plate 4-4 to 4-15.

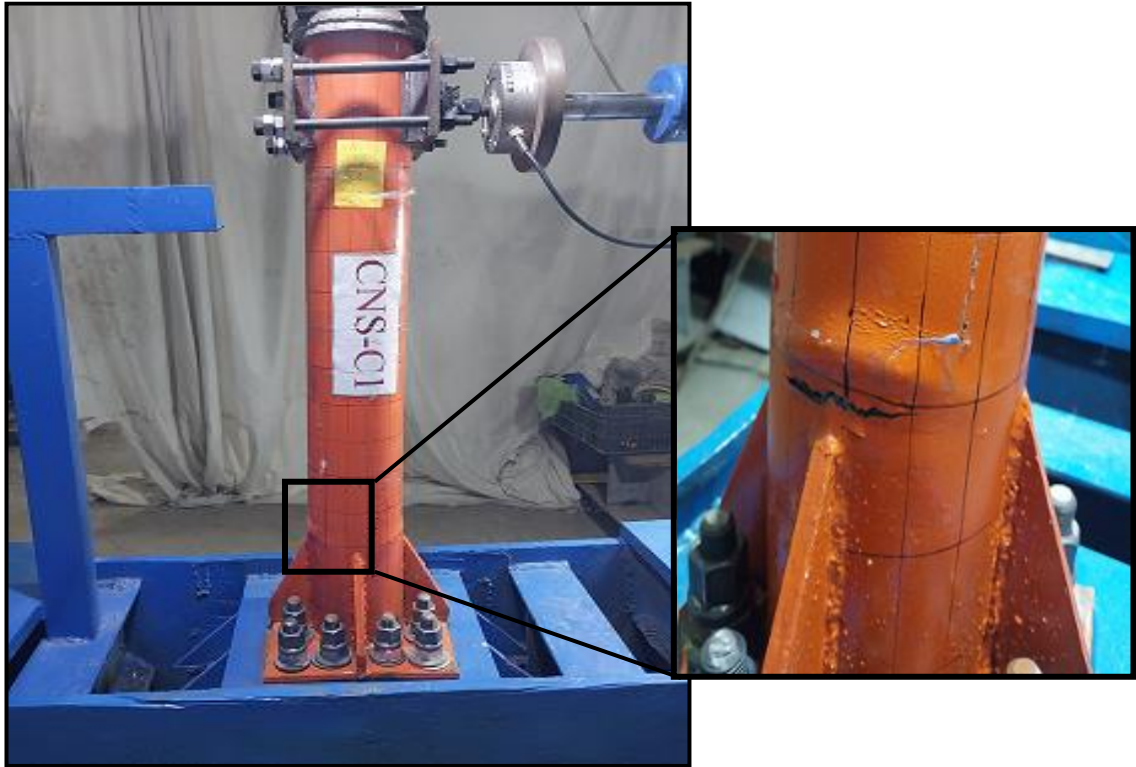


Plate 4-4 Failure Mode of CNS-C1 Specimen

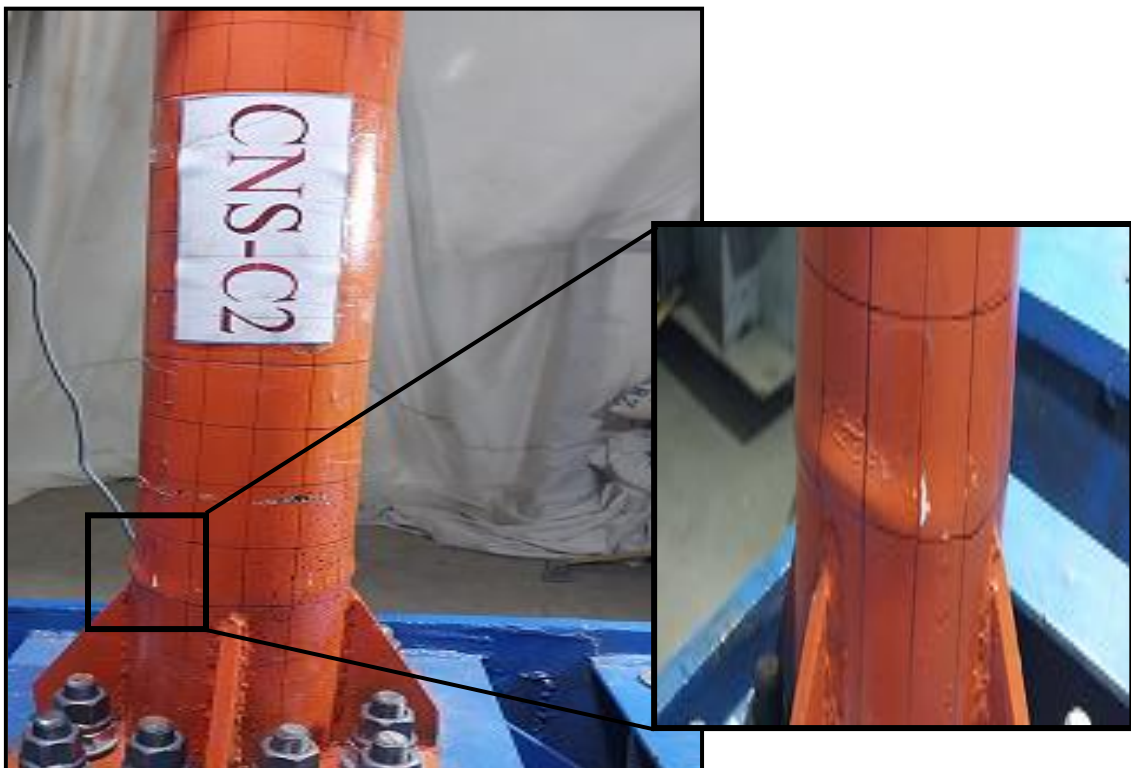


Plate 4-5 Failure Mode of CNS-C2 Specimen



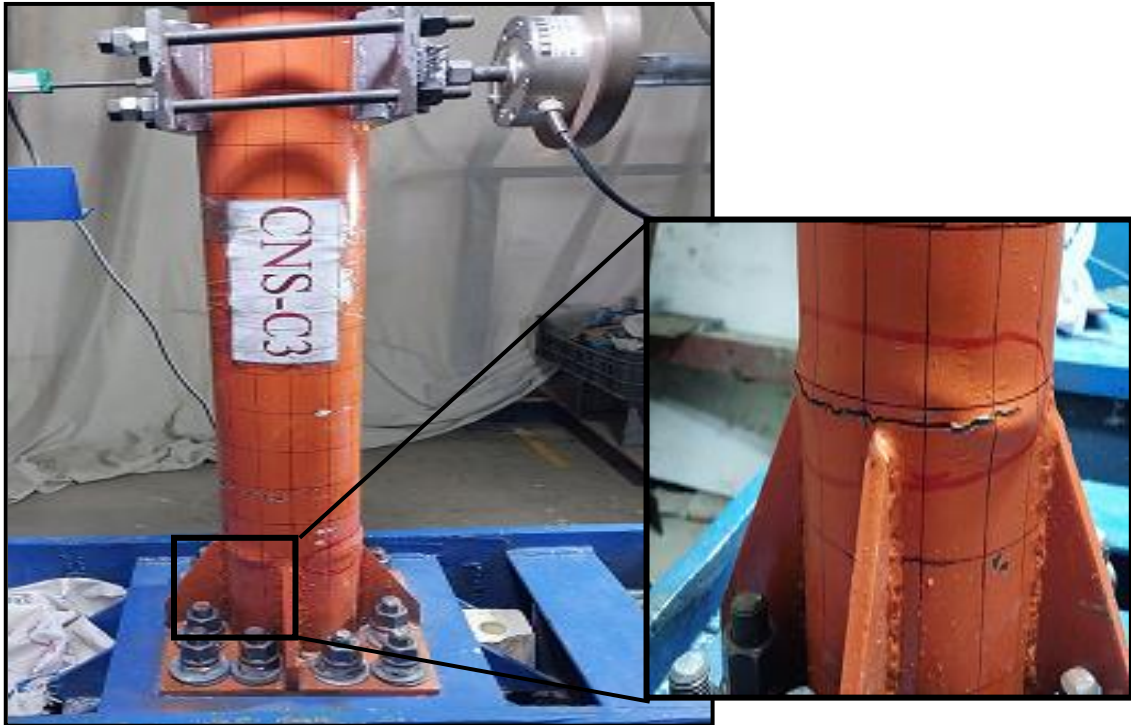


Plate 4-7 Failure Mode of CNS-S1 Specimen

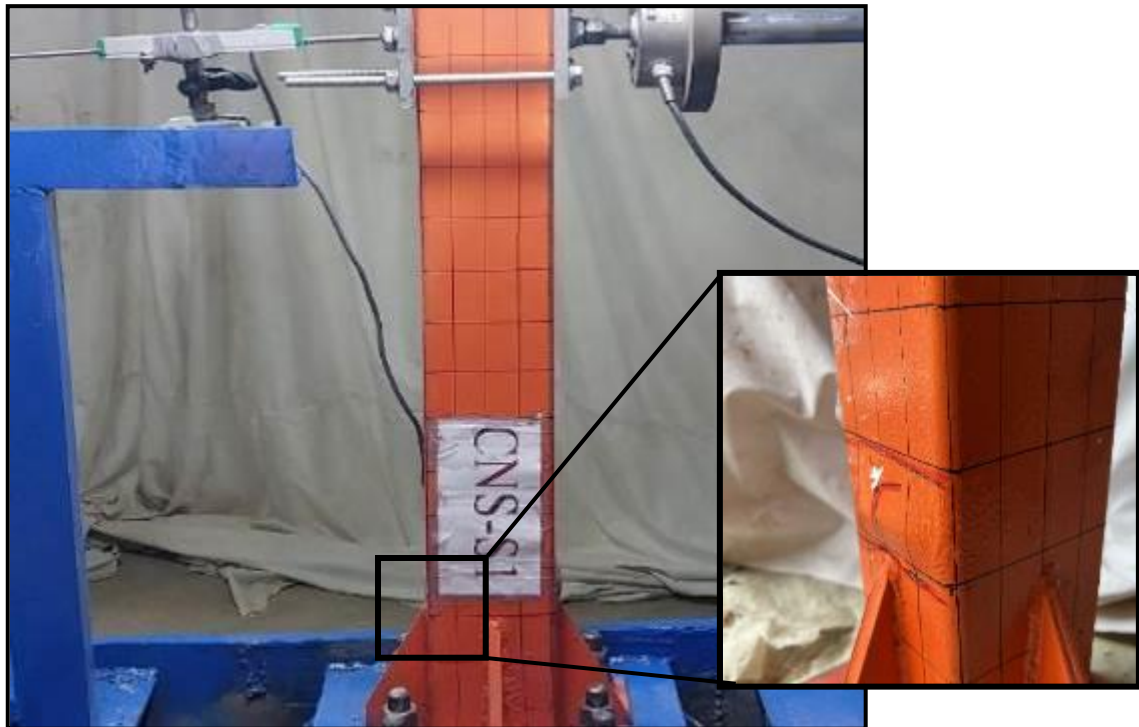


Plate 4-6 Failure Mode of CNS-C3 Specimen

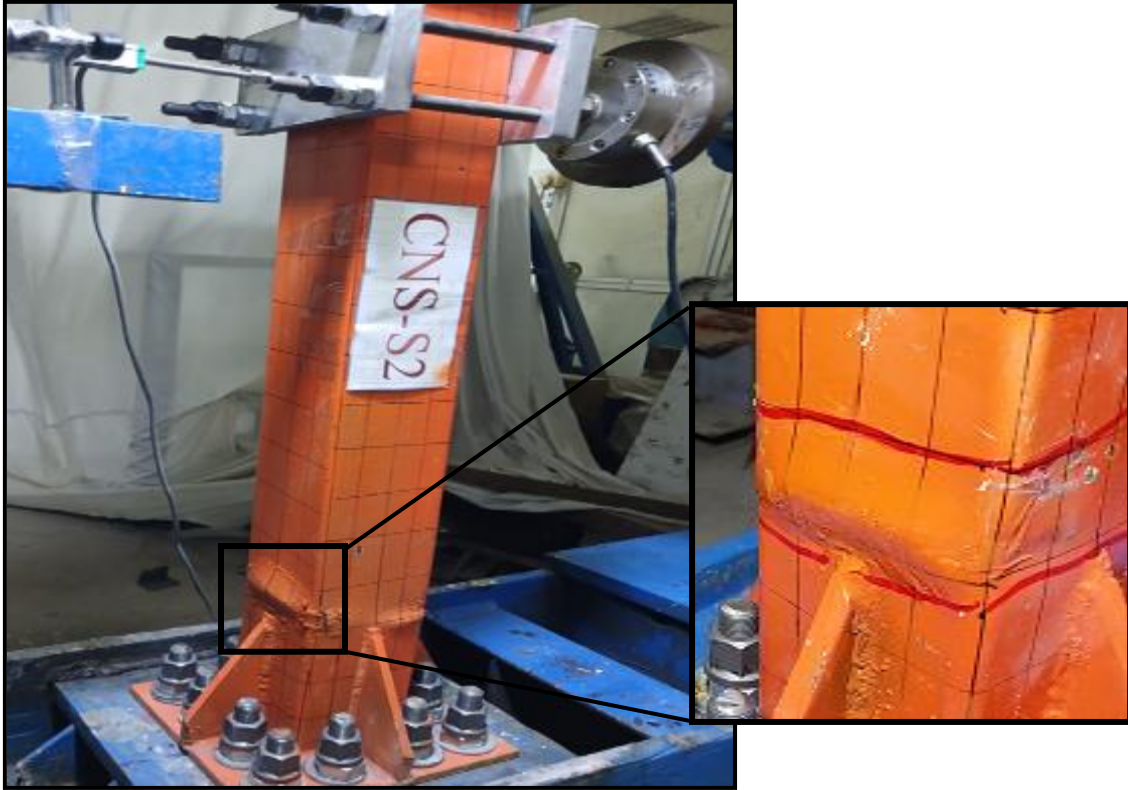


Plate 4-8 Failure Mode of CNS-S2 Specimen

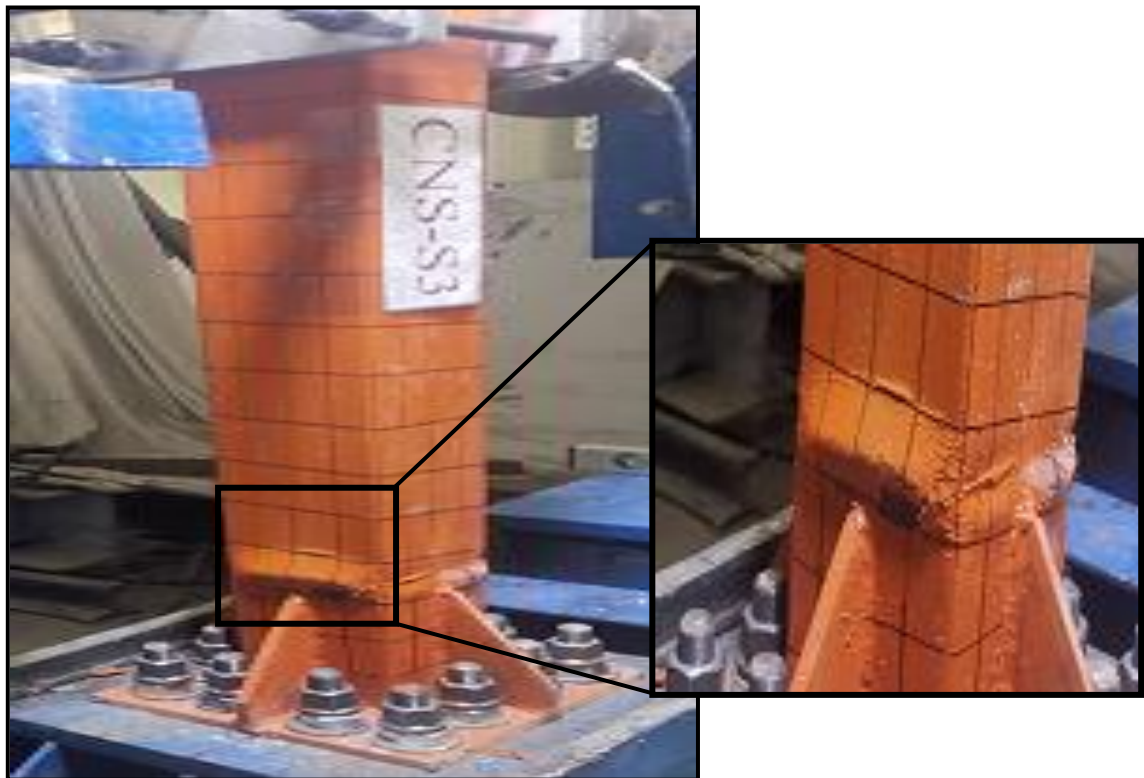


Plate 4-9 Failure Mode of CNS-S3 Specimen

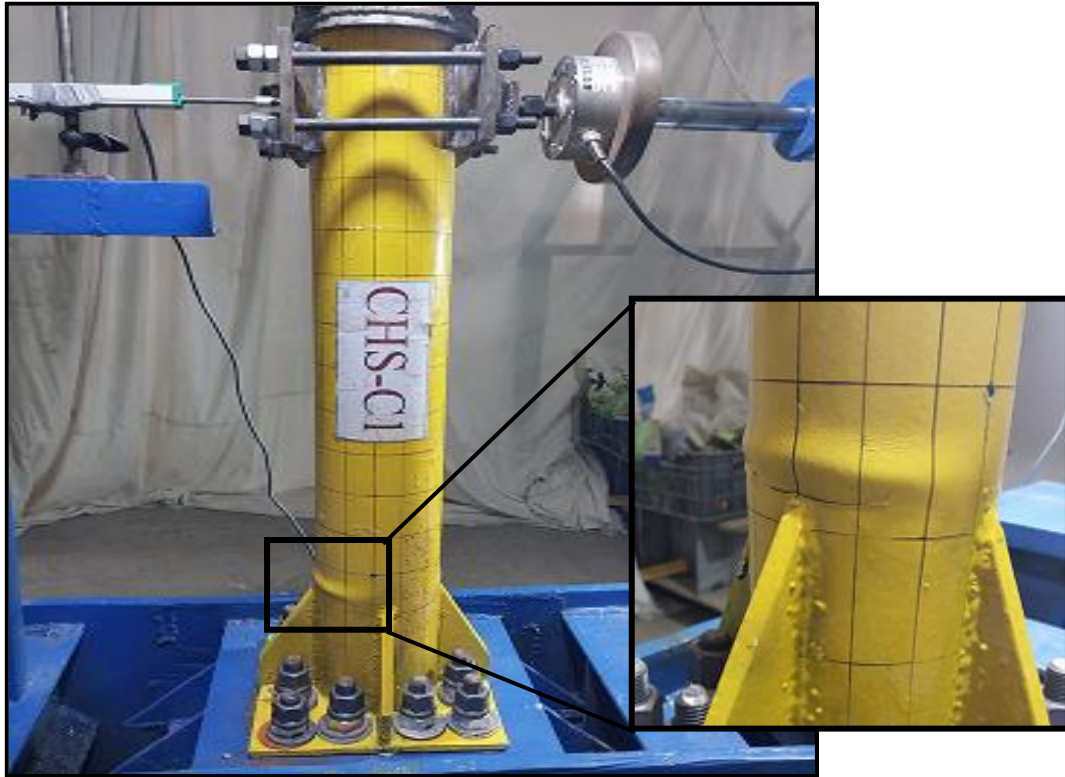


Plate 4-10 Failure Mode of CHS-C1 Specimen

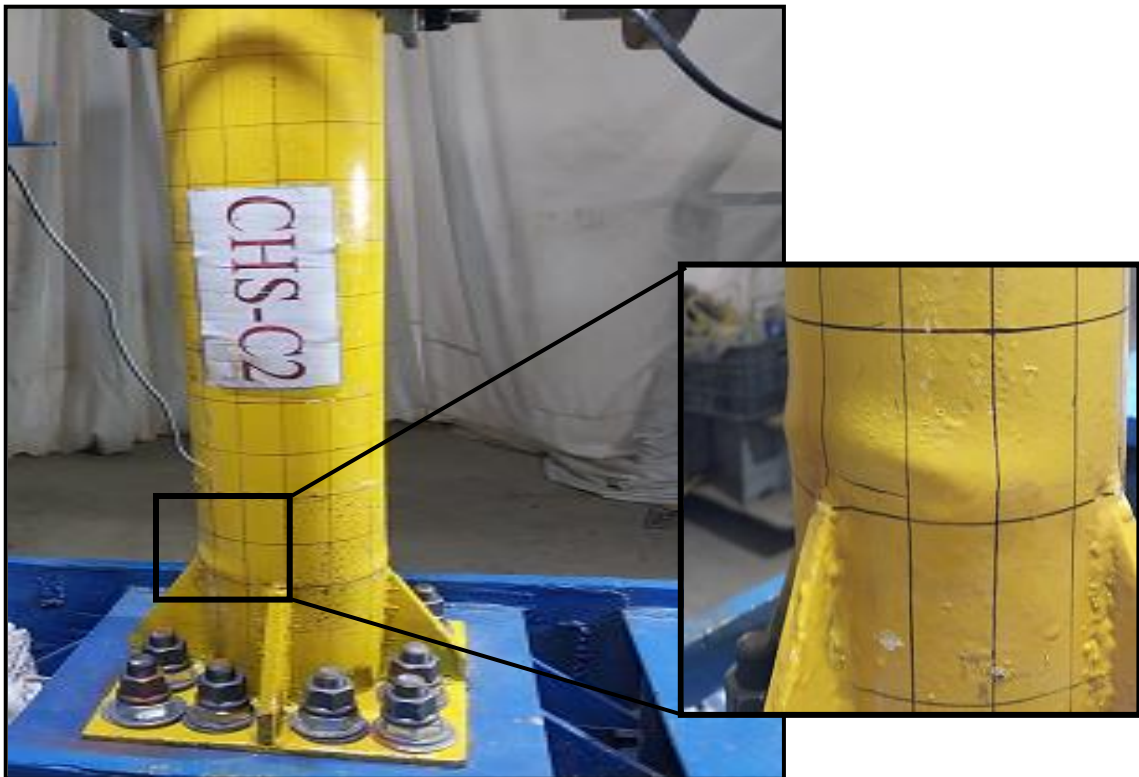


Plate 4-11 Failure Mode of CHS-C2 Specimen

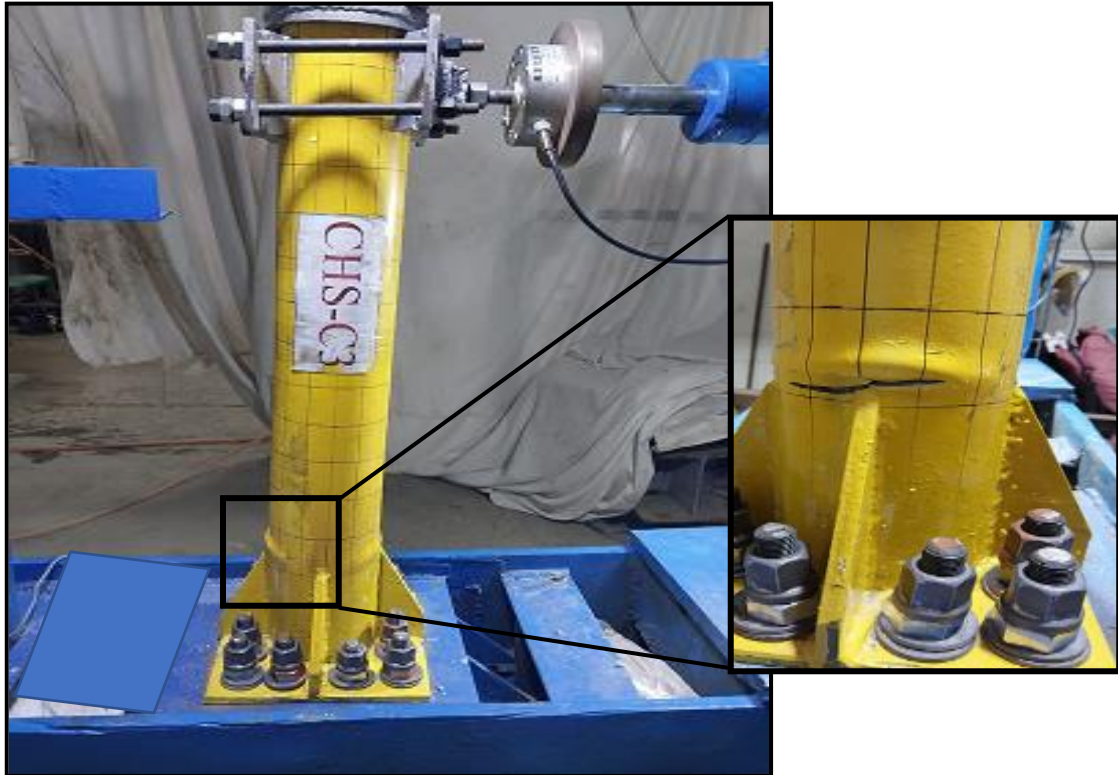


Plate 4-12 Failure Mode of CHS-C3 Specimen

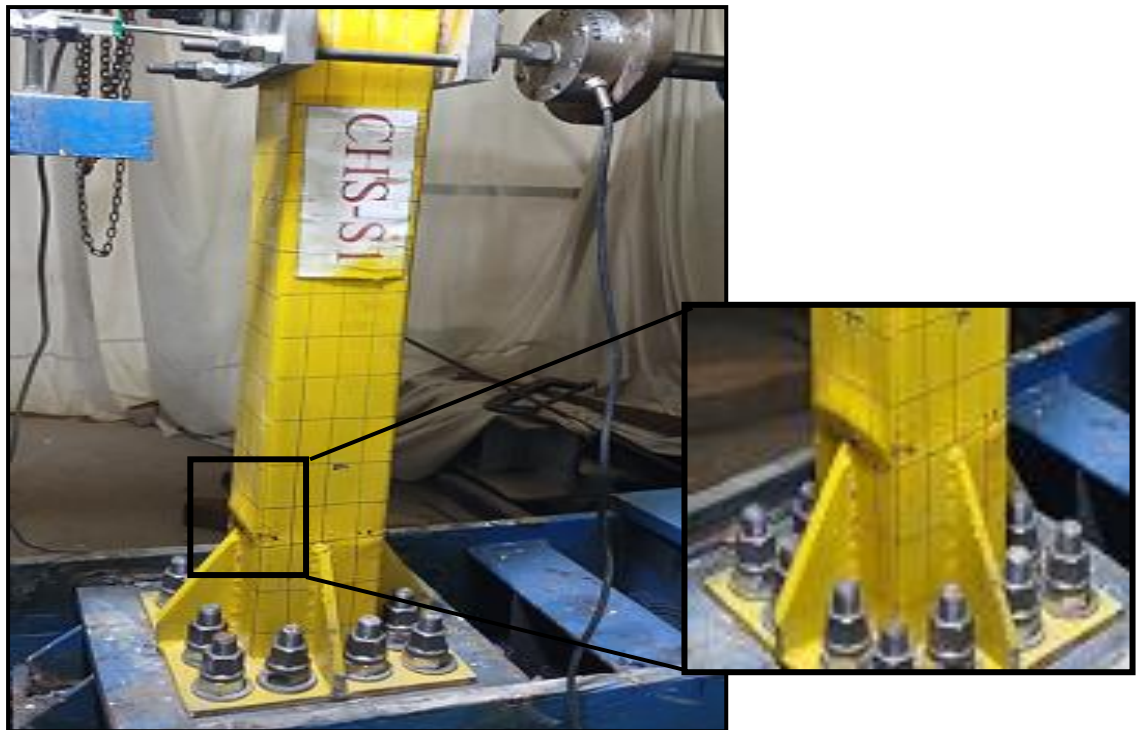


Plate 4-13 Failure Mode of CHS-S1 Specimen

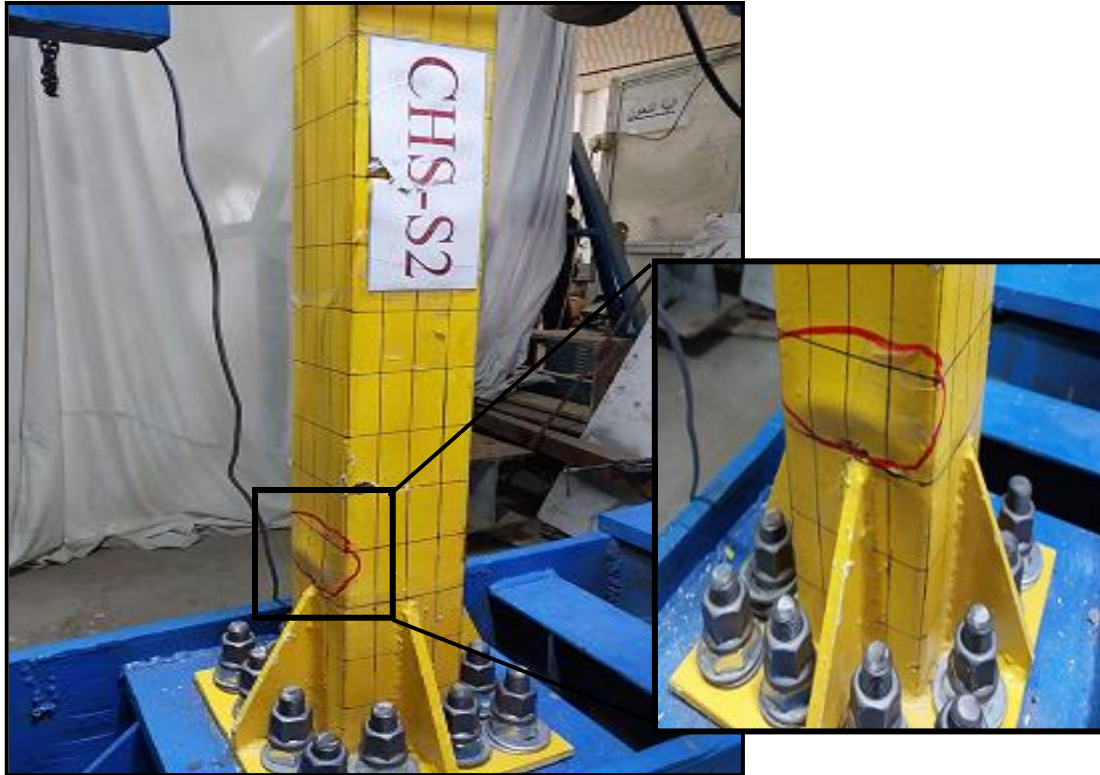


Plate 4-14 Failure Mode of CHS-S2 Specimen

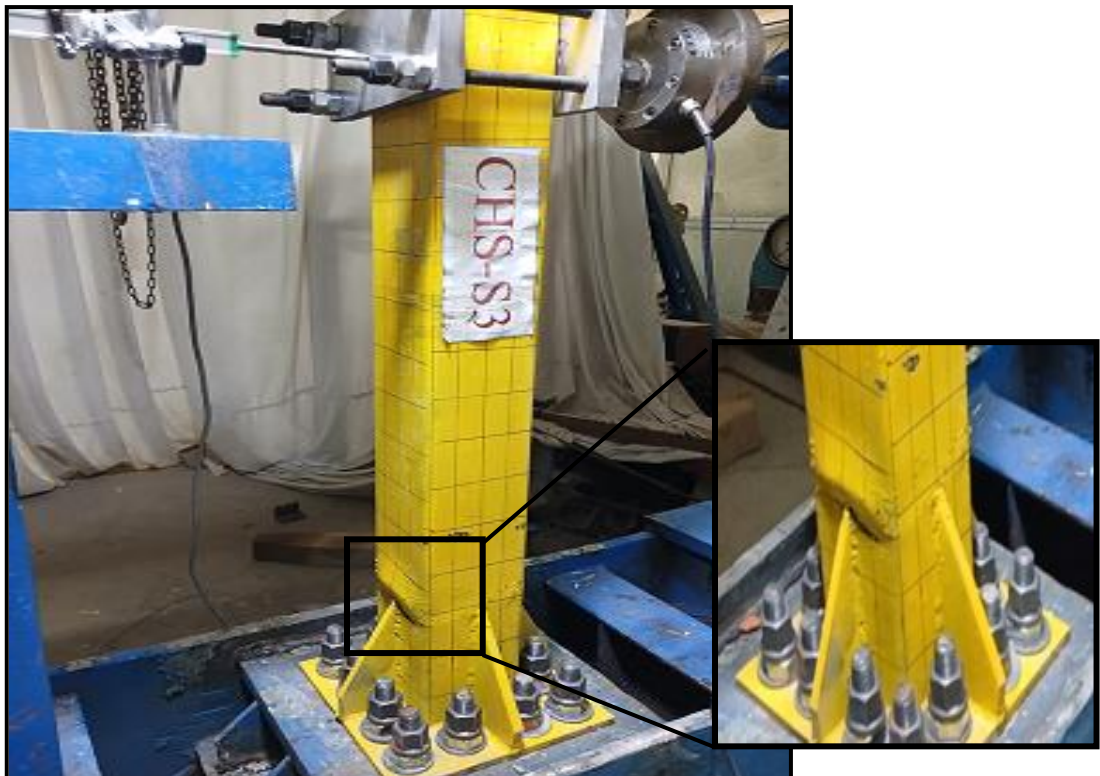


Plate 4-15 Failure Mode of CHS-S3 Specimen

From the previous pictures of specimens, the failure mode for all specimens was noticed at the bottom of columns near the stiffeners which means that the specimens reached the plastic phase at the bottom, while the top of specimens were still in the elastic phase. At the beginning phases of the cyclic load test for columns, nothing is observed. There are clear fracture sounds when the load reaches its maximum load. Subsequently, the tubes began to yield. When a load increases, the tube bends as a result of the positive and negative lateral loads. The investigation of a concrete fracture followed by the steel's achievement of maximum stress under lateral loading conditions is one of the expected possible failure scenarios for short columns. Plates 4-16 show the cracks that happened in the concrete core after the failure.



Plate 4-16 Cracks in Concrete after Failure

The failure mode of all specimens investigated near the bottom of the columns refers to the specimens reaching to plastic zone while the top of the columns were still elastic, the following was obtained:

1- All circular and square sections showed internal and external yield on the steel preceded by the occurrence of crushing concrete between the two tubes. All of the columns failed in the region near the lower support.

2-As for the circular sections, The resistance of failure occurred larger degree than the square section, due to the better confining of concrete by the circular steel tube than the square.

3- For specimens that have a high-strength concrete the failure happened decelerate than the others that have a normal concrete due to the high properties of high-strength concrete and its resistance to the high value of loads.

#### **4.5 Load-Displacement Behavior**

One LVDT was installed to record the displacement of each column in the region of lateral force action that acted by the lateral hydraulic jack. During the test, it observed that the steel started to bend and sometimes latitudinal cracks happened and a sound of concrete crushing was heard clearly before the yielding in steel happened. The load-deflection and the deflected shape of all of these columns are illustrated in Figures 4-4 to 4-15

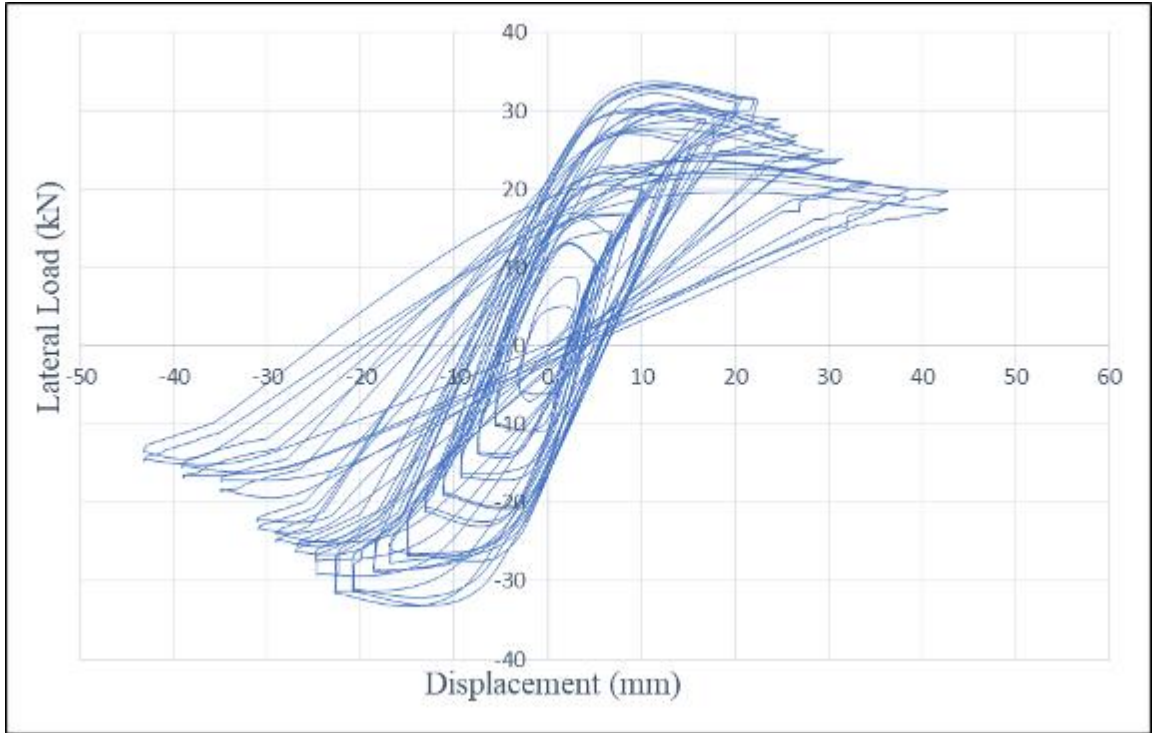


Figure 4-3 Load Displacement Diagram for CNS-C1 Specimen

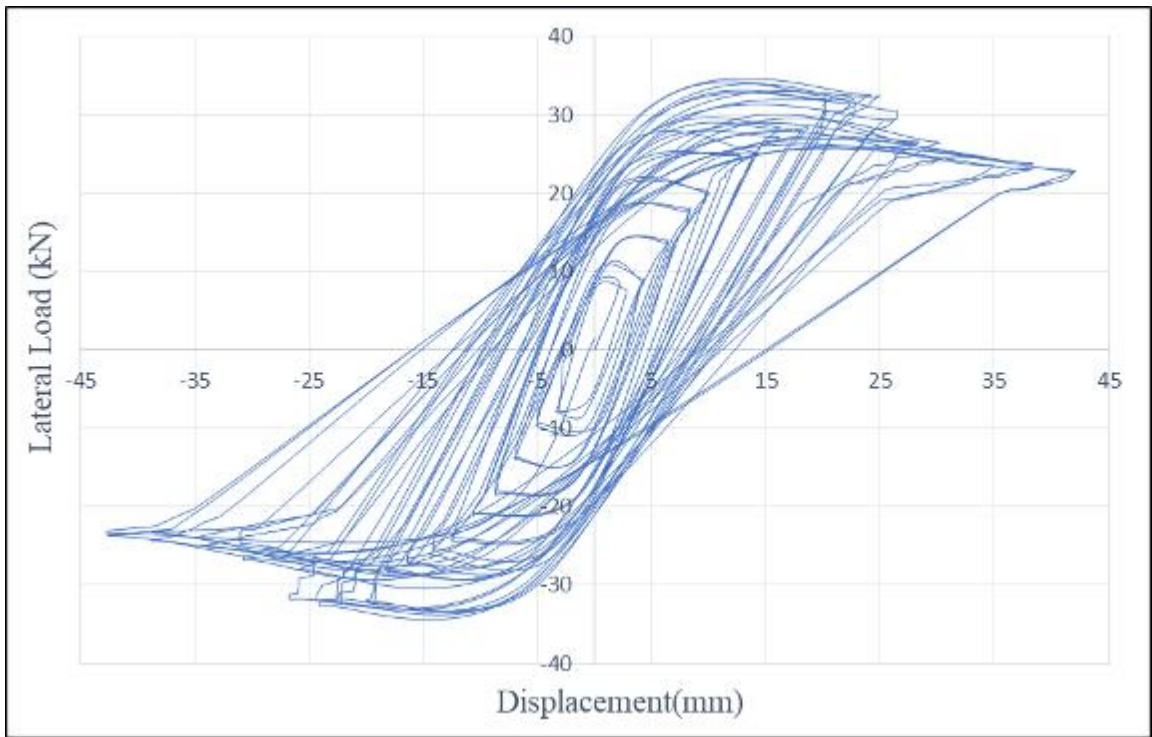


Figure 4-4 Load Displacement Diagram for CNS-C2 Specimen



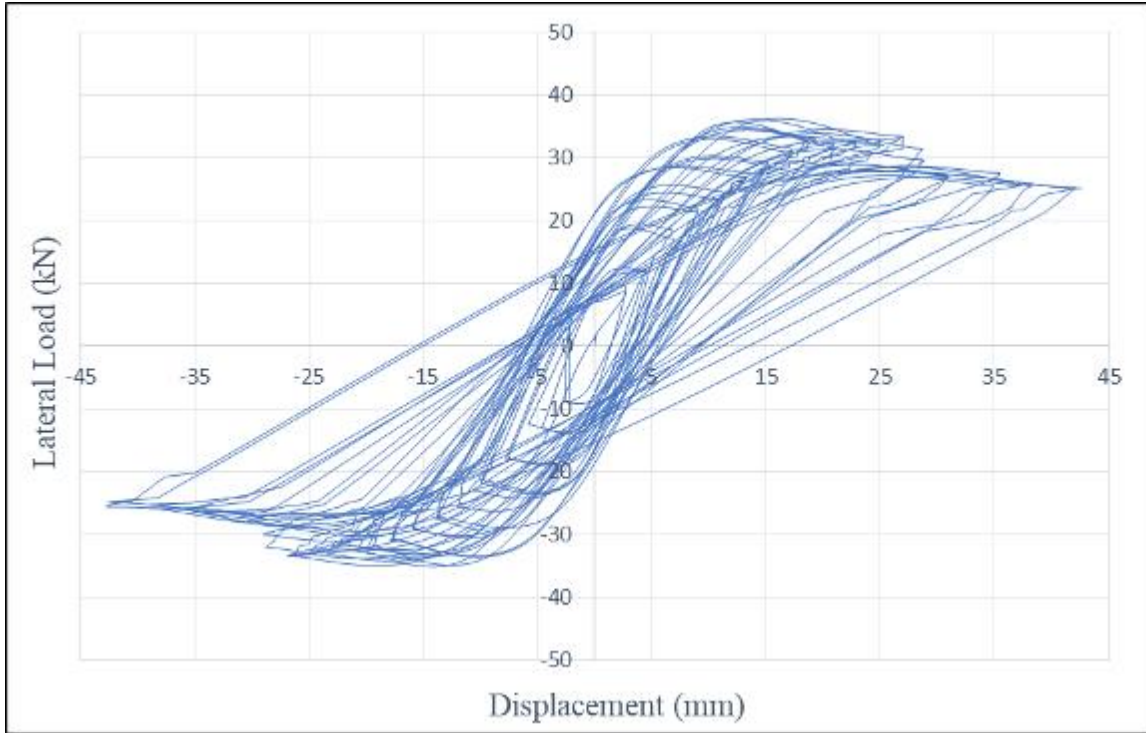


Figure 4-5 Load Displacement Diagram for CNS-C3 Specimen

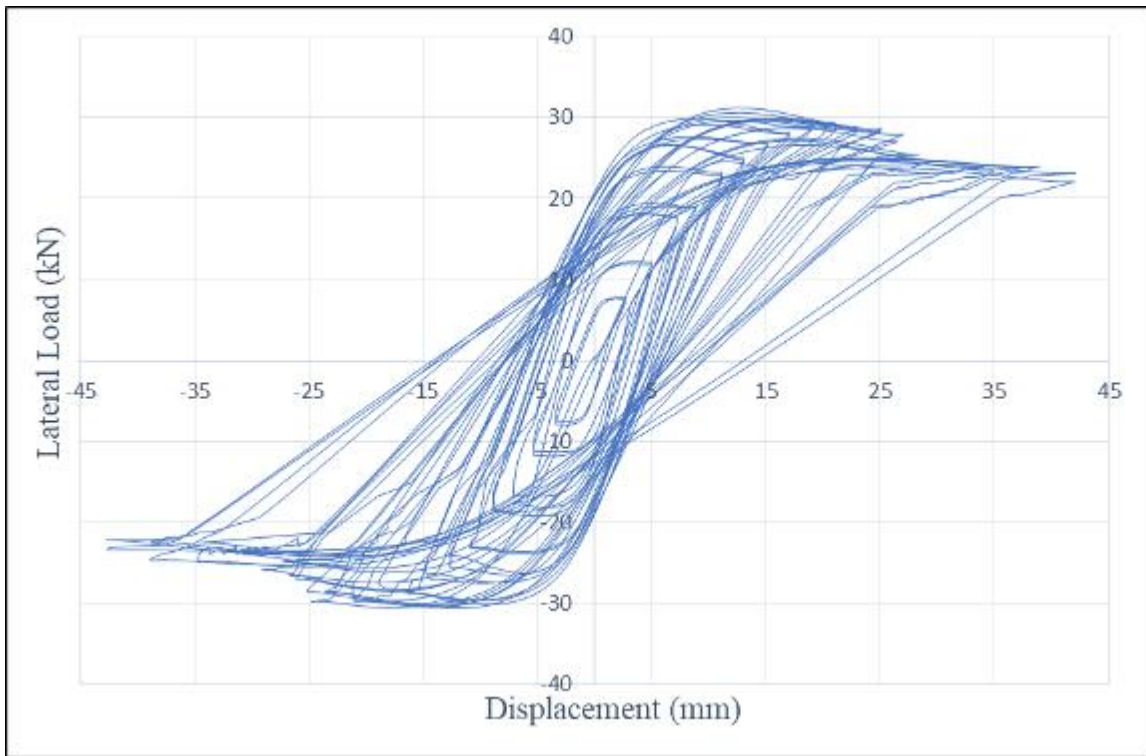


Figure 4-6 Load Displacement Diagram for CNS-S1 Specimen

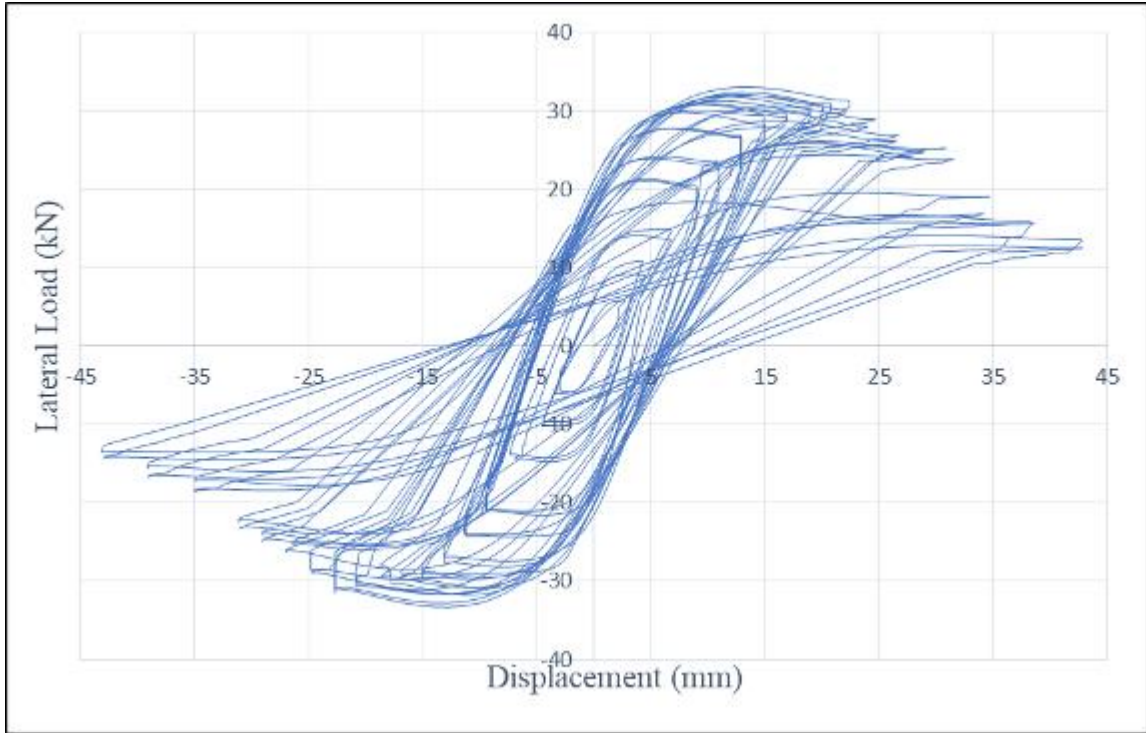


Figure 4-7 Load Displacement Diagram for CNS-S2 Specimen

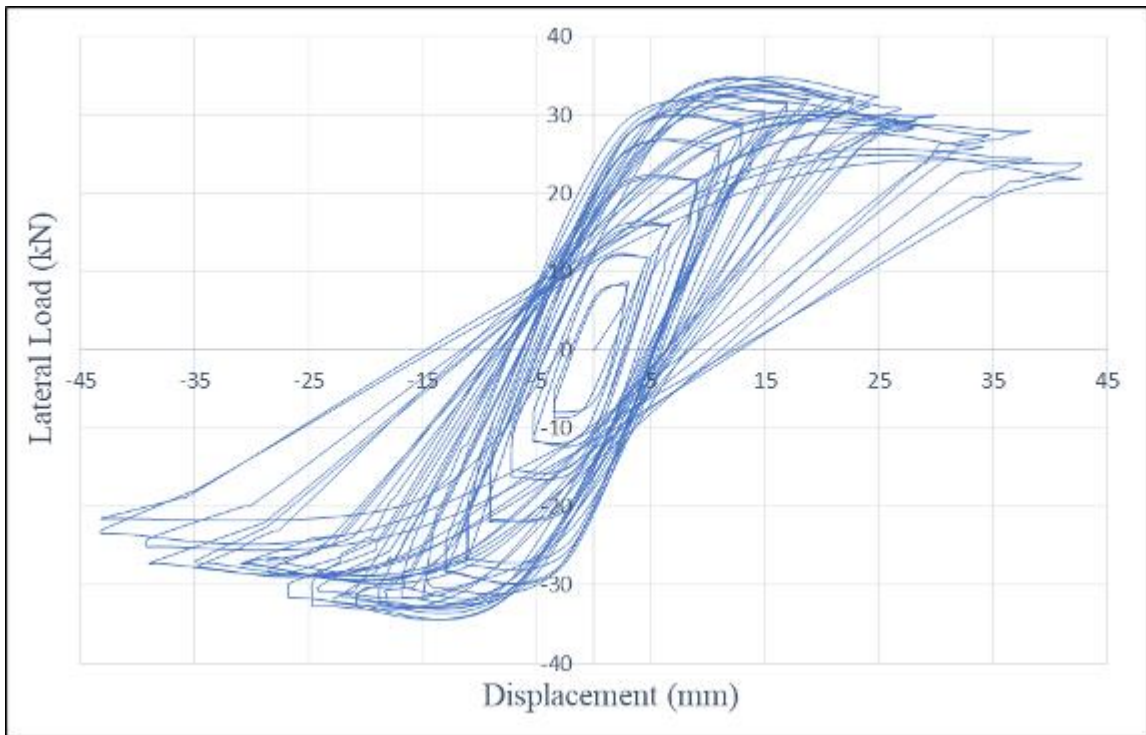


Figure 4-8 Load Displacement Diagram for CNS-S3 Specimen

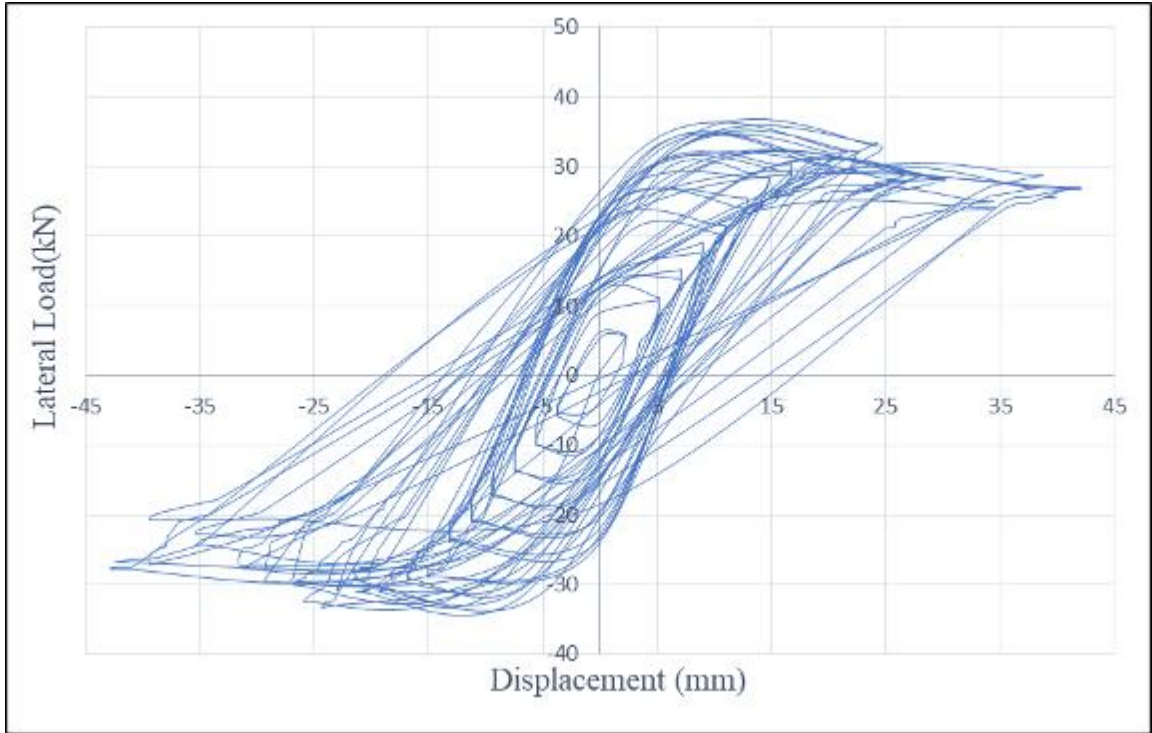


Figure 4-9 Load Displacement Diagram for CHS-C1 Specimen

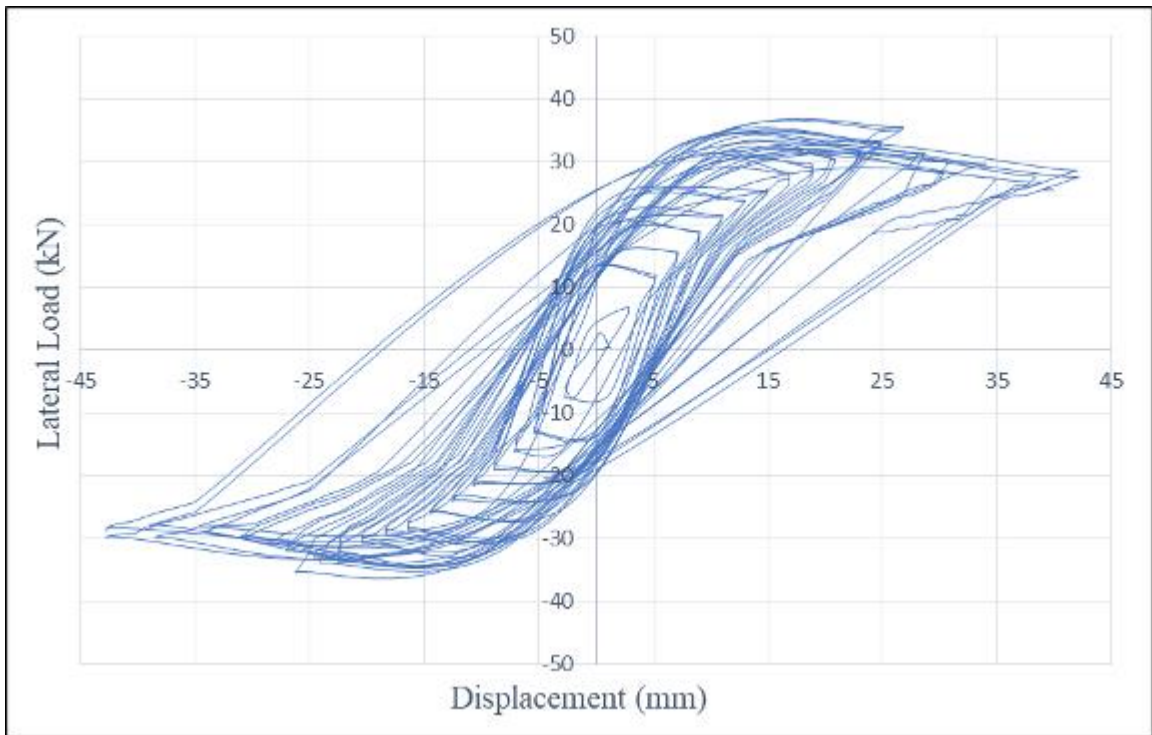


Figure 4-10 Load Displacement Diagram for CHS-C2 Specimen

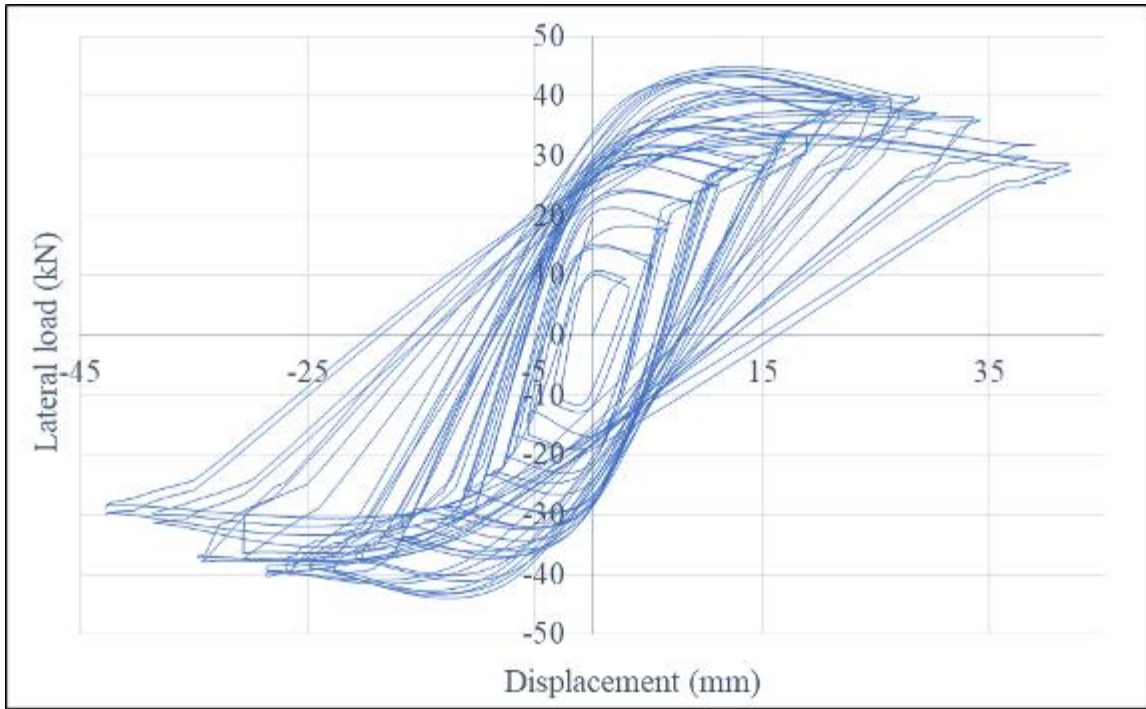


Figure 4-11 Load Displacement Diagram for CHS-C3 Specimen

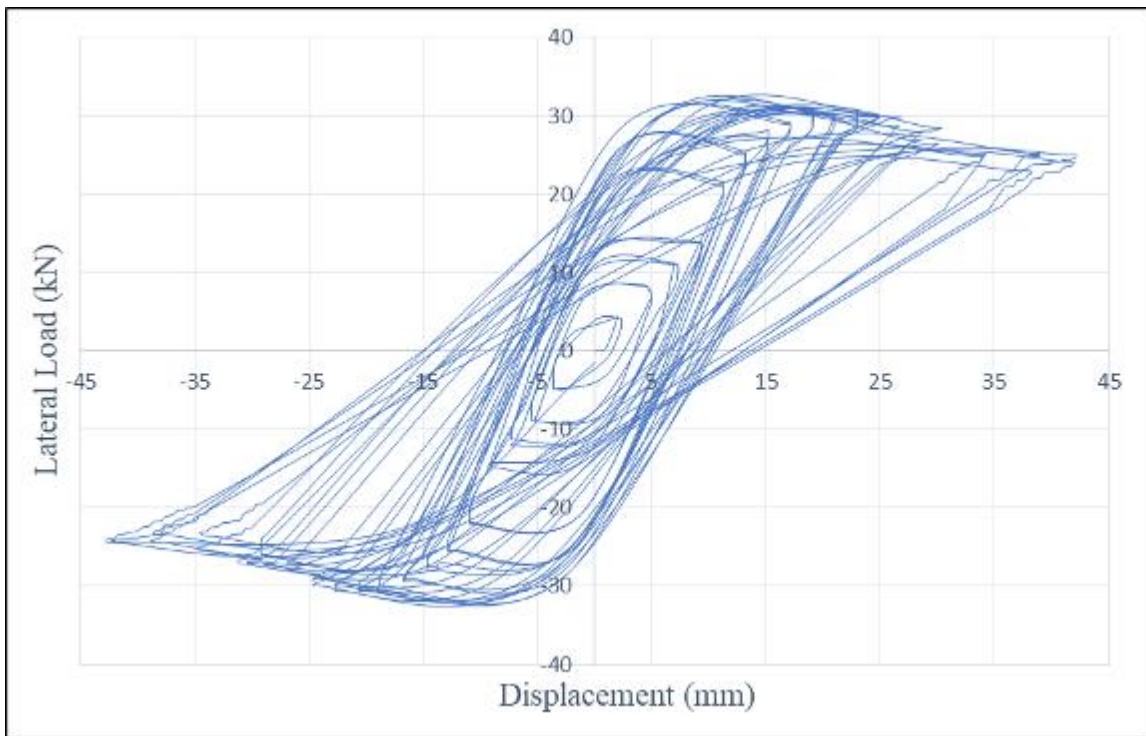


Figure 4-12 Load Displacement Diagram for CHS-S1 Specimen

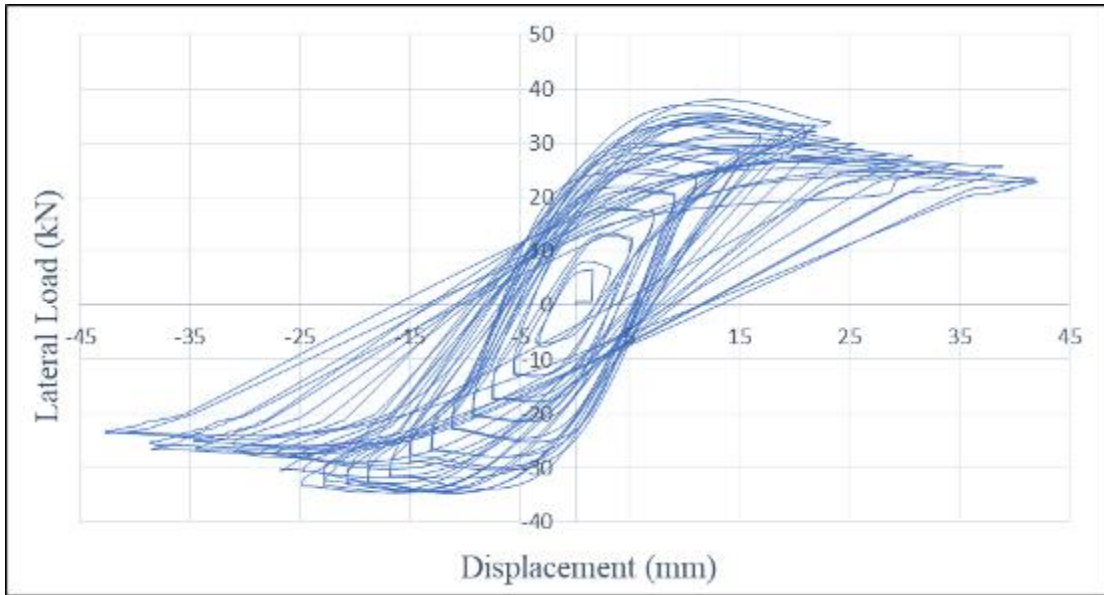


Figure 4-13 Load Displacement Diagram for CHS-S2 Specimen

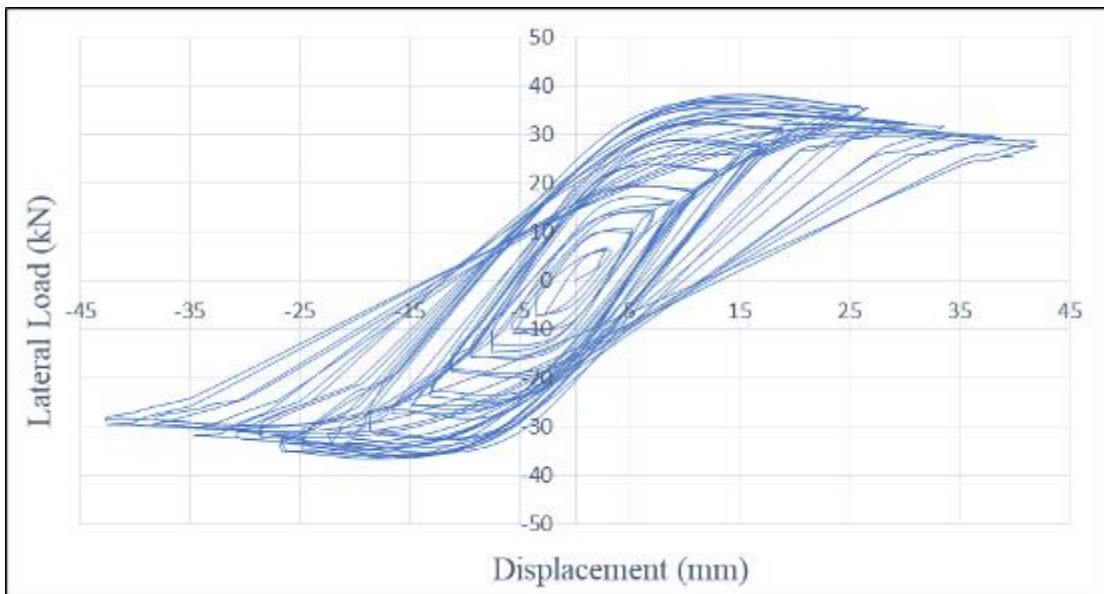


Figure 4-14 Load Displacement Diagram for CHS-S3 Specimen

The details of the symbols' names, the value of the vertical load, the maximum value of lateral load in positive and negative directions, the absolute average value of maximum lateral load, and the maximum displacement are shown in Table 4-6

Table 4-5 The failure modes of the CFDST column

No.	Symbol of Column	Max. Vertical Load (load cell1) (kN)	Max. Lateral Cyclic Load (load cell2) (kN)	Average Absolute Load (kN)	Displacement at max. lateral cyclic load (mm)
1	CNS-C1	0	31.65	31.48	22
			-31.31		-22
2	CNS-C2	38.42	32.50	32.49	24
			-32.48		-24
3	CNS-C3	71.99	33.49	33.27	26
			-33.05		-26
4	CNS-S1	0	29.36	29.62	20
			-29.88		-20
5	CNS-S2	38.34	31.39	31.42	22
			-31.45		-22
6	CNS-S3	65.49	32.42	32.51	24
			-32.6		-24
7	CHS-C1	0	33.88	33.58	24
			-33.29		-24
8	CHS-C2	47.3	35.6	35.48	26
			-35.37		-26
9	CHS-C3	72.86	39.87	40.08	28
			-40.30		-28
10	CHS-S1	0	30.44	30.53	22
			-30.62		-22
11	CHS-S2	41.5	33.91	33.39	24
			-32.87		-24
12	CHS-S3	70.8	35.94	35.61	26
			-35.28		-26

### 4.6 Skeletons Curve.

It can be gained by linking the peak points of the lateral load-displacement curve in each first cycle of cycles protocol, to create a skeleton curve. A skeleton curve is an important index for understanding inelastic seismic behavior and is used for measuring the ductility, strength, and deformation capacity of specimens. When the steel is subjected to tension in skeleton curve analysis, the loading direction is defined as positive, and the loading direction is defined to be negative when exposed to compression[12]. The skeleton curves are shown in Fig.4-15

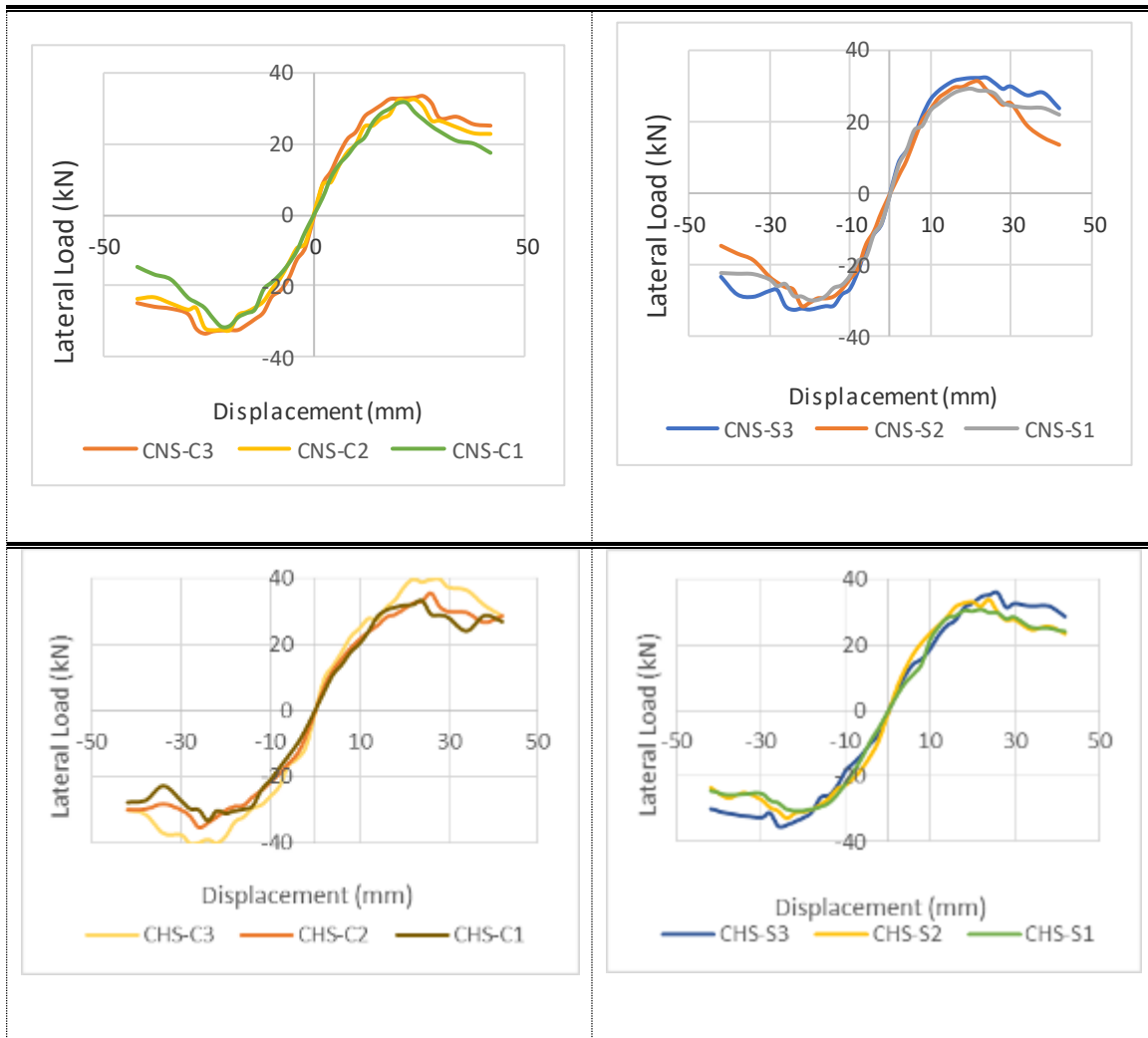


Figure 4-15 Skeleton Curve for All Specimens

## 4.7 Parameters Influence.

### 4.7.1 Influence of type of concrete:

High-strength concrete mixtures (HSC) were designed with a compressive strength of about (68) MPa, and normal-strength concrete mixtures were designed with a compressive strength of about (31) MPa. The result of the comparison between every type of axial load value with a difference of concrete type as described below:

#### 4.7.1.1 Square Section

- The lateral load of the specimen named CHS-S1 was increased than the specimen named CNS-S1 as a percentage of 3.07 % see Figure 4-16.

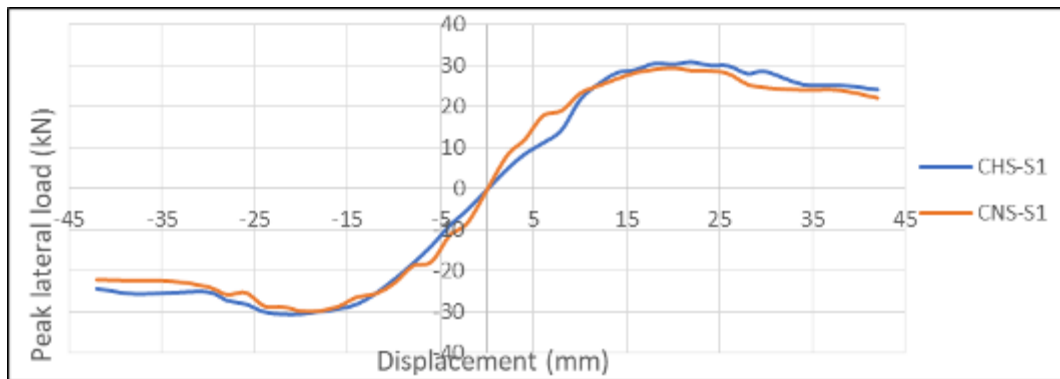


Figure 4-16 Skeleton Curve of CHS-S1 and CNS-S1

- The value of a lateral load of a specimen named CHS-S2 was increased than the specimen named CNS-S2 as a percentage of 6.26 % see Figure 4-17.

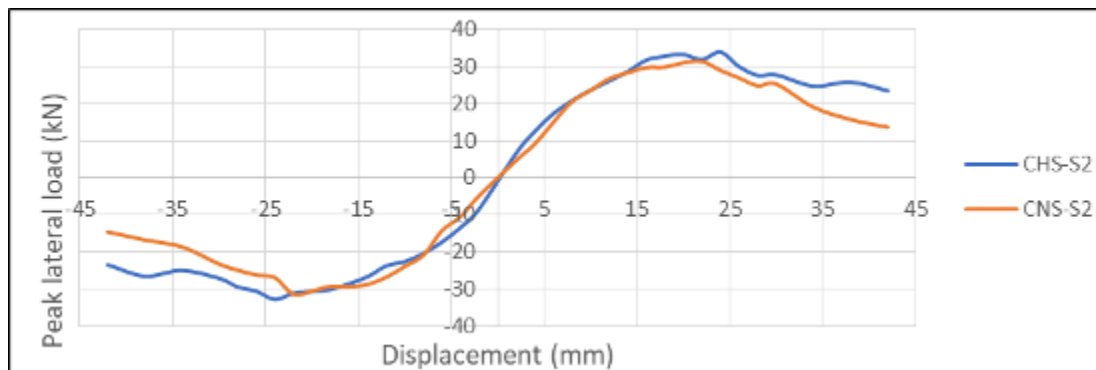


Figure 4-17 Skeleton Curve of CHS-S2 and CNS-S2



- The value of a lateral load of the specimen named CHS-S3 was increased than the specimen named CNS-S3 as a percentage of 9.53 % see Figure 4-18.

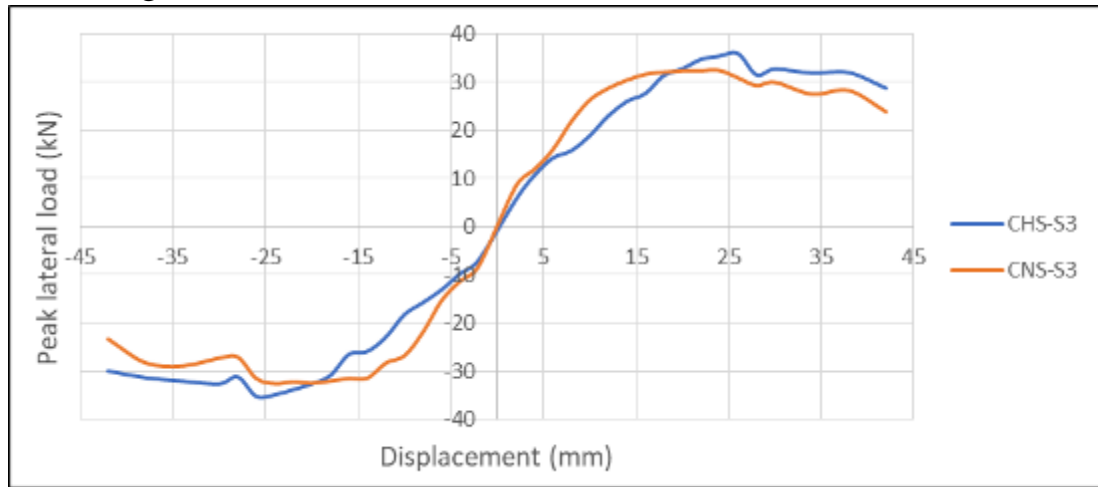


Figure 4-18 Skeleton Curve of CHS-S3 and CNS-S3

#### 4.7.1.2 Circular Section

- The lateral load of the specimen named CHS-C1 was increased than the specimen named CNS-C1 as a percentage of 6.68 % see Figure 4-19.

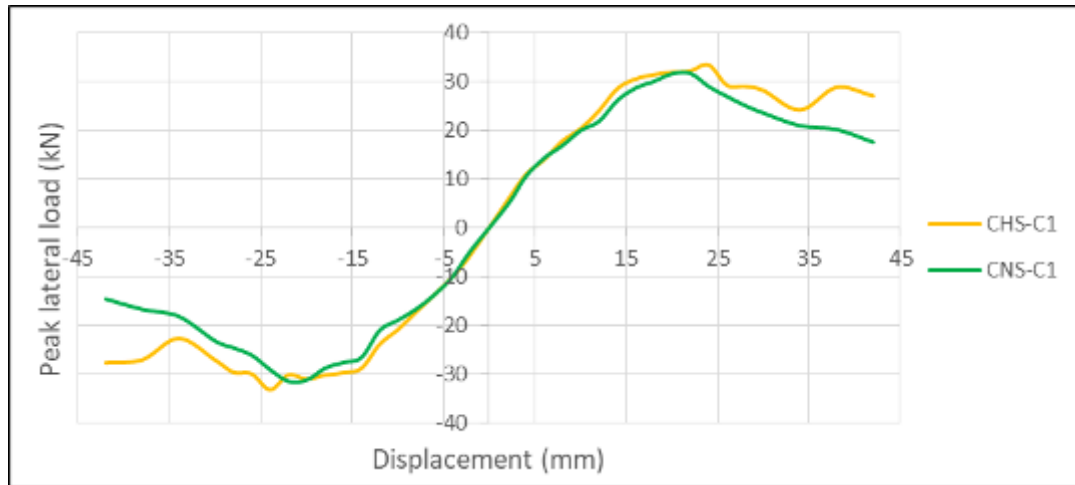


Figure 4-19 Skeleton Curve of CHS-C1 and CNS-C1

- The lateral load of the specimen named CHS-C2 was increased than the specimen named CNS-C2 as a percentage of 9.20 % see Figure 4-20.

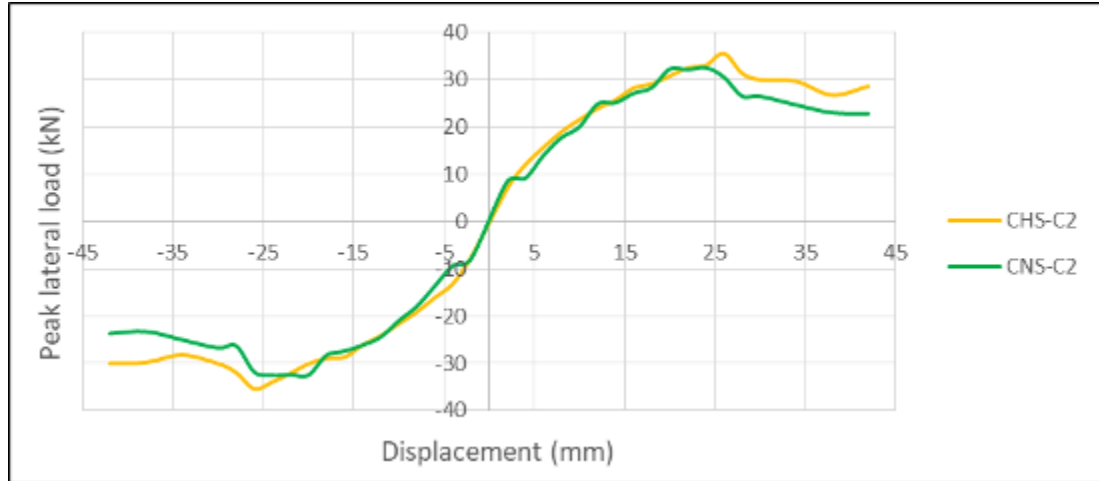


Figure 4-20 Skeleton Curve of CHS-C2 and CNS-C2

- The lateral load of the specimen named CHS-C3 was increased than the specimen named CNS-C3 as a percentage of 21.10 % see Figure 4-21.

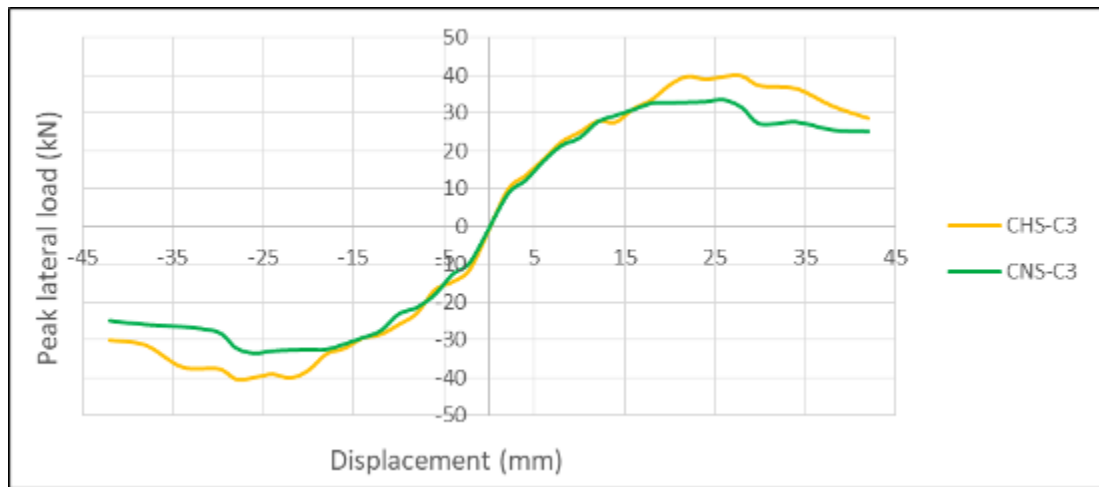


Figure 4-21 Skeleton Curve of CHS-C3 and CNS-C3

The results above proved that the influence of the high strength of concrete enhanced the performance of the resistance of composite columns to lateral loads clearly and this influence was increased whenever the value of axial load was increased.

**4.7.2 Influence of Shape of Steel Tube Cross Section:**

**4.7.2.1 High-Strength Concrete Specimens.**

- The lateral load of the specimen named CHS-C1 was increased than the specimen named CHS-S1 as a percentage of 10 % see Figure 4-22.

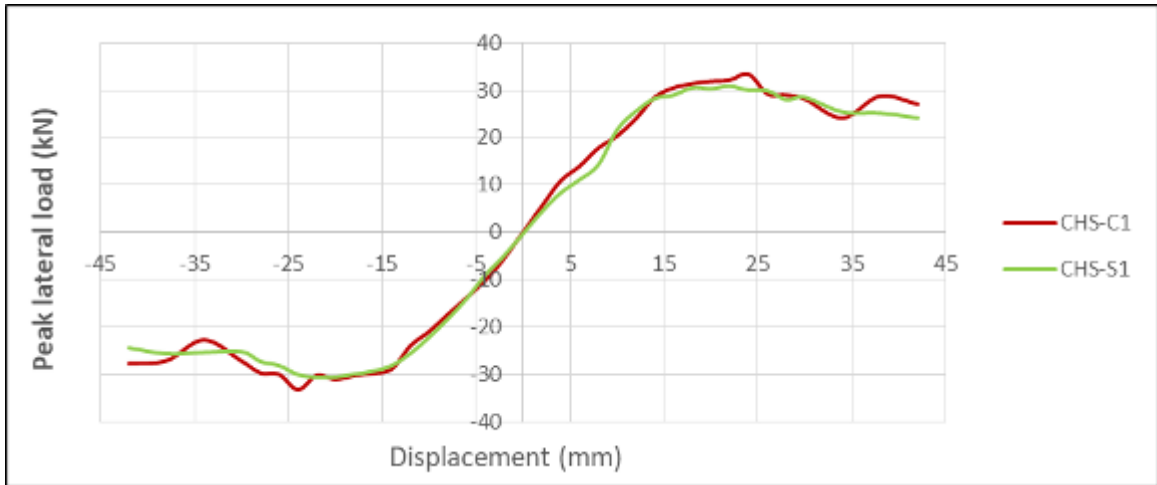


Figure 4-22 Skeleton Curve of CHS-C1 and CHS-S1

- The lateral load of the specimen named CHS-C2 was increased than the specimen named CHS-S2 as a percentage of 6.25 % see Figure 4-23.

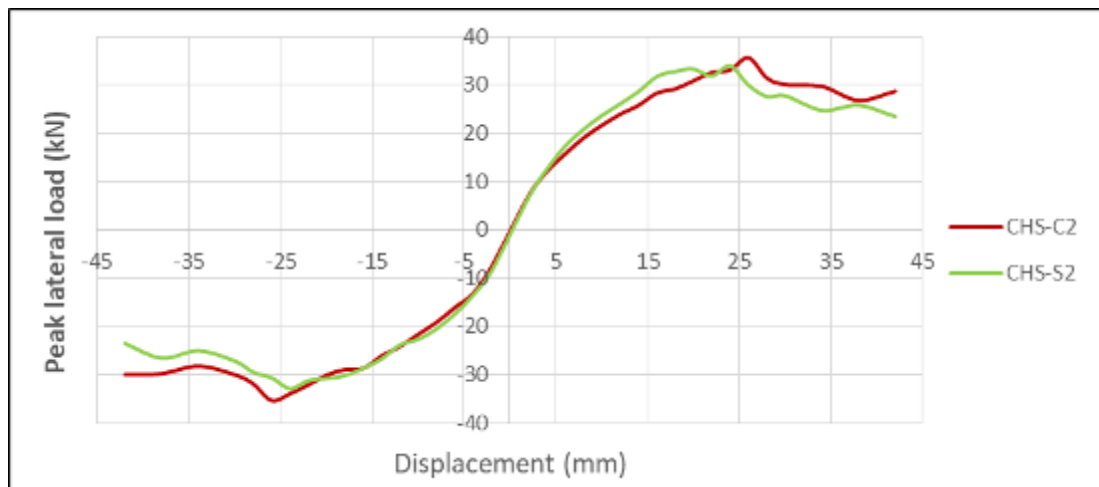


Figure 4-23 Skeleton Curve of CHS-C2 and CHS-S2

- The lateral load of the specimen named CHS-C3 was increased than the specimen named CHS-S3 as a percentage of 12.55 % see Figure 4-24.

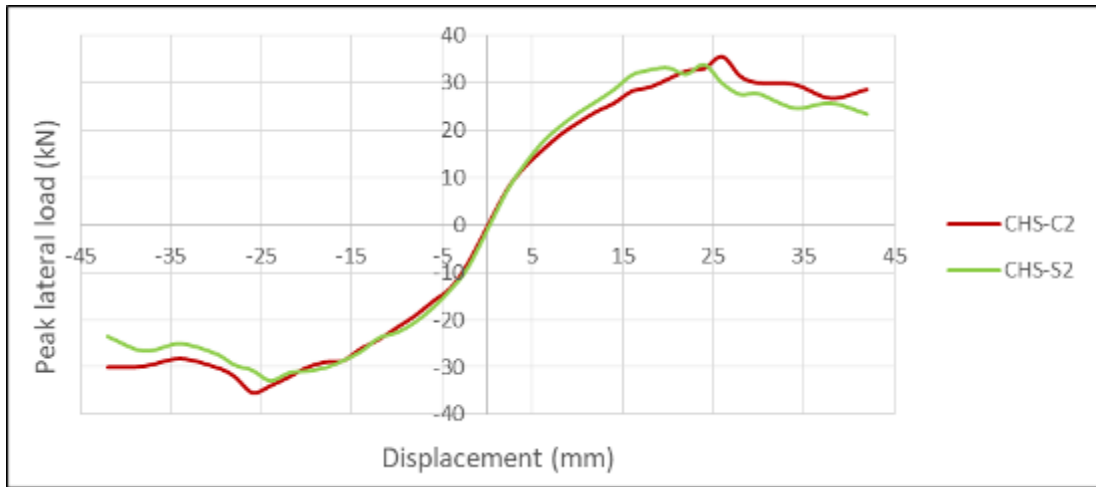


Figure 4-24 Skeleton Curve of CHS-C3 and CHS-S3

**4.7.2.2 Normal Strength Concrete Specimens.**

- The lateral load of the specimen named CNS-C1 was increased than the specimen named CNS-S1 as a percentage of 6.27 % see Figure 4-25.

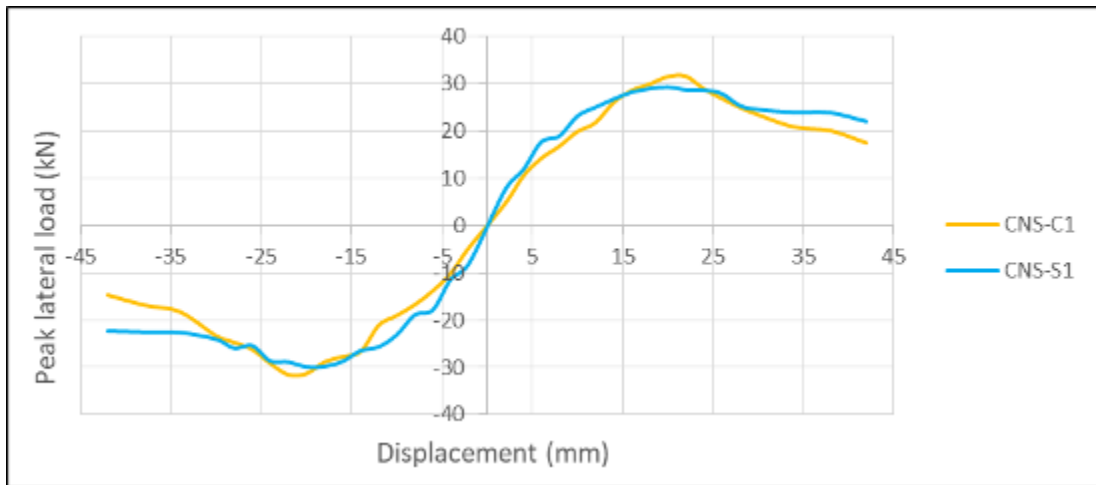


Figure 4-25 Skeleton Curve of CNS-C1 and CNS-S1

- The lateral load of the specimen named CNS-C2 was increased than the specimen named CNS-S2 as a percentage of 3.40 % see Figure 4-26.

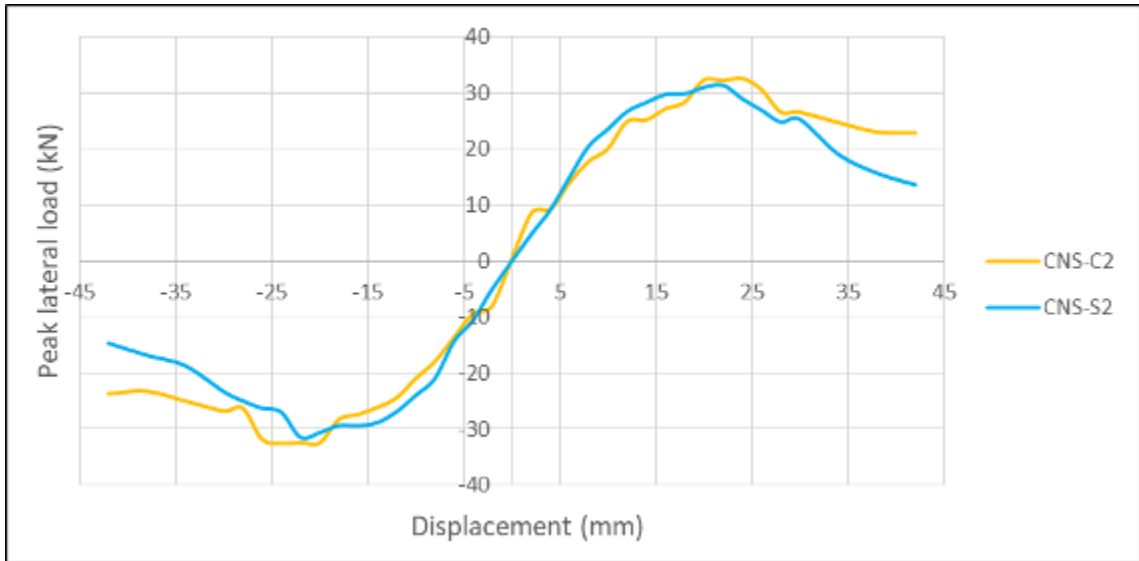


Figure 4-26 Skeleton Curve of CNS-C2 and CNS-S2

- The lateral load of the specimen named CNS-C3 was increased than the specimen named CNS-S3 as a percentage of 2.330 % see Figure 4-27.

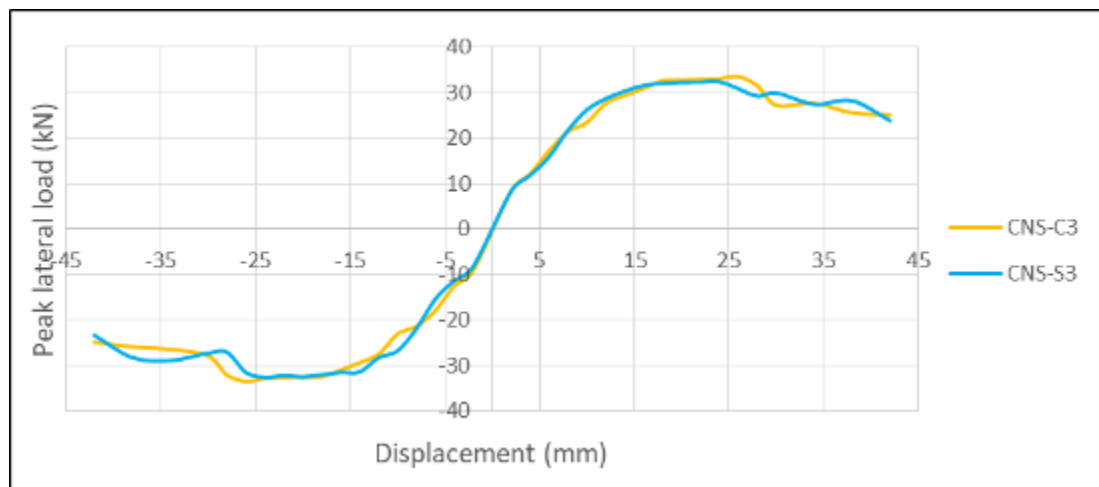


Figure 4-27 Skeleton Curve of CNS-C3 and CNS-S3

- In comparison to the precedent results to study the effect of the shape of the section of area between circular and square section area under the same conditions of the type of concrete and values of axial loads, the comparison results show that the circular section has a resistance of lateral cyclic loads greater than the square section at the same conditions that clear the circular section was more suitable than the square.

### 4.7.3 Influence of Value of Axial Loads:

#### 4.7.3.1 High-Strength Circular Specimens:

- The lateral load of the specimen named CHS-C3 was increased than the specimen named CHS-C2 by a percentage of 12.96 % see Figure 4-28

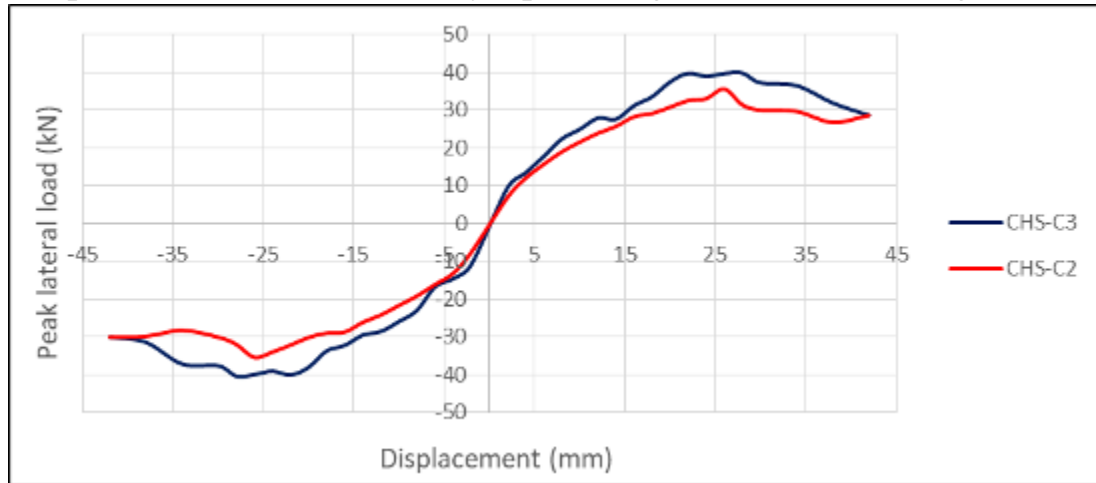


Figure 4-28 Skeleton Curve of CHS-C3 and CHS-C2

- The lateral load of the specimen named CHS-C3 was increased than the specimen named CHS-C1 as a percentage of 19.35 % see Figure 4-29.

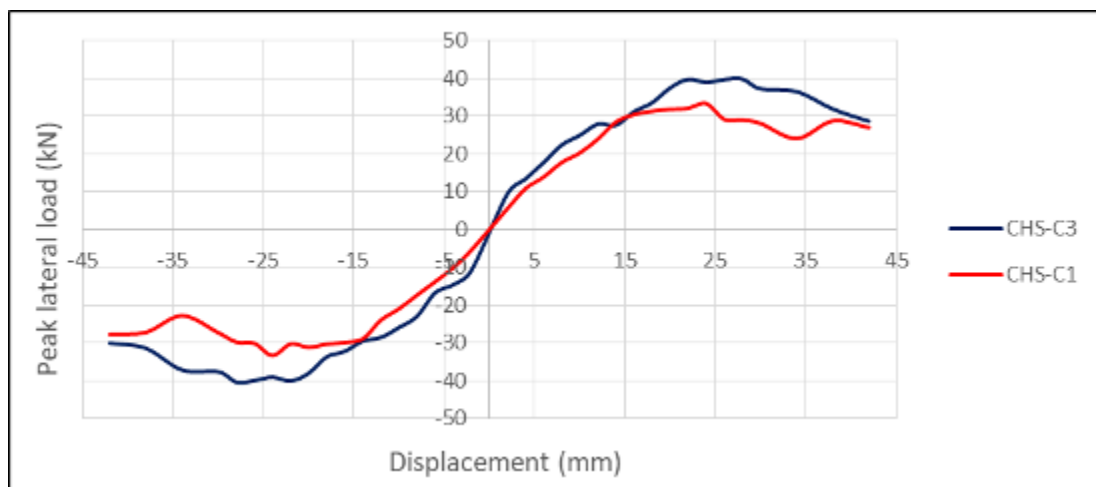


Figure 4-29 Skeleton Curve of CHS-C3 and CHS-C1

- The lateral load of the specimen named CHS-C2 was increased than the specimen named CHS-C1 by a percentage of 5.65 % see Figure 4-30.

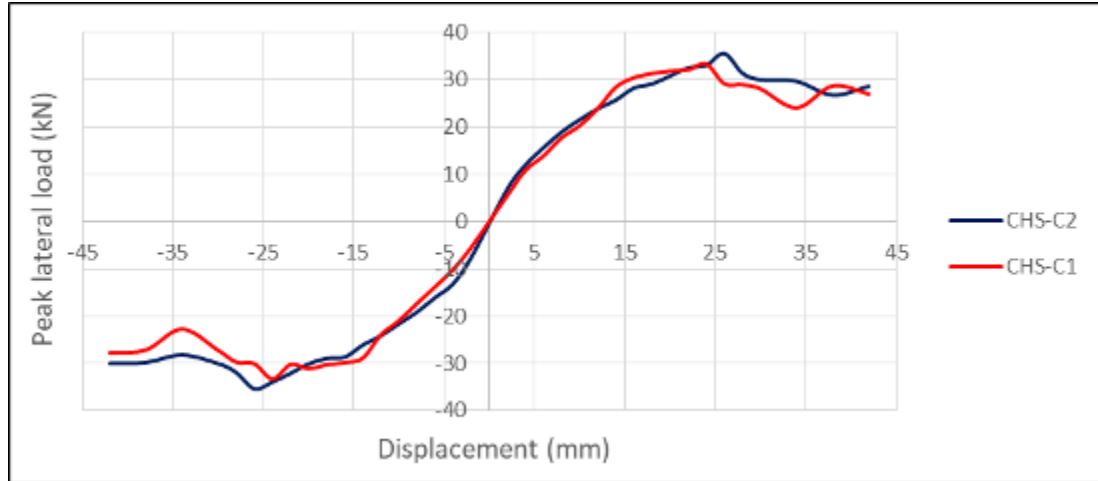


Figure 4-30 Skeleton Curve of CHS-C2 and CHS-C1

**4.7.3.2 High-Strength Square Specimens:**

- The lateral load of the specimen named CHS-S3 was increased than the specimen named CHS-S2 as a percentage of 6.64 % see Figure 4-31.

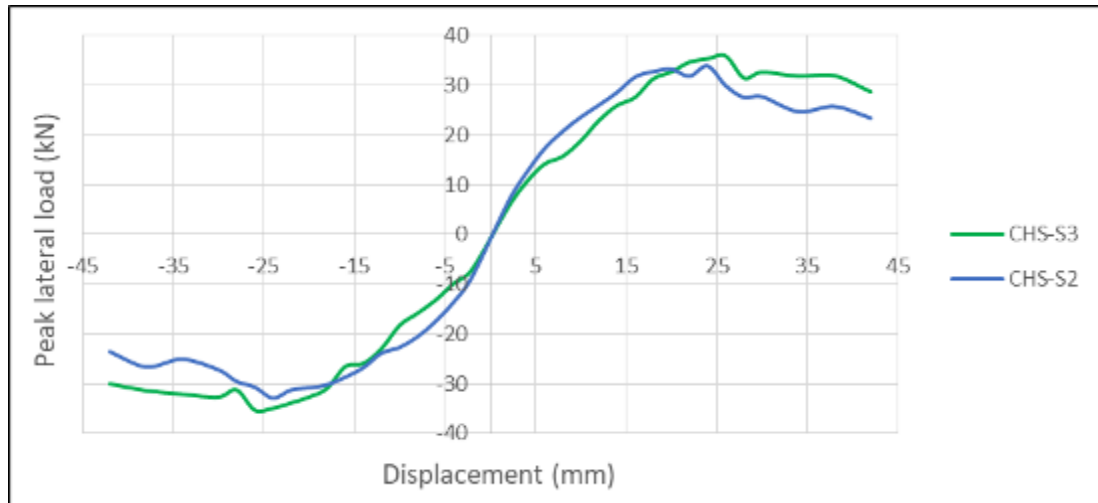


Figure 4-31 Skeleton Curve of CHS-S3 and CHS-S2

- The lateral load of the specimen named CHS-S3 was increased than the specimen named CHS-S1 as a percentage of 16.63 % see Figure 4-32.

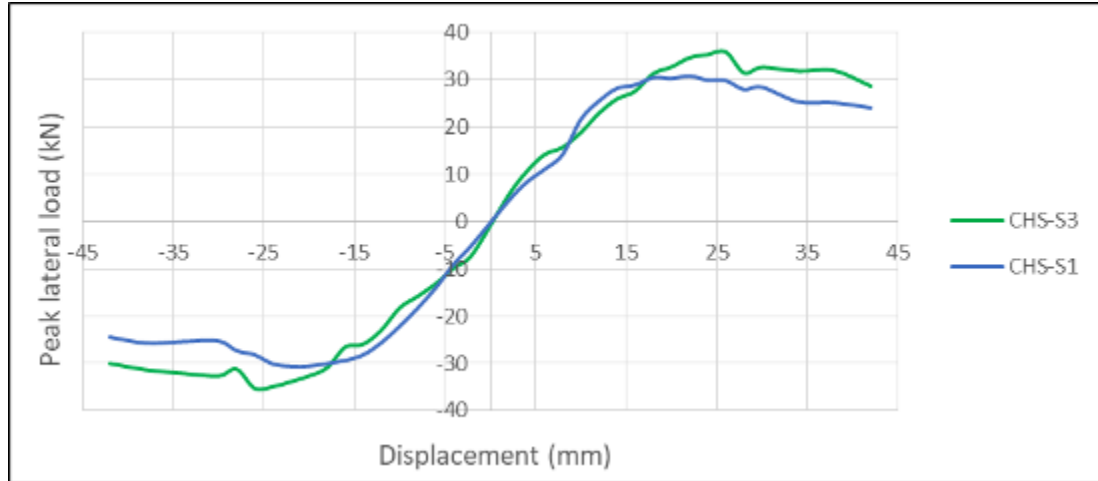


Figure 4-32 Skeleton Curve of CHS-S3 and CHS-S1

- The lateral load of the specimen named CHS-S2 was increased than the specimen named CHS-S1 as a percentage of 9.36 % see Figure 4-33.

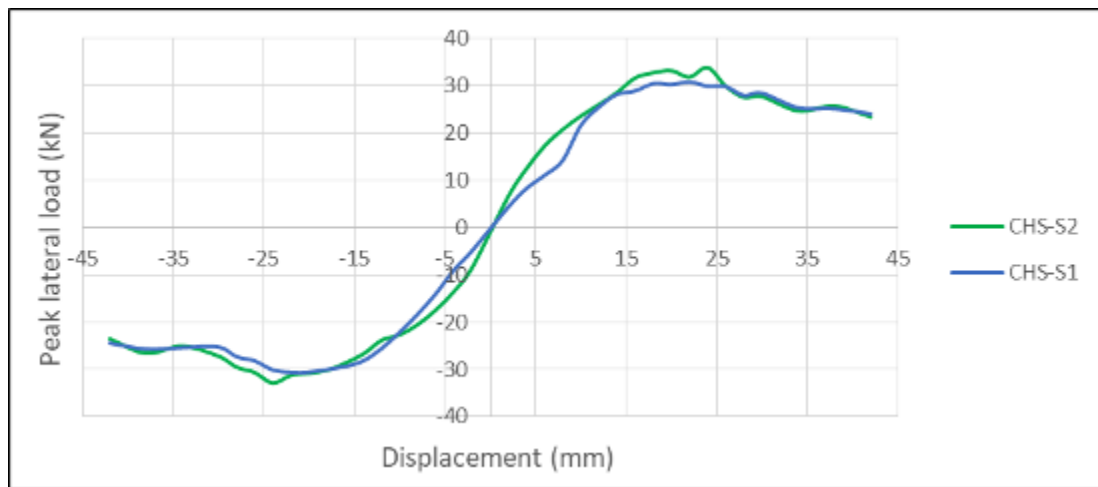


Figure 4-33 Skeleton Curve of CHS-S2 and CHS-S1

**4.7.3.3 Normal Strength Circular Specimens:**

- The lateral load of the specimen named CNS-C3 was increased than the specimen named CNS-C2 as a percentage of 2.40 % see Figure 4-34.



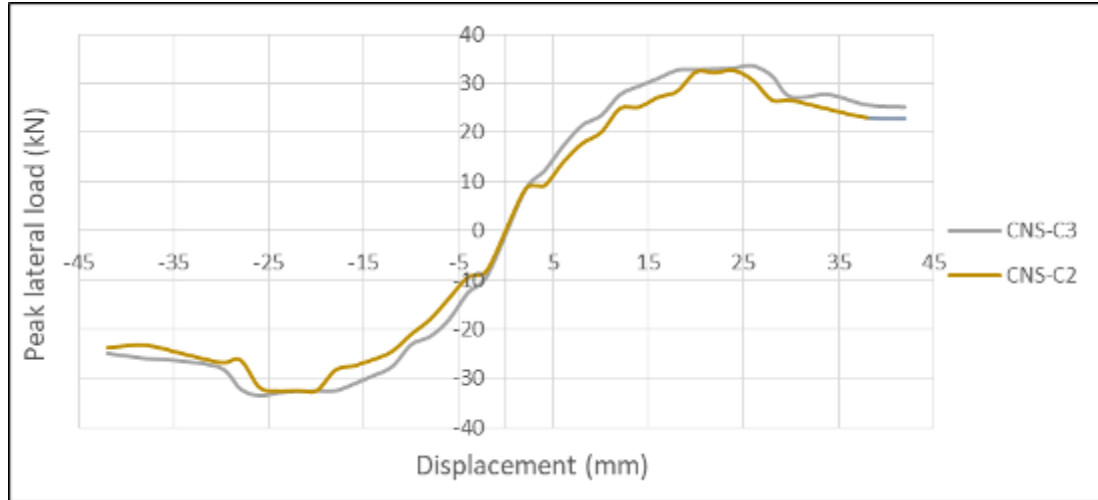


Figure 4-34 Skeleton Curve of CNS-C3 and CNS-C2

- The lateral load of the specimen named CNS-C3 was increased than the specimen named CNS-C1 as a percentage of 5.68 % see Figure 4-35.

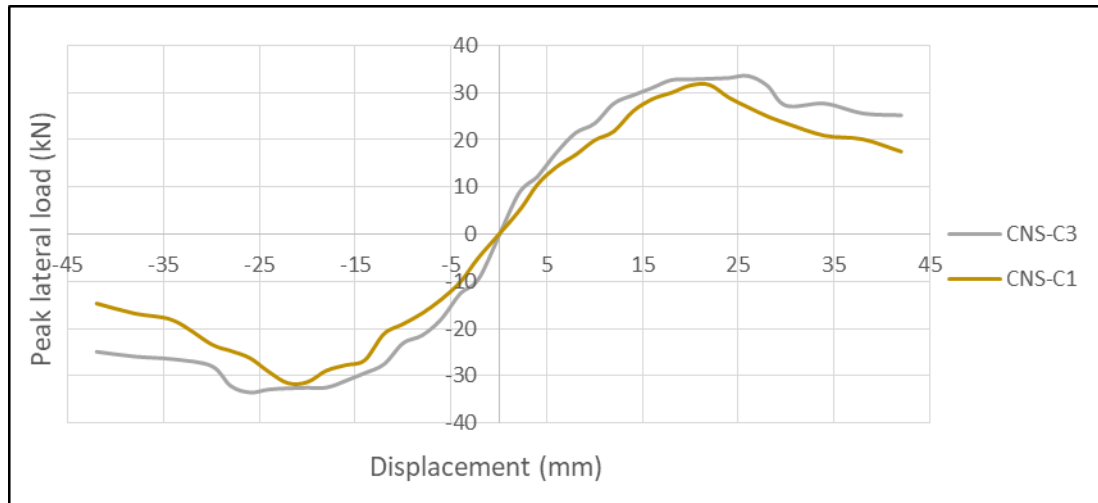


Figure 4-35 Skeleton Curve of CNS-C3 and CNS-C1

- The lateral load of the specimen named CNS-C2 was increased than the specimen named CNS-C1 as a percentage of 3.20 % see Figure 4-36.

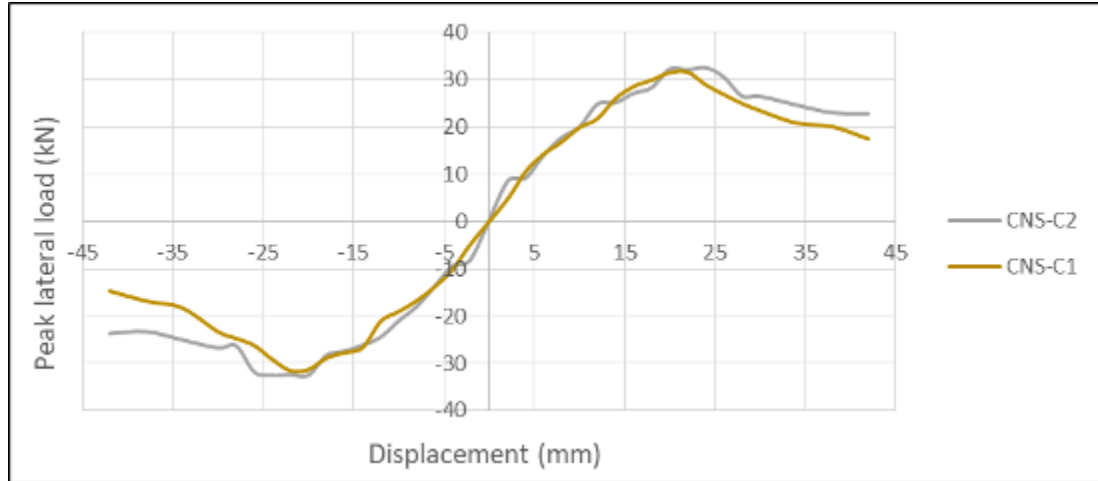


Figure 4-36 Skeleton Curve of CNS-C2 and CNS-C1

**4.7.3.4 Normal Strength Square Specimens:**

- The lateral load of the specimen named CNS-S3 was increased than the specimen named CNS-S2 as a percentage of 3.46 % see Figure 4-37.

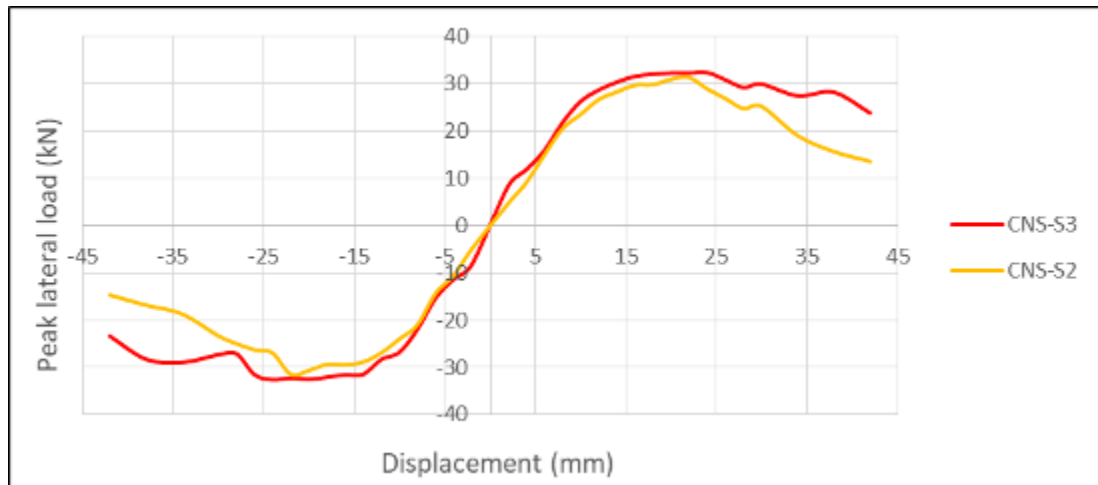


Figure 4-37 Skeleton Curve of CNS-S3 and CNS-S2

- The lateral load of the specimen named CNS-S3 was increased than the specimen named CNS-S1 as a percentage of 9.75 % see Figure 4-38.

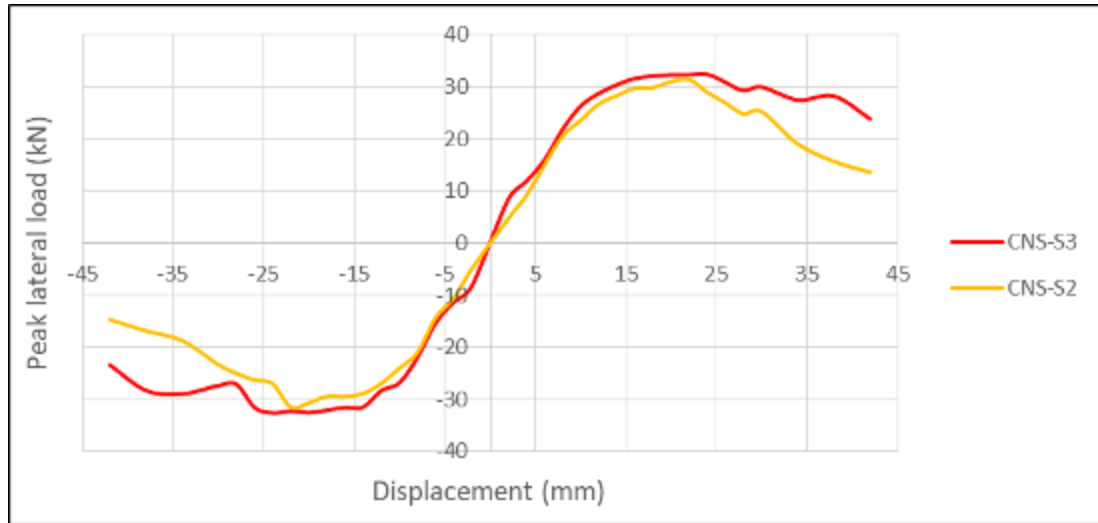


Figure 4-38 Skeleton Curve of CNS-S3 and CNS-S1

- The lateral load of the specimen named CNS-S2 was increased than the specimen named CNS-S1 as a percentage of 6.07 % see Figure 4-39.

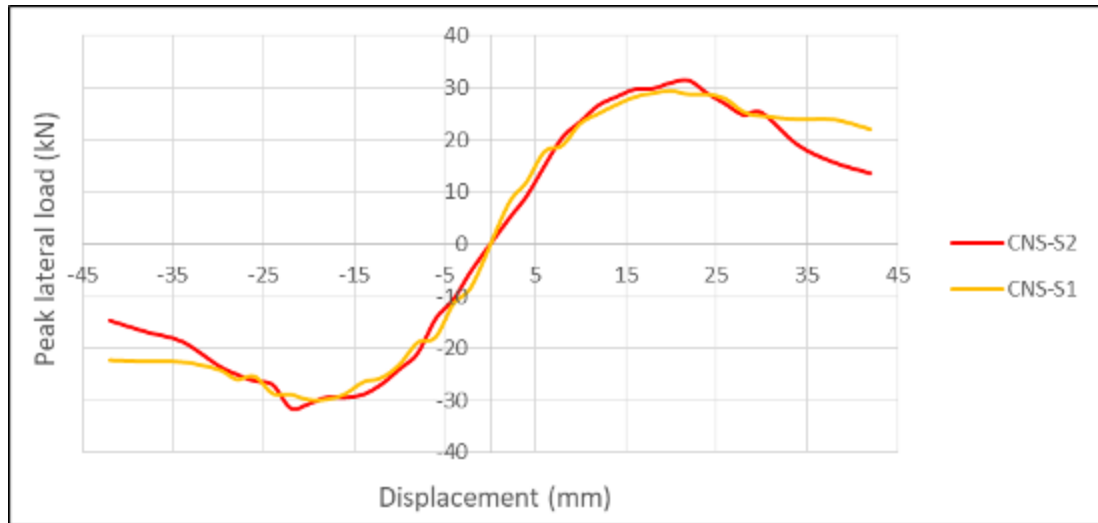


Figure 4-39 Skeleton Curve of CNS-S2 and CNS-S1

In general, the resistance of lateral load was increased significantly when the values of axial loads were increased at the same conditions of the type of concrete and shape of the cross-section area of specimens.

***CHAPTER***

***FIVE***

## **Chapter5 : Finite Element Simulation**

### **5.1 General**

Large simulation models are frequently needed to obtain a thorough knowledge of design details as design complexity increases. The Finite element applications (FEA) system should allow the analyst to efficiently use available computing resources to run big problems. Abaqus uses the most recent high-performance features of General-purpose graphics processing units (GPGPUs), High-performance computing (HPC) architectures, and Central processing units (CPUs) to ensure that you rarely cannot achieve an adequate simulation due to model size limits. Because the code completes complex jobs on time, users value being able to stick to timelines. Realistic representations rapidly reveal how painstakingly the code designers attended to the intricacies. Large model needs from real life are met with resilience by Abaqus. In this chapter, the Abaqus program (version 2021) was used to represent and simulate the composite columns samples that were tested experimentally in the lap and ensure the accuracy of the results.

### **5.2 Parts of Model**

One of Abaqus's features provides a multipurpose modeling stage and it can import components from other programs, such as AutoCAD, using appropriate and varied file extensions. Generally, geometrical modeling was implemented in 3D elements. Additionally, depending on the simulation condition, some of the elements are deformable, while others are stiff. Geometrical modeling requires six parts in total for two models square and circular cross-section columns. They are as follows: Concrete column, outer steel tube, inner steel tube, stiffeners (four numbers), top and bottom plate.

Concrete columns, stiffeners, and top and bottom plates for two models were constructed by using 3D- Deformamable –Solid Element(C3D8R), and outer and inner steel tubes were constructed by using 3D- Deformamable –Shell Element (S4R) as shown below in Figure 5-1and Figure 5-2.

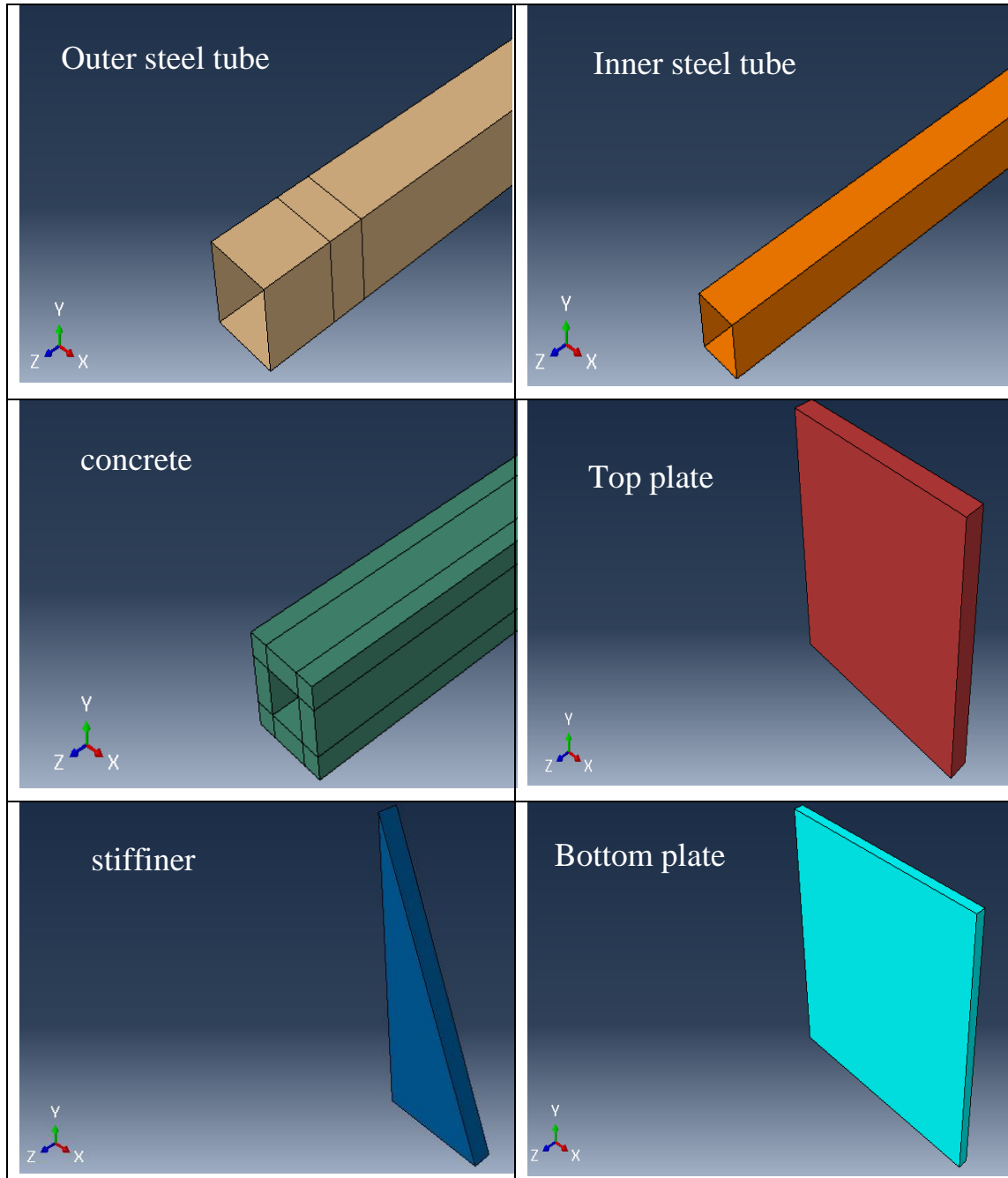


Figure 5-1 Part Modeling for Square Columns

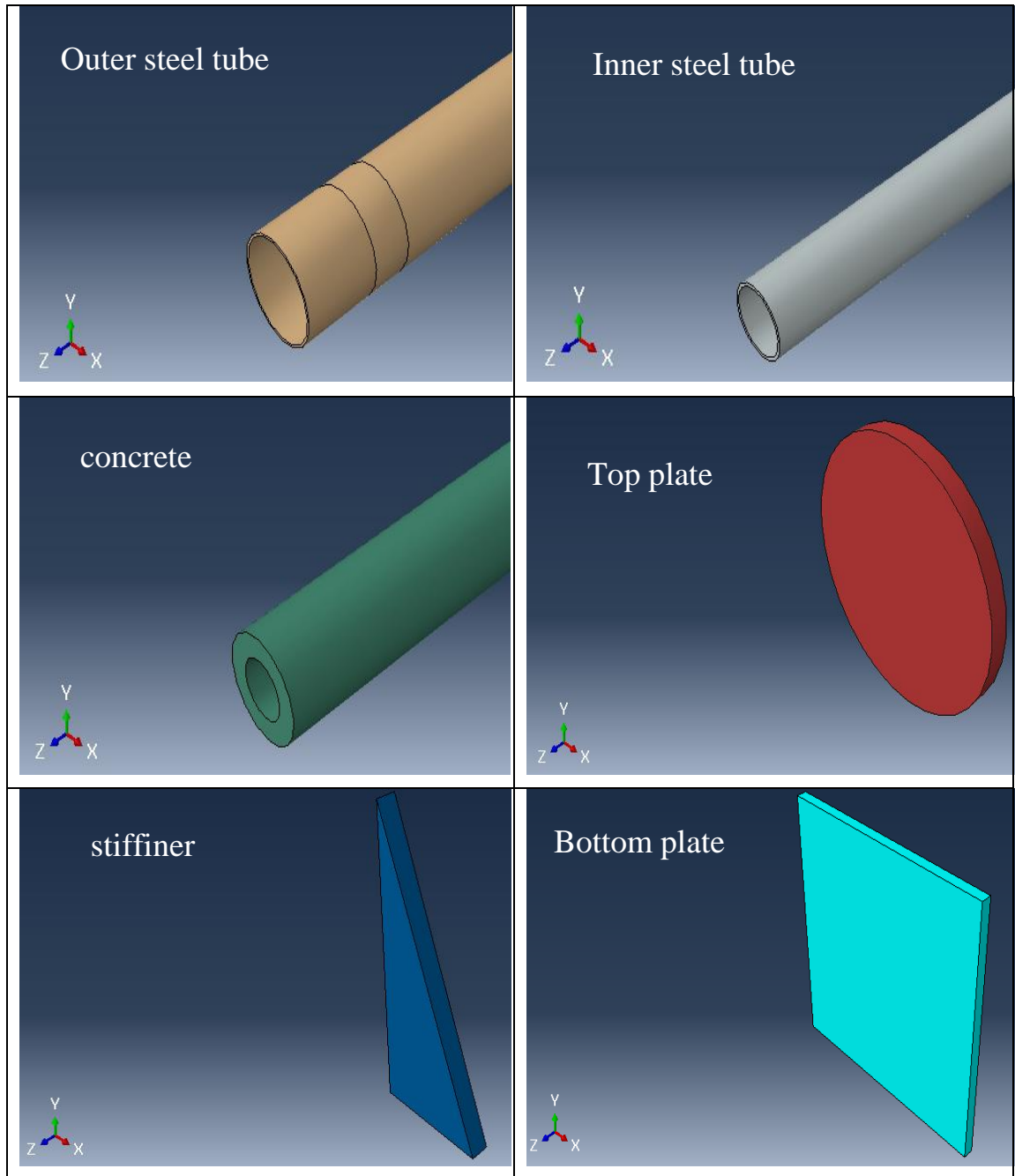


Figure 5-2 Part Modeling for Circular Columns

### 5.3 Materials Properties

Abacus have different material properties that indicate their behaviors under various conditions, and types of materials used like concrete, and steel.

### 5.3.1 Concrete Material Representing.

Elastic and plastic phases are employed to simulate concrete elements. The elastic phase is modeled for isotropic materials, presenting simple linear elasticity with the material constants being the Poisson ratio ( $\nu_c$ ) and the Young modulus of elasticity ( $E_c$ ). The International Federation for Structural Concrete (FIB) model code indicates that Poisson's ratio parameter ranges from 0.1 to 0.2. Numerous academics advise that the default value for concrete be set at 0.17 and  $E_c$  about 37658.9 MPa for high-strength concrete and used  $\nu_c$  at 0.18 and  $E_c$  about 30588.56 MPa for normal concrete. In the plastic phase concrete damages plasticity because of its ability to predict the behavior of concrete under different conditions. The value of the parameters selected is shown in Table 5-1 below:

Table 5-1 Concrete Damage Plasticity Value[48]

parameter	Dilatation angle ( $\Psi$ )	Eccentricity ( $\epsilon$ )	$f_{b_o}/f_{c_o}$	K	Viscosity parameter ( $\mu$ )
High strength	40	0.1	1.16	0.667	0.001
Normal strength	30	0.1	1.16	0.667	0.001

The dilatation angle ( $\Psi$ ) influences the degree of plastic deformation within the K volume. It varied between 20°–45° in values. Additional characteristics included, the plasticity number (K), which determines the yield surface's form and is the rate at which the tensile to compressive transition occurs. It can be acquired by utilizing the formulas listed in Table (5.1), where default values were chosen from the Abaqus user handbook. The shape of the plastic potential surface in the meridional plane is described by the eccentricity of the flow potential ( $\epsilon$ ). The viscosity



parameter ( $\mu$ ) is employed to guarantee the proper convergence of the study[49]. In compressive behavior used curve in the plastic region represents the stress-strain curve as shown in Figure 5-3

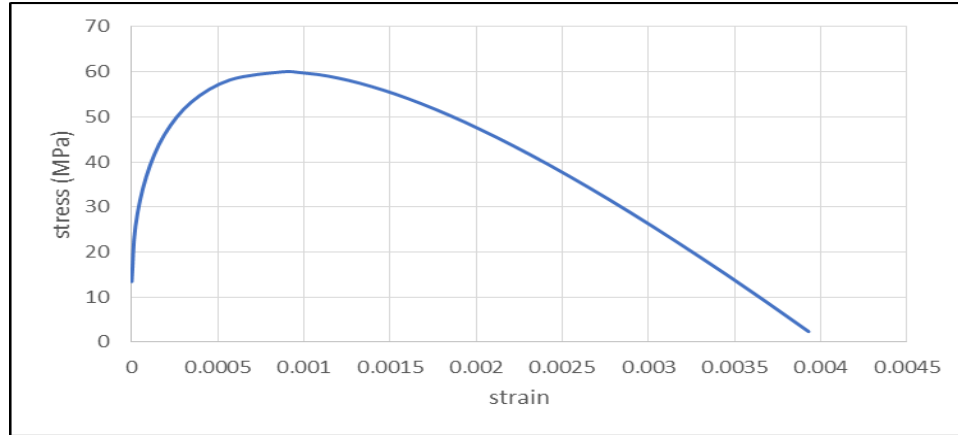


Figure 5-3 Compressive Stress-Strain Behavior

In tensile behavior, the curve of stress-strain simulated in the plastic region has a detail as shown in Figure 5-4

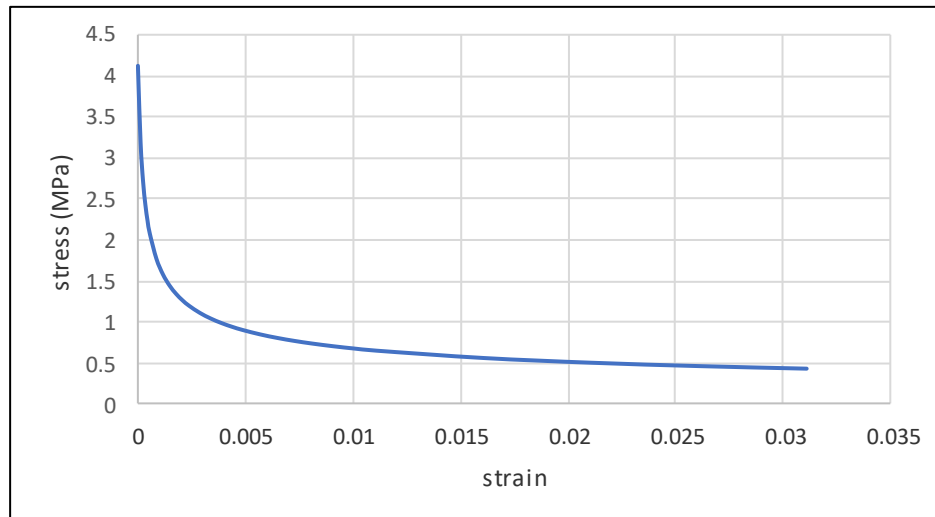


Figure 5-4 Tensile Stress-Strain Behavior

### 5.3.2 Steel Material Representing

In this study, elastic and plastic properties of steel were implemented assuming Poison's ratio ( $\nu_s$ ) and modulus of elasticity  $E_s$  for all steel is 0.3

and 201229 MPa respectively. With the plastic phase the yield stress  $f_y$  for steel used in the tube assumed as 315 MPa was calculated from the steel test as mentioned in chapter three, and the yield stress  $f_y$  for the top and bottom plate and stiffeners assumed 600 MP a higher than the same of steel tube to ensure that it is not collapsed firstly.

### 5.3.3 Sections

Generally, all materials in Abaqus require a section definition. A section contains details about the parts. The characteristics of the chosen sections depend on the type of part being simulated. The section of concrete, top and bottom plate, and stiffeners had been assigned as a “solid homogeneous” and the outer and inner tube had been assigned as a “shell homogeneous” and the order( assigned section )used to connect the parts with materials.

### 5.4 Assembly

Assembly module means that every part of the model was collected in the coordinate system and made independent of the other parts in the model.

The assembly parts of the models are shown in Figure 5-5

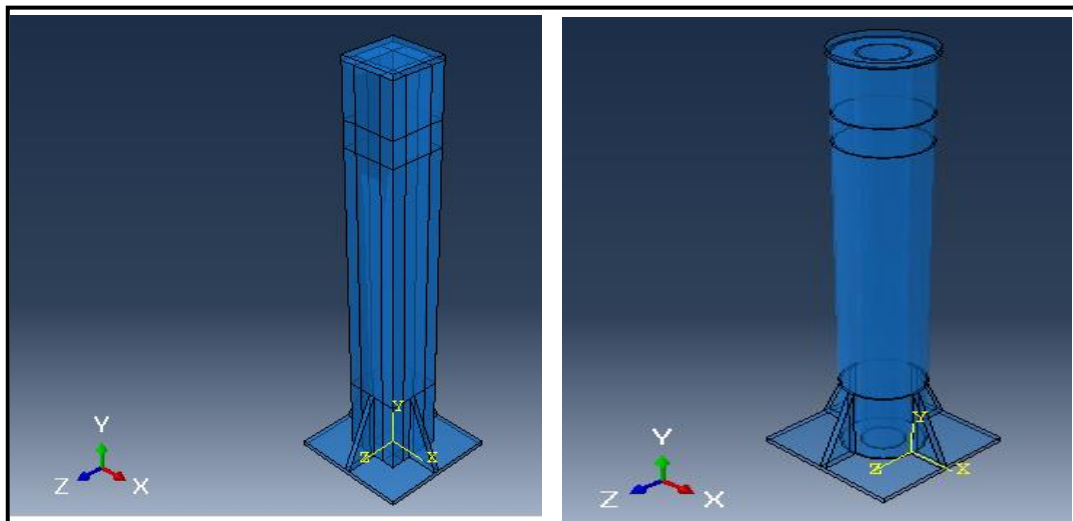


Figure 5-5 Assembly for Square and Circular Models

### 5.5 Interaction

In this study several types of interaction were used as the properties and requirements of the model, Coupling constraints were used in the region that the displacement effected, and (Tie interactions) were used between the vertical side of stiffeners (master surface) and the bottom part of outer steel tube (slave surface), Tie interaction was used between the bottom surface of stiffeners (master surface) and the bottom plate (slave surface), the other parts of the model interacted with surface to surface between concrete and steel tube, the formula of friction is Penalty, Isotropic, and the coefficient of friction is used 0.7. The reference point of the load (lateral and axial) had been interacted by coupling with the surface that it had been effected. Figure 5-6 show the details of interactions.

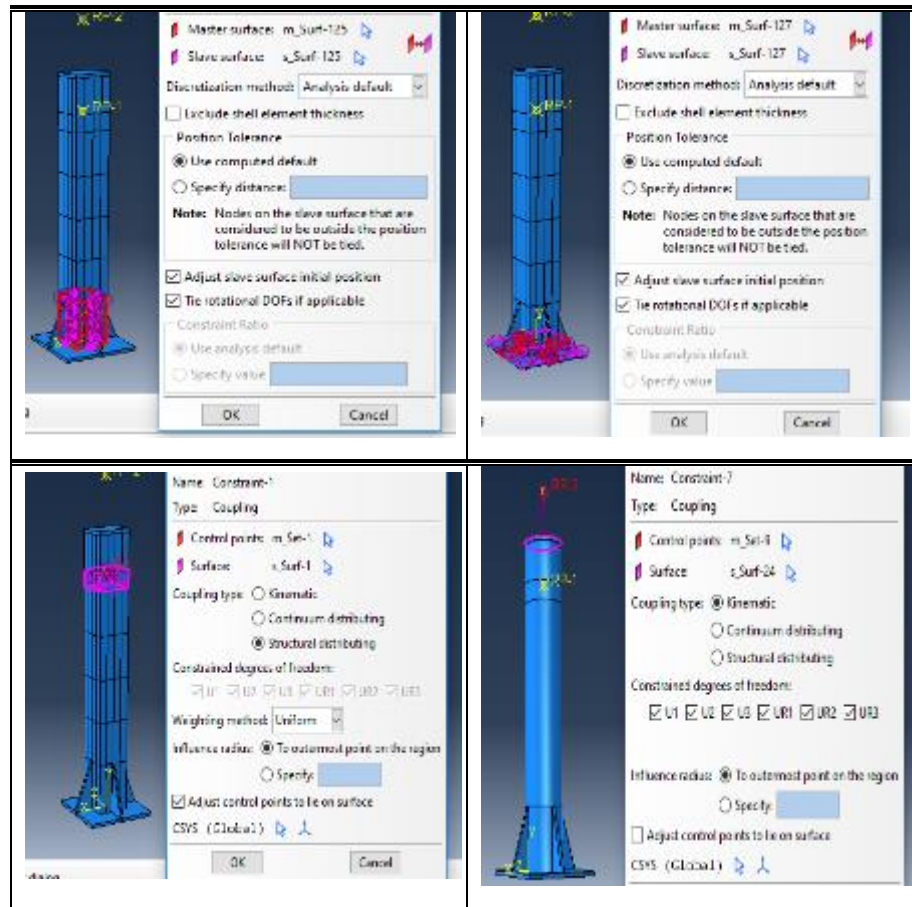


Figure 5-6 Models Interaction Simulations

## 5.6 Meshing

The most important phase in finite element modeling is mesh size selection. An adequate pre-analysis of several mesh densities was carried out before the analysis to identify the optimal density that provides the required accuracy given the complexity of the analysis. A reasonable amount of elements divided into the model leads to an adequate convergence of the results. This is essentially observed when a small change in the mesh size affects the outcome. To determine the proper mesh size, a convergence study was performed on the columns model in the current FEM. Finding the ideal model mesh size with the fewest possible elements and maximum convergence with the experimental test findings is the primary goal of the convergence study. To do the convergence investigation, the model's element size was reduced from 25,20 and 10 mm. discovered that 20mm was more in line with the lab findings, and it was accepted as shown in Figure 5-7 and Table (5-2) show the agreeable size of mesh.

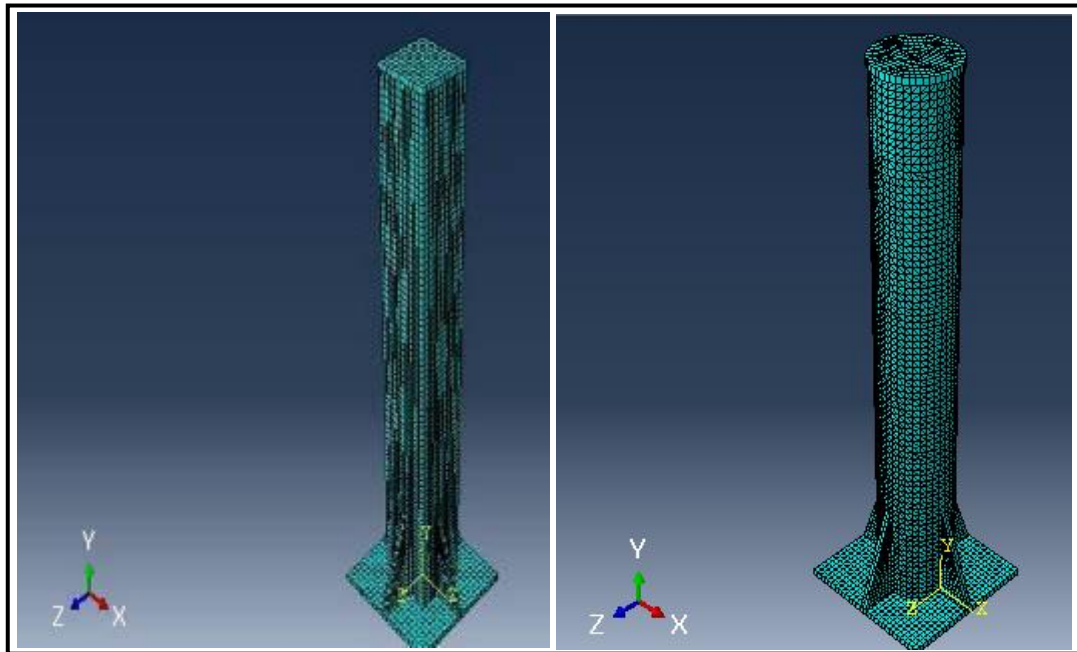


Figure 5-7 Typical Applied Meshing for Square and Circular Model

Table 5-2:Effect of Mesh Size on Ultimate Load and Deflection

Mesh size (mm)	Name	Ultimate load (kN)	Maximum deflection (mm)
10	Exp.	31.48	22
	Num.	40.55	29
20	Exp.	31.48	22
	Num.	32.92	21.46
25	Exp.	31.48	22
	Num.	27.89	16.7

### 5.7 Loading and boundary conditions

In structural analysis, Abaqus offers an extensive number of methods and features for using mechanical, thermal, or a mix of the two. In general, forces, pressures, defined displacements, and inertia forces (such as gravity) can be used to characterize mechanical loading. In this process, initial mechanical displacement/rotation had been selected to investigate the fixed case at the support (bottom plate), and at step 1 at the first case that has no axial load, mechanical displacement/rotation had been also implemented to represent the displacement applied at (100) mm from the top of the column as experimental work implemented, to investigate the lateral cyclic case excel sheet with positive and negative value start with (2,-2) till(42,-42) mm had been input as an amplitude by define the lateral displacement (U1) and fixed other values, this mechanism of load made the numerical model looks like the same in experimental work. Many academics advise using the adopted method because it can solve the majority of divergent problems. Furthermore, Abaqus generated 6 degree of freedom for each node as shown in Figure 5-8

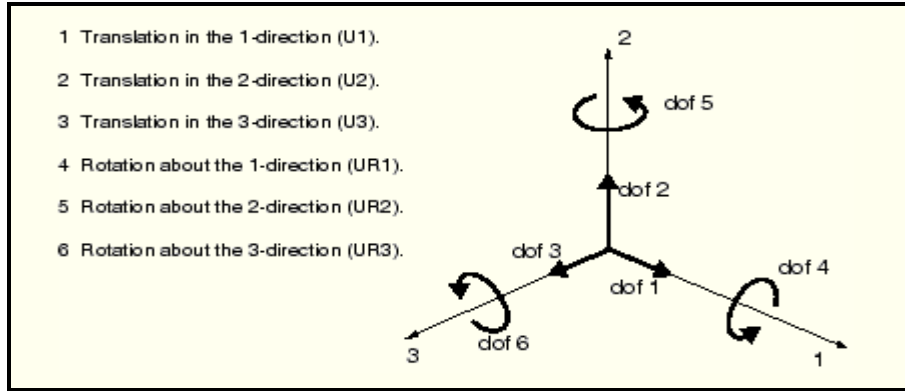


Figure 5-8 Displacement and Rotation Degree of Freedom

The simulation of boundary condition at the support and displacement control at step 1 shown in Figure 5-9 below represents case one that has lateral cyclic load only without axial loads as the same case in experimental work.

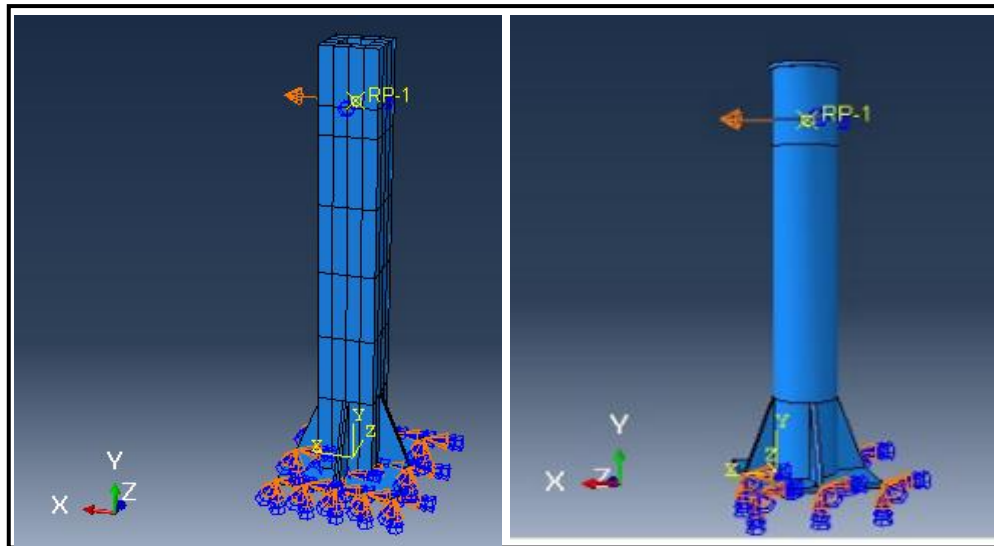


Figure 5-9 Boundary Conditions and Lateral Displacement on Model

The second case of simulation is that the specimens have an axial load in step 1 in addition to the lateral cyclic load with two types of value. The first value represents the implemented dead load only, and the other value of an axial load represents dead and live load together. An axial load entered in this step as a concentrated force that was calculated in Appendix B on the

surface area of the top plate of the column in step1 and it was entered as an amplitude represented time with load by making the axial load constant along the time of the step was 40 kN for dead load and 70 kN for dead and live load and implemented at the same time of projecting the lateral load as it has done in experimental work see Figure 5-10.

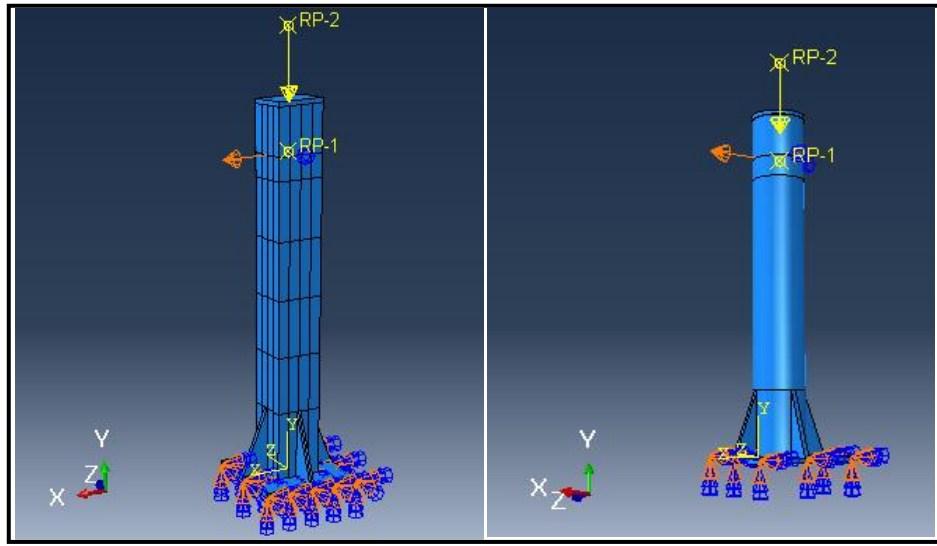


Figure 5-10 Boundary Conditions, Lateral Displacement, and Axial Force on Model

The Dynamic Implicit step analysis was implemented at step 1 to apply displacement and loads in this study, dynamic analysis can be done if the simulated system is dependent on time. During a dynamic step a time period was assigned to the analysis, because it is necessary for the amplitude options. Abaqus/Standard defaults to a time period selected as (1). Incrementation was assigned Automatic. The field output and history output were created to simulate forces, displacement, energy, stress, strain, and failure/fracture.

## 5.8 Results and Analysis

In this part, the numerical justification concerning the experimental study findings was completed in terms of the load–deflection curves for all of the specimens. The consequences of the finite element analysis were

assembled, arranged, and compared with the results that obtained from experimental work. The comparison was dependent significantly on the ultimate lateral load capacity relation with displacement, and failure mode.

### 5.8.1 Validation of Numerical Study

In this section, the load-deflection curves for each specimen were obtained, along with a numerical validation based on the experimental work findings. Concerning the ultimate deflection and load-carrying capacity of columns, all numerical calculations showed good and close agreement with experimental results. Figure 5-11 shows that the failure mode of the numerical model is the same as experimental. The numerical results of the specimens are presented together with their load-deflection behavior, Table 5-3 represents the observed percentage of variance for the load capacity and the corresponding deflection.

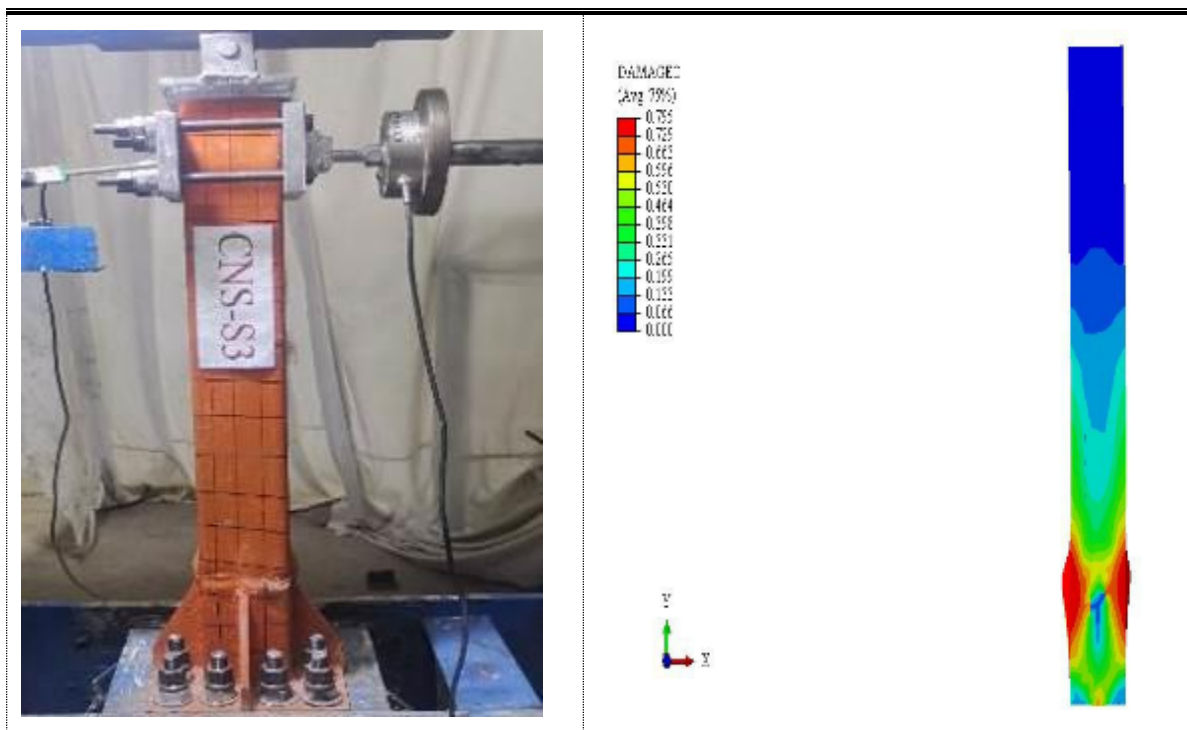


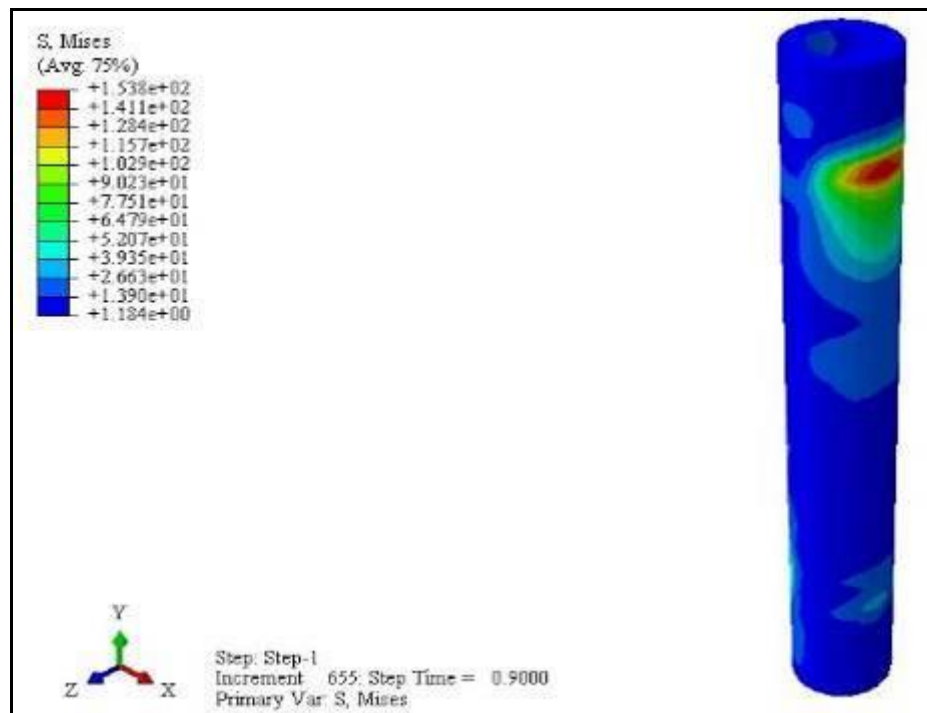
Figure 5-11 Failure Mode Validation between Experimental and F.E Work



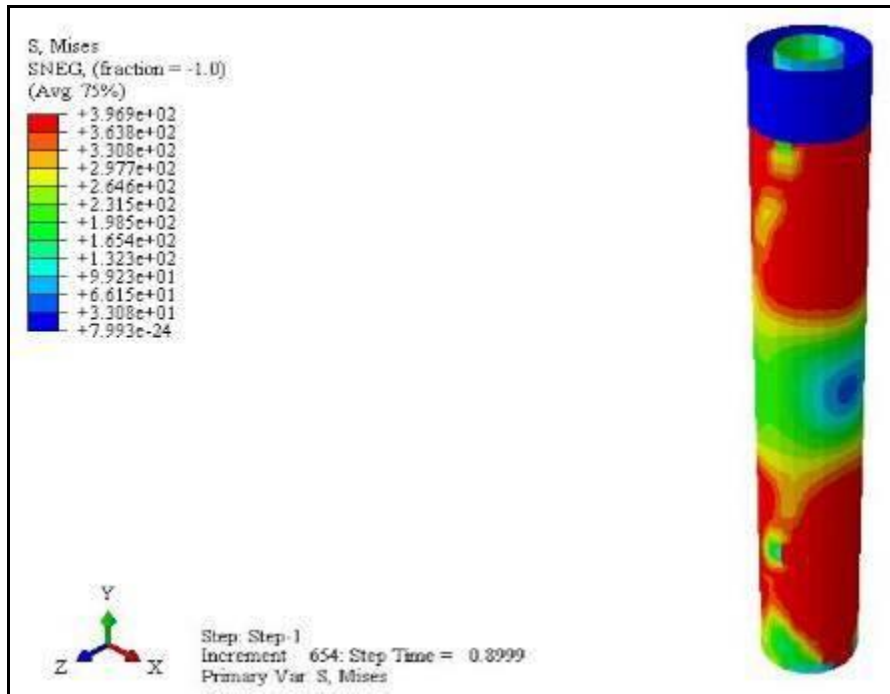
Table 5-3 Validation of Lateral Load Value of Experimental and Numerical Results

No.	Symbol of Column	Max. Lateral Cyclic Load in experimental work (kN)	Average Absolute Load in experimental work(kN)	Max. Lateral Cyclic in F.E (kN)	Average Absolute Load in F.E(kN)	P Lateral in F.E/P Lateral in experimental work
1	CNS-C1	31.65	31.48	32.98	32.92	1.045
		-31.31		-32.87		
2	CNS-C2	32.50	32.49	33.50	33.56	1.032
		-32.48		-33.62		
3	CNS-C3	33.49	33.27	35.56	35.66	1.071
		-33.05		-35.76		
4	CNS-S1	29.36	29.62	31.79	31.64	1.068
		-29.88		-31.50		
5	CNS-S2	31.39	31.42	32.40	32.35	1.029
		-31.45		-32.30		
6	CNS-S3	32.42	32.51	34.50	34.36	1.056
		-32.6		-34.22		
7	CHS-C1	33.88	33.58	35.50	35.10	1.045
		-33.29		-34.69		
8	CHS-C2	35.6	35.48	36.96	37.00	1.042
		-35.37		-37.15		
9	CHS-C3	39.87	40.08	40.44	40.87	1.020
		-40.30		-41.31		
10	CHS-S1	30.44	30.53	31.85	31.87	1.043
		-30.62		-31.90		
11	CHS-S2	33.91	33.39	34.50	34.56	1.03
		-32.87		-34.62		
12	CHS-S3	35.94	35.61	37.25	37.10	1.04
		-35.28		-36.9		

The validation between the numerical results and experimental findings shows little difference, in general, the numerical results appear more than the same in experimental with a maximum value of difference of about (1.071). This difference may be caused by the accuracy of using finite element programs more than that found in experimental work, like the application of boundary conditions and loads. The peak lateral displacement that the yielding failure reached was approximately the same between numerical models and the experimental work that has the same conditions, except for a few negligible differences. More details about the distribution of stresses for the concrete, steel tubes, and stiffeners are shown in Figures 5-12 to 5-15.

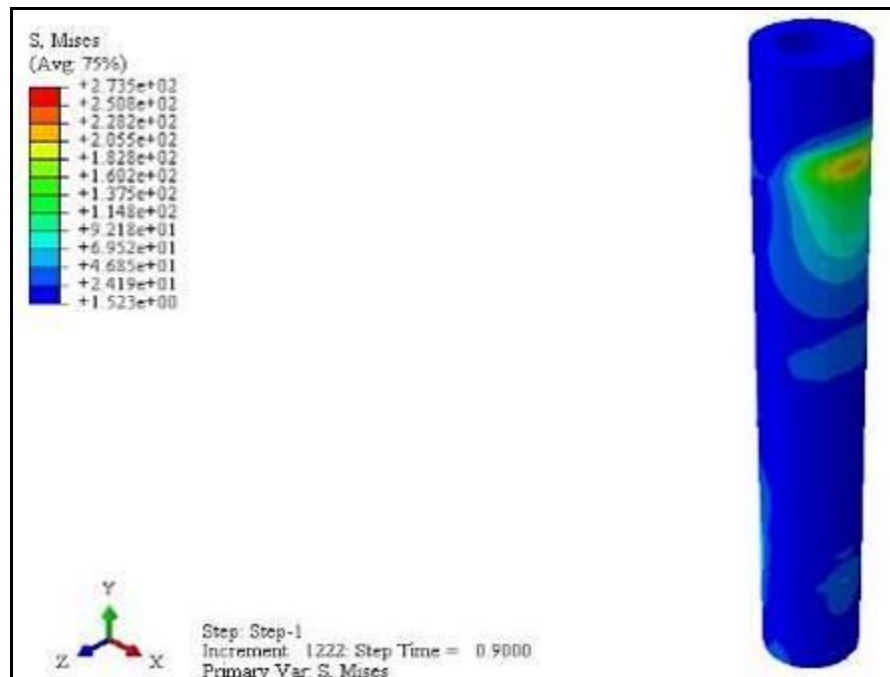


(a)

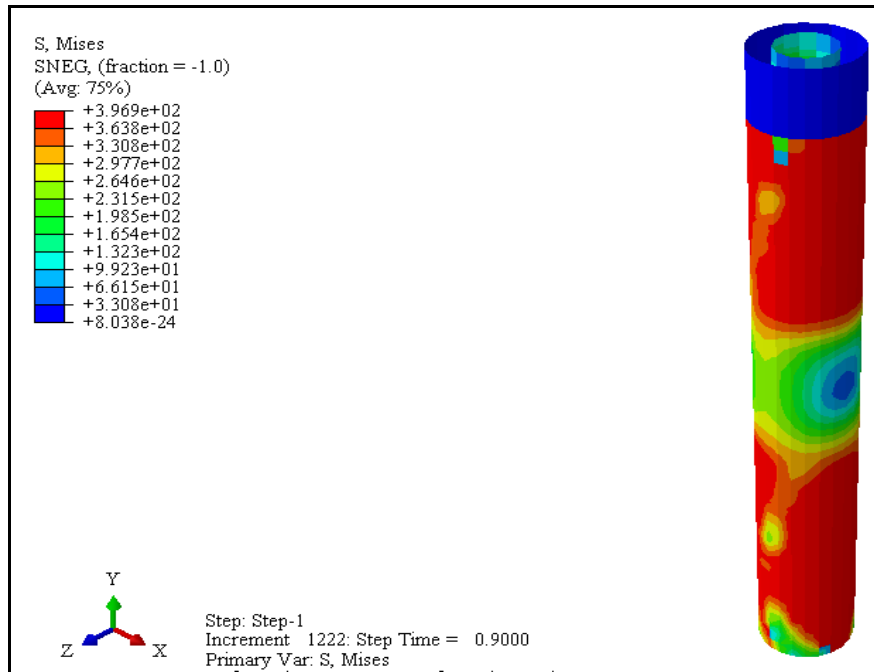


(b)

Figure 5-12 Stresses in Model Group One CNS-C (a) Stresses in Concrete(b) Stresses in Steel Tube

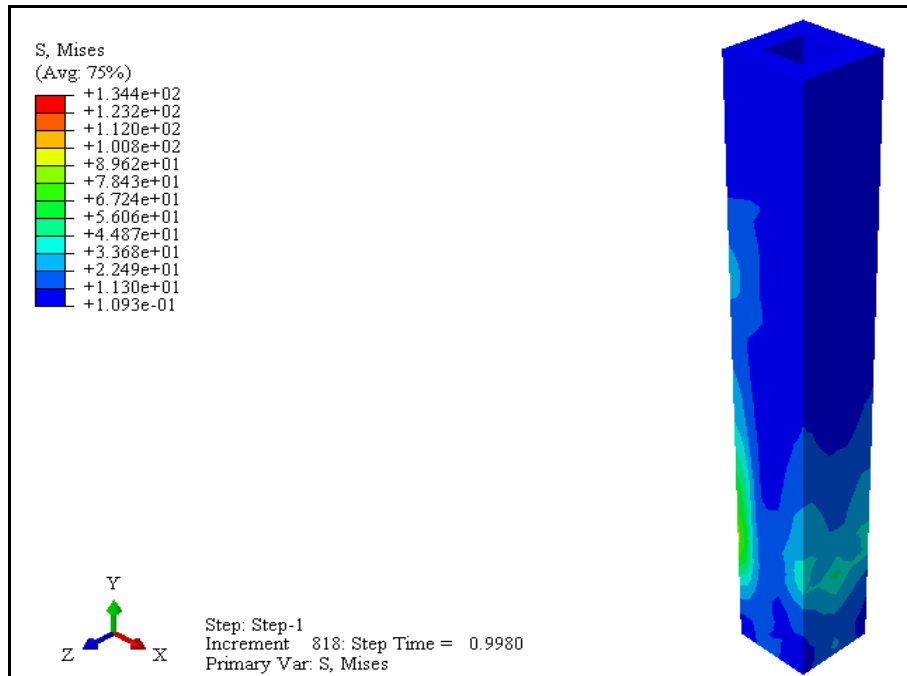


(a)

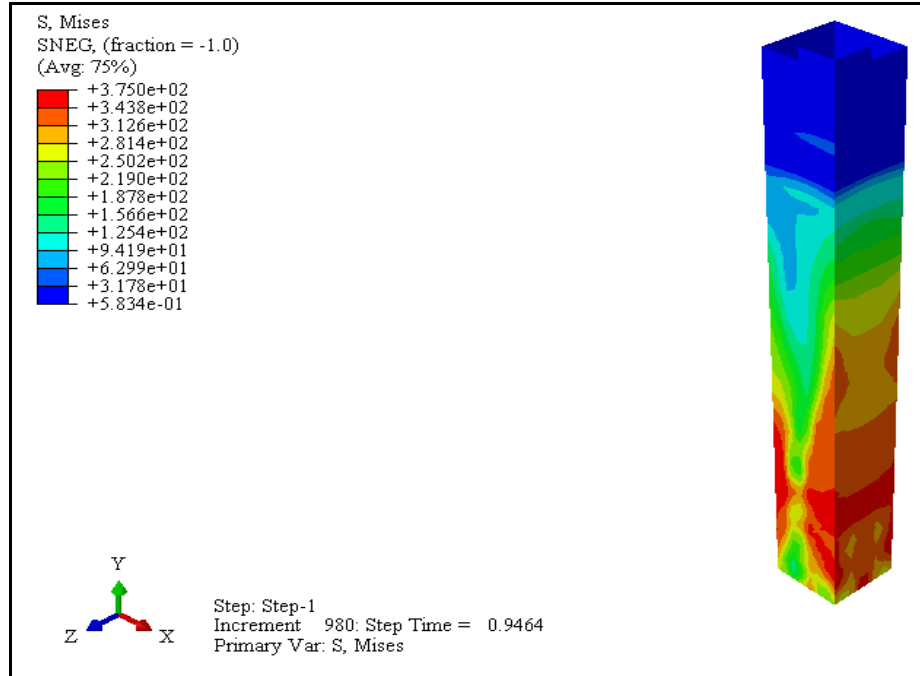


(b)

Figure 5-13 Stresses in Model Group Two CHS-C (a) Stresses in Concrete(b) Stresses in Steel Tube

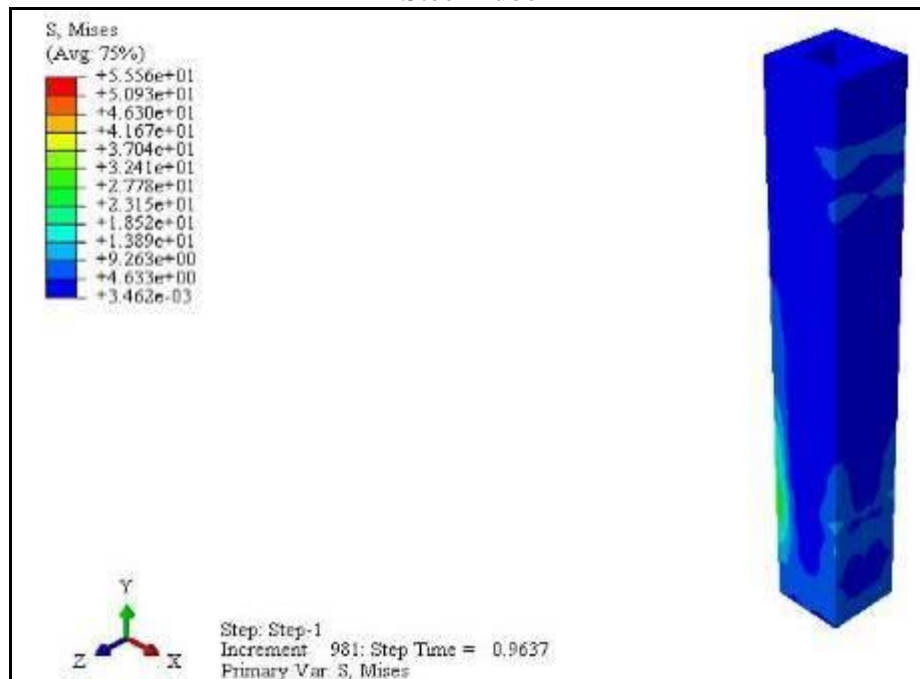


(a)

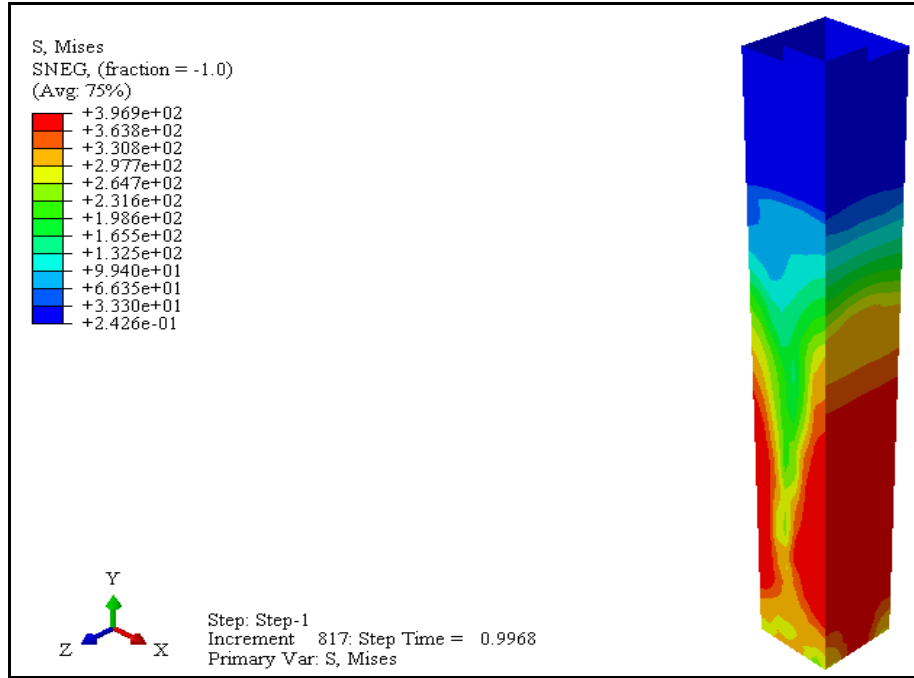


(b)

Figure 5-14 Stresses in Model Group Three CNS-S (a) Stresses in Concrete(b) Stresses in Steel Tube



(a)



(b)

Figure 5-15 Stresses in Model Group Four CHS-S (a) Stresses in Concrete (b) Stresses in Steel Tube

The validation between load-deflection curves for the experimental work and the FEA models is shown in Figures 5-16 to 5-27 below.

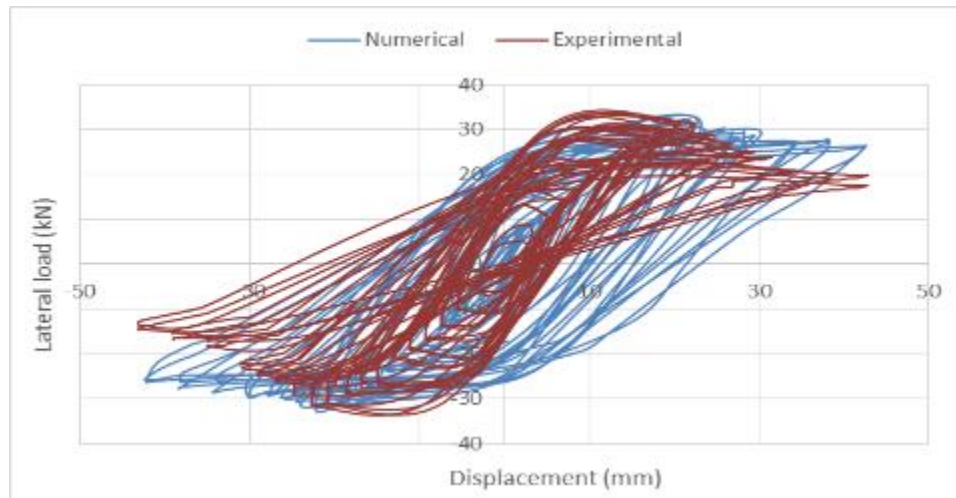


Figure 5-16 Load Displacement Diagram for CNS-C1 Specimen

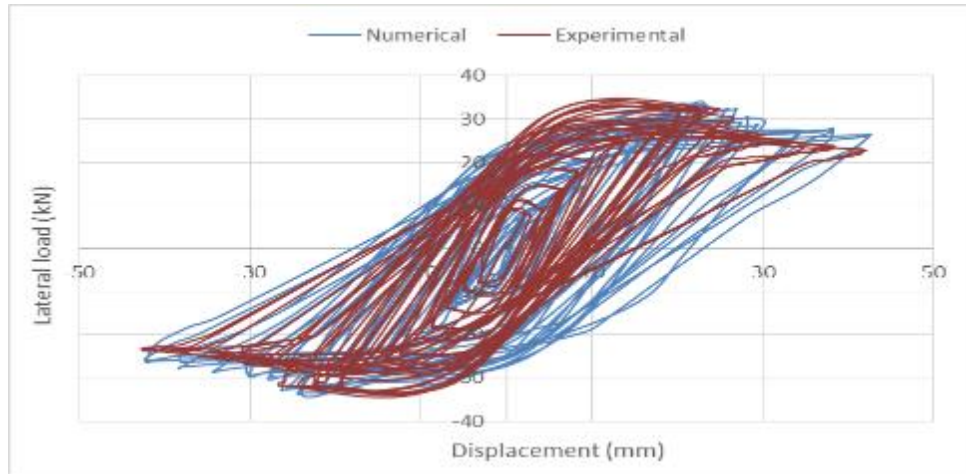


Figure 5-17 Load Displacement Diagram for CNS-C2 Specimen

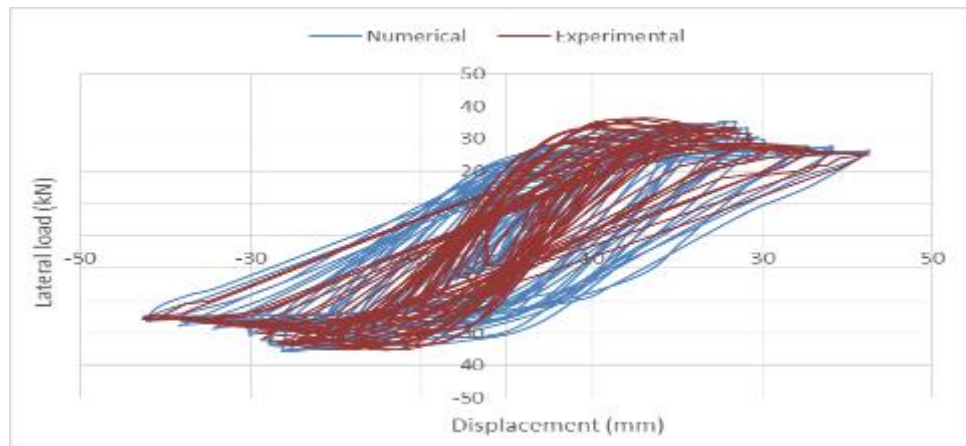


Figure 5-18 Load Displacement Diagram for CNS-C3 Specimen

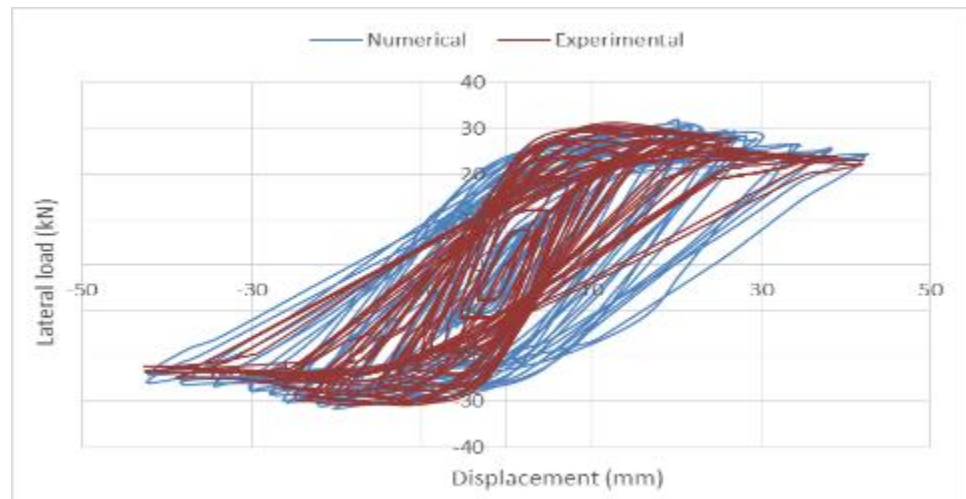


Figure 5-19 Load Displacement Diagram for CNS-S1 Specimen

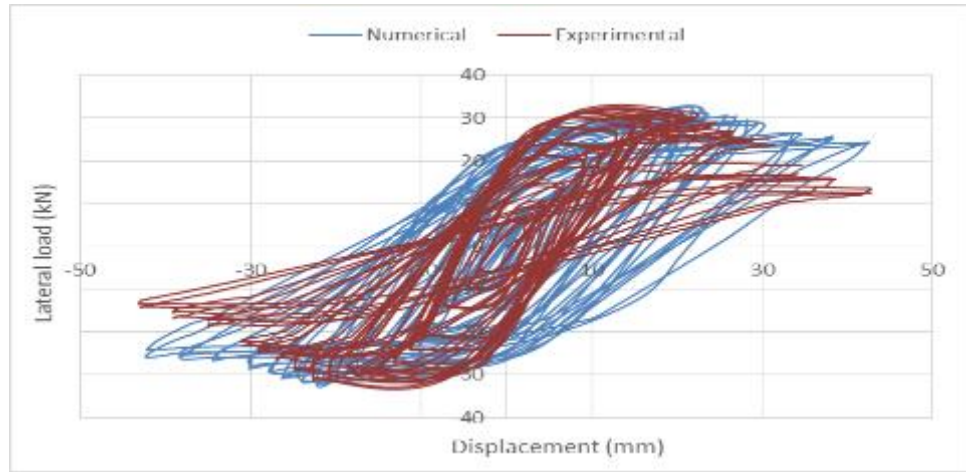


Figure 5-20 Load Displacement Diagram for CNS-S2 Specimen

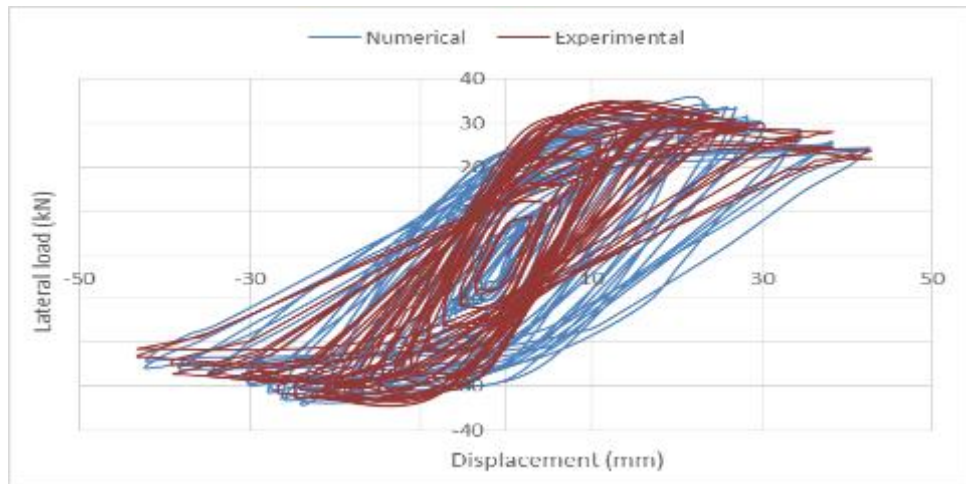


Figure 5-21 Load Displacement Diagram for CNS-S3 Specimen

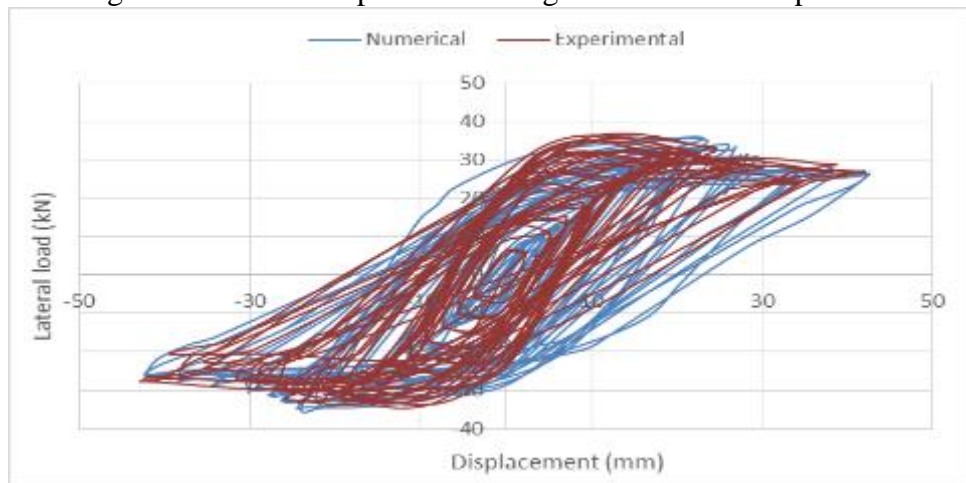


Figure 5-22 Load Displacement Diagram for CHS-C1 Specimen



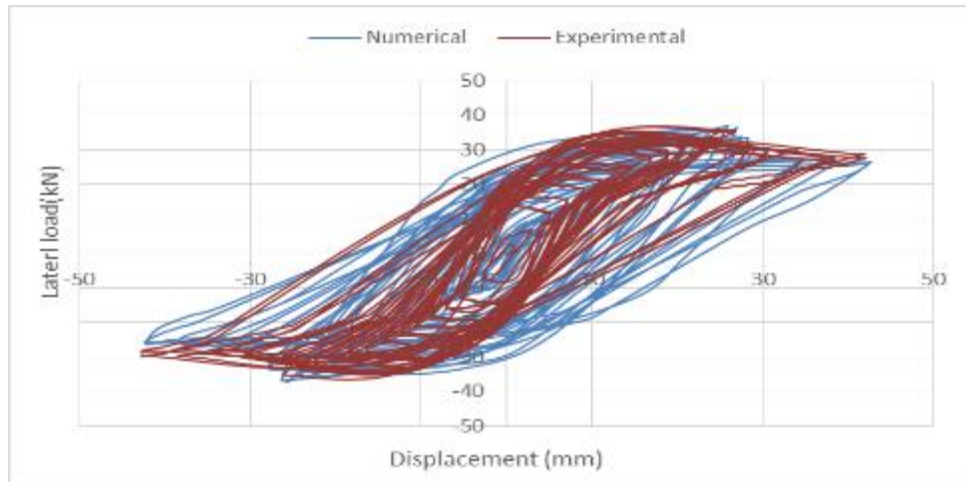


Figure 5-23 Load Displacement Diagram for CHS-C2 Specimen

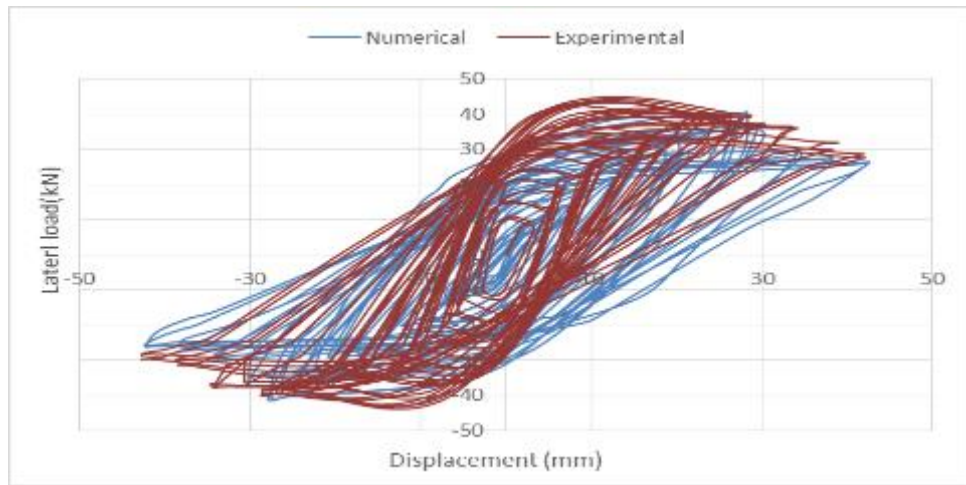


Figure 5-24 Load Displacement Diagram for CHS-C3 Specimen

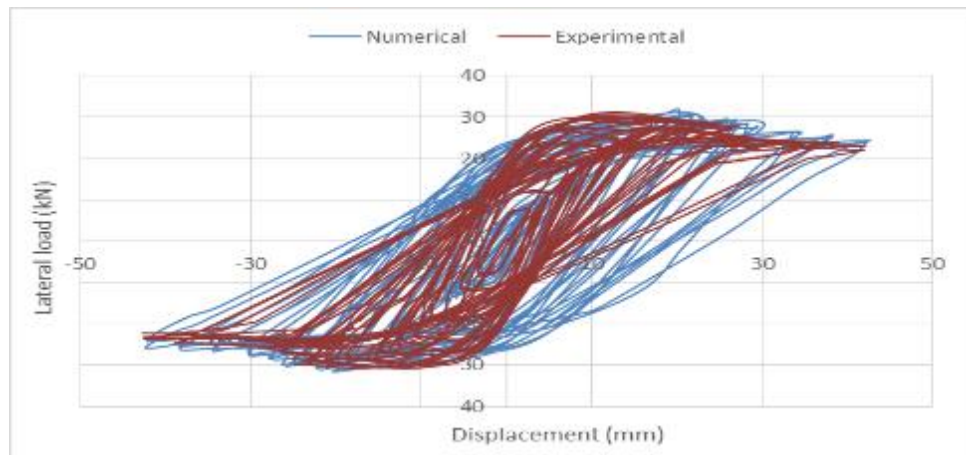


Figure 5-25 Load Displacement Diagram for CHS-S1 Specimen

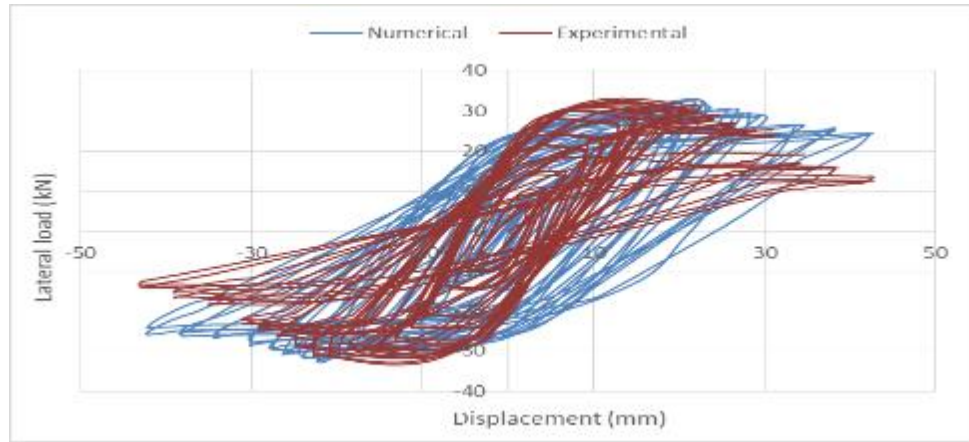


Figure 5-26 Load Displacement Diagram for CHS-S2 Specimen

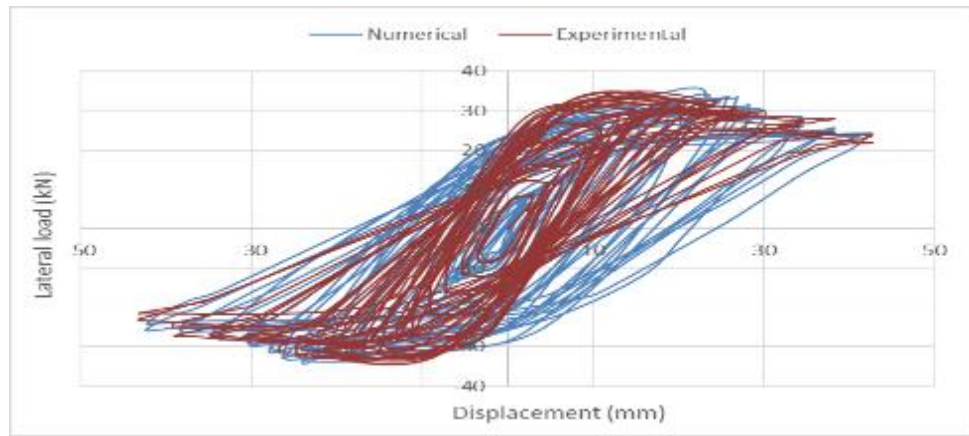


Figure 5-27 Load Displacement Diagram for CHS-S3 Specimen

From the results and stress figures, it can be observed that when the columns were still in the elastic zone at the top it reached the plastic mode at the bottom of the columns. Figure 5-28 shows the deformation in the shape of the composite column that represented the mode of failure.

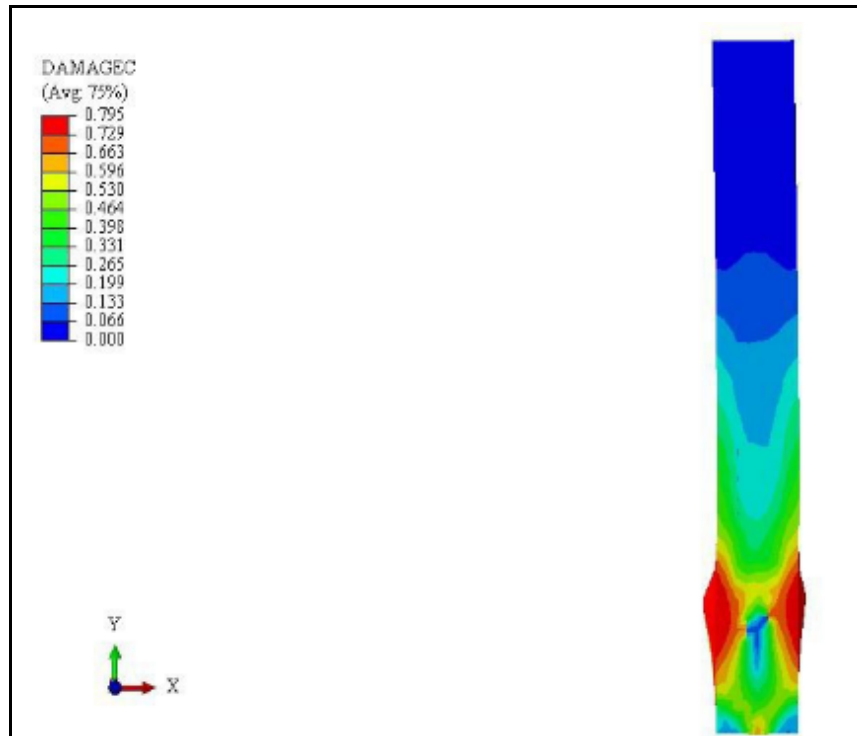


Figure 5-28 The Deformed Shape of Composite Column Model

at the representation of the finite element model concrete crushing and steel yielding were the failure modes expected. The compressive yield strength in concrete precedes the yield stress of the steel tube at the bottom of the column. Maximum compressive stress had been found near the bottom of the column, this conclusion of failure mode was demonstrated by comparing the stresses of steel and the strength of concrete, clear that the concrete failed in compression and tension before the steel reached the yield stress.

## 5.9 Parametric Study

The selected techniques, material models, and analysis techniques used to simulate and validate the experimental work results were presented and shown in the previous section of this chapter. When compared to the outcomes of the experimental studies, the finite element method produced accurate results. For further parametric research, this item has adopted the

previous configuration that was provided. The parametric study requires the addition of longitudinal Reinforcement bars and stirrups to the specimens to study the increasing lateral cyclic load strength.

### **5.9.1 Reinforcement specimens simulation**

Geometrical modeling requires seven parts in total for two models square and circular cross-section columns. They are as follows: Concrete column, outer steel tube, inner steel tube, stiffeners (four numbers), top and bottom plate. Concrete columns, stiffeners, and top and bottom plates for two models were constructed using 3D- Deformamable –Solid Element(C3D8R), outer and inner steel tubes were constructed using 3D-Deformamable –Shell Element (S4R), and steel reinforcement(longitudinal and stirrups) were constructed by using 3D- Deformamable-Wire Element (T3D2). Two specimens (square and circular) with high-strength concrete were used in this parametric study and the case of 70kN axial load was implemented this case represented the maximum value of lateral cyclic load from previous experimental and numerical study. All other details and boundary conditions from properties, assembly, interaction, mesh, loads, and boundary conditions are the same as in the previous study.

### **5.9.2 Reinforcement Details**

Reinforcement steel bars consist of longitudinal steel bars with a diameter of (6) mm and its number was four for square section specimens and six for circular section specimens. the stirrup diameter was (4)mm and distributed into three regions the two regions near the upper and lower supports were 50 mm, and the third region at the middle with distribution of 100 mm. the details of reinforcement and dimensions are shown in Figure 5-29 below.

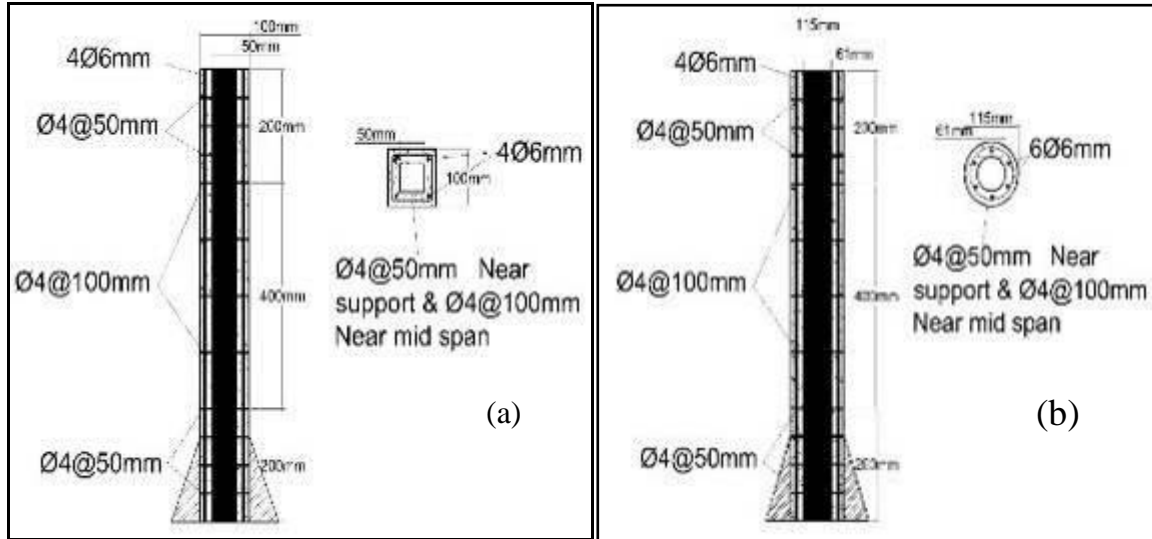


Figure 5-29 Reinforcement Details for Specimens (a) Square Section Specimens (b) Circular Section Specimens

### 5.9.3 Parametric Study Results and Analysis

In this section, the numerical justification concerning the experimental study findings was completed in terms of the load–deflection curves for all of the specimens. The consequences of the finite element analysis were assembled, arranged, and compared with the results that obtained from previous numerical studies and experimental work. The comparison was dependent significantly on the ultimate lateral load capacity relation with displacement, and failure mode.

#### 5.9.3.1 Validation of parametric study

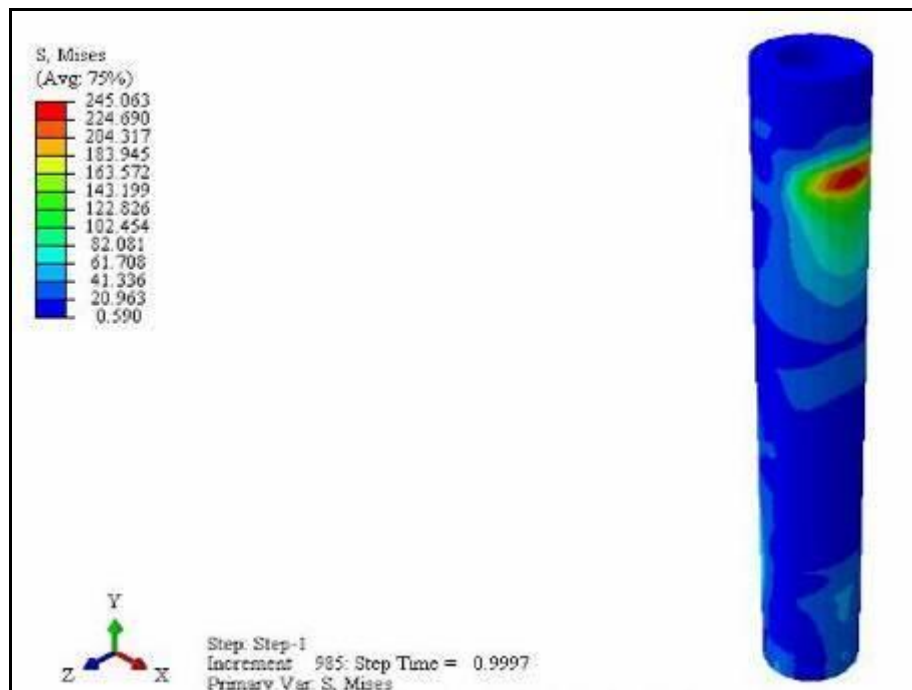
In this section, the load-deflection curves for two specimens were obtained, along with a numerical validation based on the previous numerical study and experimental work findings. Concerning the ultimate deflection and load-carrying capacity of columns, the numerical calculations after strengthening the specimens with steel reinforcement showed a relative increase with previous numerical studies and experimental results. The numerical results of the specimens are presented together with their load-

deflection behavior, Tables 5-3 represent the observed percentage of variance for the load capacity and the corresponding deflection.

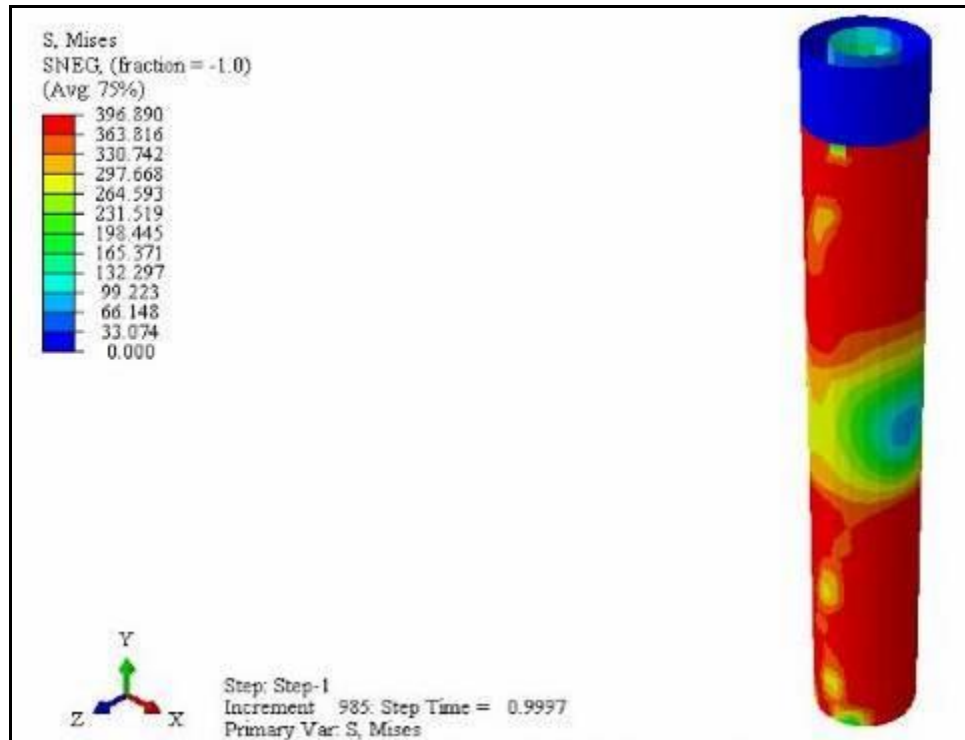
More details about the distribution of stresses for the concrete, steel tubes, and stiffeners are shown in Figures 5-30 and 5-31.

Table 5-4 Validation between Lateral Load for The Model in F.E and Model Strengthen with Reinforcement Steel

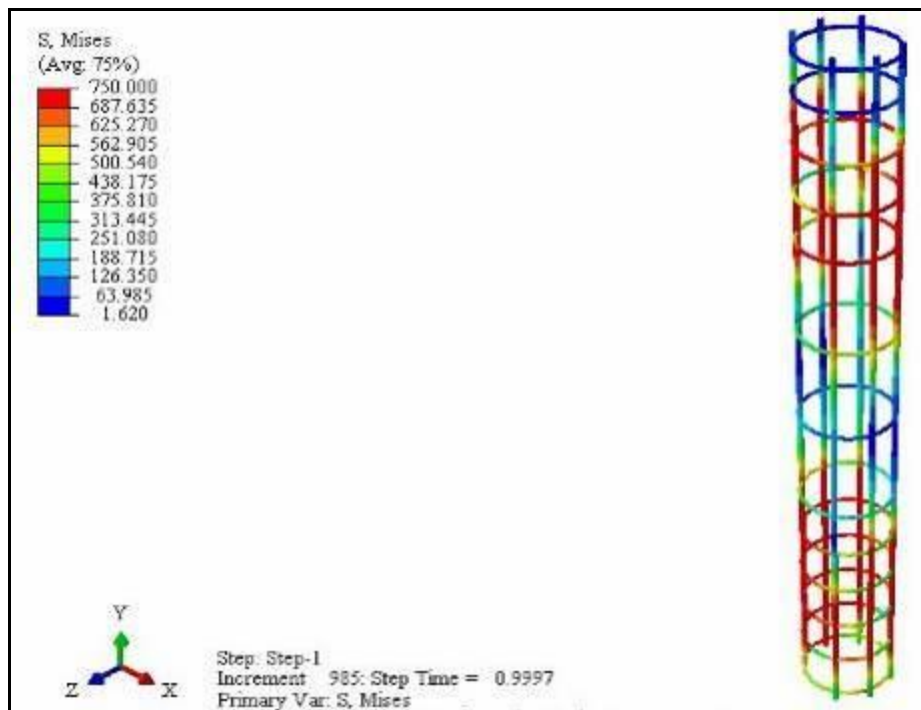
No.	Symbol of Column	Max. Lateral Cyclic in F.E (kN)	Average Absolute Load in F.E (kN)	Max. Lateral Cyclic in F.E after strengthening (kN)	Average Absolute Load in F.E after strengthen (kN)	P Lateral in F.E after strengthen/ P Lateral in F.E
1	CHS-C3	40.44	40.87	45.56	45.57	1.11
		-41.31		-45.59		
2	CHS-S3	37.25	37.10	37.94	37.87	1.02
		-36.9		37.81		



(a)

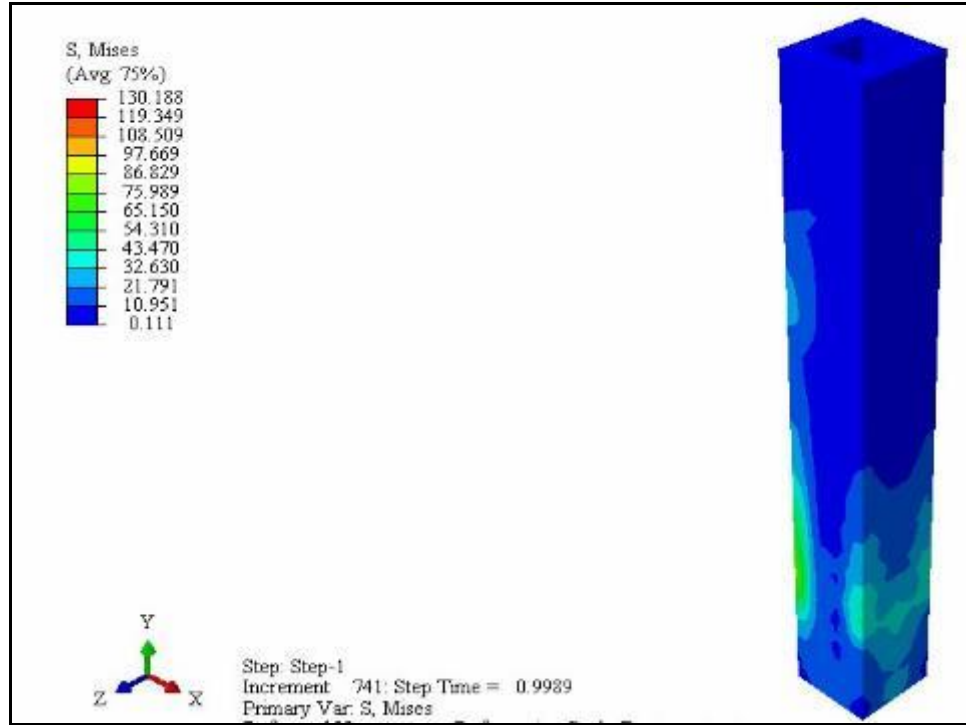


(b)

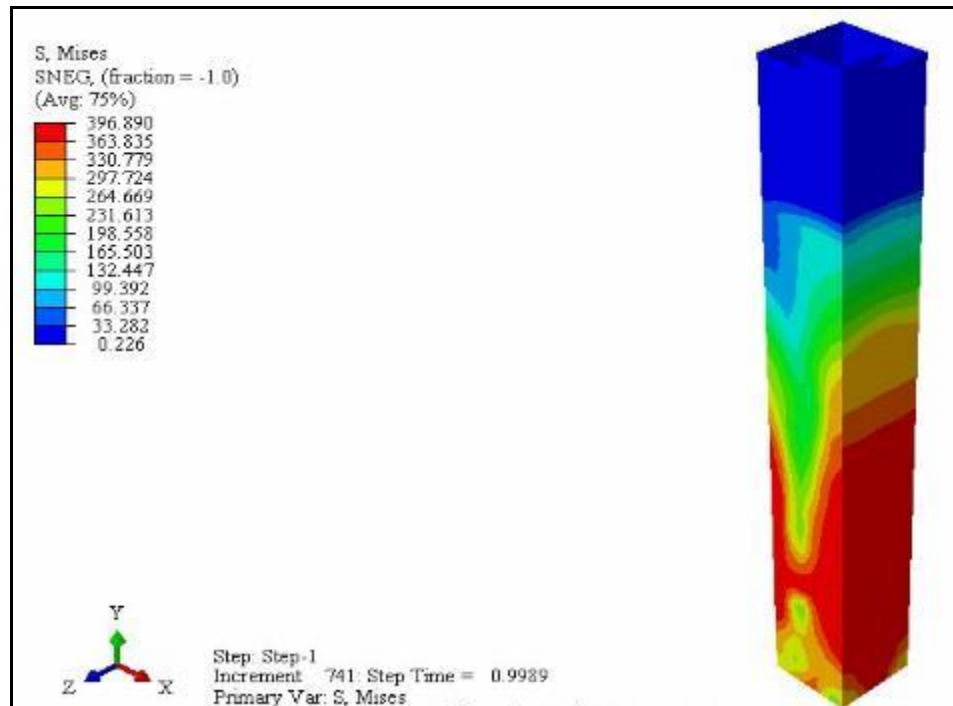


(c)

Figure 5-30 Stresses in Strengthened Circular Columns CHS-CR (a) Stresses in Concrete (b) Stresses in Steel Tube (c) Stresses in reinforcement steel

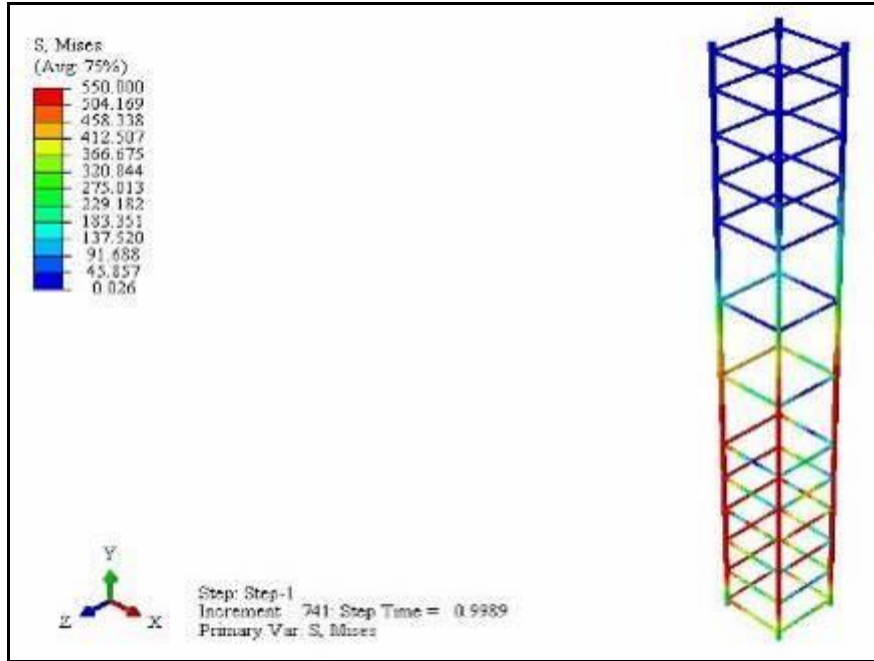


(a)



(b)





(c)

Figure 5-31 Stresses in Strengthen Square Columns CHS-SR (a) Stresses in Concrete(b) Stresses in Steel Tube(c) Stresses in reinforcement steel

The validation between load-deflection curves for the numerical study without reinforcement steel and the model strengthened with reinforced steel for cases with high-strength concrete and 70 kN axial load for circular and square section specimens. as shown in Figures 5-32 and 5-33 below.

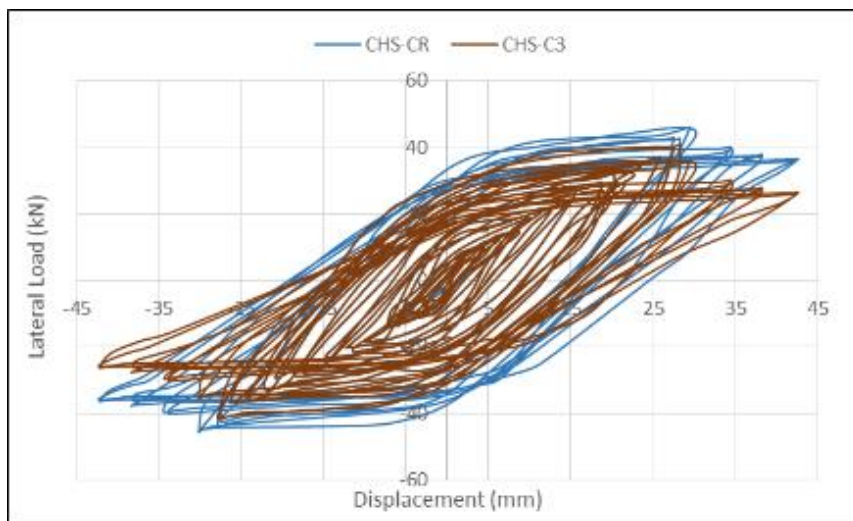


Figure 5-32 Comparison of Load Displacement Diagram between CHS-C3 and CHS-CR

Mode

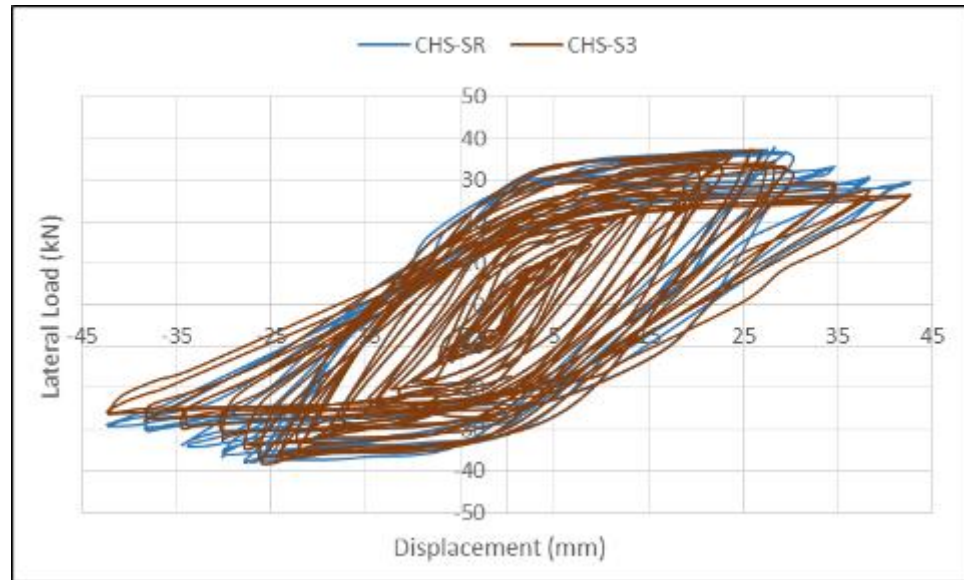


Figure 5-33 Comparison of Load Displacement Diagram between CHS-S3 and CHS-SR Model

The result of comparison between the models with a circular section, high-strength concrete, and the case with dead and live load (70 kN) with the model has the same condition of cross-section, type of concrete, and the value of axial load, in addition to use reinforcement steel to strength the model, found that the addition of steel bars and stirrups made noticeable enhancement in the lateral load resistance with an increasing percentage than the model without strengthen about 1.11, and the displacement that the model reached yield failure on it is 30 mm while it was 28mm with the model without strengthen, that made the addition of steel to the model is suitable and useful. The result of comparison between the models with a square section, high-strength concrete, and the case with dead and live load (70 kN) with the model has the same condition of cross-section, type of concrete, and the value of axial load, in addition to use reinforcement steel to strength the model, found that the addition of steel bars and stirrups made little enhancement in the lateral load resistance with an increasing

percentage than the model without strengthen about 1.02, and the displacement that the model reached yield failure on it is 28 mm while it was 26 mm with the model without strengthen, that made the addition of steel to the model for square section has a high cost in comparison with its advantages.

# ***CHAPTER***

***Six***

## **Chapter6 : Conclusions**

### **6.1 Introduction**

The effects of the type of concrete and shape of steel tube cross-section under different axial loads subjected to lateral cyclic loads in double-skin tubular columns are experimentally and numerically investigated and presented in this study. Twelve double-skin columns were manufactured and tested, six of them with circular cross-section and the other six columns having a square cross-section all samples were divided into normal and high concrete strength. The columns were split into three groups. Each column measured 800 mm in length and 115 mm (diameter) for the outer circular steel tube and 100 mm side length for the outer square steel tube. The current study brought to light several significant ideas in the philosophy of the effect of cyclic loads in composite columns with different parameters. The primary conclusions drawn from the composite column's experimental results are as follows.

### **6.2 Conclusions**

- 1- The failure mode of all specimens where at the bottom of columns near the lower support and it represented yielding failure in the steel outer and inner tube preceded by crushing in concrete.
- 2- As for the circular sections, the resistance of failure occurred to a larger degree than the square section, due the confining of concrete by the circular steel tube was better than the square.
- 3- The ultimate resistance of lateral loads of composite columns filled with high-strength concrete(HSC) under the same conditions of axial load value: first group without axial load, the second group subjected to dead load only, and the third group subjected to dead and live loads, for

- circular cross-section show an increase of (6.68 %,9.20%,20.19%) respectively compared with columns filled with normal concrete (NSC), and for square cross-section show an increase of (3.07%, 6.26%, 9.53%) respectively compared with columns filled with normal concrete (NSC), this difference means that the influence of high strength concrete enhanced the performance of the resistance of composite columns to lateral loads clearly, and the confining of concrete by the steel tube
- 4- The ultimate resistance of lateral loads of composite columns that have a circular cross-section under the same conditions of axial load value: first group without axial load, the second group subjected to dead load only, and the third group subjected to dead and live loads, and filled with normal strength concrete show an increase of (6.27 %,3.30%,2.33%) respectively compared with columns that have a square cross-section, and for columns filled with high strength concrete a circular columns show an increase of (10 %, 6.25%, 12.29%) respectively compared with columns have a square cross-section, the previous results show that a circular section column has a resistance of lateral cyclic loads greater than the square section at the same conditions that clear the circular section was more suitable than the square.
  - 5- In general, under the same condition of column section shape, and type of concrete filled in steel tubes, the lateral load capacity increases with increasing axial compressive stress value.
  - 6- The external confining of concrete by steel tubes can enhance the performance of columns by reducing the brittle behavior of high-strength concrete, increase the strength of specimens, and the steel tubes can be used as forms for pouring concrete.

- 7- Numerical simulation of samples gives a good agreement with experimental results and a maximum difference between numerical results and the same with experimental work about (1.071), it can be observed that when the columns are still in the elastic mode at the top it reached the plastic mode at the bottom of the columns The compressive yield strength in concrete precede the yield stress of steel tube. Maximum compressive stress had been found near the bottom of the column this conclusion of failure mode was demonstrated by comparing the stresses of steel and the strength of concrete, clear that the concrete failed in compression and tension before the steel reached the yield stress.
- 8- Parametric study was conducted ,by adding reinforced steel bars to the previous specimens for two samples ,the first has a circular cross – section, and the other has a square cross – section, the two samples filled with a high –strength concrete and subjected to 70 kN axial load, the results showed that adding reinforced steel bars to the circular specimens may enhanced the resistance of lateral load about (1.11) than the numerical model without reinforced steel bars, but for the square there is negligible increasing in the lateral loads resistance.

### **6.3 Recommendations**

- 1- Study the effect of other types of concrete like reactive powder (RPC) in composite columns with reinforced bars compared with composite columns filled with high-strength concrete (HSC).
- 2- To change the failure mode position, strengthen the bottom of the tube by welded plates from inside the tubes, or use (an FRP) jacket from the outside of the tube.

- 3- Study the effects of different types of outer and inner steel tubes (use the outer square section with the circular inner tube and versa).
- 4- In this study tried to strengthen the specimens, using reinforced steel bars with steel tubes, but it was difficult to fill them with concrete, because of the small free area between reinforced bars and steel tubes, and the samples had been neglected, but in case study in finite element this parameter was taken into consideration, so in the practical side with the same characteristics of the test, the cross-section of specimens must be larger than the current.



# ***REFERENCES***

## References

- [1] “Composite Columns,” *ACI Journal Proceedings*, vol. 27, no. 11, 1930. doi: 10.14359/8187.
- [2] D. W. Hoepfner, “Cyclic {Loading} and {Cyclic} {Stress},” vol. 691–698. 2013.
- [3] S. K. Paul, “A critical review of experimental aspects in ratcheting fatigue: microstructure to specimen to component,” *J. Mater. Res. Technol.*, vol. 8, no. 5, pp. 4894–4914, 2019, doi: 10.1016/j.jmrt.2019.06.014.
- [4] ASTM-C39, “Standard Test Method for Compressive Strength of Cylindrical Concrete,” *Annu. B. ASTM Stand.*, no. February, 2010, doi: 10.1520/C0039.
- [5] H. G. Russell Chairman Arthur R Anderson Jack O Banning Irwin G Cantor *et al.*, “ACI 363R-92 State-of-the-Art Report on High-Strength Concrete Reported by ACI Committee 363,” vol. 92, no. Reapproved, 2010.
- [6] M. Johansson and K. Gylltoft, “Mechanical Behavior of Circular Steel–Concrete Composite Stub Columns,” *J. Struct. Eng.*, vol. 128, no. 8, pp. 1073–1081, 2002, doi: 10.1061/(asce)0733-9445(2002)128:8(1073).
- [7] L. Xu, J. Pan, and J. Chen, “Mechanical Behavior of ECC and ECC/RC Composite Columns under Reversed Cyclic Loading,” *J. Mater. Civ. Eng.*, vol. 29, no. 9, pp. 1–11, 2017, doi: 10.1061/(asce)mt.1943-5533.0001950.
- [8] S. Vernardos and C. Gantes, “Experimental behavior of concrete-filled double-skin steel tubular ( CFDST ) stub members under axial compression : A comparative review,” *Structures*, vol. 22, no. May, pp. 383–404, 2019, doi: 10.1016/j.istruc.2019.06.025.
- [9] A. Behnamnia and M. Barati, “Seismic Behavior of Steel-Concrete

References.....

Composite Columns Under Cyclic Lateral Loading,” vol. 2019, no. November, pp. 183–192, 2019, doi: 10.22034/JCEMA.2019.99690.

[10] F. Ding and Z. Yu, “Composite action of rectangular concrete-filled steel tube columns under lateral shear force,” no. September, pp. 5–9, 2020, doi: 10.1002/suco.202000283.

[11] S. İpek and E. Mete, “Nonlinear finite element analysis of double skin composite columns subjected to axial loading,” 2020, doi: 10.1007/s43452-020-0012-x.

[12] A. bellah Alsamawi and N. Boumechra, “Behaviour of fully encased composite columns under cyclic loads,” *Ce/Papers*, vol. 4, no. 2–4, pp. 564–569, 2021, doi: 10.1002/cepa.1331.

[13] A. Gautham and D. R. Sahoo, “Behavior of steel-reinforced composite concrete columns under combined axial and lateral cyclic loading,” *J. Build. Eng.*, vol. 39, no. August 2020, p. 102305, 2021, doi: 10.1016/j.jobbe.2021.102305.

[14] A. B. Alsamawi, N. Boumechra, and K. Hamdaoui, “Numerical Parametric Study of Fully Encased Composite Columns Subjected to Cyclic Loading,” *Civ. Eng. J.*, vol. 8, no. 1, pp. 45–59, 2022, doi: 10.28991/CEJ-2022-08-01-04.

[15] P. Kar, A. C. Borsaikia, and K. D. Singh, “Experimental investigation of partially confined concrete-filled steel tubular square columns under lateral cyclic loading,” *J. Constr. Steel Res.*, vol. 201, no. December 2022, p. 107751, 2023, doi: 10.1016/j.jcsr.2022.107751.

[16] C. Cho, Y. Kim, L. Feo, and D. Hui, “Cyclic responses of reinforced concrete composite columns strengthened in the plastic hinge region by HPFRC mortar,” *Compos. Struct.*, vol. 94, no. 7, pp. 2246–2253, 2012, doi: 10.1016/j.compstruct.2012.01.025.

References.....

- [17] A. P. C. Duarte, B. A. Silva, N. Silvestre, J. de Brito, E. Júlio, and J. M. Castro, “Experimental study on short rubberized concrete-filled steel tubes under cyclic loading,” *Compos. Struct.*, vol. 136, pp. 394–404, 2016, doi: 10.1016/j.compstruct.2015.10.015.
- [18] T. Yu, Y. M. Hu, and J. G. Teng, “Cyclic lateral response of FRP-confined circular concrete-filled steel tubular columns,” vol. 124, pp. 12–22, 2016, doi: 10.1016/j.jcsr.2016.05.006.
- [19] P. Faustino, P. Frade, and C. Chastre, “Lateral Cyclic Behaviour of RC Columns Confined With Carbon Fibres,” *Structures*, vol. 5, pp. 196–206, 2016, doi: 10.1016/j.istruc.2015.11.004.
- [20] C. Oucif, K. Ouzaa, V. Stoian, and C. Alexandru, “Numerical Modeling of Reinforced Concrete Strengthened Columns Under Cyclic Loading,” 2017, doi: 10.1007/s13369-017-2533-z.
- [21] F. Yuan, M. Chen, and J. Pan, “Experimental study on seismic behaviours of hybrid FRP–steel-reinforced ECC–concrete composite columns,” *Compos. Part B Eng.*, vol. 176, no. June, p. 107272, 2019, doi: 10.1016/j.compositesb.2019.107272.
- [22] Z. Huang, D. Li, B. Uy, H. T. Thai, and C. Hou, “Local and post-local buckling of fabricated high-strength steel and composite columns,” *J. Constr. Steel Res.*, vol. 154, pp. 235–249, 2019, doi: 10.1016/j.jcsr.2018.12.004.
- [23] Y. Yan, H. Liang, Y. Lu, Z. Liu, and T. Gong, “Behaviour of RC columns strengthened with SCC-filled steel tubes under cyclic loading,” *Eng. Struct.*, vol. 199, no. December 2018, p. 109603, 2019, doi: 10.1016/j.engstruct.2019.109603.
- [24] H. Elci, “Seismic strengthening of improperly repaired reinforced concrete columns using CFRP confinement,” *Structures*, vol. 28, no. April,

References.....

pp. 266–275, 2020, doi: 10.1016/j.istruc.2020.08.072.

[25] F. C. Wang and H. Y. Zhao, “Experimental investigation on blast furnace slag aggregate concrete filled double skin tubular (CFDST) stub columns under sustained loading,” *Structures*, vol. 27, no. April, pp. 352–360, 2020, doi: 10.1016/j.istruc.2020.05.046.

[26] V. Ishvarbhai, Q. Quan, and M. N. S. Hadi, “Numerical analysis of high-strength concrete- fi lled steel tubular slender beam-columns under cyclic loading,” *JCSR*, vol. 92, pp. 183–194, 2014, doi: 10.1016/j.jcsr.2013.09.008.

[27] J. Zhang, X. Li, W. Cao, and C. Yu, “Cyclic behavior of steel tube-reinforced high-strength concrete composite columns with high-strength steel bars,” *Eng. Struct.*, vol. 189, no. March, pp. 565–579, 2019, doi: 10.1016/j.engstruct.2019.04.006.

[28] B. Lai, J. Y. R. Liew, and M. Xiong, “Experimental study on high strength concrete encased steel composite short columns,” *Constr. Build. Mater.*, vol. 228, p. 116640, 2019, doi: 10.1016/j.conbuildmat.2019.08.021.

[29] J. T. Wang, X. H. Wu, B. Yang, and Q. Sun, “Bearing capacity and damage behavior of HCFTST columns under cyclic loading,” *Structures*, vol. 32, no. April, pp. 1492–1506, 2021, doi: 10.1016/j.istruc.2021.03.102.

[30] J. Xiao and C. Zhang, “Seismic behavior of RC columns with circular, square and diamond sections,” *Constr. Build. Mater.*, vol. 22, no. 5, pp. 801–810, 2008, doi: 10.1016/j.conbuildmat.2007.01.010.

[31] W. Zhu, J. Jia, J. Gao, and F. Zhang, “Experimental study on steel reinforced high-strength concrete columns under cyclic lateral force and constant axial load,” *Eng. Struct.*, vol. 125, pp. 191–204, 2016, doi: 10.1016/j.engstruct.2016.07.018.

[32] E. Farajpourbonab, S. Y. Kute, and V. M. Inamdar, “Steel - reinforced

References.....

concrete - filled steel tubular columns under axial and lateral cyclic loading,” *Int. J. Adv. Struct. Eng.*, no. 2012, 2018, doi: 10.1007/s40091-018-0186-0.

[33] J. Ci, H. Jia, M. Ahmed, S. Chen, D. Zhou, and L. Hou, “Experimental and numerical analysis of circular concrete-filled double steel tubular stub columns with inner square hollow section,” *Eng. Struct.*, vol. 227, no. June 2020, p. 111400, 2021, doi: 10.1016/j.engstruct.2020.111400.

[34] ACI-318M, *Building Code Requirements for Structural Concrete (ACI 318M-14) and Commentary (ACI 318RM-14)*. 2014.

[35] No.5, “Iraqi Specifications for Portland Cement,” *Ministry of Planning - Central Organization For Standardization And Control Quality*. 2019.

[36] “Iraqi Specifications No. (45), 1984 for Aggregates of Natural Resources used for Concrete and Construction.” [Online]. Available: <https://www.scribd.com/document/395467049/Iraqi-Standard-Materials-Specification-Construction-Works>.”

[37] ASTM C1240, “Astm C1240,” *Stand. Specif. Silica Fume Used Cem. Mix.*, vol. 15, pp. 1–7, 2005.

[38] M. Description and S. Precautions, “MasterRoc MS 610 MasterRoc MS 610 Densified silica fume for cast and sprayed concrete,” pp. 1–2.

[39] M. O. F. Action and T. Applications, “MasterGlenium® 54”.

[40] ASTM C 494/C 494M - 04, “Standard Specification for Chemical Admixtures for Concrete, ASTM International, West Conshohocken, PA, 2004, [www.astm.org](http://www.astm.org),” *Am. Soc. Test. Mater.*, no. February, pp. 15–17, 2013.

[41] S. T. Methods, “Standard Test Methods and Definitions for Mechanical Testing of Steel Products 1”.

[42] B. Statements, “Standard Test Method for,” pp. 1–4.

References.....

- [43] C. C. Test, T. Drilled, C. Concrete, B. Statements, and C. Testing, “Standard Test Method for Compressive Strength of Cylindrical Concrete Specimens 1,” vol. 04, no. October, pp. 1–5, 2003.
- [44] C. C. Test, T. Drilled, C. Concrete, and B. Statements, “Standard Test Method for Splitting Tensile Strength of Cylindrical Concrete,” pp. 1–5.
- [45] C. C. T. Speci-, T. D. Cores, and C. C. T. Speci-, “Standard Test Method for Flexural Strength of Concrete ( Using Simple Beam with,” pp. 1–3.
- [46] H. Lime, “Standard Specification for Mixing Rooms , Moist Cabinets , Moist Rooms , and Water Storage Tanks Used in the Testing of Hydraulic Cements,” pp. 1–3.
- [47] I. 978-1-64195-193-7 Standard, ACI and Building, *Building Code Requirements for Structural Concrete Reinforced with Glass Fiber-Reinforced Polymer (GFRP) Bars-Code and Commentary Copyright*.
- [48] V. K. Kytinou, C. E. Chalioris, and C. G. Karayannis, “Analysis of residual flexural stiffness of steel fiber-reinforced concrete beams with steel reinforcement,” *Materials (Basel)*., vol. 13, no. 12, pp. 1–25, 2020, doi: 10.3390/ma13122698.
- [49] C. C. Chou and S. C. Wu, “Cyclic lateral load test and finite element analysis of high-strength concrete-filled steel box columns under high axial compression,” *Eng. Struct.*, vol. 189, no. March, pp. 89–99, 2019, doi: 10.1016/j.engstruct.2019.03.052.

# ***APPENDIXES***



# Appendixes

## Appendix A

### Silica Fume Properties



## MasterRoc MS 610

Densified silica fume for cast and sprayed concrete

### MATERIAL DESCRIPTION

MasterRoc MS 610 is a high-quality silica fume powder for high performance concretes. It changes the porous structure of the concrete making it denser and more resistant to any type of external influence.

### APPLICATIONS

- Wet-mix sprayed concrete applications
- Pre-cast concrete
- Cast in-situ concrete
- High strength concrete
- Underwater concrete
- Concrete with low cement content
- Annulus grouting (TBM)

### FEATURES AND BENEFITS

- Increased strength
- Substantially improved resistance to chemical and mechanical attack
- Prevents bleeding and segregation in fresh concrete
- Reduced accelerator consumption
- Very thick layers possible

### PACKAGING

MasterRoc MS 610 is supplied in 10 kg bags.

### TYPICAL PROPERTIES\*

Properties listed are for guidance and are not a guarantee of performance.

Appearance	Grey Powder
Density	0.55 -0.7 kg/l
Chloride content	<0.1%

### SAFETY PRECAUTIONS

Avoid contact with eyes and prolonged contact with skin. If contact occurs, wash thoroughly with water and seek medical advice.

For further information refer to the product Material Safety Data Sheet.

### COMBINATION

The use of superplasticizers is recommended for any silica fume concrete. For frost resistance, an additional air-entraining agent must be added.

### MIXING

MasterRoc MS 610 is added to the concrete during batching. Minimum mixing time is 90 seconds. The recommended dosage is 5 to 15% of the cement weight.

### STORAGE

If stored dry and in tightly closed original bags, MasterRoc MS 610 has a shelf life of 12 months from date of manufacture when stored in undamaged, unopened packaging.



## MasterRoc MS 610

### Densified silica fume for cast and sprayed concrete

#### NOTE

Technical support, where provided, does not constitute supervisory responsibility. For additional information contact your local MB Construction Chemicals Solutions South Africa (Pty) Ltd representative. MB Construction Chemicals Solutions South Africa (Pty) Ltd shall not be liable for technical advice provided.

MB Construction Chemicals Solutions South Africa (Pty) Ltd reserves the right to have the true cause of any difficulty determined by accepted test methods. Undertaking such tests is not, and shall not be deemed to

be, an admission of liability or an assumption of any risk, loss, damage or liability.

#### QUALITY AND RESPONSIBLE CARE

All products originating from MB Construction Chemicals Solutions South Africa (Pty) Ltd are manufactured under a management system independently certified to conform to the requirements of the quality standards ISO 9001, environmental and occupational health and safety standards.

\* Properties listed are based on laboratory controlled tests

#### DISCLAIMER

The technical information and application advice given in this MB Construction Chemicals Solutions South Africa (Pty) Ltd publication are based on the present state of our best scientific and practical knowledge. As the information herein is of a general nature, no assumption can be made as to a product's suitability for a particular use or application and no warranty as to its accuracy, reliability or completeness either expressed or implied is given other than those required by law. The user is responsible for checking the suitability of products for their intended use.

## Superplasticizer (Glenium 54)



### MasterGlenium® 54

A high performance concrete superplasticiser based on modified polycarboxylic ether

#### DESCRIPTION

**MasterGlenium 54** has been developed for applications primarily in precast but also readymix concrete industries where the highest durability and performance is required.

#### MECHANISM OF ACTION

**MasterGlenium 54** is differentiated from conventional superplasticisers, such as those based on sulphonated melamine or naphthalene formaldehyde condensate as it is based on a unique carboxylic ether polymer with long lateral chains. This greatly improves cement dispersion. At the start of the mixing process the same electrostatic dispersion occurs but the presence of the lateral chains, linked to the polymer backbone, generate a steric hindrance which stabilises the cement particles capacity to separate and disperse.

This mechanism provides flowable concrete with greatly reduced water demand and enhanced early strength.

#### TYPICAL APPLICATIONS

The excellent dispersion properties of **MasterGlenium 54** make it the ideal admixture for precast or ready-mix where low water cement ratios are required. This property allows the production of very high early and high ultimate strength concrete with minimal voids and therefore optimum density. Due to the strength development characteristics the elimination or reduction of steam curing in precast works may be considered as an economical option.

- High workability without segregation or bleeding
- Less vibration required
- Can be placed and compacted in congested reinforcement
- Reduced labour requirement
- Improved surface finish

**MasterGlenium 54** may be used in combination with **MasterMatrix** for producing Smart Dynamic Concrete (SDC). The technology produces advanced self-compacting concrete, without the aid of vibration. For economic, ecological and ergonomic ready-mix / precast concrete production.

**MasterGlenium 54** can be used to produce very high early strength floor screeds. For screed mix designs consult Master Builders Solutions Technical Services.

#### PACKAGING

**MasterGlenium 54** is available in 208 L drums and in bulk tanks upon request.

#### STANDARDS

ASTM C-494 Type F & G  
BS EN 934-2

#### TYPICAL PROPERTIES\*

Appearance	Whitish to straw coloured liquid
Relative density	1.07
pH value	4.0 - 7.0

#### APPLICATION GUIDELINES

**MasterGlenium 54** is a ready to use admixture that is added to the concrete at the time of batching.

The maximum effect is achieved when the **MasterGlenium 54** is added after the addition of 70% of the water. **MasterGlenium 54** must not be added to the dry materials.

Thorough mixing is essential and a minimum mixing cycle, after the addition of the **MasterGlenium 54**, of 60 seconds for forced action mixers is recommended.



## MasterGlenium® 54

The normal dosage for **MasterGlenium 54** is between 0.50 and 1.75 L/100kg of cement (cementitious material). Dosages outside this range are permissible subject to trial mixes.

### MIXING

**MasterGlenium 54** is suitable for mixes containing all types of Portland cement and cementitious materials as follows:

- Microsilica
- Fly ash (PFA)
- Ground granulated blast furnace slag GGBS

Note: **MasterGlenium 54** is not compatible with **MasterRheobuild** superplasticizers.

### EFFECT ON HARDENED CONCRETE

- Increased early and ultimate compressive strengths
- Increased flexural strength
- Better resistance to carbonation
- Lower permeability
- Better resistance to aggressive atmospheric conditions
- Reduced shrinkage and creep
- Increased durability

### STORAGE AND SHELF LIFE

**MasterGlenium 54** should be stored above 5°C in closed containers or storage tanks to protect from evaporation and extreme temperatures. The shelf life is 12 months when stored as above.

The occurrence of a surface layer with **MasterGlenium 54** is normal and will have no effect on the performance of the product.

### HEALTH AND SAFETY

**MasterGlenium 54** contains no hazardous substances requiring labelling. For further information refer to the Material Safety Data Sheet.

### QUALITY AND CARE

All products originating from Master Builders Solutions Dubai, UAE facility are manufactured under a management system independently certified to conform to the requirements of the quality, environmental and occupational health & safety standards ISO 9001 and ISO 14001.

\* Properties listed are based on laboratory controlled tests.

® = Registered trademark of the MBCC Group in many countries.

MBS\_CC-UAE/GI\_54\_09\_87v2#03\_16v3/01\_23

### STATEMENT OF RESPONSIBILITY

The technical information and application advice given in this Master Builders Solutions publication are based on the present state of our best scientific and practical knowledge. As the information herein is of a general nature, no assumption can be made as to a product's suitability for a particular use or application and no warranty as to its accuracy, reliability or completeness either expressed or implied is given other than those required by law. The user is responsible for checking the suitability of products for their intended use.

### NOTE

Field service where provided does not constitute supervisory responsibility. Suggestions made by Master Builders Solutions either orally or in writing may be followed, modified or rejected by the owner, engineer or contractor since they, and not Master Builders Solutions, are responsible for carrying out procedures appropriate to a specific application.

Master Builders Solutions  
Construction Chemicals LLC  
P.O. Box 37127, Dubai, UAE  
Tel: +971 4 8090600  
www.master-builders-solutions.com/en-ae

Disclaimer: The TUV mark relates to certified management system and not to the product mentioned on this datasheet



A brand of  
**MBCC GROUP**

## Appendix B

### Design of Axial and Lateral Load for( CFST ) Columns

#### Axial load design ( $P_o$ ):

The AISC 360-16 specification provides an approach for predicting the Nominal strength of CFST columns within the specified limitations (TABLE I1.1b). The compressive strength of CFST columns is determined by the CFST section classification for local buckling, as shown below:

#### For square section

$$\lambda = \frac{B}{t} = \frac{100}{2.75} = 36.36$$

$$\text{where } \lambda_p = 2.26 * \sqrt{\frac{Es}{fy}} = 2.26 * \sqrt{\frac{201229}{315.33}} = 57$$

$$\text{and } \lambda_r = 3 * \sqrt{\frac{Es}{fy}} = 3 * \sqrt{\frac{201229}{315.33}} = 75.78$$

$$\lambda \leq \lambda_p \text{ The section is compact and less than } 5 * \sqrt{\frac{Es}{fy}} = 126.33 \therefore \text{ok}$$

#### For a circular section

$$\lambda_p = 0.09 \frac{Es}{Fy}$$

$$\lambda_r = 0.31 \frac{Es}{Fy}$$

$$\lambda = \frac{D}{t} = \frac{115}{2.75} = 41.8$$

$$\text{where } \lambda_p = 0.09 * \frac{201229}{315.33} = 57.4$$

$$\text{and } \lambda_r = 0.31 * \frac{201229}{315.33} = 198$$

$$\lambda \leq \lambda_p \text{ The section is compact and less than}$$

$$0.31 * \frac{E_s}{F_y} = 198 \therefore \text{ok}$$

**The thickness of the steel tube has been satisfied The ACI-code 318(10.3.1.6) shall be not less than (a) or (b):**

$$(a) \quad b\sqrt{\frac{f_y}{3E_s}} \quad \text{for each face of width (square)}$$

$$100 * \sqrt{\frac{315.33}{3 * 201299}} = 2.29 \text{mm}$$

$$t_{used} = 2.75 \text{ mm} > 2.29 \text{mm} \therefore \text{ok}$$

$$(b) \quad h\sqrt{\frac{f_y}{8E_s}} \quad \text{for circular sections of diameter } h$$

$$115 * \sqrt{\frac{315.33}{8 * 201299}} = 1.6$$

$$t_{used} = 2.75 \text{ mm} > 1.6 \text{ mm} \therefore \text{o.k}$$

**Nominal Axial Load:**

$$P_o = 0.85 * f_{c'} * A_c + f_y * A_s$$

$$f_{c'} = 68.16 \text{ MPa for high-strength concrete}$$

$$f_{c'} = 31.66 \text{ MPa for normal-strength concrete}$$

$$f_y = 315.33 \text{ MPa}$$

**For square tube:**

$$A_c = 6430 \text{ mm}^2$$

$$A_s = 1650 \text{ mm}^2$$

**For normal -strength**

$$P_o = .85 * 31.66 * 6430 + 315.33 * 1650 = (693) \text{ kN}$$

**For high-strength**

$$P_o = 0.85 * 68.16 * 6430 + 315.33 * 1650 = (893) \text{ kN}$$

**For circular tube:**

$$A_c = 6494 \text{ mm}^2$$

$$A_s = 1520 \text{ mm}^2$$

**For normal -strength**

$$P_o = 0.85 * 31.66 * 6494 + 315.33 * 1520 = (654) \text{ kN}$$

**For high-strength**

$$P_o = 0.85 * 68.16 * 6494 + 315.33 * 1520 = (856) \text{ kN}$$

**Moment of Inertia:**

**For square tube**

$$I_x = \frac{bh^3}{12}$$

$$I_x = \frac{(100 * 100^3 - 50 * 50^3)}{12}$$
$$= 7.8 * 10^6 \text{ mm}^4$$

Total area of cross-section composite column =  $A_c +$

$$A_s = 6430 + 1650 = 8080 \text{ mm}^2$$

The radius of gyration =  $R_s = \sqrt{\left(\frac{I_{sc}}{A_{sc}}\right)}$

$$= 31 \text{ mm}$$

**For circular tube**

$$I_x = \frac{\pi (D^4)}{64}$$

$$I_x = \frac{\pi (115^4 - 61^4)}{64}$$

$$= 7.9 \times 10^6 \text{ mm}^4$$

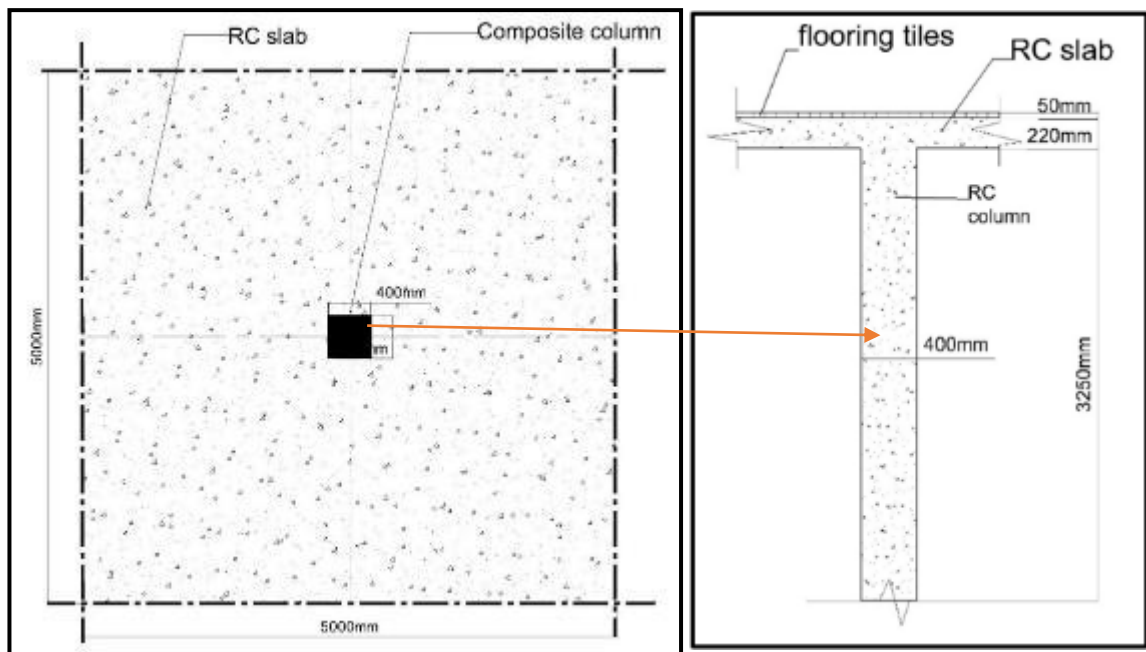
The total area of the cross-section composite column =  $6494 + 1520 = 8014 \text{ mm}^2$

$$\text{The radius of gyration} = R_s = \sqrt{\left(\frac{I_{sc}}{A_{sc}}\right)}$$

$$= 31.4 \text{ mm}$$

### Dead and Live Load scale calculations

The effect of dead load plus live load as a self-weight of typical slab assumed to have a dimension (5000\*5000) mm with (220 mm) thickness and the finishing tiles over it (50) mm, and live load about (1-1.25) kN/m<sup>2</sup> that carried by a short column with dimensions of (400\*400\*3250) mm. The samples were selected by multiplying these loads and dimensions assuming a scale factor (1:4). as shown in Figure below.



(a)

(b)

Actual column details(a)section in slab (b)section in column



Appendixes.....

$$\text{Slab dimensions} = 5000 * 5000 = 25 * 10^6 \text{ mm}^2$$

$$\text{Thickness of slab} = 220 \text{ mm}$$

$$\text{Self weight of slab} = 24 * \frac{220}{1000} = 5.28 \text{ kN/m}^2$$

$$\text{Flooring Tiles} = 23 * \frac{50}{1000} = 1.15 \text{ kN/m}^2$$

$$\text{Total dead load} = 6.5 \text{ kN/m}^2$$

$$\text{D.L} = (5 * 5) \text{ m}^2 * 6.5 \text{ kN/m}^2 = 162 \text{ kN} \text{ (dead load transferred to actual column).}$$

$$\text{Scale factor} = \frac{\text{Sample length}}{\text{Actual length}} = \frac{800}{3250} = \frac{1}{4}$$

$$\text{D.L of specimen} = 162 * \frac{1}{4} = 40 \text{ kN}$$

$$\text{L.L assumed} = 1.25 \text{ kN/m}^2$$

$$\text{D.L} + \text{L.L} = 70 \text{ kN}$$

## الخلاصة

يعد سلوك الأعمدة المركبة تحت تأثير الاحمال الجانبية الدورية هو أحد الأساليب المستخدمة في الوقت الحالي، فان قوة الشد العالية للفولاذ، والفائدة الاقتصادية، والقدرة العالية للخرسانة على مقاومة قوة الضغط ، جعل المادتين تعملان معاً بشكل جيد. وتشمل الدراسة: الاعمدة المركبة المكونة من أنبوبين خارجي وداخلي مثبتين معاً بشكل جيد واملء الفراغ بينهما بنوعين من الخرسانة: خرسانة ذات مقاومة عالية واخرى ذات مقاومة اعتيادية. ويمثل عدد عينات الاختبار العملي 12 عموداً مركباً ، ستة منها مربعة المقطع ، والاخرى دائرية. وقد تم تقسيمها إلى ست مجموعات جميعها معرضة الى قوة جانبية دورية: تتألف المجموعة الأولى من عيّنتين؛ احدهما ذات مقطع دائري والاخرى ذات مقطع مربع. وقد ملئت هذه العينات بخرسانة اعتيادية وخضعت فقط للحمل الجانبي الدوري. اما المجموعة الثانية هي بنفس مواصفات المجموعة السابقة،بالاضافة الى تعرضها الى حمل محوري (عمودي) يمثل الحمل الميت فقط مايعادل (40 كيلو نيوتن). وكان للمجموعة الثالثة أيضاً نفس مواصفات المجموعتان الأولى والثانية، وتعرضت لاحمال محورية (ميتة وحية) تبلغ حوالي (70) كيلو نيوتن. وتتألف المجموعة الرابعة من عيّنتين، احدهما ذات مقطع دائري والاخرى ذات مقطع مربع. وكانت هذه العينات مملوءة بخرسانة عالية المقاومة ، وخضعت فقط للحمل الجانبي الدوري. وكانت المجموعة الخامسة هي بنفس مواصفات المجموعة الرابعة، وتعرضت لحمل محوري (عمودي) يبلغ حوالي (40 كيلو نيوتن) يمثل الحمل الميت فقط. اما المجموعة السادسة فهي ايضا بنفس الوصف للمجموعتين الرابعة والخامسة، وقد خضعت لاحمال محورية (ميتة و حية) تبلغ حوالي (70) كيلو نيوتن. وتشمل متغيرات العمل ، شكل المقطع العرضي للأنبوب، ونوع الخرسانة، وقيمة الحمل المحوري. وتمثل التأثيرات الديناميكية، أنماط الفشل، منحنيات العلاقة بين الازاحة الجانبية – الحمل الدوري الجانبي، بروتوكول القوة الدورية الجانبية مع الوقت، ومقارنة النتائج العملية مع النتائج العددية المستخرجة باستخدام برنامج التحليل العددي (ABACUS). وتم دراسة تأثيرنوع الخرسانة المألثة للأعمدة المركبة ووجد أن العينات ذات الخرسانة العالية (HSC) زادت عن نفس المقدار من الخرسانة العادية (NSC) ، بالنسبة للمقطع الدائري كنسبة مئوية (6.68%، 9.20%، 21.10%) بالنسبة لتغير قيمة القوة المحورية (العمودية) وفيما يتعلق بالمقطع المربع، زادت النسبة المئوية (3.37%، 6.26%، 9.53%) على التوالي بالمقارنة مع الأعمدة المملوءة بالخرسانة العادية(NSC) ، وهذا يعني أن تأثير الخرسانة ذات المقاومة العالية عزز أداء مقاومة الأعمدة المركبة للأحمال الجانبية

بوضوح. وبالنسبة لتأثير الشكل، تبين النتائج أن العينات ذات المقطع الدائري لديها مقاومة للاحمال الدورية الأفقية أكبر من العينات ذات المقطع المربع تحت نفس تأثير قيم القوة المحورية (العمودية).



جمهورية العراق  
وزارة التعليم العالي و البحث العلمي  
جامعة كربلاء  
كلية الهندسة  
قسم الهندسة المدنية

**عنوان الرسالة : دراسة عملية ونظرية للاعمدة الحديدية الانبوبية  
المزدوجة المملوءة بالخرسانة و المعرضة الى احمال جانبية دورية**

رسالة مقدمة الى مجلس كلية الهندسة / جامعة كربلاء وهي جزء من متطلبات نيل درجة /  
الماجستير في علوم الهندسة المدنية  
المؤلف:

اسم الطالب : زينب فاضل كاظم / بكالوريوس هندسة مدنية (2003-2004)

باشراف :

أ.م. د. بهاء حسين العباس ، أ.م. د. علي غانم عباس الخفاجي